BULLETIN

of the

Polish Hydrogen and Fuel Cell Association

3RD POLISH FORUM

SMART MATERIALS

FOR HYDROGEN AND RENEWABLE ENERGY

SET PLAN SATELLITE CONFERENCE 29-30 NOV. 2011 WARSAW

CHAIRMAN: Janina Molenda

Highlights:
achievements of Polish Scientists in the fields of
- **hydrogen storage,**
- **fuel cells: PEMFC, SOFC**
- **Li-ion batteries**
- **supercapacitors**
- **photovoltaics**
- **photocatalysts for solar energy conversion**
- **photoelectrochemical cells**

forum.hydrogen.edu.pl

POLSKIE STOWARZYSZENIE WODORU I OGNIW PALIWOWYCH * PSWiOP *

Reviewers:
Prof. dr hab. inż. Janina Molenda (AGH UST)
Prof. dr hab. Roman Dziembaj (UJ)
Prof. dr hab. inż. Janusz Szmyd (AGH UST)
Prof. dr hab. inż. Marek Danielewski (AGH UST)

Acknowledgement:
The Bulletin was financially supported from the European Institute of Innovation and Technology, under the KIC InnoEnergy NewMat project.

Rocznik informacyjny nr 6 (2011)
Polskiego Stowarzyszenia Wodoru i Ogniw Paliwowych
ISSN 1896-7205, nakład 500 egz
Redaktor naczelny: Janina Molenda

Adres redakcji:
Polskie Stowarzyszenie Wodoru i Ogniw Paliwowych
Akademia Górniczo-Hutnicza im. Stanisława Staszica, Wydział Energetyki i Paliw
Al. Mickiewicza 30, 30-059 Kraków, e-mail: hydrogen@agh.edu.pl

www.hydrogen.edu.pl

Ladies and Gentlemen,

Cordially welcome for the sixth time on the columns of the Bulletin of the Polish Hydrogen and Fuel Cells Association!

I would like to inform those, who for the first time have contact with our periodical that, almost seven years old, Polish Hydrogen and Fuel Cells Association is an initiative of polish scientific societies associated with universities, research institutions, Centers of Excellence and local organizations concerned with preservation of natural environment. The basic aim of the Association is propagation and dissemination of the development of the hydrogen and fuel cells technologies as well as consolidation of the scientific society around problems involved in the broadly understood hydrogen based power industry.

We are very pleased, that our Association is continuously developing – presently counts 157 ordinary members (including over 50 professors or senior scientists in this figure). Polish Association represents huge intellectual potential and in this regard we distinguish as against other European hydrogen associations. Polish Hydrogen and Fuel Cells Association is a member of international organizations: European Hydrogen Association (EHA) and Partnership for Advancing the Transition to Hydrogen (PATH).

I cherish vast hope that activity of the Association contributes to the popularization of the ideas of clean, modern power technologies, including the hydrogen technologies. We are pleased to inform, that during 6 editions of the "Best thesis in the field of hydrogen technology and fuel cells" competition, every year an increasing number of master and Ph.D. theses are submitted for the contest. Academic lectures at AGH Open Technical University in the field of hydrogen technologies are organized annually. For the 3rd time we had organized the Summer School of Hydrogen and Fuel Cells for young scientists, Ph.D. students and power industry employees. The current issue of the Bulletin coincides with the III Polish Forum of Hydrogen and Fuel Cells, which took place on the 29-30 November in Warsaw. This year the conference has wider formula - "Smart Materials for Hydrogen and Renewable Energy" and is a satellite to the major Strategic Energy Technology Plan Conference 2011 (www.setplan2011.pl), which is related to Polish EU Presidency. The conference is devoted to the presentation of Polish achievements in the area of materials for the hydrogen technologies, fuel cells and renewable energy systems. In the Bulletin you can find the papers originating from the leading scientific centers in Poland, which were presented during the III Forum „Smart Materials for Hydrogen and Renewable Energy". The contents of the Bulletin shows that in Poland there is significant scientific potential in the field of new materials for modern energy technologies, i.e. fuel cells and hydrogen technologies, solar conversion systems and energy storage. In Poland we have large achievements concerning design of functional materials for high- and low-temperature fuel cells, hydrogen storage, photovoltaics, water photolysis, Li-ion batteries and supercapacitors. Today it seems that nanomaterials are the future for modern power technologies.

You are always welcome to visit and contribute to the Association website: www.hydrogen.edu.pl.

I hope that Polish Hydrogen and Fuel Cells Association will create a solid scientific background and will be lobbing for development of the clean power technologies in Poland.

Prof. Janina Molenda
President of the
Polish Hydrogen and Fuel Cell Association

Contents

EIT KIC InnoEnergy Lighthouse Innodriver on „New Materials for Energy Systems" (NewMat) - bridging a gap between science and industry

Aleksandra Czyrska-Filemonowicz, Beata Dubiel
AGH University of Science and Technology, International Centre of Electron Microscopy for Materials Science & Faculty of Metals Engineering and Industrial Computer Science,
30-059 Kraków, Al. Mickiewicza 30, Poland

The InnoEnergy Knowledge and Innovation Community (KIC InnoEnergy) was designated by the European Institute of Innovation and Technology (EIT) Governing Board on the 16 December 2009 in Budapest [1, 2] and the priority area which this KIC addresses is a Sustainable Energy. The KIC InnoEnergy consortium is structured in six Co-location Centres (CC). One of these centres is the CC Poland Plus, coordinated by the AGH University of Science and Technology.

Innovation in energy issues sets new challenges for materials development. Therefore a co-operative "NewMat" project, the Lighthouse Innodriver project of the CC Poland Plus, proposes a new strategy for materials innovation for a better co-development between materials design and implementation in energy devices.

The NewMat project, coordinated by the AGH University of Science and Technology, concerns the implementation of new materials for enhancement of the existing- and introduction of innovative technologies of energy production. New materials with improved properties should increase performance and efficiency of clean energy production, but also contribute to cost savings.

The project is structured around three types of activities, known as the Knowledge Triangle (Fig.1): research, higher education and innovation.

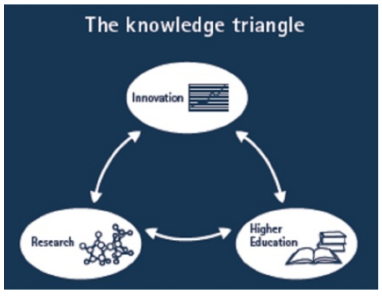

Fig.1. The Knowledge Triangle [1].

At present, the NewMat consortium consists of ten partners from education, research and industry sectors, representing five Co-location Centres of the KIC InnoEnergy. The list of the NewMat partners is given in the Table 1 and presented on Fig.2.

To solve the materials' problems defined by industry, NewMat project offers complex interdisciplinary research and education based on horizontal- and visionary concepts. It comprises multi-scale material investigations in atomistic-/ nano-/ micro-/ meso-/ macro- and engineering scales. To develop the new materials, a cross disciplinary studies, including materials science, mechanics, physics and chemistry subjects, are carried out. In particular, materials for innovative energy sources, like advanced fossil fuel power plants, clean coal technologies, nuclear power plants, renewables, smarts grids, membranes and energy storage are investigated. Transformational advances in materials facilitate the targets of future energy policy.

The key objectives of the NewMat project are:

- to develop and share expertise of the research community and industry partners on new materials for clean energy systems,
- to train a new generation of engineers and researchers,
- to solve the materials' problems defined by industry by complex interdisciplinary research based on horizontal and visionary concepts.

To reach the objectives of the activities given above, the NewMat project is divided into two stages. At present, we conduct the STAGE 1 (2011-2014) of the NewMat project, which comprises the research of new materials (design, modelling, processing, characterization, optimisation) necess-

Table 1. NewMat project partners.

	Partner	Co-location Centre	Organization type
1	AGH-UST AGH University of Science and Technolgy	CC Poland Plus	Education
2	UJ Jagiellonian University	CC Poland Plus	Education
3	BZF Bay Zoltán Foundation for Applied Research, Institute for Logistics and Production Systems	CC Poland Plus	Research
4	IFK Universität Stuttgart	CC Germany	Education
5	UU Uppsala University	CC Sweden	Education
6	IST Instituto Superior Técnico Lisboa	CC Iberia	Education
7	INP Grenoble Institute of Technology	CC Alps Valleys	Education
8	EDP Energias de Portugal, SA	CC Iberia	Industry
9	EDF Electricité de France	KIC level partner	Industry
10	RAFAKO S.A	CC Poland Plus	Industry

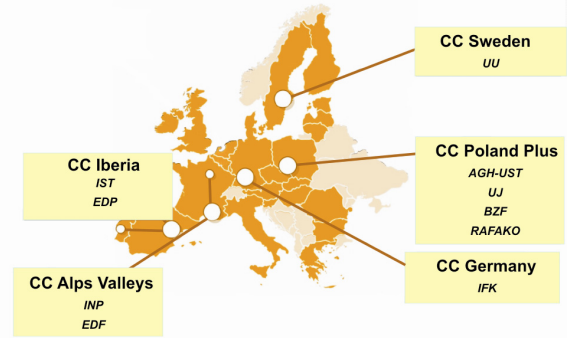

Fig.2. Pan-European NewMat consortium: ten partners from five Co-location Centres.

ary before production of the demonstrators made from new materials and their application in pilot components/plants (to be conducted in the STAGE II of the NewMat project; 2014-2017).

The project consists of eleven Work Packages, including two innovation activities, seven research activities, one joint education activity and one coordination activity:

WP0: Market analysis and business opportunities
WP1: Materials for high efficiency „zero-emission" fossil fuel power plants
WP2: Advanced materials for clean coal technologies
WP3: Materials for nuclear power plants
WP4: Materials for renewable energy storage and conversion systems (fuel cells, Li-ion batteries, photovoltaics, photoelectrochemical cells)
WP5: Membranes for energy production
WP6: Smart grids materials
WP7: Development of characterisation and modelling methods of power plant components made from innovative materials
WP8: Education on materials for energy systems
WP9: Project coordination and promotion
WP10: Exploitation plan

On the basis of the market watch for development of materials for energy systems, the research packages of the NewMat project are oriented towards solving industrial problems by:

- characterisation of micro/nanostructure and properties of new materials,
- tailoring materials' microstructure for desired properties,

- design by modelling and processing of new materials,
- optimisation, verification, application.

New methods of characterisation- and modelling of components made from innovative materials address dedicated microstructural characterisation down to a nano-and atomic scale, measurements of desired properties, modelling, monitoring and life-time prediction. It will be facilitated by the use of the one most advanced and powerful electron microscopes, Titan G2 60-300 with Cs probe corrector and ChemiSTEM system for analytical high resolution microscopy at high (300 kV) and low (60 kV) voltage (Fig.3), installed recently in the International Centre of Electron Microscopy for Materials Science at the AGH University of Science and Technology in Kraków [3].

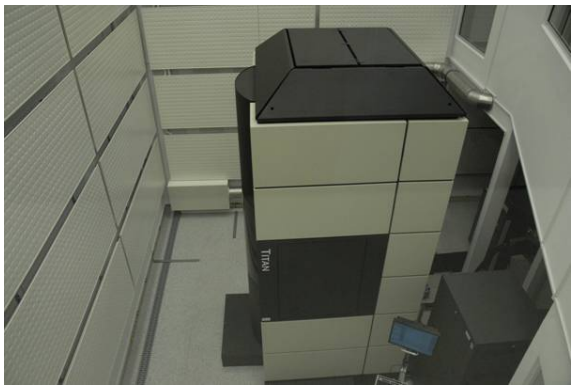

Fig.3. Titan Cubed G2 60-300 with Cs probe corrector and ChemiSTEM system for analytical high resolution microscopy recently installed in the International Centre of Electron Microscopy for Materials Science at the AGH University of Science and Technology in Kraków (photo: S. Malik).

Education activities within NewMat project address the high-level education programmes in the field of energy in Europe. The teachers and students mobility is designed according to common criteria established by InnoEnergy for the EIT label and implemented by the InnoEnergy partners. It will result in mobility of professors and students, on-site industrial internships, co- supervision of PhD students as well as transnational access to laboratory infrastructure.

Organization of the Schools and Workshops is focused on spreading the information in Sustainable Energy among the InnoEnergy partners. Specific workshops dedicated to industry-driven objectives should benefit in integration of academia and industry communities.

In order to commercialize and exploit the business opportunity of demonstration and application of New Materials in pilot components/ plants, business models and business plan for technology, product, service and new ventures will be defined.

The realization of the NewMat project closely integrates all corners of the Knowledge Triangle of research, higher education and innovation and bridge the gap between science and industry.

Acknowledgements

The authors acknowledge a financial support from the European Institute of Innovation and Technology, under the KIC InnoEnergy NewMat project.

References

1. European Institute of Innovation and Technology, http://www.eit.europa.eu
2. KIC InnoEnergy, http://www.kic-innoenergy.com
3. International Centre of Electron Microscopy for Materials Science, http://www.tem.agh.edu.pl

Zinc Oxide by Atomic Layer Deposition for the second and third generation of photovoltaic cells

Marek Godlewski[1,2], Grzegorz Łuka[1], Krzysztof Kopalko[1], Elżbieta Guziewicz[1]

[1]Institute of Physics, Polish Acad. Sciences, Al. Lotników 32/46, 02-668 Warsaw, Poland

[2]Dept. Math. and Natural Sciences College of Science, Cardinal S. Wyszyński Univ., Warsaw, Poland

Abstract

ZnO films deposited by Atomic Layer Deposition (ALD) method at different growth conditions have required electron concentrations and electron mobilities for applications as n-type partners to p-type CdTe (ZnO layers with a reduced free electron concentration) and the transparent conductive oxide (TCO, metallic ZnO films). In the latter case their electrical properties are comparable to those of ITO and ZnO:Al (AZO) films obtained by a sputtering. We also demonstrate that ZnO films deposited by the ALD are suitable for construction of hybrid structures (semiconductor/organic material) for applications in novel photovoltaic (PV) panels based on organic materials (PV cells of the third generation).

I. Introduction

Photovoltaic (PV) effect and its application are known from the XIX century. It was discovered by A.E. Becquerel in 1839, whereas the first practical applications were proposed in 1870s by Hertz and in 1883 by Charles Fritts. The first modern solar cell was patented in 1946 by Russell Ohl. In 1954 Bell Laboratories developed the first PV cell (with 4% efficiency) based on a crystalline silicon. This led to a first generation of PV cells, which are based on a p-n junction of monocrystalline or polycrystalline Si. This PV generation is still dominant, accounting for more than 80% of the solar cell market (after [1]). For further development new ideas and materials are needed to reduce a payback time for the PV devices [1-5]. PV cells based on amorphous silicon and thin films of II-VI and III-V materials are now intensively tested. They can lower a price of PV cells and thus lead to a boom in solar cells industry.

The first thin film PV cells of the second generation, based on amorphous silicon, were demonstrated by Wronski and Carlson in 1976. Many other possible materials were tested (GaAs, $CuInSe_2$, CdTe). Band gap of the latter materials is ideally suited for PV devices of an increased efficiency, due to optimization of the absorption with the solar spectrum. Moreover, a direct band gap of these materials results in large absorption coefficients. In the consequence, much thinner material is enough to absorb fully the solar light.

Third (fourth in some sources) generation of PV cells do not rely on semiconductor-based p-n junctions. Photo-electrochemical (PEC) cells and organic/polymer cells belong to this category, with materials costs reduced to a few $ per m^2. The main limitation is still relatively low efficiency and time stability (lifetime) of devices based on organic materials. We demonstrated recently that by coating of an organic material with ZnO films devices stable in time can be constructed. High rectification rations of Schottky junctions for such hybrid junctions were recently demonstrated by us for P3HT/ZnO system [2].

In the present work we also demonstrate that the Atomic Layer Deposition (ALD) can be used to deposit TCO contacts for solar cells.

II. Technique of Atomic Layer Deposition

Atomic Layer Deposition is a self-limiting growth process, often claimed to be a version of Chemical Vapor Deposition (CVD). The main difference between the ALD and CVD is that in the ALD process precursors (commonly organic ones) are introduced sequentially and their pulses are separated by purging processes with a neutral gas. Vapors of the second precursor react only with the first precursor adsorbed at the surface of the growing film. They do not react in a gas phase, as happens in the CVD processes. In the consequence, very reactive precursors can be used, since they will not pre-react in a gas form. Moreover, thermal decomposition of the precursors is not required. This results in the two very attractive properties of the method:

1) ALD enables growth at a low temperature.
2) ALD enables very uniform covering of 3D structured surfaces.

For example, ZnO with good structural properties can be grown at a very low temperature, well below 200 °C [6-10]. The most effective zinc precursors turned out to be diethylzinc (DEZn) and dimethylzinc (DMZn) with deionized water used as an oxygen precursor. Growth temperature could be reduced to about 100 °C, which enabled us construction of hybrid structures of the type ZnO/organic material [2,11]. This is very important advantage of the ALD method, important for applications in PV devices based on organic materials.

III. Results and discussion

A. CdTe/ZnO PV cells

Use of material with a low band gap (such as silicon) enables absorption of light in a wide range of energies, but results in a low produced voltage. Therefore, for optimum PV devices we should use direct band gap materials with a band gap ~1.5 eV.

CdTe exhibits a forbidden gap of 1.45 eV at room temperature, which is spectrally close to the one required for a material with a maximum of solar energy conversion efficiency. In the consequence, the predicted light conversion efficiency is relatively large (27% [4]) for CdTe-based PV devices. This is why thin films of CdTe (PVs of the second generation) are intensively studied for PV applications.

Use of CdTe in PV devices was difficult due to problems with contacts to p-type CdTe [4]. The best back-contacts were prepared by using materials such as Sb_2Te_3 or As_2Te_3 or graded CdTe/ZnTe structures. Importantly, it was demonstrated recently that coating with heavily n-type ZnO can help to solve problems with a back contact [12]. This results from an alignment of CdTe, ZnTe and ZnO bands. Due to this favorable alignment carriers can easily tunnel from CdTe/ZnTe region to metal contact via a conduction band of ZnO [12]. This is the first reason why ZnO is an interesting partner of CdTe for PV applications. The second relates to the fact that as-grown CdTe is of p-type. CdTe can be doped for n-type using Al, In, Ga. However, in the case of polycrystalline thin films these dopants segregate at the grain boundaries giving rise to metallic paths that shunt the CdTe layers [4]. Thus in PV devices only p-type CdTe is used and n-type partner is needed to construct p-n junctions. Even though most of the works concentrated on use of CdS, ZnO is still considered as an attractive n-type partner of CdTe in PV cells [4]. We tested such possibility by depositing of lightly n-type doped ZnO by the ALD process on top of as-grown p-type CdTe layers. The p-n junction constructed by us had a rectification factor of 10^4 and a good photoresponse under the solar light illumination.

B. ZnO grown by ALD as the TCO material

Another important approach to reduce costs of PV devices concentrates on introduction of alternative transparent contact materials. The presently widely used In_2O_3:Sn (ITO) becomes too expensive, which is due to a rapidly increasing price of indium. Several alternative TCO materials were tested [13], with ZnO being the best candidate for the ITO replacement [13]. ZnO films doped with aluminum (or indium) produced by the sputtering show required properties for the TCO applications [4,13]. Doping may cause some problems, since the ZnO:Al layers may not be stable in time due to Al diffusion [4,14]. Electron mobility in these films is limited by scattering at grain boundaries [15].

In the present work we tested if the TCO layers can be deposited by the ALD method. We report that ZnO films deposited by the ALD have desired electrical parameters. A high free electron concentration, relatively high mobility (as for polycrystalline films), and high transparency (transparency above 90% is achieved in a wide spectral region) makes them suitable for the TCO applications [11,16]. Relevant results are shown in Figs. 1 and 2 for films grown using DEZn as the zinc precursor.

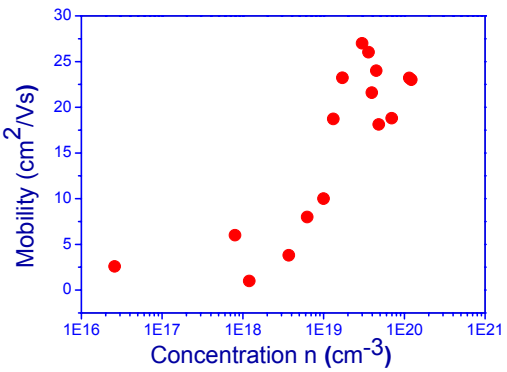

Fig. 1: Electrical properties (electron mobility at room temperature) of ZnO films grown by the ALD using DEZn at temperature varied between 60 and 240 °C (see Godlewski et al [11] for further details).

In most of the cases films with a higher n show lower electron mobility, because scattering on ionized impurities determines carrier mobility. Scattering on grains boundaries is also important. We can modify the role of the two dominant scattering mechanisms mentioned above. In fact, we could select growth parameters to increase carrier mobility with an increasing growth temperature. For films grown at such conditions the rise of free electron concentration is observed together with the rise in their mobility (see Fig. 1). These properties and a high transparency (see Fig. 2) makes them suitable for the TCO applications. Further increase of layers conductivity we achieved by doping ZnO with Al.

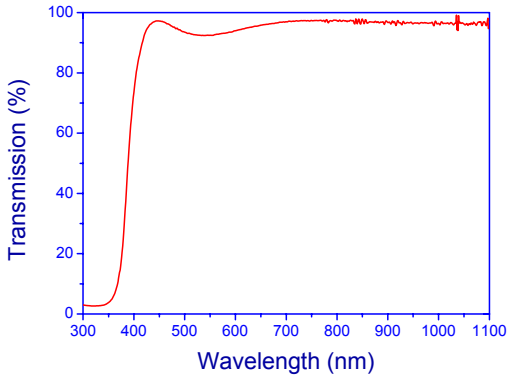

Fig. 2: Transmission spectrum of 215 nm thick highly conductive ZnO film (with free electron concentration at room temperature n=2x10^{20} cm^{-3} and mobility 25.5 cm^2/Vs) grown by the ALD on a sapphire substrate (see Godlewski et al [11] for further details).

C. *ZnO grown by ALD for PV cells of the third generation*

Organic materials show several attractive properties for applications in solar cells of the third generation. Their wider use is limited by time stability of the devices. Fortunately, their coating with transparent wide band gap materials can improve time stability [17]. For coating of organic materials a low thermal budget of growth and the post-growth treatment processes is required. This makes the ALD technique and the ALD deposited ZnO films very attractive. We tested several possible configurations of PV cells covered by the ALD with ZnO films. Pentacene, OPV8 and P3HT (Poly (3-Hexylthiophene)) were used as organic materials. The so-obtained diodes showed good rectifying properties (10^4) [2] and a very good PV response. Films coated with ZnO are stable in time.

IV. Conclusion

We demonstrate suitability of the ALD method for construction PV devices of the second and third type. ZnO films obtained by the ALD can act as the TCO material. They can also be used as the n-type partner in CdTe-based solar cells. Importantly, a very low growth temperature enables construction of hybrid ZnO/organic structures. This opens the chances of constructing several PV devices belonging to the third generation of solar cells.

Acknowledgement

This work was supported in part by the European Union within European Regional Development Fund, through grant Innovative Economy (POIG.01.01.02-00-108/09).

References

1. 2007 Survey of Energy Resources World Energy Council 2007
2. E. Katsia, N. Huby, G. Tallarida, B. Kutrzeba-Kotowska, M. Perego, S. Ferrari, F. C. Krebs, E. Guziewicz, M. Godlewski, G. Łuka, Appl. Phys. Lett. 94, 2009, p. 143501.
3. R. McConnell, Semiconductors 38, 2004, p. 931.
4. A. Bosio, N. Romeo, S. Mazzamuto, V. Canevari, Progress in Crystal Growth and Characterization of Materials 52, 2006, p. 247.
5. J.A. Aranovich, D. Golmayo, A.L. Fahrenbruch, R.H. Bube, J. Appl. Phys. 51, 1980, p. 4260.
6. N. Huby, S. Ferrari, E. Guziewicz, M. Godlewski, V. Osinniy, Appl. Phys. Lett. Vol. 92, 2008, p. 023502.
7. E. Guziewicz, I.A. Kowalik, M. Godlewski, K. Kopalko, V. Osinniy, A. Wójcik, S. Yatsunenko, E. Łusakowska, W. Paszkowicz,, J. Appl. Phys. 103, 2008, p. 033515.
8. K. Kopalko, M. Godlewski, J.Z. Domagala, E. Łusakowska, R. Minikayev, W. Paszkowicz, A. Szczerbakow, Chemistry of Materials 16, 2004, p. 1447.
9. A. Wójcik, M. Godlewski, E. Guziewicz, R. Minikayev, W. Paszkowicz, J. Cryst. Growth 310, 2008, p. 284.
10. T. Krajewski, E. Guziewicz, M. Godlewski, Ł. Wachnicki, I.A. Kowalik, K. Kopalko, A. Wójcik, V. Osinniy, M. Guziewicz, Microelectron. J. 40, 2009, p. 293.
11. M. Godlewski, E. Guziewicz, G. Łuka, T. Krajewski, M. Łukasiewicz, Ł. Wachnicki, A. Wachnicka, K.

Kopalko, A. Sarem, B. Dalati, Thin Solid Films 518, 2009, p. 1145.
12. B. Späth, J. Fritsche, F. Säuberlich, A. Klein, W. Jaegermann, Thin Solid Films 480-481, 2005, p. 204.
13. O. Bamiduro, H. Mustafa, R. Mundle, R.B. Konda, A.K. Pradhan, Appl. Phys. Lett. 90, 2007, p. 252108.
14. T. Strachowski, W. Lojkowski, E. Grzanka, A. Presz, J. D. Fidelus, M. Godlewski, S. Yatsunenko, H. Matysiak, R.R. Piticescu, C.J. Monty, J. Appl. Phys. 102, 2007, p. 075513.
15. K. Ellmer and R. Mientus, Thin Solid Films Vol. 516, 2008, p. 5829.
16. M. Godlewski, E. Guziewicz, T. Krajewski, P. Kruszewski, Ł. Wachnicki, K. Kopalko, A. Wójcik, V. Osinniy, Microelectronic Engineering 85, 2008, p. 2434.
17. See F.C. Krebs, in Degradation and Stability of Polymer and Organic Solar Cells ed. F.C. Krebs Solar Energy Materials & Solar Cells 92, 2008, p. 685.

Smart photocatalysts for solar energy conversion

Wojciech Macyk
Faculty of Chemistry, Jagiellonian University, Ingardena 3, 30-060 Kraków, Poland

Heterogeneous photocatalysis – what is it?

Renewable energy sources have become very trendy, so more and more efforts are undertaken to utilize solar energy in various processes, in particular related to its conversion into electrical or chemical energy. The use of photovoltaic cells is limited by the variability of sunlight, high dispersion of solar energy, efficiency of conversion processes and the cost of the equipment itself. The issue of converting solar energy into the chemical one is even worse. Attempts of hydrogen photogeneration or artificial photosynthesis of fuel compounds generally did not go far beyond the walls of laboratories and the process of plant photosynthesis remains still an unequalled design. So should the attempts to use solar energy be abandoned? I am convinced that solar energy could and should be used to everyone's benefit, and photocatalysis is one of the ways to reap the benefit.

It all began in the 1960s with several articles showing oxidation of organic substances in the presence of titanium dioxide irradiated with UV light. However, those works did not focus too much attention and it was not until the seventies when research data on photocatalytic decomposition of water initiated the rapid development of heterogeneous photocatalysis. Unfortunately, to date researchers failed to develop a photocatalyst that could be readily applied in hydrogen production. Nevertheless, the work carried out over the years have resulted in many important discoveries and technologies.

Heterogeneous photocatalysts are usually oxides and sulfides of transition metals. The basic processes resulting in the photocatalytic effect are shown in Figure 1. Absorption of light leads to the generation of hole and electron in the valence and conduction bands, respectively (process 1). Those charges may migrate within the semiconductor particle, and can be trapped at surface sites (e_r^-, h_r^+; process 2). They can also participate in the interfacial electron transfer processes involving the molecules of electron acceptor A and donor D (process 3). Subsequent reactions of primary reduction/oxidation products, $A^{\bullet-}$ and $D^{\bullet+}$, lead to stable end products A_{red} and D_{ox}. The unwanted side processes include: charge recombination (processes 4 and 5) and redox reaction between $A^{\bullet-}$ and $D^{\bullet+}$ resulting in reproduction of the acceptor and the donor (process 6).

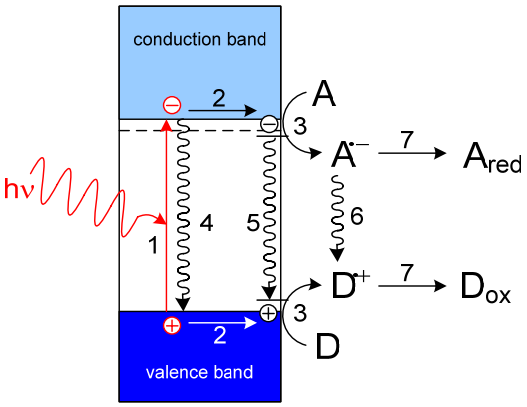

Fig. 1. Primary physical and chemical processes occurring in the presence of irradiated photocatalyst.

So much for basic theory. How can it be used in practice? If the processes 3 in the Figure 1 would stand for the reactions of water reduction and oxidation, then they could be used for hydrogen production. This is a difficult task and so far cannot be realized with satisfactory efficiencies in purely photocatalytic systems (*vide infra*). If the reactants A and D in the process 3 are organic substances, the reaction generates free radicals, which can combine to form new C-C or C-N bonds. Such "photosynthesis" can be performed with fairly good efficiency and selectivity in the presence of cadmium or zinc sulfides as photocatalysts. But most frequently oxygen and water play the role of A and D, respectively. In this case usually titanium dioxide or zinc oxide are used as photocatalysts, while superoxide anion ($O_2^{\bullet-}$) and hydroxyl radical ($OH^{\bullet}$) are the primary redox products. Those reactive radicals are responsible for most of the oxidation of organic substances. Importantly, oxidation under these conditions is usually complete, giving H_2O and CO_2 as the final products. The reactions can therefore be used in the processes of water, air or surface purifi-

cation. Since microorganisms also find the reactive radicals difficult to bear, ZnO and TiO_2 can be useful in photodisinfection.

How to "paint" the photocatalyst?

One key feature of TiO_2 and ZnO should be emphasised: those materials can absorb only ultraviolet radiation (photon energy above ~3.2 eV), and this fact significantly limits their application in photocatalysis. However, there are methods of "activation", or photosensitization of TiO_2 towards visible light – then the photocatalyst gains a colour.

In our work carried out at the Faculty of Chemistry, Jagiellonian University and a fellow group of Professor Horst Kisch at the University of Erlangen, we have successfully applied a number of methods for TiO_2 photosensitization. One of them is based on synthesis of TiO_2 in the presence of various organic compounds that are precursors of highly unsaturated carbon compounds. Excitation of such materials with visible light (e.g. blue or green) results in generating holes in the valence band and electrons in the conduction band, which in turn reduce the adsorbed oxygen molecules. Redox reactions produce a number of reactive oxygen species at the surface of the material. The discovery of carbon-doped TiO_2 (that is how this type of materials is usually called) in 2001 initiated an intensive development of other TiO_2-based photocatalysts of this type. Such photocatalysts have already been applied as ingredients of the photoactive paints for indoor painting, where the intensity of ultraviolet light is negligible.

Looking closer at the photosensitization process one can consider titanium dioxide crystal with some dopants which introduce donating or accepting electron levels (Figure 2a). Depending on the dopant nature light absorption can result in electron excitation from the donor level to conduction band, or from the valence band to the acceptor level. Carbon-doped TiO_2 obeys the former mechanism. The photogenerated hole is a weaker oxidant than that formed in the latter case, but the electrons from conduction band are capable of molecular oxygen reduction. This is a very important process, because it leads to generation of so called reactive oxygen species presented in the Figure 2. Another approach to titanium dioxide painting (photosensitization) involves synthesis of hybrid materials composed of two semiconductors – TiO_2 and another one (e.g. CdS) characterized by a narrower band gap, and energy of electrons in its conduction band suitable for the electron injection to titanium dioxide. Although charge separation in such systems prevents from an efficient and unwanted charge recombination, usually such systems suffer unacceptable photocorrosion processes which lead to loss of photoactivity in a relatively short time.

Surface coordination compounds may also influence spectral and redox properties of the semiconductor particle – photosensitization towards a lower photon energy, as well as shift of the band edges, may be achieved. A specific class of surface complexes formed at titanium dioxide comprises titanium(IV) complexes synthesized upon chemisorption of organic or inorganic ligands onto TiO_2.

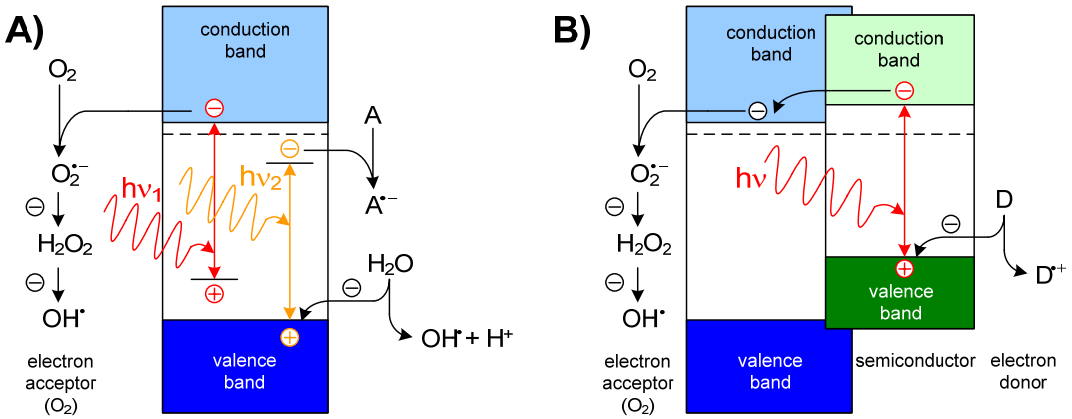

Fig. 2. Photosensitization of titanium dioxide achieved by: a) doping with electron donating or accepting levels; b) hybrid of two semiconductors. In both cases electrons from conduction band of TiO_2 can be used for reduction of oxygen to superoxide ($O_2^{\bullet-}$) and further to hydrogen peroxide (H_2O_2) and hydroxyl radical ($OH^{\bullet}$).

The ligands particularly easily chemisorbed at TiO_2 surface belong to the following groups: carboxylic acids, chelating ligands (derivatives of catechol, phthalic acid or salicylic acid), fluorides, cyanides, phosphates etc. (Figure 3). Similar moieties may also be used as anchoring groups binding external complexes to the surface. Ligand-to-metal charge transfer excitation (LMCT) in this case is equivalent to the injection of electron to the conduction band – in both cases the Ti^{III} species is formed. Therefore in such situation the photoinduced charge transfer can be described as a ligand-to-band charge transfer (LBCT) instead of LMCT (Figure 4a). This mechanism is valid also for TiO_2 sensitized with chemisorbed cyanide complexes of Fe^{II}, Ru^{II}, Os^{II}, Mo^{IV}, W^{IV} and Re^{III}. An effective photosensitization of titanium dioxide by surface complexes can be achieved only under certain circumstances: (i) the energy of LBCT is lower than the bandgap energy of TiO_2 (<3.2 eV) and (ii) absorption coefficient of the LBCT transition is high (allowed transition). However, practical applications of such materials are determined by efficiency of back electron transfer and stability of the surface complex. We have developed a series of transparent colloids of TiO_2 photosensitized by derivatives of catechol, phthalate and salicylate.

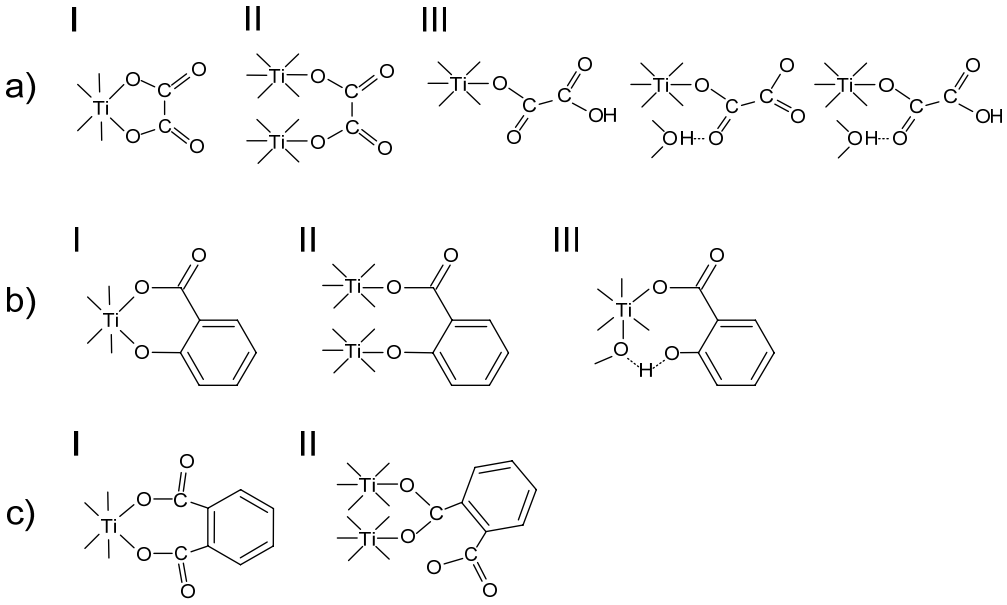

Fig. 3. Coordination modes of selected chelating ligands: a) oxalate; b) salicylate; c) phthalate. Various structures may be distinguished: bidentate chelating (I), bidentate bridging (II), monodentate with possible stabilization by hydrogen bonds (III).

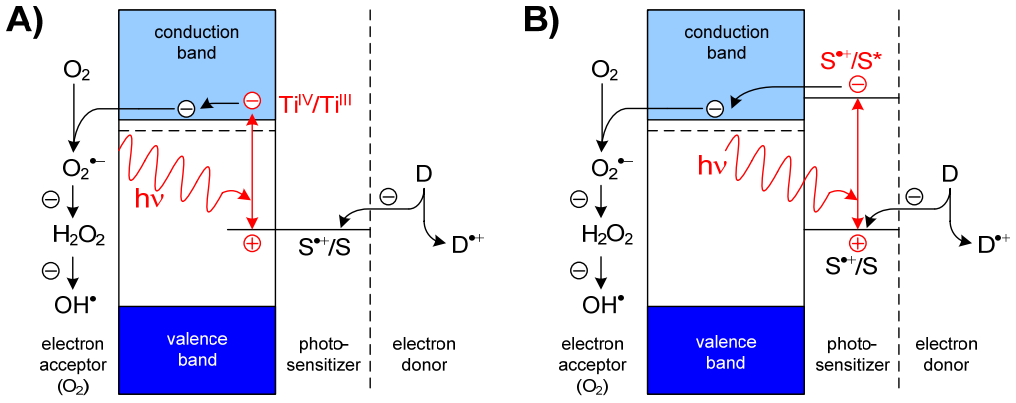

Fig. 4. Mechanisms of titanium dioxide photosensitization achieved by surface modifications: a) direct photosensitization (optical charge transfer) observed in the presence of surface LMCT Ti^{IV} complexex; b) dye-photosensitization involving electron injection to the conduction band from the excited photosensitizer (typical for dye sensitized solar cells).

The most important features of these yellow to brown colloidal solutions are: (i) good stability in aqueous solutions at neutral pH (usually colloids of titanium dioxide are stable in strongly acidic solutions) and (ii) high efficiency of photocatalytic processes induced by visible light. We have demonstrated an efficient bacteria inactivation in the presence of these colloids upon visible light irradiation. The results of bacteria inactivation tests made in the presence of modified nanocrystalline TiO_2 show a big potential for further development of these systems. Although photostability of materials modified with organic ligands is limited, these photocatalysts may find broad applications wherever disinfection is required (single-use equipment in hospitals, households) or even as photoactivated antibiotics.

Photosensitization of TiO_2 by surface complexes is based on the interaction of adsorbed or chemisorbed photosensitizer (S) with the semiconductor support (Figure 4b). The excited state energy ($S^{\cdot+}/S^*$ redox pair) should be higher than the energy of conduction band edge of the semiconductor. The electron injection from the excited state S* to the conduction band takes place with concomitant formation of $S^{\cdot+}$ transient species. Regeneration of the photosensitizer is assured in the presence of an electron donor D. Electrons from the conduction band reduce adsorbed oxygen thus generating reactive oxygen species. TiO_2 photosensitization according to this mechanism takes place in the case of platinum(IV) chloride complexes chemisorbed at the TiO_2 surface or in dye sensitized solar cells containing TiO_2 modified with derivatives of $[Ru(bpy)_3]^{2+}$ complex.

Photocatalysis – solar to electrical energy conversion

Photosensitized titanium dioxide may find applications not strictly associated to photocatalytic oxidation processes. An example may come from modern photovoltaic devices. Colourless titanium dioxide with attached deeply red or brown ruthenium(II) complexes is used to construct quite efficient dye sensitized solar cells (DSSC). Such material being in a good contact with a transparent electrode is excited with visible light (Figure 5). Upon excitation the photosensitization process (analogous to that from Figure 4b) takes place. Instead of oxygen reduction, the electron transfer to the conducting electrode results in the photocurrent flow. On the other hand, the oxidized form of ruthenium complex (Ru^{III}) is reduced back to Ru^{II} by iodide anions present in the electrolyte solution. The reversible I_3^-/I^- redox pair transmits electrons between the platinum electrode and the photosensitizer. Possible structures of ruthenium(II) complexes playing the role of photosensitizers are shown in Figure 6. A similarity between the interfacial redox processes taking place in DSSC and photocatalytic oxidation of organic pollutants should be stressed: the main difference between these two applications of photosensitized systems consists in reversibility of these reactions. While irreversible oxidation of organic matter is achieved in the process of water or air detoxification, completely reversible redox processes should govern operation of DSSC.

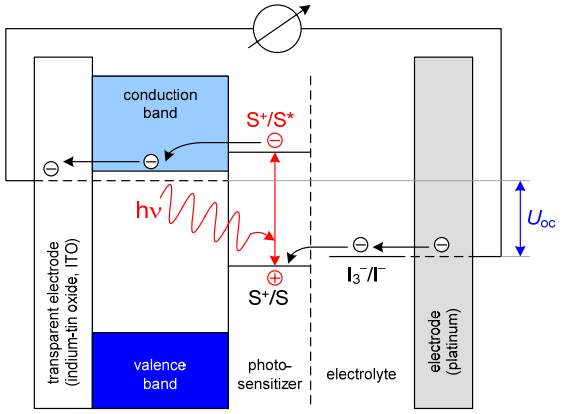

Fig. 5. Mechanism of photocurrent generation in dye sensitized solar cell.

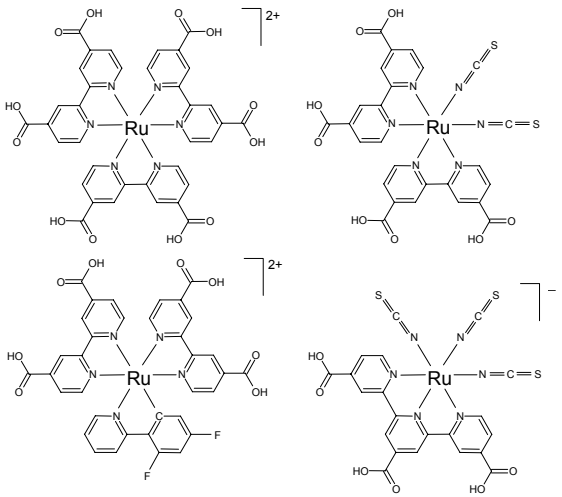

Fig. 6. Possible structures of ruthenium(II) complexes used as photosensitizers in DSSCs.

It should be mentioned, that DSSC is not only an academic concept born from research on photovoltaic or photocatalytic systems. Dye sensitized solar cells are working devices introduced already to the market. Their main weakness is associated to a limited stability of the dye – in the presence of even traces of oxygen organic ligands of ruthenium complexes decompose.

Conversion of light to electricity can also be applied in information processing. Photosensitized TiO_2-based materials may be used for construction of photoelectrochemical logic gates and switches. Photoelectrochemical properties of titanium dioxide sensitized by binuclear [L_nFe-CN-TiL_n] complexes are particularly interesting. This group of materials, involving hexacyanoferrate and pentacyanoferrate moieties bound to the surface of TiO_2, shows the PEPS effect (*PhotoElectrochemical Photocurrent Switching*, Figure 7). The direction of photocurrent generated at the electrode covered by such material depends on the applied potential (and therefore on the oxidation state of iron), on wavelength of incident light and composition of the electrolyte. Only the reduced form of iron moiety (Fe^{II}) can contribute to cathodic photocurrent generation. Presence of the oxidized surface complex changes the behaviour of the material – it behaves then like unmodified TiO_2. Excitation of the photoelectrodes made of titanium dioxide modified with surface binuclear complexes within the metal-to-band charge transfer bands (MBCT) results in most cases in generation of cathodic photocurrents (Figure 7b, photocurrents marked in red), while a direct excitation of the semiconductor (UV light) results in either cathodic or anodic photocurrents, depending on the photoelectrode potential (Figure 7a).

The switching potential at which the photocurrent direction changes correlates very well with redox potential of the iron moiety. At potentials higher than $E_{½}$ of the surface complex the excitation of the surface species does not take place – under these conditions only excitation of the semiconductor matrix with ultraviolet light may result in photocurrent generation (anodic, Figure 8a). Excitation of the reduced surface species generates an electron in the conduction band as a result of $Fe^{II} \rightarrow Ti^{IV}$ charge transfer. Due to a significant negative polarization of the electrode the electron transfer from the conduction band to the electrode is not favoured, what facilitates the reverse process, i.e. reduction of the electron acceptor in the electrolyte and a concomitant electron transfer from the electrode to the photochemically oxidized surface species (Figure 8b). These processes are responsible for the cathodic photocurrent generation. In the case of air-equilibrated systems oxygen molecule plays the role of the electron acceptor (E_{O_2/O_2^-} = –0.16 V vs. NHE). A direct excitation of the semiconductor also results in cathodic photocurrents (Figure 8c). Switching of the photocurrent direction by changes in either electrode potential or colour of incident light (photon energy) may be used for construction of chemical switches. Input values are attributed then to high or low potentials (input 1) and high or low photon energies (input 2). Anodic or cathodic photocurrents correspond to various output values.

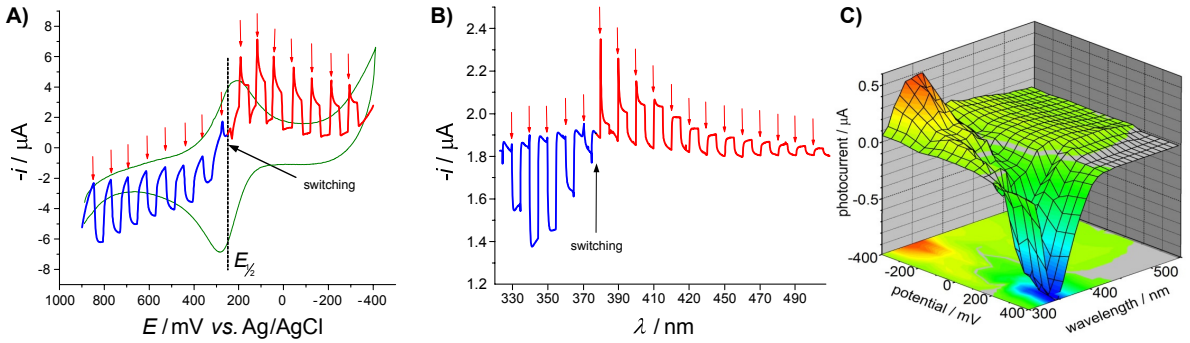

Fig. 7. Dependence of photocurrent generated at electrode covered with $[Fe(CN)_6]^{4-}$-modified TiO_2 on applied potential (a; λ = 350 nm, scan rate 10 mV s^{-1}), excitation wavelength (b; E = 200 mV vs. Ag/AgCl) and both potential and wavelength (c). Anodic photocurrents are shown in blue, cathodic – in red. For comparison the cyclic voltammogram recorded in the dark for the $[Fe(CN)_6]^{4-}$-modified TiO_2 electrode is shown (a). Arrows indicate opening of the shutter.

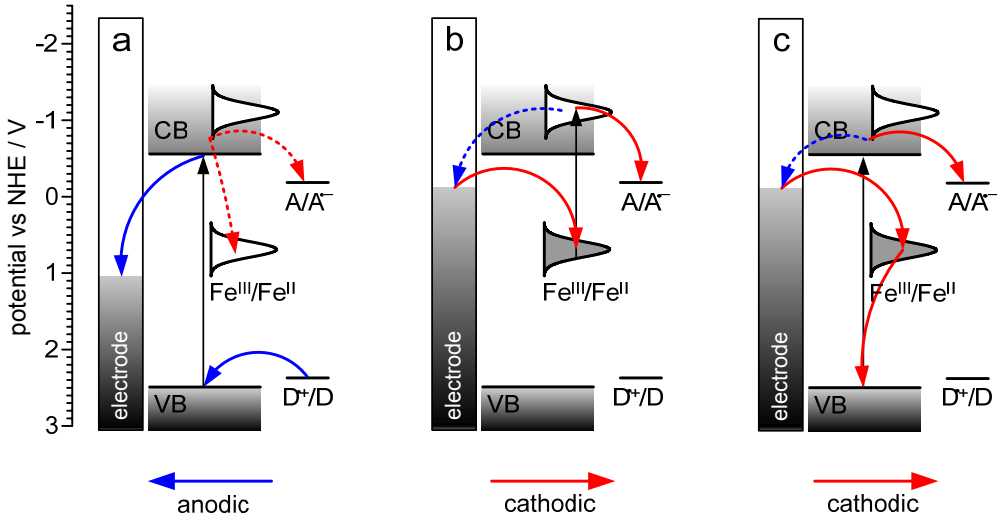

Fig. 8. The mechanism of photocurrent generation at electrodes made of TiO_2 modified with iron cyanide complexes upon UV (a, c) and visible (b) light generation. High electrode potentials (a) ensure presence of Fe^{III} surface species, while Fe^{II} prevails at low potentials (b, c).

Photocatalysis – solar to chemical energy conversion

Let us come back to the roots of photocatalysis. Its primary goal was to facilitate water splitting and enable cheap, efficient and environmental-friendly production of hydrogen. After almost five decades we know, that this challenging task is much more difficult to be brought into life than anybody could expect. Research on water splitting (Figure 9) focuses on two main redox processes: water reduction (Figure 9a) and oxidation (Figure 9b). The latter one appears particularly difficult since water oxidation to molecular oxygen is a four electron process. Catalysts facilitating it must decrease activation energy, but also work as a sink of holes available for this multielectron reaction. Combination of water reduction and oxidation at a single photocatalyst particle (Fig. 9c) still remains an unattainable challenge.

Reduction of water appears an easier task. It can be realized, for instance, at the surface of zinc sulphide (Figure 10). This material, engineered by Kisch *et al.*, offers a particularly low reduction potential of electrons excited to the conduction band. Although quantum yields of hydrogen generation are relatively high, the oxidation path of this system requires an expensive sacrificial electron donor, like e.g. 2,5-dihydrofuran, which is consumed in the process. The choice of this donor arises from a good stability of generated allyl radicals which undergo coupling or dismutation reactions. On the other hand, the overall reaction taking place in this system involves H_2 production and C-C coupling (dehydrodimer formation). Both products store chemical energy that can be released during combustion reaction. Solar energy absorbed by semiconductor particles is therefore converted into chemical energy.

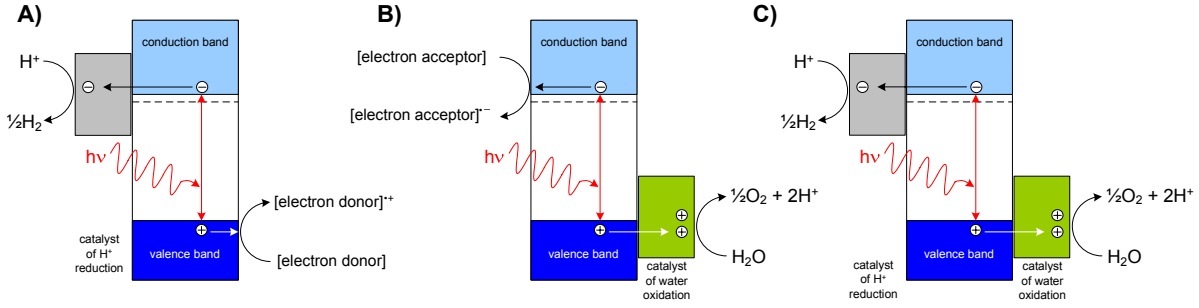

Fig. 9. Photocatalytic water reduction (a), oxidation (b) and splitting (c).

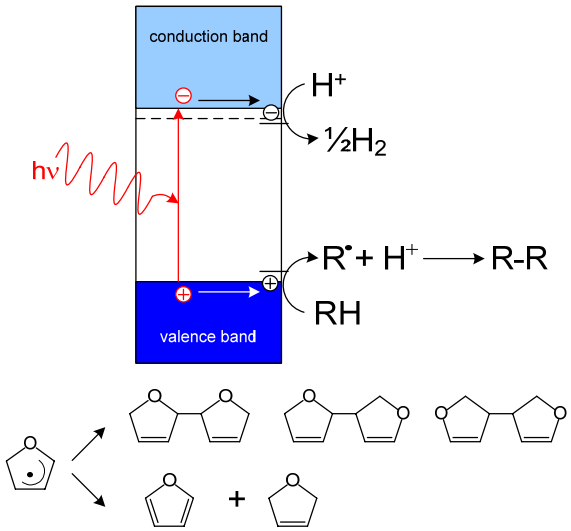

Fig. 10. Photocatalytic water reduction at ZnS in the presence of 2,5-dihydrofuran as an electron donor.

Another example of photocatalytic C-C or C-N coupling reactions is based on CdS photocatalyst (Figure 11). Redox properties of this semiconductor facilitate generation of two organic radicals, which upon coupling reaction form bigger, sometimes quite complex molecules. Although products of these reactions cannot be used as fuels, presented method offers a unique way of fine chemicals production. It is worthy to mention that both, yields and selectivity of product formation, facilitate practical application of such systems.

What will the future bring?

Presented examples of photocatalytic systems show a huge potential use of photocatalysts in solar energy utilization processes. Some of them evolved already from laboratory experiments to practical applications, however predicting future is – as usual – not easy. One has to keep in mind, that solar energy is dispersed. This implies a necessity of large areas to get sufficient number of photons required to produce considerable amounts of fuels or chemicals. Application of artificial light sources cannot solve any energy production issues, however they can be considered when production of high-value chemicals (e.g. pharmaceuticals) can be realized in photocatalytic systems. Future research will be focused on development of new photocatalysts and co-catalysts, engineered to improve quantum efficiencies of solar energy conversion and to extend response of photoactive materials to a broader range of solar spectrum. It is evident, that photocatalysis can be a bright tool to use solar energy in an elegant way.

Acknowledgements

The author would like to thank the members of Coordination and Bioinorganic Physicochemistry Group, Faculty of Chemistry, Jagiellonian University, for a fruitful common work on discussed topics and to people from Centre for Innovations, Technology Transfer and University Development (CITTRU) for an efficient collaboration on bringing ideas to life.

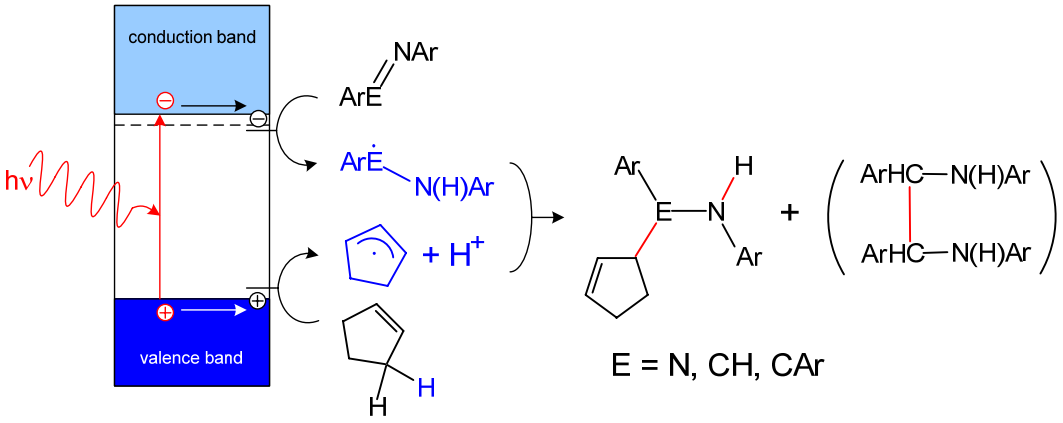

Fig. 11. Photocatalytic C-C and C-N coupling reactions performed at cadmium sulphide surface.

Selected reading

1. Stochel, G.; Brindell, M.; Macyk, W.; Stasicka, Z.; Szaciłowski, K., *Bioinorganic Photochemistry*. Wiley: Chichester, 2009.
2. Szaciłowski, K.; Macyk, W.; Drzewiecka-Matuszek, A.; Brindell, M.; Stochel, G., *Chem. Rev.* 2005, *105*, 2647-2694.
3. Linsebigler, A. L.; Lu, G.; Yates Jr., J. T., *Chem. Rev.* 1995, *95*, 735-758.
4. Kamat, P. V.; Meisel, D., *C. R. Chimie* 2003, *6*, 999-1007.
5. Hoffmann, M. R.; Martin, S. T.; Choi, W.; Bahnemann, D. W., *Chem. Rev.* 1995, *95*, 69-96.
6. Hagfeldt, A.; Grätzel, M., *Acc. Chem. Res.* 2000, *33*, 269-277.
7. Moser, J. E.; Bonnote, P.; Grätzel, M., *Coord. Chem. Rev.* 1998, *171*, 245-250.
8. Macyk, W.; Kisch, H., *Chem. Eur. J.* 2001, *7*, 1862.
9. Kisch, H.; Macyk, W., *ChemPhysChem* 2002, *3*, 399-400.
10. Macyk, W.; Burgeth, G.; Kisch, H., *Photochem. Photobiol. Sci.* 2003, *2*, 322.
11. Kisch, H.; Burgeth, G.; Macyk, W., *Adv. Inorg. Chem.* 2004, *56*, 241.
12. Macyk, W.; Szaciłowski, K.; Stochel, G.; Buchalska, M.; Kuncewicz, J.; Łabuz, P., *Coord. Chem. Rev.* 2010, *254*, 2687–2701.
13. Hebda, M.; Stochel, G.; Szaciłowski, K.; Macyk, W., *J. Phys. Chem. B* 2006, *110*, 15275-15283.
14. Macyk, W.; Stochel, G.; Szaciłowski, K., *Chem. Eur. J.* 2007, *13*, 5676-5687.
15. Szaciłowski, K.; Macyk, W.; Hebda, M.; Stochel, G., *ChemPhysChem* 2006, *7*, 2384-2391.
16. Macyk, W.; Stochel, G.; Szaciłowski, K., *Chem. Eur. J.* 2007, *13*, 5676-5687.
17. Szaciłowski, K.; Macyk, W., *Comp. Rend. Chimie* 2006, *9*, 315-324.
18. Szaciłowski, K.; Macyk, W., *Solid-State Electronics* 2006, *50*, 1649-1655.
19. Szaciłowski, K.; Macyk, W., *Chimia* 2007, *61*, 831-834.
20. Szaciłowski, K.; Macyk, W.; Stochel, G., *J. Am. Chem. Soc.* 2006, *128*, 4550-4551.
21. Hörner, G.; Johne, P.; Künneth, R.; Twardzik, G.; Kisch, H., *Chem. Eur. J.* 1999, *5*, 208-217.
22. Kisch, H.; Hopfner M., *Novel Organic Syntheses through Semiconductor Photocatalysis* in "Electron Transfer in Chemistry. Volume 4: Heterogeneous Systems, Solid State Systems, Gas Phase Systems. Section 1: Catalysis of Electron Transfer", V. Balzani (ed.), Wiley, 2001, 232-275.

Titanium dioxide for hydrogen generation in photo-electrochemical cells

M. Radecka[1], K. Zakrzewska[2]

[1]Faculty of Materials Science and Ceramics, AGH University of Science and Technology, al. Mickiewicza 30, 30-059 Cracow, Poland

[2]Faculty of Electrical Engineering, Automatics, Computer Science and Electronics, AGH University of Science and Technology, al. Mickiewicza 30, 30-059 Cracow, Poland

Hydrogen, its generation, storage, transportation and sensing have been recently recognized as the most promising scientific issues to undertake in order to work out the way to overcome the economic and ecological problems associated with the overwhelming use of fossil fuels. In order to replace traditional fuels with non-polluting, environmentally friendly energy carrier such as hydrogen, a great deal of research has to be done especially in the field of material science. Since the publication of the pioneering paper of Fujishima and Honda [1] in 1972, the photoelectrolysis of water in a photoelectrochemical cell (PEC) with titanium dioxide photoanode has been recognized as a promising method of hydrogen generation. The main factor limiting the practical application of this method is its low conversion efficiency, at this moment less than 10%.

1. Photoelectrolysis of water

As shown in Fig.1, the principle of the photoelectrochemical decomposition of water, i.e., water splitting, involves creation of an electron-hole pair upon interaction with light according to the following reaction:

$$h\nu \xrightarrow{TiO_2} e' + h^{\bullet} \quad (1)$$

A photon with an energy hv, equal or higher than the band gap energy, E_g, of a semiconductor (e.g. TiO_2) is absorbed promoting electrons e' into the conduction band (CB) and electron holes $h^{\bullet}$ into the valence band (VB).

The photoelectrochemical cell (PEC) is composed of two electrodes, immersed in an aqueous electrolyte. The photoanode is made of an n-type semiconductor exposed to light. Metallic cathode is usually based on Pt covered with a Pt-black layer.

The electric field at the electrode/electrolyte interface prevents the recombination of the photoinduced electron-holes pairs, i.e., the rate of the reaction (1) in the opposite direction is low.

Photoinduced holes participate in the anode reaction at the semiconductor/electrolyte interface:

$$2h^{\bullet} + H_2O \rightarrow \frac{1}{2}O_2 + 2H^+ \quad (2)$$

Gaseous oxygen evolves at the photoanode while hydrogen ions H^+ are transported to the cathode through the aqueous electrolyte. Electrons migrate over the external circuit to the cathode where they reduce hydrogen ions to gaseous hydrogen according to:

$$2H^+ + 2e' \rightarrow H_{2(gas)} \quad (3)$$

Photon energy necessary to split water into hydrogen and oxygen can be calculated from the overall reaction:

$$H_2O_{(liquid)} \rightarrow H_{2(gas)} + \frac{1}{2}O_{2(gas)} \quad (\Delta G^o = +237.14\ \mathrm{kJmol^{-1}}) \quad (4)$$

The change of standard free enthalpy of the reaction (4), ΔG^o, is +237.14 $kJmol^{-1}$ or 2.46 eV per H_2O molecule. As two electron-hole pairs are involved in the splitting of one water molecule, the energy required for one electron-hole pair (or one absorbed photon) is 1.23 eV. Taking into account the overvoltage losses and an excess of energy in order to drive the process at a reasonable rate, the threshold energy of photons for the photoelectrolysis increases to 1.7 – 1.9 eV [2]. Thus, in practice, the band gap energy of the semiconductor photoe-

lectrode of about 1.7 – 1.9 eV is sufficient for the process to take place and as a consequence even the narrow band gap semiconductors could be used.

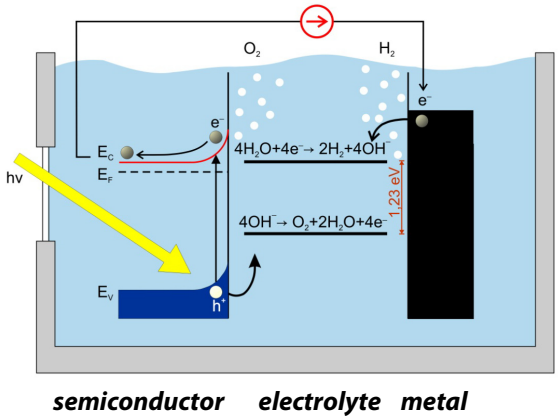

Fig. 1. Photoelectrochemical cell for water photoelectrolysis.

2. Photoanodes based on TiO_2

Fundamental requirements for an efficient photoactive semiconductor can be summarized [3,4] as follows:

a) high stability and resistivity to corrosion and photocorrosion;
b) low cost and availability;
c) conduction band CB minimum and the dopant states above H_2/H_2O level;
d) effective absorption of photons over the visible range, i.e., 1.6-2.5 eV;
e) sufficient overlap between the intragap and band states of a photocatalyst in order to provide a fast transfer of photoexcited carriers to the reactive states at the surface within their lifetime.

As opposed to III-V semiconductors, e.g., GaAs that are not irresistible to corrosion and photocorrosion, TiO_2 meets almost all conditions. Biological and chemical inertness, resistance against corrosion, non-toxicity, high photo-oxidation potential, as well as a reasonable price [3,5,6] are its important advantages. However, too wide a band gap of TiO_2 (3.0 eV for rutile and 3.2 eV for anatase) constitutes a serious obstacle on the way to reach the appropriate efficiency of the photoconversion process within the visible range of the light spectrum.

A large variety of modifications of TiO_2 have been proposed [7-44] in order to gain a better match between the absorption edge of TiO_2 with the solar spectrum while still preserving other properties important for photocatalysis. Majority of work has been directed toward metal ion doping [7-14], dye sensitization [35-37], incorporation of noble metals [30-34], formation of solid-solutions [2,4-10] and hybrid structures [40-44]. Recently, one can observe a growing interest in anion doping with nitrogen, carbon, etc. [3, 15-20], and taking advantage of co-doping of both anion and cation sublattices [45]. Some examples of these modifications of TiO_2 photoanodes are listed in Table 1.

Metal-loaded, i.e. substitutional cation doped TiO_2 has been extensively studied with a moderate success [7-14]. Both donor- and acceptor-type metals such as vanadium, molybdenum, chromium, niobium, iron, magnesium, tungsten, etc. have been reported. It has been realized [4,11,46] that the presence of metal ion dopants in the cationic sublattice of TiO_2 affects considerably the charge carrier recombination and interfacial electron-transfer rates. The reasons for this unsatisfactory behaviour of modified materials can be sought in the formation of localized states of a dopant, deep in the band gap of titanium dioxide [4,11].

First suggested by Asahi and co-workers [15], incorporation of non-metals such as carbon, nitrogen, fluorine, phosphorus or sulphur into the anionic sublattice of TiO_2 [3,15-21] offers much promise for an improvement in the photocatalytic and photoelectrochemical behaviour in comparison with unmodified TiO_2, especially over the visible range of the light spectrum [15,16].

Theoretical calculations followed by experimental results have shown that the shift in the fundamental absorption edge towards the visible range can be achieved in the case of nitrogen doped anatase polymorphic form of TiO_2 [15,47]. Asahi attributed this shift to the narrowing of the forbidden band gap due to the mixing of N 2p with O 2p orbitals in the valence band [15]. This interpretation has been contested by the group of Di Valentin [47] on the basis of spin-polarized DFT calculations that yielded the presence of localized N 2p level in the forbidden band gap of TiO_2 even at high concentration of nitrogen.

Table 1. Modifications of TiO_2 photoanode materials.

Modiffication			References
Bulk modification	Cationic site	Al^{3+}, Co^{2+}, Cr^{3+}, Fe^{3+}, Mn^{2+}, Mn^{3+}, Nd^{3+}, Ni^{2+}, Mo^{5+}, Nb^{5+}, W^{6+},	7-14
	Anionic site	N, C, S	3, 15-21
	Non-stoichiometric	TiO_{2-x}	22-24
	Solid-solutions	TiO_2-VO_2, TiO_2-SnO_2	25-29
	Nanocermet	Ag, Au, Pd, Pt, Ru	30-34
Surface modification	Organic dyes Discontinuous noble metal	cyanine, rhutenium(II) complex, rose bengal Ag, Au, Pd, Pt, Ru	31, 35-39
Hybrid-structure		TiO_2/CdSe TiO_2/CdS TiO_2/SnO_2 TiO_2/ZnO	40-44

It is believed that simultaneous occurrence of N impurities and oxygen vacancies may be responsible for a synergetic effect in the enhancement of photoactivity. According to [48,49] oxygen deficiency, through its significant influence on the N-doping configuration, affects the visible light photocatalysis.

However, the increased charge recombination and trapping, inherently related to any sort of modification of TiO_2 still remain the most important problem as far as an efficiency of the energy conversion is concerned. High expectations for improvement are due to the emerging nanotechnologies that yield functionalized nanomaterials.

Applications of nanomaterials to photocatalysis and photoelectrochemistry is based on the general belief that transport properties could be affected by the size, form and geometry of the nanostructures: nanotubes, nanorods, nanowires, nanograins, etc. Shorter distance to the surface or interface providing faster diffusion of charge carriers can reduce the charge recombination [6,50-52]. Nanosized TiO_2 particles generally demonstrate higher photocatalytic activity than those with larger particle sizes, thanks to the enhanced redox potential of photogenerated electrons and holes.

3. Concise overview of the own work

Our research on the application of TiO_2-based materials for water splitting started in 2002 with the work on TiO_2-VO_2 [26]. Since then, we have been involved in numerous investigations on: non-stoichiometric thin films and polycrystalline ceramics, anatase/rutile polymorphic forms, cation and anion doping of TiO_2, nanocermets, and solid solutions. Photocatalytic decomposition of organics has been a subject of several papers as well [29, 53,54]. Recently, we focus our attention on the nanomaterials.

Thin films were deposited by dc-pulsed magnetron and rf sputtering [20,21,23,26,29-31,53,56]. Sol-gel and co-precipitation as well as Flame Spray Synthesis were used for nanopowders and polycrystalline ceramics. The methods of analysis of the properties of the synthesized materials are given in Table 2.

In the case of powder TiO_{2-x} samples [24] we have demonstrated that slight nonstoichiometry enhances the photocurrent response in the photoelectrochemical cell for water splitting. Deviation from stoichiometry towards oxygen deficiency in TiO_{2-x} causes a decrease in the electrical resistance which is important in the case of electron-hole transport from the bulk to the surface [24,55]. Im-

provement in the photoelectrochemical behaviour has been reported by our group for FSS-made TiO_2:Cr nanopowders in [53]. Controlled preparation of nitrogen-doped nanosized TiO_2 thin films has been achieved [56]. TiO_{2-x} films with small deviation from stoichiometry are considered the most promising for substitutional N-doping. The photocurrent response of the system Ti-N-O over the full compositional range has been investigated.

Table 2. The methods of analysis of the properties of TiO_2 photoanode materials.

Property	Thin films, ceramics and nanopowders
Chemical composition and structure	RBS, NRA, XPS, GID XRD
Morphology	AFM, SEM, TEM
Optical	spectrophotometry-classical configurations and with an integrating sphere
Electrical	conductivity (four-point-probe), impedance spectroscopy
Photoelectrochemical	$I_{ph}(V)$, $I_{ph}(\lambda)$, $I_{ph}(t)$

Fig. 2 demonstrates the columnar growth of thin films and close correspondence between the images provided by AFM and SEM. In order to study the influence of nitrogen flow rate η_{N2} on the optical spectra of stoichiometric and nonstoichiometric titanium dioxide thin films the wavelength λ corresponding to the transmittance T equal to 60% has been plotted as a function of η_{N2}. The red-shift towards the visible range is more pronounced for nonstoichiometric TiO_{2-x}:N than for stoichiometric TiO_2:N thin films. It has been shown that doping with nitrogen improves the photoelectrochemical properties over the visible range of the light spectrum in the case of nonstoichiometric samples.

The most fundamental problem of charge recombination, detrimental to the PEC device performance requires the basic studies of the nature of the recombination centres that can be addressed by the application of more advanced techniques available at synchrotron facilities. Such studies are now in progress.

Moreover, the use of thin films of ZnO and ZnO/TiO_2 for photoanodes is underway. ZnO thin films grown with a preferred crystallographic orientation to the substrate have shown a considerable photocurrent over the UV range.

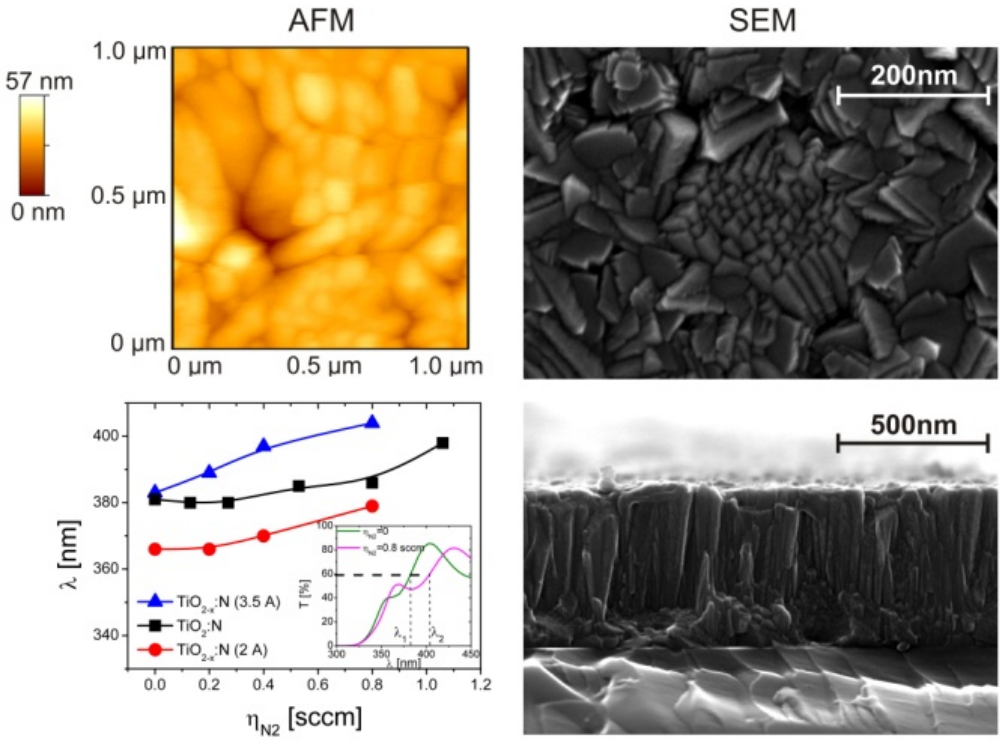

Fig. 2. AFM, SEM images of the columnar growth in nonstoichiometric TiO_{2-x} thin films and influence of nitrogen flow rate η_{N2} on the optical spectra of stoichiometric and nonstoichiometric titanium dioxide thin films; T – optical transmittance; λ – wavelength corresponding to T=60%.

Acknowledgement

The authors acknowledge financial support from the European Institute of Innovation and Technology, under a KIC Inno Energy, NewMat project.

References

1. A. Fujishima, K.Honda, *Nature,* 238 (1972) 37
2. J.A. Turner, *Science,* 285 (1999) 687
3. A.V. Emeline, V. N. Kuznetsov, V.K. Rybchuk, N. Serpone, *Int. J. Photoenergy*, (2008) doi: 10.1155/2008/258394
4. M. Radecka, M. Rekas, A. Trenczek-Zajac, K. Zakrzewska, *J. Power Sources,* 181 (2008) 46
5. A.Mills, S. Le Hunte, *J. Photochem. Photobiol., A,* 108 (1997) 1
6. M. Grätzel, *Nature*, 414 (2001) 338
7. H.P. Maruska, A.K. Ghosh, *Solar Energy Materials*, 1 (1979) 237
8. G. Campet, J.Verniolle, J-P. Doumerc, J. Claverie, *Mat. Res. Bull*., 15 (1980) 1135
9. L.Kavan, M.Grätzel, *Electrochim. Acta*, 40 (1995) 643
10. K.T. Ranjit, B. Viswnathan, J. *Photochem. Photobiol. A: Chemistry*, 107 (1997) 215
11. K.Wilke, H.D. Breuer, *J. Photochem. Photobiol. A: Chemistry*, 121 (1999) 49
12. M. Radecka, K. Zakrzewska, M. Wierzbicka, A. Gorzkowska, S. Komornicki, *Solid State Ionics*, 157 (2003) 379
13. M.Radecka, P.Sobas, A.Trenczek and M.Rekas, *Polish J.Chem*., 78 (2004) 1925
14. A.Trenczek-Zając, M.Radecka, M.Rękas, *Physica. B, Condensed Matter*, 399 (2007) 55
15. R. Asahi T. Morikawa, T. Ohwaki, K. Aoki and Y. Taga, *Science,* 293 (2001) 269
16. H. Irie, Y. Watanabe and K. Hashimoto, J. Phys. Chem. B, 107 (2003) 5483
17. X. Chen and S. Mao, *Chem. Rev*., 107 (2007) 2891
18. T. Ohno, T. Mitsui, M. Matsumura, *Chem.Lett*., 32 (2003) 364
19. H. Wang, J.P. Lewis, *J.Phys.: Condens. Matter*, 18 (2006) 421
20. M. Radecka, E. Pamula, A. Trenczek-Zajac, K. Zakrzewska, A. Brudnik, E. Kusior, N.-T. H. Kim-Ngan, A. G. Balogh, *Solid State Ionics*, 192 (2011) 693
21. A. Trenczek-Zajac, M. Radecka, K. Zakrzewska, A. Brudnik, E. Kusior, S. Bourgeois, M.C. Marco de Lucas and L. Imhoff, *J. Power Sources,* 194 (2009) 93
22. J.F. Houlihan, D.B. Armitage, T. Hoovler, D. Bonaquist, D.P. Madacsi and L.N. Mulay, *Mat.Res.Bull*., 13 (1978) 1205
23. A. Brudnik, A. Gorzkowska-Sobas, E. Pamula, M. Radecka, K. Zakrzewska: *J. Power Sources*, 173 (2007) 774
24. M.Radecka, A.Trenczek-Zajac, K.Zakrzewska and M.Rekas, *J. Power Sources*, 173 (2007) 816
25. G. Zhao, H. Kozuka, H. Lin, T.Yoko, *Thin Solid Films,* 339 (1999) 123
26. A. Gorzkowska, M. Radecka, *Molecular Physics Reports,* 35 (2002) 126
27. M. Avudaithai, T.R.N. Kutty, *Mat.Res.Bull*., 24 (1989) 1163
28. M. Radecka, P. Pasierb, K. Zakrzewska, M. Rekas, *Solid State Ionics*, 119 (1999) 43
29. K.Zakrzewska, M.Radecka, *Thin Solid Films,* 515 (2007) 8332
30. K.Zakrzewska, M.Radecka, A.Kruk and W.Osuch, *Solid State Ionics*, 157 (2003) 349
31. A.Gorzkowska-Sobaś, E.Kusior, M.Radecka, K.Zakrzewska, *Surface Science*, 600 (2006) 3964
32. Y-K. Choi, S-S. Seo, K-H. Chjo, Q-W. Choi, S.M.Park, *J.Electrochem.Soc*., 139 (1992) 1803
33. G. Zhao, H. Kozuka, T. Yoko, *Thin Solid Films,* 277 (1996) 147
34. Y. Matsumoto, T. Shimizu, E.Sato, *Electrochemica Acta,* 27 **(**1982) 419
35. A.K. Ghosh, H.P.Maruska, *J.Electrochem.Soc*., 124 (1977) 1516
36. M. Gómez, J. Rodríguez, S.-E. Lindquist, C.G. Granqvist, *Thin Solid Films,* 342 (1999) 148
37. M.K. Nazeeruddin, A. Kay, I. Rodicio, R. Humphry-Baker, E. Müller, P. Liska, N. Vlachopoulos, M. Grätzel, *J.Am.Chem.Soc*., 115 (1993) 6382
38. N. Chandrasekharan, P.V.Kamat, J.Hu, *J. Phys. Chem., B,* 104 (2000) 11103
39. A.Sclafani, J-M.Herrmann, *J.Photochem. Photobiol .A:Chemistry*, 113 (1998) 118
40. Di. Liu, P.V. Kamat, *J.Phys. Chem*., 97 (1993) 10769
41. R. Vogel, K. Pohl, H.Weller, *Chem.Phys. Letters,* 174 (1990) 241
42. P.V. Kamat, M. Flumiani, A. Dawson, *Colloids & Surfaces A-Physicochemical & Eng.Aspects,* 202 (2002) 269
43. S. Rühle, M. Shalom, A. Zaban, *Chem.Phys.Chem,* 11 (2010) 2290

44. X.Gan, X. Li, X. Gao, F. Zhuge, W.Yu, *Thin Solid Films*, 518 (2010) 4809
45. M.E. Kurtoglu, T. Longenbach, K.Sohlberg, Y. Gogotsi, *J. Phys. Chem. C*, 115 (2011) 17392
46. U. Diebold, *Surf. Sci. Rep*., 48 (2003) 53
47. C. Di Valentin, E. Finazzi, G. Pacchioni, A. Selloni, S. Livraghi, M.C. Paganini and E. Giamello, *Chem. Phys*., 339 (2007) 44
48. S.-H. Lee, E. Yamasue, K.N. Ishihara and H. Okumura, *Appl. Catal. B-Environ,* 93 (2010) 217
49. M. Batzill, E.H. Morales and U. Diebold, *Phys. Rev. Lett*., 96 (2006) 026103
50. P.V. Kamat and D. Meisel, *C. R. Chimie,* 6 (2003) 999
51. G. Li and K.A. Gray, *Chem. Phys*., 339 (2007) 173
52. Z. Zhang, C.-C. Wang, R. Zakaria and J.Y. Ying, *J. Phys. Chem*. B, 102 (1998) 10871
53. M. Radecka, M. Rekas, E. Kusior, K. Zakrzewska, A. Heel, K.A. Michalow and T. Graule, J. *Nanosci. Nanotechnol*., 10 (2010) 1032
54. M.Radecka, B.Lyson, M.Lubecka, A.Czapla, K.Zakrzewska, *Acta Physica Polonica A*, 117 (2010) 415
55. S.N. Subbarao, Y.H.Yun, R.Kershaw, K. Dwinghta and A.Wold, *Inorg. Chem*., 18 (1979) 488
56. A. Trenczek-Zajac, M. Radecka, E. Pamula, K. Zakrzewska, A. Brudnik, E. Kusior, K. Kowalski, A. Reszka, *J. Nanosci. Nanotechnol*. 2011 (in print)

Functional Materials Letters
Vol. 4, No. 2 (2011) 107–112

Material problems and prospects of Li-ion batteries for vehicles applications

Janina Molenda
Faculty of Energy and Fuels, AGH University of Science and Technology,
al. Mickiewicza 30, 30-059 Kraków, Poland

The paper reviews material issues of development of Li-ion batteries for vehicles application. The most important of them is safety, which is related to application of nonflammable electrolyte with large electrochemical window and possibility of forming protective SEI (solid/electrolyte interface) to prevent plating of lithium on carbon anode during fast charge of the batteries. The amount of electrical energy, which a battery is able to deliver, depend on the electromotive power of the cell as well as on its capacity – both these factors are related to the chemistry of electrode materials. Nanotechnology applied to electrode materials may be a breakthrough for Li-batteries performance due to extreme reactivity of nanoparticles in relation to lithium. The electrode-electrolyte interface phenomena are decisive for a cell lifetime. Review of physicochemical properties of intercalated transition metal compounds with layered, spinel or olivine-type structure is provided in order to correlate their microscopic electronic properties, i.e. the nature of electronic states, with the efficiency of lithium intercalation process, which is controlled by the chemical diffusion coefficient of lithium. Data concerning cell voltage and character of discharge curves for various materials are correlated with the nature of chemical bonding and electronic structure. Proposed electronic model of the intercalation process allow for prediction and design of operational properties of intercalated electrode materials. Proposed method of measuring the $Li_xM_aX_b$ potential on the basis of the measurement of the electromotive force of the $Li/Li^+/Li_xM_aX_b$ electrochemical cell is a powerful tool of solid state physics allowing for direct observation of the Fermi level changes in such systems as a function of lithium content.

Keywords: Li-ion batteries; Electric vehicles; Cathode materials; Intercalation.

1. Introduction

The market of reversible electrochemical cells (rechargeable batteries) is flourishing at present due to a huge interest of car manufacturers in using them in electrically driven (Battery electric vehicles BEVs) and hybrid cars. Popular Ni-Cd and NiMH batteries have already reached their technological limits. Li-ion battery technology seems, however, to have a bright future ahead, given the recent remarkable development in the field. It has already dominated portable electronics market and it is now fighting to access electric drive vehicles market. The required capacity of a Li-ion battery for vehicle applications is much bigger than for portable electronics – 20-100 kWh. The security of usage of that kind of batteries is an important issue. The bigger the capacity, the more energy is accumulated – therefore, more strict security measures must apply. This raises numerous challenges to develop new material technologies – cell components with a better chemical and thermal stability, as well as to solve problems such as heat dissipation dependent on the cell housing system. The lack of experimental data on real lifetimes of Li-ion batteries in changeable climatic conditions – from +40°C to -40°C (the required lifetime of batteries is ten years for vehicles and 1-4 years for laptops) constitutes also a big problem. Furthermore, high capacity Li-ion batteries may play an important role in managing renewable energy. The fact that the output power of renewable energy sources such as solar cells or wind power plants depends on meteorological conditions causes problems when it comes to connecting them directly to an electricity distribution system. Unstable supply causes electric current frequency to fluctuate and decreases the power quality. If the power generated from renewable sources were stored in high capacity Li-ion batteries, it could be then transferred to the electricity distribution system with stable operating parameters.

High capacity Li-ion batteries are packs comprising a series chain of cells. In the present paper however, we will only examine active materials in a single Li-ion cell, that is to say – electrode materials and electrolyte. In particular, methods of enhancing their operational parameters, including increased stability will be scrutinized.

2. Fundamentals of Li-ion batteries

Li-ion batteries use the capability of transition metals compounds M_aX_b (M = transition metal; X = O, S) with layered or tunnel structure to reversibly insert lithium (one or more mol Li per mol M_aX_b) at room temperature without significant changes in their crystallographic structure.[1-3] In this process, the basic elements of the structure do not undergo any changes, except for minor reversible variations of lattice parameters. Stability of structure during the whole process is due to strong ionic and covalent bonds between M and X atoms. The intercalation of lithium (which is always a combined ionic-electronic transport process, involving insertion of Li^+ ions and an equivalent number of electrons) to transition metal compounds M_aX_b can be put down as follows:

$$xLi^+ + xe^- + M_aX_b = Li_xM_aX_b. \qquad (1)$$

This reaction makes use of deep d-type energy levels in transition metal compounds, with the energy of several eV/atom, which can accumulate the energy of several kWh/kg; thus enabling construction of a power supply with significant volumetric and gravimetric energy density.

Fig. 1a shows adjustment of electronic structures of electrode materials and an electrolyte in a perfectly reversible Li-ion cell with conducting electrodes, which guarantees thermodynamic stability of the cell. Energy gap (electrochemical window) of an electrolyte, E_g, should be wider than 4 eV. The electrochemical potential of electrons (Fermi level, E_F) of both electrode materials should be situated within the electrochemical window of the electrolyte. At the same time, Fermi level of the anode material should be situated below the bottom of the electrolyte conduction band (below LUMO – Lowest Unoccupied Molecular Orbital – level). This prevents transfer of electrons from the anode material to the electrolyte (electrolyte will not undergo reduction and anode material will not undergo oxidation). As for Fermi level of the cathode material, it should be situated above the top of the electrolyte valence band (HOMO – Highest Occupied Molecular Orbital – level) in order to prevent electron transfer from the electrolyte to the cathode material (electrolyte will not undergo oxidation, cathode material will not undergo reduction). In reality, the desired adjustment of cell components (electrode materials and electrolyte) from the point of view of their electronic structures is not achieved (Fig. 1a). For any element anodes (Li, Si, carbon) Fermi level is situated above the electrolyte LUMO level, practically for all known non-aqueous electrolytes.[4] The use of such anode is possible owing to the formation of a passive SEI (Solid Electrolyte Interface) layer which is a result of reaction between the electrolyte and anode material. The layer prevents further anode–electrolyte reaction and capacity loss. Good properties of SEI layer in the case of Li anode are obtained when the electrolyte is based on ethylene carbonate (EC).[5] The SEI layer lets only the lithium ions pass and protects the electrolyte from reduction. However, the SEI layer itself is very fragile and easy to destroy. Upon charging of a cell with metallic lithium, the SEI layer is destroyed and lithium ions moving towards the anode undergo reduction to metallic lithium in the electrolyte (without the SEI layer, electrons can easily be transferred from anode material to the electrolyte). This results in the formation of lithium dendrites which short-circuit the cell.

This mechanism caused that $Li/Li^+/Li_xTiS_2$ cell technologies were withdrawn from the market in the 70'ties of the XX-th century. In 1991, a new generation of lithium batteries, *i.e.* Li-ion batteries, was commercialized by Sony Corp. The metallic lithium anode was replaced with graphite, which has the ability to reversibly intercalate lithium and has a reasonably low potential versus lithium. Similarly as in lithium, the electrochemical potential of electrons (E_F) in graphite is also above the LUMO level of the electrolyte (Fig. 1b) and proper functioning of the cell is dependent on the formation of the SEI layer. It has been proven[5] that adding VC to the electrolyte (EC, DEC, DMC) helps to reconstruct the destroyed SEI layer upon cell charging. Nevertheless, the rate of lithium ions transfer through the SEI layer towards the anode and the rate of SEI layer reconstruction (healing) still limit the charging rate of the carbon anode and consequently that of the

Li-ion batteries. Graphite is still thought to be the best anode material. Its layered structure with three strong covalent bonds with sp^2 hybridization on a graphite plane and the half-filled p_z orbital perpendicular to the graphite plane which interacts with lithium 2s orbital, effectively limit graphite swelling upon lithium intercalation but also limit the overall quantity of inserted lithium (maximum of 1 lithium atom per 6 carbon atoms). Still, its capacity (approx. 380 mAh/g) is by far bigger than the capacity of the best cathode materials. Silicon has a significantly higher capacity for lithium intercalation, but its increase in volume during the process reaches 300% which effectively destroys the SEI layer. Furthermore, the reaction between the electrolyte and silicon proceeds continuously, which eliminates this material from practical use.

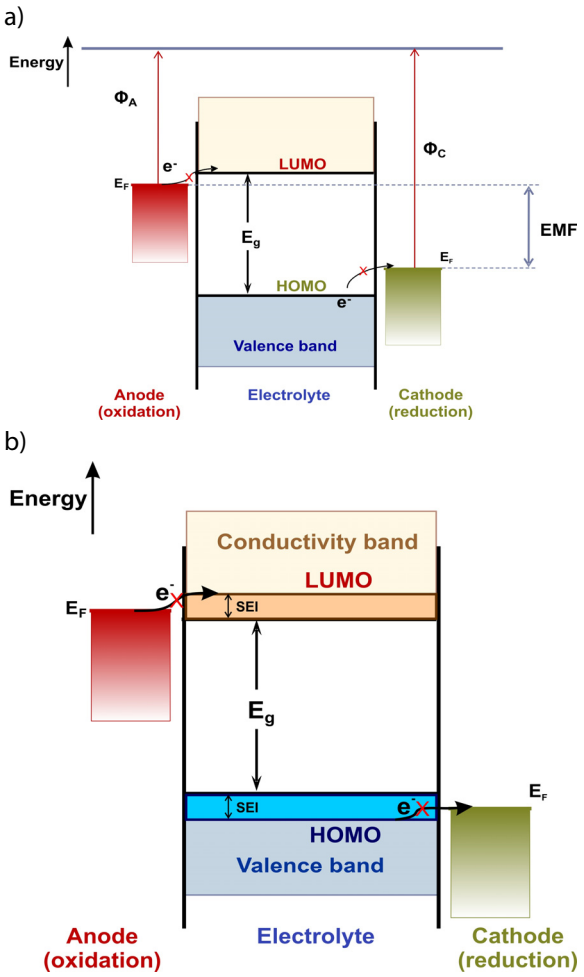

Fig. 1. Electronic structures of electrode materials and an electrolyte in (a) a perfectly reversible Li-ion cell and (b) cell with passive layers at electrode-electrolyte interfaces. W_A and W_C denote work function of cathode and anode materials respectively.

A similar situation leading to the formation of a passive SEI layer can be observed at the cathode material/ electrolyte interface (Fig. 1b). The SEI layer constitutes an energy barrier for electron transfer from the electrolyte to the cathode material and prevents further electrolyte – cathode material reactions. The formation of SEI has also some negative effects: it limits the electric contact between active particles of the cathode material and the current collector when the electrolyte penetrates along the cathode material grain boundaries. This effect can be significantly diminished by covering the active particles of cathode material with carbon or nanoscale amorphous oxides (such as Al_2O_3, ZnO, Bi_2O_3, MgO) and other,[6,7] which gives rise to discontinuities in the SEI layer (carbon or other foreign particles will not form the SEI because they have much lower potential versus HOMO of the electrolyte). The discontinuities in the SEI layer provide spots for charge transfer to and from the cathode material during the cell charging and discharging.

3. parameters of Li-ion batteries

Li-ion batteries $Li_xC_6/Li^+/Li_{1-x}M_aX_b$ principle parameter, *i.e.* energy density – per unit mass or volume, dependent on the cell electromotive force and its capacity, is defined by electronic and crystallographic structure of both electrode materials in relation to lithium intercalation reaction
on anode:

$$C_6 + xLi^+ + xe^- \leftrightarrow Li_xC_6. \qquad (2)$$

and on cathode:

$$Li_1M_aX_b \leftrightarrow Li_{1-x}M_aX_b + xLi^+ + xe^-. \qquad (3)$$

Current density of the cell depends on ionic-electronic transport properties in both electrode materials (ambipolar diffusion). Consequently, the cell voltage, capacity, energy density and current density are defined by properties of the cathode and anode materials. The number of charge and discharge cycles and cell lifetime are significantly conditioned by processes taking place on electrode material/electrolyte interfaces. Cell safety depends on thermal and chemical stabilities of electrode materials and electrolyte. It has been shown,[8] that graphite anode does not limit Li-ion batteries oper-

ational parameters such as current density or voltage. Therefore, better performance of the Li-ion batteries can be achieved by development of better cathode materials.

4. Electronic aspect of Li-ion batteries

Author's long-term research into numerous Li_x-M_aX_b systems, such as: Li_xTiS_2,[9] Li_xVO_2,[10] Li_xCoO_2,[11] Li_xNbSe_2,[12] $LiNiO_2$,[13] Li_xWO_3,[14] Li_xWSe_2,[15] $Li_xYBa_2Cu_3O_7$,[16] $Li_xBi_2Sr_2CaCu_2O_8$,[17] $Li_xMn_2O_4$,[18,19] Li_xFePO_4,[20] Li–graphite,[8] has shown that electronic structure of an intercalated material plays an important role in the intercalation process. Electrons introduced to the cathode material during the electrochemical intercalation (together with the equivalent number of lithium ions) occupy the available electronic levels and raise Fermi level according to the state-density function. Variations of the electromotive force of $Li/Li^+/Li_xM_aX_b$ cell (Fig. 1a), for which the anode potential is constant (constant Li^+ ion concentration in the electrolyte), corresponds to the variations of electrochemical potential of electrons (Fermi level) in the cathode material. This is because the changes in lithium ions chemical potential in the intercalated structure are small, *i.e.* of the order of k_BT (k_BT at room temperature equals ~0.025 eV).[19] The changes in electrons electrochemical potential may be equal to the bandwidth, *i.e.* 1 eV or more. This approach to the description of the intercalation process makes it possible to predict and design the cathode material operational properties on the basis of its electronic properties. High monotonous density of states at Fermi level of the cathode material and delocalized states lead to a weak (favorable for the envisaged application) dependence of the cathode potential on composition (x_{Li}), wide range of lithium non-stoichiometry (high cell capacity) and to high current density as a result of fast cathode material relaxation (Fig. 2a).

A discontinuous state-density function N(ε) and the related occurrence of localized electronic states near Fermi level constitute a kinetic barrier for lithium intercalation (lithium ions and electrons ambipolar diffusion), which effectively lowers current density and does not permit to use full capacity of the cathode material (Fig. 2b). The nature of electronic states near Fermi level of the cathode material is thus crucial for the effectiveness of the intercalation process because charge transfer is performed at Fermi level.

Operational parameters of Li-ion batteries which are based on the energy of *d*-electrons of transition metal, are by their very nature limited. A pristine cathode material, which on one hand would have high energy density (high potential versus lithium and high capacity), and on the other hand high current density, is impossible to develop. This negative correlation is illustrated in the electronic diagram (energy vs. density of states) of commercial cathode materials with indicated Fermi level versus lithium and resulting electromotive force of the cell (Fig. 3).

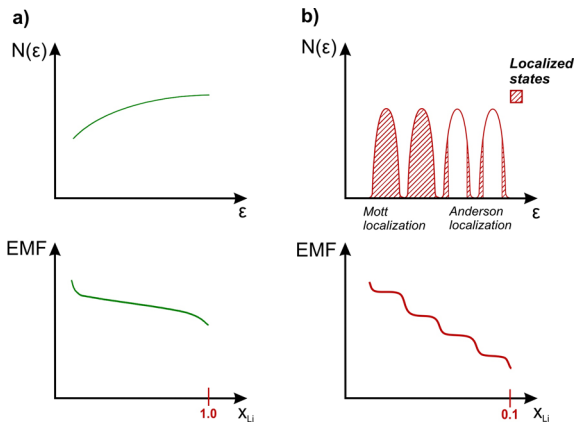

Fig. 2. Relationship between density of states of the cathode material (N(ε)) and dependence of electromotive force (EMF) of $Li/Li^+/LiM_aX_b$ cell on composition of the cathode material (x_{Li}).

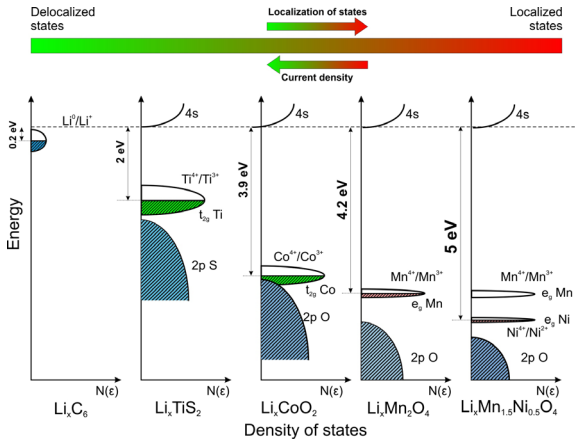

Fig. 3. Electronic diagram (energy vs. density of states) of commercial cathode materials with indicated Fermi level versus lithium and resulting electromotive force of the cell.

The best electron transport properties appear for layered TiS_2 due to the wide d (t_{2g}Ti) band and delocalized electronic states near Fermi level. Good ionic and electronic transport properties lead to high current densities, however, the $Li/Li^+/Li_xTiS_2$ cell voltage reaches only 2 V. $LiCoO_2$ shows worse electronic transport properties. The t_{2g}Co band is significantly narrower, electronic states are localized and in order to obtain the required current densities, the macroscopic conductivity of the $LiCoO_2$-based cathode material needs to be improved by addition of conductive carbons. The $LiCoO_2$ cathode cell voltage is high, reaching 3.9 V. As for the manganese spinel $LiMn_2O_4$ and $LiMn_{1.5}Ni_{0.5}O_4$, during lithium intercalation/deintercalation processes the energy is obtained from even deeper electronic levels (e_gMn, e_gNi) that have a higher localization degree (polaron states), which results, on one hand, in a high cell voltage, of 4.2 and 5 V respectively, and on the other hand, in a much lower current densities. Fig. 4 shows the cell voltage and electrical conductivity of the cathode material at cell operating temperature (300K). The higher the cell voltage, the lower the electrical conductivity of the cathode material (lower current densities). Modification of the cathode material chemical composition can increase the cell voltage whereas grain refinement to nanometric-size significantly improves current density, which is due to shortening of the effective diffusion path for lithium.

5. Commercial cathodes

Investigations on cathode materials for Li-ion batteries conducted by Molenda[21-24] show that electrochemical properties of cathode materials based on $Li(Co,Ni,Mn)O_2$ layered oxides, their chemical stability and reversible capacity can still be significantly improved. $LiCoO_2$ uses only half of its theoretical capacity.

This is due to the fact that lithium electrochemical intercalation/ deintercalation is reversible only in the compositional range $LiCoO_2$ – $Li_{0.5}CoO_2$, which results in low capacity of 130 mAh/g. Upon electrochemical deintercalation of lithium in the range Li_1CoO_2 – $Li_{0.5}CoO_2$, electrons are extracted from the t_{2g}Co band (together with the equivalent number of Li^+ ions) (Fig. 3). Electron holes are formed in the t_{2g}Co band and the Fermi level is located within this band.[21] Further lithium deintercalation implies lowering of the Fermi level within the t_{2g}Co band. When the Fermi level reaches the top of oxygen 2p band (Fig. 3), electrons are extracted from this band, oxygen is oxidized (O^{2-} ions) and leaves the Li_xCoO_2 structure. Oxygen reacts with the organic electrolyte (exothermic reaction) and causes a danger of battery explosion. The examination of lattice parameters, oxygen content and the average cobalt valency in samples at high degree lithium deintercalation confirms this model.[21] Author's extensive research[21-24] on optimization of cathode materials on the basis of layered transition metal oxides aims at improving their chemical stability through introduction of manganese ($LiNi_{1-y-z}Co_yMn_zO_2$). It is deemed possible because of the electron configuration of $Mn^{3+/4+}$ ions (t_{2g}^3 $e_g^{1/0}$) and shift of the oxygen 2p band beyond the range of Fermi level variations ($Co^{3+/4+}$, $Ni^{2+/4+}$) in the intercalation/deintercalation process. Furthermore, the studies underway aim at establishing optimal ionic and electronic transport properties, which are indispensable for the intercalation reaction to be highly effective.

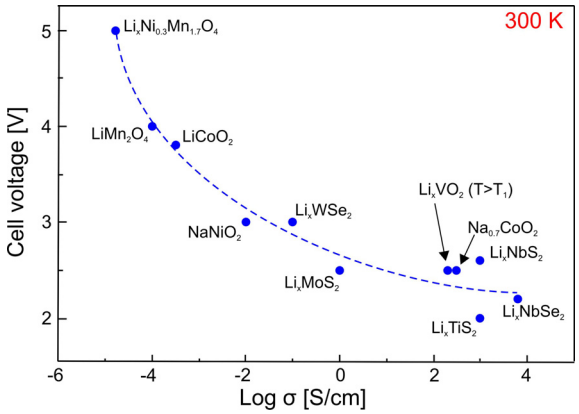

Fig. 4. Correlation between cell voltage and electrical conductivity of the cathode material at cell operating temperature (300K).

The manganese spinel $LiMn_2O_4$ – a cathode material considered very promising – undergoes phase transformation[2,18,19,25] near the cell working temperature (290 K) and it progressively looses capacity with increasing number of charge / discharge cycles. This is due to its limited chemical stability versus the liquid electrolyte, which causes its partial dissolution and decomposition related to the disproportionation reaction:

$$2Mn^{3+}(s) \rightarrow Mn^{4+}(s) + Mn^{2+}(l). \quad (4)$$

An increase in chemical stability of the manganese spinel versus the electrolyte may be attained by surface modification with a carbon (or $LiCoO_2$) coating or by modification of its chemical composition, *e.g.* substitution of oxygen by fluorine or sulfur.[26,27] It has been shown[19] that substitution of manganese by transition metal ions (Cr^{3+}, Fe^{3+}, Co^{3+}, Ni^{2+}, Cu^{2+}) eliminates the undesirable phase transformation, and that in the case of substitution by copper, the electrical conductivity increases by two orders of magnitude.

$LiFePO_4$ with the olivine structure (commonly known as phospho-olivine)[28,29] is also seen as very promising because of several important advantages: high theoretical capacity (170 mAh/g), the highest of all known cathode materials chemical stability, which guarantees cell security, and stable capacity which does not decrease with the increasing number of work cycles. Its hexagonal close-packed oxygen sublattice has one-dimensional channels, which constitute potential fast diffusion paths for lithium ions. However, due to the specific crystal structure (FeO_6 octahedra linked via corners lead to a significant, 3.8 Å, Fe-Fe distance, while the M-M distance for conductive oxides is below 3 Å) phospho-olivine is practically an electronic insulator. Its electrical conductivity at room temperature (*i.e.* at the cell working temperature) is very small as for a cathode material, and equals 10^{-9} S/cm (several orders of magnitude smaller than that of $LiCoO_2$). The conditions set forth above explain why the observed mechanism of $LiFePO_4$ delithiation is not, unfortunately, a diffusional mechanism, which would be described by the following reaction:

$$LiFePO_4 - xLi^+ - xe^- \leftrightarrow Li_{1-x}FePO_4. \quad (5)$$

and which would lead to a homogenous material with a variable lithium content. Lithium extraction/insertion into $LiFePO_4$ during the charge/discharge process is based on the coexistence of two phases – one which contains lithium and the other - completely lithium-free:

$$LiFePO_4 - xLi^+ - xe^- \rightarrow xFePO_4 + (1-x)LiFePO_4. \quad (6)$$

Reversibility of charging and discharging processes is due to high similarity of $LiFePO_4$ and $FePO_4$ structures (the same space group) and a minor difference in volume – 6.81%. This behavior of the cathode material is highly disadvantageous, since only the surface of grains works effectively, *i.e.* current density of the cell is low. The low ionic-and-electronic conductivity is the principal reason of the two-phase delithiation mechanism.

Much hope for commercial Li-ion batteries is associated with Chiang's revolutionary report on phospho-olivine doping,[30] indicating a possibility of electrical conductivity increase by a factor of 10^7. According to some theoretical studies, it is possible to obtain metallic conductivity of phospho-olivine. However, examination of doped phospho-olivine surfaces by Molenda *et al.*[31,32] and the results published by Nazar[33] have proved that the high values of conductivity of doped phospho-olivine are not due to bulk metallic properties but due to the formation of metallic iron phosphides on the surface of phospho-olivine grains, which are the effect of partial reduction of $LiFePO_4$ to Fe_2P during the synthesis. Current efficiency of the cell is not improved significantly because the bulk ionic-electronic transport has not been activated.

The most challenging issue in the search for cathode materials based on phospho-olivine is to develop phospho-olivine with mixed ionic-electronic conduction. This should activate the diffusional mechanism of the intercalation/deintercalation process and improve current efficiency, being at present the only drawback of lithium cells based on phospho-olivine. Enhancement of the $LiFePO_4$ electrical conductivity is therefore crucial for the technological development of cathode materials based on phospho-olivine.

Intensive studies on the improvement of transport properties of phospho-olivine, *i.e.* on the development of phospho-olivine with mixed ionic-electronic conduction,[32,34] conducted by Molenda *et al.* indicate that the goal can be achieved through iron substitution by a transition metal with relevant electronic configuration versus iron, so that the electron transfer from ion to ion could be generated. It seems, that still other possibilities are available to increase the ionic-electronic transport, *e.g.* through substitutions in iron sublattice or in the polyanion $(PO_4)^{3-}$. Probably the best solution to improve electrochemical effectiveness of the cathode based on phospho-olivine would be through the synthesis of nanostructured material as it might lead to shortening of the effective diffusion path for lithium and to better current efficiency. Finally, it is

worth-while to note that materials engineering methods allow obtaining electrochemically very active nanograins with "open" fast diffusion paths for lithium.[35]

6. Acknowledgement

This work was financially supported by EU under the grant No. UDA-POIG 01.01.02-00-108/09-01.

The author acknowledge a financial support from the European Institute of Innovation and Technology, under the KIC InnoEnergy NewMat project.

7. References

1. M. S. Whittingham, *Prog. Solid State Chem.* 12, 41 (1978).
2. J.-M. Tarascon, M. Armand, *Nature* 414, 359 (2001).
3. *Lithium Batteries, New Materials, Development and Perspectives*, ed. G. Pistoia (Elsevier, 1994).
4. J. B. Goodenough, Y. Kim, *Chem. Mater.* 22, 587 (2010).
5. R. Fong, U. van Sacken, J. R. Dahn, *J. Electrochem. Soc.* 137, 2009 (1990).
6. J. Liu, A. Manthiram, *J. Electrochem. Soc.* 156, A833 (2009).
7. Y. Wu, A. Manthiram, *Solid State Ionics* 180, 50 (2009).
8. J. Molenda, *Bull. Pol. Acad. Sci. Chem.* 45, 449 (1997).
9. D. Than, J. Molenda and A. Stokłosa, *Electrochim. Acta* 36, 1555 (1991).
10. Molenda and T. Bąk, *Phys. Stat. Sol. (a)* 135, 263 (1993).
11. Molenda and A. Stokłosa, *Solid State Ionics* 36, 43 (1989).
12. J. Molenda, T. Bąk and J. Marzec, *Phys. Stat. Sol.(a)* 156, 159 (1996).
13. J. Molenda, P. Wilk and J. Marzec, *Solid State Ionics* 146, 73 (2002).
14. J. Molenda and A. Kubik, *Solid State Ionics* 117, 57 (1999).
15. J. Molenda and T. Bąk, *Phys. Stat. Sol. (b)* 178, 205 (1993).
16. J. Molenda, T. Bąk and A. Stokłosa, *Physica C* 207, 147 (1993).
17. J. Molenda *et al.*, *Solid State Ionics* 119, 61 (1999).
18. J. Molenda *et al.*, *Solid State Ionics* 135, 53 (2000).
19. J. Molenda *et al.*, *Solid State Ionics* 171, 215 (2004).
20. J. Molenda *et al.*, Solid State Ionics 177, 2617 (2006).
21. J. Molenda, J. Marzec, Funct. Mater. Lett. 2, 1 (2009).
22. J. Molenda, A. Milewska, *J. Power Sources* 194, 88 (2009).
23. M. Gozu, K. Świerczek, J. Molenda, *J. Power Sources* 194, 38 (2009).
24. Milewska, M. Molenda, J. Molenda, *Solid State Ionics* (2010), doi: 10.1016/j.ssi.2010.11.026.
25. J.-M. Tarascon and D. Guyomard, *Electrochim. Acta* 38, 1221 (1993).
26. G. G. Amatucci, N. Pereira, T. Zheng, J.-M. Tarascon, *J. Electrochem. Soc.* 148, A171 (2001).
27. Y.-K. Sun, *Electrochem. Comm.* 2, 6 (2000).
28. K. Padhi *et al.*, *J. Electrochem. Soc.* 144, 1609 (1997).
29. J. B. Goodenough, in Lithium Ion Batteries, eds. M. Wakihara and O. Yamamoto (Kodansha 1998).
30. S. Y. Chung, J. T. Bloking and Y. M. Chiang, *Nat. Mater.* 1, 123 (2002).
31. J. Marzec, W. Ojczyk and J. Molenda, *J. Mater. Sci. Pol.* 24, 69 (2006).
32. J. Molenda, J. Marzec, *Funct. Mater. Lett*. 1, 97 (2008).
33. P. S. Herle *et al.*, *Nat. Mater.* 3, 147 (2004).
34. W. Ojczyk *et al.*, *J. Power Sources* 173, 700 (2007).
35. Kang, G. Ceder, *Nature* 458, 190 (2009).

The above manuscript appeared in the Functional Materials Letters Vol. 4, No. 2 (2011) 107–112 ©World Scientific Publishing Company. Reprinted with permission.

Smart carbon coatings for Li-ion batteries

Marcin Molenda
Faculty of Chemistry, Jagiellonian University, Ingardena 3 Str., 30-060 Krakow, Poland

Introduction

High performance lithium ion batteries require electrode (cathode and anode) materials showing high enough ionic and electronic conductivities as well as high chemical stability. Currently, the standard composite cathodes used in Li-ion cells are prepared as physical mixture of powders (active material, carbon and binder) [1]. Thus, aggregation of the fine carbon particles may occur, increasing heterogeneity of the cathodes and lowering the reversible cell capacity due to limitation in the charge transport [2]. Higher performances of cathode as well as anode materials may be achieved by lowering the size of active material grains. Nano-sized grains reveal better electrochemical properties and also lower chemical stability towards electrolyte [3, 4]. The latest may provide dangerous and uncontrolled self ignition of a cells. Coating of active material by conductive carbon layers (CCL) increased the chemical stability and safety of the composite cathode [5]. Many reports points to improvement of electrochemical performances of the cathode materials caused by carbon coating [6-12]. There are several trials to improve the carbon coatings, starting from mechanical mixtures of various resins, carboxylic acids, or sugars solutions with the active materials, carbonized further to get the final composites. However, the morphology of these layers was not discussed in detail. Characteristic of the carbon coatings deposited on electrodes is that they react with the electrolyte thereby giving rise to the formation of passive insulating layers. To avoid these destructive effects, the carbon conductive layers (CCL) should stick well to the electrode material and be able to reduce an interface area of the electrode/electrolyte composite. This is needed for optimal formation of solid electrolyte interface (SEI) that is responsible for the magnitude of ion transport across the interface. In view of the above, the formation of micro canals in the CCL (the appropriate porous structure) can provide suitable pathways for the transport of ions (e.g. Li^+) from the electrolyte to active material and vice versa. Such a composite material should assure also a sufficient electrical conductivity. On the other hand, the carbon matrix is applied in silicon, tin or antimony based high capacity composite anodes [13-17]. In such composites the carbon coating act as electrically conducting and stress buffering agent compensating volume changes. The volume changes during lithium insertion-deinsertion from active anode material (*e.g.* Sn, Si) may reach 300%, thus the electrical contact in the composite may be lost and cell damaged. A high capacity anodes requires a nano-sized grains of active materials which reveal high chemical reactivity thus composites preparation is difficult. A novel method of preparation of conductive carbon layer with controlled morphology on fine particle powders, based on direct polymer deposition, has been proposed in recent works [18-21].

The goal of the work was to show applicability of the CCL composite idea in preparation of cathode as well as anode composites for Li-ion batteries in water mediated process using hydrophilic polymers as carbon precursor. The influence of polymer precursors composition, conditions of deposition and pyrolysis process on morphology and electrical properties of the formed CCL was studied on model composite system CCL/α-Al_2O_3. CCL cathode composites were prepared from $LiMn_2O_{4-y}S_y$ ($0 \le y \le 0.1$) lithium manganese spinel materials while anode composite was prepared from nano-sized tin(IV) oxide obtained by reverse microemulsion method. The textural, chemical as well as electrical properties of the obtained electrode composites were characterized and discussed.

Experimental

Schematic process of CCL/α-Al_2O_3 composite preparation is presented in Fig. 1. Two methods of the composite precursors formation were applied. In the first, the free-radical precipitation polymerization of freshly distilled acrylonitrile (AN) was performed in the presence of α-Al_2O_3 grains (POCh, Poland, 99.99 %, S_{BET} = 24 $m^2 g^{-1}$). The details of procedure was described in previous paper [19]. In

brief, α-Al_2O_3 grains were suspended in water solution of AN (7 wt%) and the polymerization was initiated by 2,2'-azobis(isobutyramidine hydrochloride) (Aldrich), upon which the obtained PAN/α-Al_2O_3 samples were washed, filtered and dried in the vacuum at 50°C. In the second method , the α-Al_2O_3 grains were wet impregnated with polymers in water solutions. The polymers used, were poly-N-vinylformamide (PNVF) obtained by radical-free polymerization from N-vinylformamide (Aldrich) [5] and modified by pyromellitic acid (PMA) (5-10 wt%) PNVF (MPNVF) [20, 21]. To achieve the impregnation, α-Al_2O_3 grains were suspended in the solutions of respective polymers in water (8-15 wt%). The suspensions were stirred continuously until the solvent evaporated and the viscosity of the solutions became high enough to avoid sedimentation. Then the samples were dried in an air drier at 90°C overnight. To obtain CCL/α-Al_2O_3 composites, following the preparation, the PAN/α-Al_2O_3, PNVF/α-Al_2O_3 and MPNVF/α-Al_2O_3 composite precursors were pyrolysed in a tube furnace under the flow of 99.999 % argon (5 dm^3/h) at 550° and 600°C for 24h. The CCL/α-Al_2O_3 composites obtained were deep black with foamed slag-like structure, the one prepared from the MPNVF precursor being special in that it looked glassy and lustrous like a graphite. The composites had their carbon content determined by temperature programmed oxidation (TPO) using thermal-gravimetric analysis (TGA) [19].

Lithium manganese spinel $LiMn_2O_{4-y}S_y$ ($0 \le y \le 0.1$) materials for CCL composites were prepared by sol-gel method [5]. The grains of cathode material were coated by MPNVF polymer precursor in wet impregnation process (Fig. 1). Then the obtained MPNVF/$LiMn_2O_{4-y}S_y$ composite precursors were carefully pyrolysed under controlled conditions (10 dm^3/h Ar 99.999%, 400°C/6h), to avoid the oxide decomposition providing carbon layer combustion. The optimal conditions of the pyrolysis process were determined by thermal analysis techniques (EGA-TGA/DTG/SDTA) [18].

Carbon/tin anode composites were prepared in following process. As tin precursor a nano-sized $Sn(OH)_4$ obtained by reverse (w/o, water in oil) microemulsion method. Two w/o microemulsions were prepared. They contained 22% wt. of water phase, 48% wt. of cyclohexane (POCh) as oil phase and 30% wt. of surfactant (Triton X-100, Aldrich) and co-surfactant (n-Hexanol, POCh) with a ratio 2:1 by weight. In the water phase of the first microemulsion tin (IV) chloride ($SnCl_4 \cdot 5H_2O$, POCh) was dissolved. The water phase of the second microemulsion contained the precipitating agent tetrapropylammonium hydroxide ($((CH_3CH_2CH_2)_4NOH$, Aldrich). The obtained two transparent w/o microemulsions were mixed together for 24h. After precipitation of tin (IV) hydroxide the resulting mixture was centrifuged and washed with acetone and water (2:1) several times providing a white powder. The nano-sized tin (IV) oxide was obtained after calcination performed under air flow at 450°C for 3h. Then, the obtained SnO_2 grains were coated by polymer carbon precursor–poly(N-vilnylformamide) modified with 5-10 wt.% pyromellitic acid (MPNVF precursor) - in wet impregnation process (Fig. 1). The obtained MPNVF/SnO_2 composite precursors were pyrolysed under Ar (99.999%, 10 dm^3/h) flow at 800°C for 3h. The optimal conditions of calcination and pyrolysis process were determined by the thermal analysis methods (EGA-TGA/DTG).

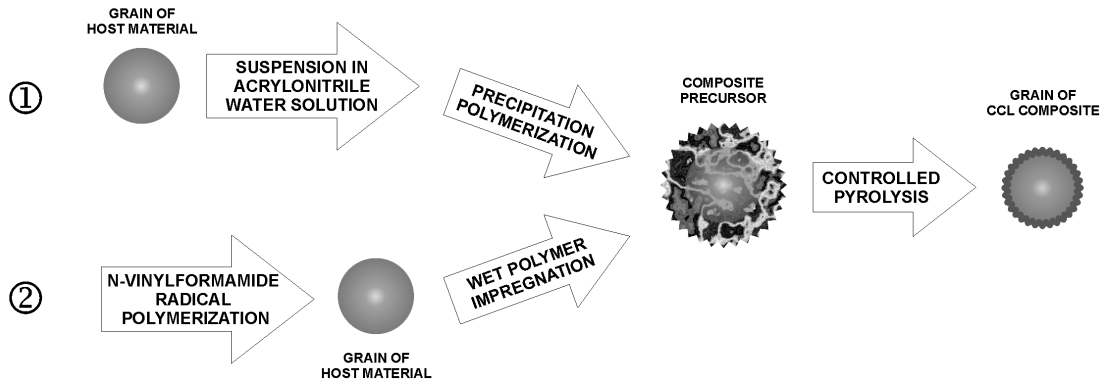

Fig. 1. Process schematic of water mediated CCL/Al_2O_3 composite formation performed by polymer precipitation polymerization in suspension (1) or by wet polymer impregnation (2).

Thermal gravimetric analyses (TGA) coupled with mass spectrometry analysis of evolved gas (MS-EGA) were performed in a Mettler-Toledo 851^e thermo-analyzer using 150 µl corundum crucibles under flow of air or argon (80ml/min), within temperature range 30-1000°C and heating rate 10°C/min. The simultaneous MS-EGA was performed using on-line joined quadruple mass spectrometer (QMS) Thermostar (Balzers). The 17, 18 and 44 m/z mass lines, ascribed to the OH, H_2O and CO_2 species respectively, were collected during the TGA experiments. The carbon content in the composites was determined by the temperature programmed oxidation (TPO) [19].

The differential scanning calorimetry (DSC) experiments were performed in Mettler-Toledo 821^e equipped with intracooler Haake, in 40µl aluminum crucibles under constant flow of argon (80 ml/min). The measurements of chemical stability of the composite cathode towards electrolyte (1M $LiClO_4$ in EC:DMC) were performed within temperature range +25÷+500°C with heating rate of 10°C/min.

The Raman spectroscopy measurements were performed on thin pellets containing 10 mg of the carbon sample and 200 mg of KBr. The carbon samples were prepared by pyrolysis under the same process conditions as those applied in the composites preparation. The spectra were recorded at room temperature using a triple grating spectrometer (Jobin Yvon, T 64000) equipped with a liquid nitrogen cooled CCD detector (Jobin Yvon, Model CCD3000). The spectral resolution of 2 cm^{-1} was set. An excitation wavelength at 514.5 nm was provided by an Ar-ion laser (Spectra-Physics, Model 2025). The laser power at the sample position was about 20 mW. Raman scattered light was collected with a 135° geometry, and 5000 scans were accumulated to ensure acceptable signal-to-noise ratio.

The crystal structure of the obtained carbon composites were characterized at room temperature by powder X-ray diffraction (XRD) method in a PW3710 Philips X'Pert apparatus equipped with a graphite monochromator using Cu $K_{\alpha 1}$ radiation. The average crystallites size was calculated from reflections broadening using the Scherrer equation.

The specific surface area measurements of the composites were performed in Micrometrics ASAP 2010 using the BET isotherm method. For that about 500 mg of each sample was degassed at 250-300°C for 8 h under a pressure of 0.26-0.4 Pa and subjected to N_2 sorption at -195.8°C. The pore size distribution was determined using the BJH method.

Electrical conductivity was measured using the *ac* (33Hz) 4-probe method within temperature range of 40÷55°C. The carbon coated composite powders were elastic that the standard preparation of pellets was impossible. The fine powder samples were placed into a glass tube and pressed by a screw-press between parallel gold disc electrodes (∅=5mm) till the measured resistance remains constant.

Transmission electron microscopy investigation was performed using TECNAI G F20 (200 kV) coupled with an energy dispersive X-ray spectrometer (EDAX). In order to fully describe morphology of obtained composite grains, the analysis was carried out in a bright filed (BF) and high resolution (HREM) modes.

Results and Discussion

Model CCL/α-Al_2O_3 composites

The results of the Raman spectroscopy (RS) measurements are presented in Fig. 2. The degree of carbon materials graphitization was characterized using the intensity ratio D/G, where the D band (defect mode; at about 1350 cm^{-1}) corresponds to sp^3 diamond-like carbon structures and the G band (about 1600 cm^{-1}), to sp^2 graphitic structures [23-26]. It was found that the graphitization degree increased with a decrease in the D/G ratio. The lowest value of the D/G ratio was observed for MPNVF precursor. This indicates the formation of the highest amounts of the graphene domains in the carbonized sample compared to the other precursors. Also, the G peak of the carbonized MPNVF precursor was downshifted and its width decreased, which suggests 2D ordering (1st phase of graphitization) [24]. Thus, the modification of PNVF by pyromellitic acid improves the polymer carbonization and the carbon layer formation. This may result from the fact that the planar structure of the PMA molecules serves as a nucleus of the graphene domains, which compete with the formation of the disordered structures. Likewise, for the same precursor the highest carbonization efficiency (the lowest loss of the carbon atoms from the precursor) was achieved (Table 1).

Table 1. Mass ratios of polymer precursors to α-Al_2O_3 applied in the composite precursors preparation, and the carbon content in the resulting C/α-Al_2O_3 composites.

Polymer precursor (PP)	PP/α-Al_2O_3 ratio	Carbon content in C/α-Al_2O_3, wt%	Carbonization efficiency, wt%
PAN	0.4	1.6	4.0
	0.8	5.1	6.9
	1.2	10.3	9.6
	1.6	20.6	16.3
	2.0	37.2	29.6
PNVF	1.0	6.6	7.0
	1.2	8.1	7.3
	1.4	9.6	7.5
	1.6	11.5	8.1
	2.4	25.3	14.1
	3.2	31.9	14.6
	4.8	47.7	14.7
MPNVF	0.2	2.0	11.7
	0.4	5.6	16.0
	0.6	9.7	18.2
	0.8	13.5	18.7
	1.1	17.4	18.6
	1.8	23.8	17.4
	3.3	40.0	20.0

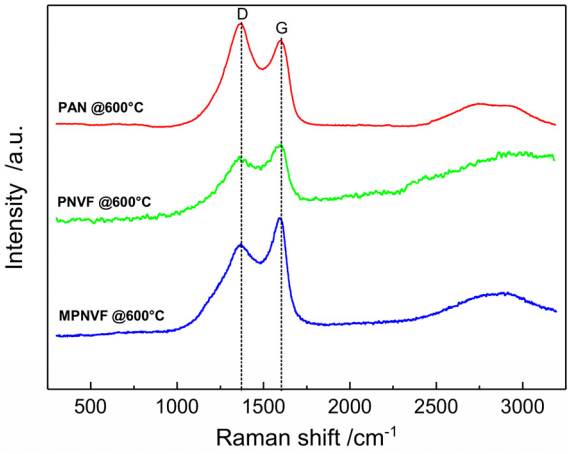

Fig. 2. Raman spectra of pyrolysed carbons derived from PAN, PNVF and MPNVF precursors.

The results of the electrical conductivity measurements carried out on the CCL/α-Al_2O_3 samples are presented in Fig. 3. As expected, the electrical conductivity of the composites increased with an increase in carbon loading. For the PNVF precursor, however, this increase was found much slower above 12 wt% of C. Such an effect was not observed for the CCL obtained from the PAN and MPNVF precursors. By contrast, the activation energy of electrical conductivity remained nearly constant in the range of carbon content studied, suggesting a preservation of the conductivity mechanism of the CCL. Of the samples examined, the best electrical properties, i.e. the highest conductivity and the lowest activation energy, were revealed by the composite based on the MPNVF precursor. Taking into account the results of the RS measurements, it may be concluded that the improvement of the electrical conductivity arose from the action of the pyromellitic acid modifier facilitating the achievement of the 2D ordered graphene structure. This way the desired value of the electrical conductivity of 10^{-2} S cm^{-1} was achieved. Simultaneously, the lowest activation energy (about 0.08 eV) of the electrical conductivity for these composite materials was observed.

The change in specific surface area with carbon content of the CCL/α-Al_2O_3 composites is presented in Fig. 4. For all the samples studied the specific surface areas increased linearly with carbon loading up to 25-30 wt%, the rate of this increase being dependent on the polymer precursor. This suggests that the initial porous structure of the CCLs was

preserved regardless of the carbon content. Interestingly, for the PNVF precursor the surface areas measured in the low carbon loading region were found much higher than those for MPNVF. This difference means that the modification of PNVF with the PMA modifier resulting in MPNVF, brought about the formation of another type of CCL, where most probably the formed graphene domains are locally arranged in a manner that they limit the formation of disordered carbon.

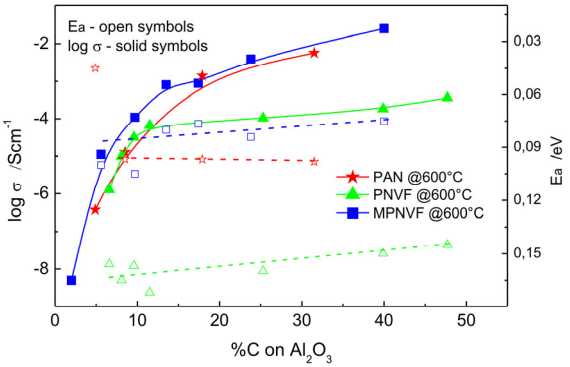

Fig. 3. Electrical properties of CCL/Al_2O_3 composites affected by composition of polymer precursor.

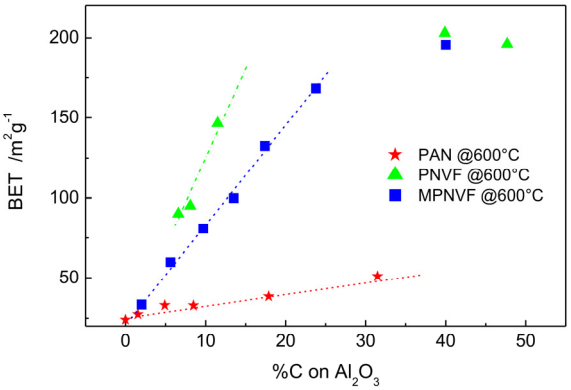

Fig. 4. Specific surface area of CCL/Al_2O_3 composites derived from different polymer precursor.

The N_2-adsorption-desorption isotherms and pore size distributions of CCL/α-Al_2O_3 composites are presented in Fig. 5. The observed shapes of the isotherms (Fig. 5a-5c) correspond to the mixed I and IV types of isotherms (according to IUPAC nomenclature). Such shapes indicate the presence of micro- and mesopores within the CCLs. The hysteresis loops of the H4 type (IUPAC) suggest the slotted pores located within the intergranular spaces. The textural properties of the composites on the other hand are generally similar, but there are differences in the pore size distribution (Fig. 5d-5f). The smallest pores were found in the composite obtained from the PAN precursor. This fact can be related to the applied preparation method, i.e. the precipitation polymerization resulting in filling of the pores by carbon particles. Unlike the PAN derived composite, the PNVF derived composite (Fig. 5b and 5e) revealed a highly porous structure with a relatively high number of micro-pores (about 30%), this morphology being in agreement with the highest specific surface area (Fig. 4). By contrast, the composite derived from the MPNVF precursor showed a very uniform distribution of the mesopores with sizes within the range of 3-4.5 nm (Fig. 5f). Also, the specific surface area of this composite that is lower by about 50 % than that of the unmodified precursor (PNVF) (Fig. 4) suggests that a tighter carbon film with a lower content of the disordered carbon was formed in this sample. These morphological properties together with the electrical properties (Fig. 3) classify the MPNVF derived composite as the optimal preparation.

Based on the electrical and morphological properties determined for the CCL/α-Al_2O_3 composites derived from the polymer precursors under investigation, the following structural model of these materials may be proposed (Fig. 6). The CCL obtained from the PAN precursor (Fig. 6a) consists of tightly packed small carbon particles, while that obtained from the PNVF precursor (Fig. 6b) is built of carbon whiskers, this latter structure being reflected in a high specific surface area and a high share of the micropores in this sample. This same PNVF precursor, when modified with pyromellitic acid (MPNVF precursor), strongly diminishes the specific surface area of the resulting composite, which is due to the formation of a tight, highly conductive carbon film with the defined porous structure that is dominated by mesopores with a narrow size distribution (Fig. 6c).

The sample result, of the performed HR-TEM studies on CCL/α-Al_2O_3 composites obtained from MPNFV precursor, is presented in Figs. 7. It is observed a uniform dispersion of well sticked nanosized carbon coatings on ceramic grains.

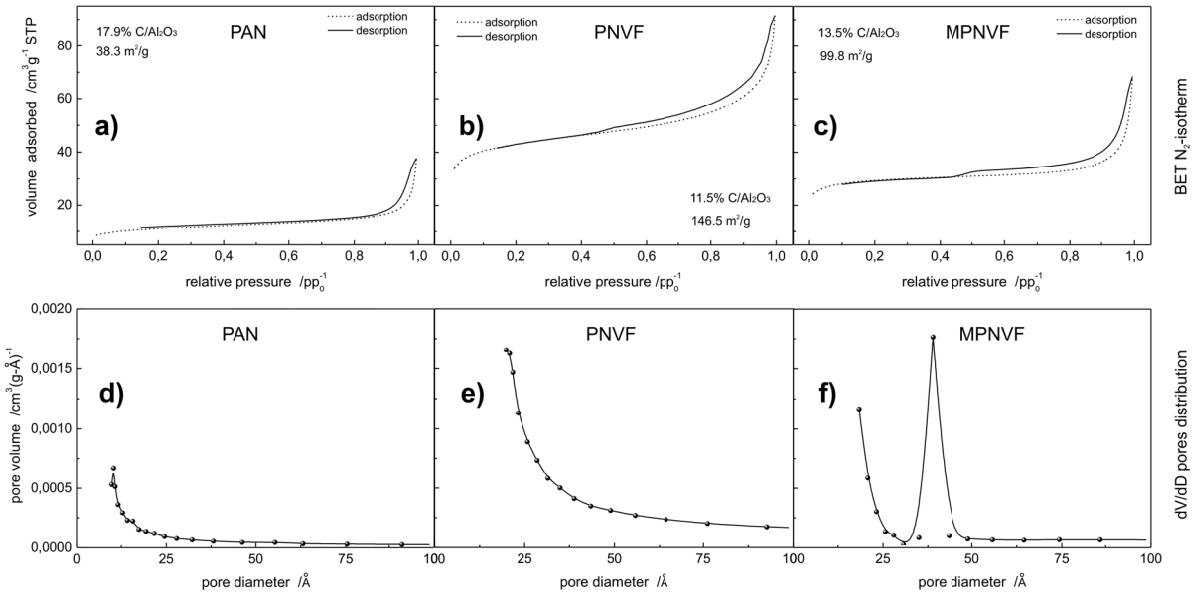

Fig. 5. Typical BET N_2-isotherms of CCL/Al_2O_3 composites.

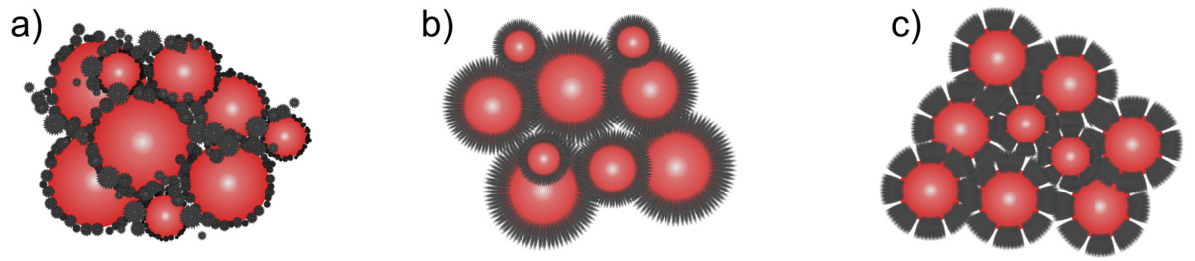

Fig. 6. Model cross-section of CCL composites derived from: PAN (a), PNVF (b) and MPNVF (c) precursors.

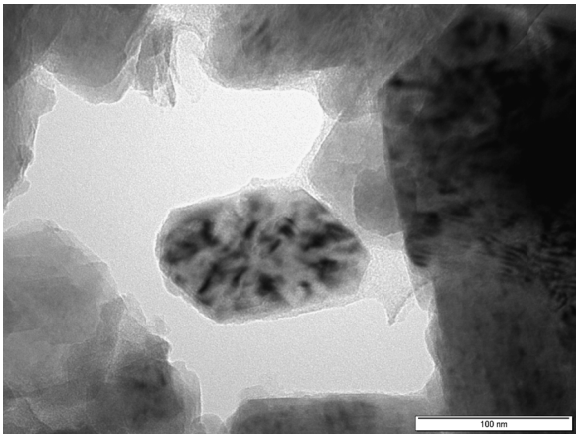

Fig. 7. HR-TEM cross-section of the C/Al_2O_3 composite obtained from MPNVF precursor.

CCL/$LiMn_2O_{4-y}S_y$ cathode composites

Thermal decomposition (pyrolysis) of the MPNVF/$LiMn_2O_{4-y}S_y$ precursor composites revealed similar behavior to decomposition of the PNVF/$LiMn_2O_{4-y}S_y$ precursor composites described in details elsewhere [18]. The temperature of the process, performed in argon atmosphere, had to be limited to 400°C because of oxidative decomposition of the spinel material causing carbon layer combustion. This effect was also observed for the others carbon polymer precursors (polyacrylonitrile, poly(N-vinylformamide) or co poly(styren, acrylonitrile)). The XRD patterns of CCL/$LiMn_2O_{4-y}S_y$ composites revealed typical feature of cubic $LiMn_2O_4$ spinel structure without any reflexes related to carbon deposit and this leads to conclusion that the obtained carbon layer was amorphous.

Electrical properties of the CCL/$LiMn_2O_{4-y}S_y$ cathode composites obtained from MPNVF precursor are presented in Fig. 8. One can notice decrease in the electrical conductivity of the carbon-spinel composites in comparison to uncoated $LiMn_2O_4$. This is due to too low pyrolysis temperature (400°C), but increasing of it was impossible, because the composite began to decompose. Howev-

er, the increase of electrical conductivity of the composites is observed with increase of carbon loading, what suggests that the formed carbon layer is conductive.

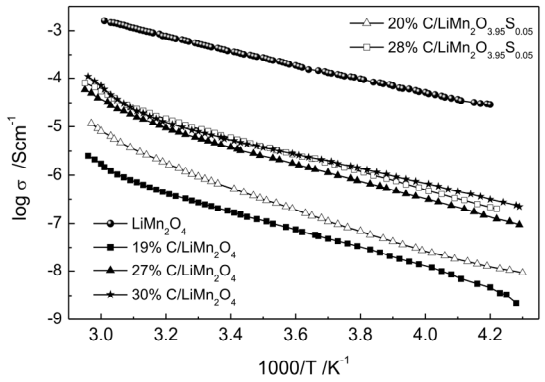

Fig. 8. Electrical Properties of CCL/$LiMn_2O_{4-y}S_y$ cathode composites obtained from MPNVF precursor.

The chemical resistance of the composites towards electrolyte (1M $LiClO_4$ in EC/DMC) was tested using DSC method. The results are presented in Fig. 9. The carbon coated materials exhibited better chemical stability in comparison to pristine ones. The heat effects related to exothermic redox reaction is shifted up toward higher temperatures of about 30-40°C. This should results in higher stability and safety of the CCL composite cathodes. The dependence of DSC heat effects of the composites on carbon content are presented in Fig. 10. The increase of carbon loading in the composites provided decrease of the heat of reaction of 25% at least. However, for the sulphur modified and carbon coated spinel this effect is much greater, in comparison to pristine $LiMn_2O_4$ cathode material (45% decrease). This strongly suggests that surface modification of the cathode material grains by CCL may significantly increase the safety of Li-ion batteries, especially in case of use of nano-sized grains of the materials.

Dependence of the specific surface area and pores size distribution on the carbon content are presented in Table 2. There is an increase in the specific surface area related to carbon coating, what was expected. An example of the BET N_2-isotherms and pores size distribution of the CCL/$LiMn_2O_{4-y}S_y$ composite are presented in Figs. 11. The observed shapes of the isotherms (Fig. 11a) correspond to the mixed I and IV type of the isotherms (according to IUPAC nomenclature). Such shapes indicate the presence of mesopores within the CCL's. Moreover, the carbon film with very uniform mesopores distribution, sizes within the range of 3-4.5 nm, was observed (Fig. 11b). The hysteresis loops of the H4 type (IUPAC) suggests the slotted pores located within the intergranular spaces. Such mesopores should provide fast path ways for lithium ion transport into cathode material. The observed morphology of the CCL/$LiMn_2O_{4-y}S_y$ composites prepared from MPNVF precursor revealed similar behavior than that for the model CCL/Al_2O_3 composites derived from the same precursor. This leads to conclusion that the morphology of the CCLs is related only to polymer carbon precursor while the overall composite morphology results from the host material texture as well.

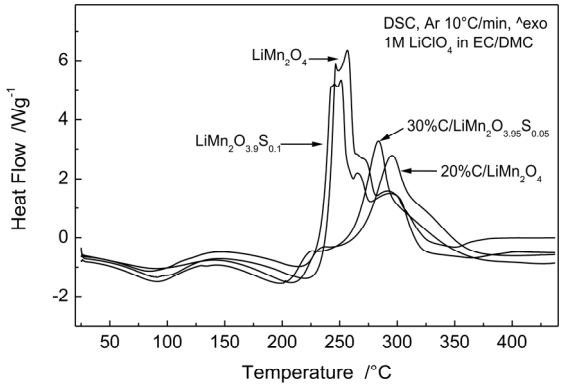

Fig. 9. Chemical stability towards electrolyte CCL/$LiMn_2O_{4-y}S_y$ cathode composites obtained from MPNVF precursor.

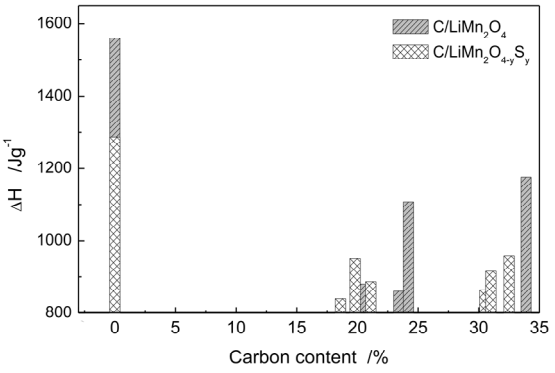

Fig. 10. Dependence of heat of reaction on carbon content in CCL/$LiMn_2O_{4-y}S_y$ cathode composites obtained from MPNVF precursor.

Table 2. Textural properties of the $LiMn_2O_{4-y}S_y$ cathode composites.

Sample	Carbon content [%]	BET specific surface area [m^2g^{-1}]	Maximum of pores size distribution [nm]
$LiMn_2O_4$	0	6.1	-
$C/LiMn_2O_{3.97}S_{0.03}$	18.6	10.2	3.4
$C/LiMn_2O_{3.97}S_{0.03}$	32.5	12.5	3.3
$C/LiMn_2O_{3.95}S_{0.05}$	21.1	9.1	3.3
$C/LiMn_2O_{3.9}S_{0.1}$	19.8	9.6	3.4
$C/LiMn_2O_{3.9}S_{0.1}$	30.5	8.4	3.4

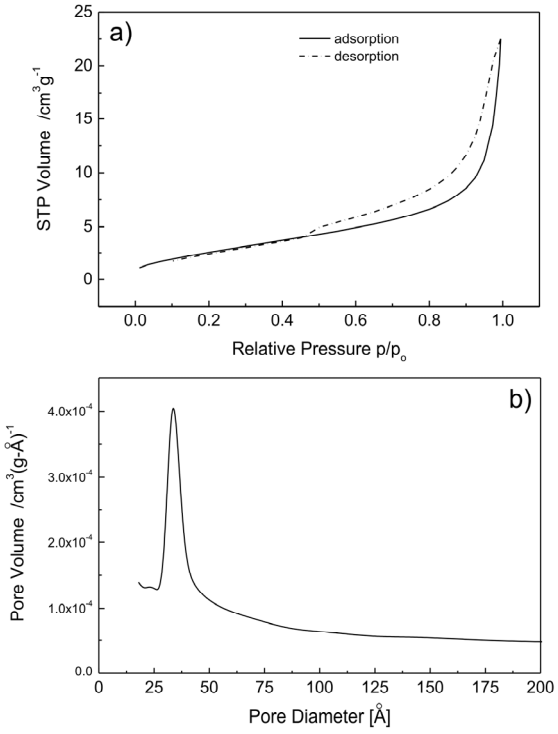

Fig. 11. BET N_2-isotherms (a) and pores size distribution (b) of CCL/$LiMn_2O_{4-y}S_y$ cathode composites.

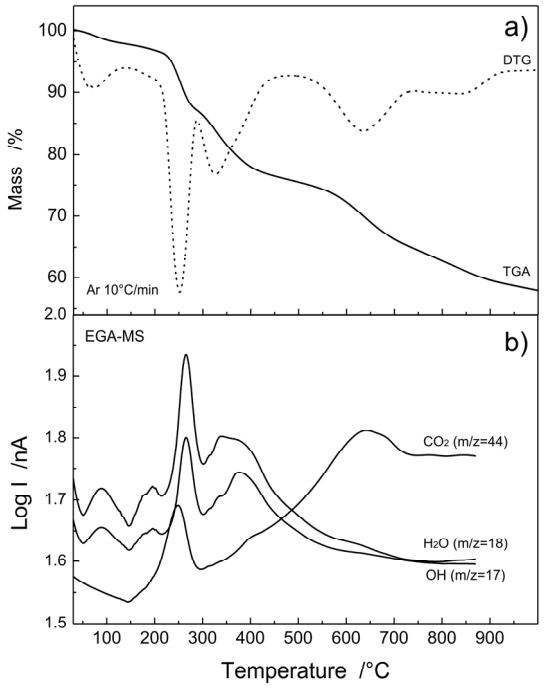

Fig. 12. Thermal decomposition of MPNVF/SnO_2 composite precursor of CCL/Sn composite.

CCL/Sn anode composites

The thermal analysis of the MPNVF/SnO_2 composite precursor decomposition process performed in argon atmosphere is presented on Figs. 12. The observed TGA curve (Fig. 12a) is very complex, however in principle two main stages can be distinguished. The first stage which started above 200°C and is related to polymer pyrolysis and formation of carbonaceous materials. Simultaneously, the evolution of water and carbon dioxide is observed in EGA curves (Fig. 12b). Above 450°C the reduction of tin (IV) oxide to metallic tin (by formed carbonaceous material) begins what is accompanied by carbon dioxide evolution. It seemed that formation of C/Sn nano-composite from MPNVF/SnO_2 precursor may be possible in simple, coupled process of pyrolysis and carboreduction, preserving the tin nano-grains against fusion.

The results of X-ray diffraction measurements of CCL/Sn anode composites revealed that the assumed composites were obtained. An example of XRD pattern of 18% C/Sn composite are presented in Fig. 13. The pattern reveals characteristic feature of metallic tin, without any reflexes related to carbon material, what suggests that carbon layers were amorphous. Only small amounts of SnO impurities was observed, what was related to incomplete carboreduction of SnO_2. The calculated from reflexes broadening average crystallite size of metallic tin was in the range of 130-140 nm. This suggests that tin nano-grains were preserved against fusion, moreover, tin nano-grains were encapsulated by CCLs.

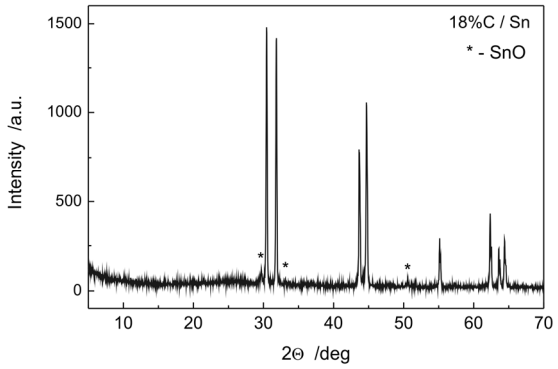

Fig. 13. XRD pattern of CCL/Sn anode composite.

The electrical properties of the obtained CCL/Sn composites are presented in Fig. 14. The results showed that the continuous path for electrical conductivity through CCL is achieved above 15% of carbon loading, and this is close to results obtained for C/Al_2O_3 model composites. Below 15% of carbon content in the composite, the formation of percolation path for electrical conductivity is observed. The activation energy of the electrical conductivity is low and not affected by carbon loading in the CCL/Sn composites, that suggests that electrical conductivity occurs only through graphite-like CCLs.

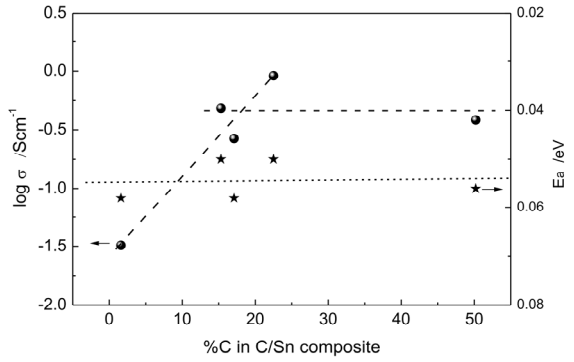

Fig. 14. Electrical properties of CCL/Sn anode composites affected by carbon loading.

The dependence of the specific surface area on the carbon content of the C/Sn composites are presented in Table 3. There is a strong increase in the specific surface area related to carbon coating, what was expected in relation to nature of the carbon precursor used (MPNVF). An example of the BET N_2-isotherms and pores size distribution of the C/Sn anode composite are presented in Figs. 15. The observed shapes of the isotherms (Fig. 15a) correspond to the mixed I and IV type of the isotherms (according to IUPAC nomenclature). Such shapes indicate the presence of micro- as well as disordered mesopores within the CCL's. The calculation of the pores size distribution (Fig. 15b) revealed two types of mesopores. The uniform pores, within sizes 3.5-5 nm, are related to pores in CCLs, while the large, disordered ones of sizes 8-18 nm are related to composite grains.

Table 3. The textural properties of the C/Sn anode composites.

Sample	Carbon content [%]	BET specific surface area [m^2g^{-1}]
C/Sn-1	1.6	25.0
C/Sn-2	15.3	65.8
C/Sn-3	18.0	107.5
C/Sn-4	22.5	79.7
C/Sn-5	48.3	161.4
C/Sn-6	50.2	108.8

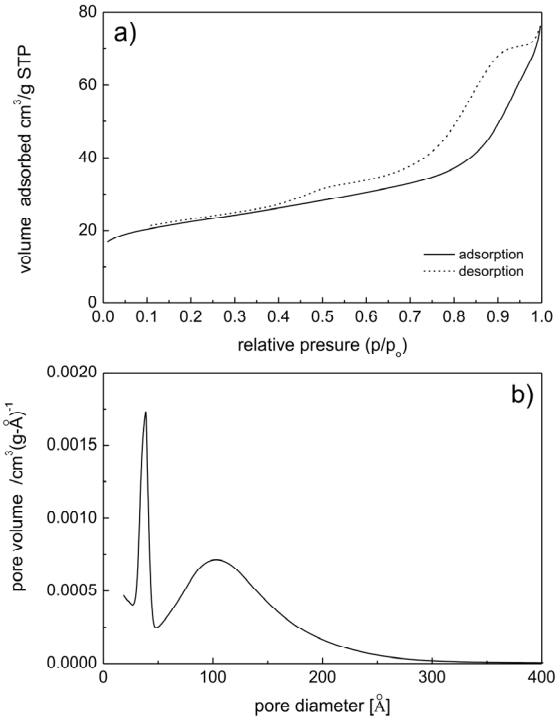

Fig. 15. BET N_2-isotherms (a) and pores size distribution (b) of CCL/Sn anode composites.

The sample HR-TEM images of C/Sn anode composites are presented in Figs. 16. Uniform dispersion of crystalline tin nano-grains in amorphous carbon matrix is observed what correlates well with XRD and BET results.

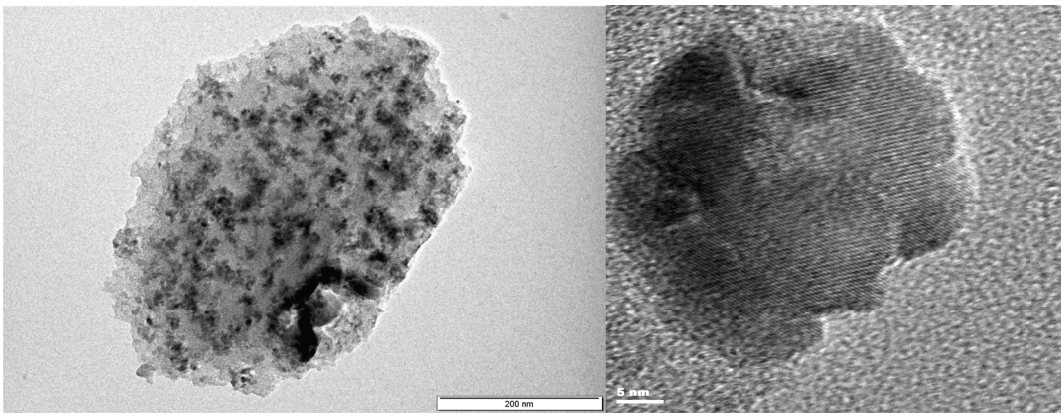

Fig. 16. HR-TEM images of CCL/Sn anode composite.

Conclusions

The electrical and morphological properties of the model CCL/α-Al_2O_3 composites showed a strong dependence on the nature of the polymer carbon precursors used to form CCLs. This leads to the conclusion that the properties of CCLs may be controlled by a proper composition of the polymer precursor. It was shown that the modification of poly-N-vinylformamide precursor with pyromellitic acid improved the electrical properties of the carbon film and gave rise to the formation of the optimal pore structure. The proposed water mediated method of smart carbon coatings preparation, is capable of creating an appropriate mesoporous structure of the CCL what may assure easy pathways for ion transport (e.g. Li^+). The method combines coating from solution and solid phase and is an easy to scale-up process. The water mediated preparation process is essential in case of future, environmental friendly technology. This feature may be used in preparation of carbon coated cathode materials composite for lithium-ion batteries. Moreover, these carbon films exhibit good electrical properties, which already fulfill the demand for low-conducting cathode materials (e.g. $LiFePO_4$, Li_2MSiO_4) to be applied in lithium-ion batteries. Also, due to its tightness, the CCL formed with use of the MPNVF precursor should be capable of improving chemical resistance of the cathode materials to the action of the electrolyte in the battery. The results obtained on cathode as well as anode composites obtained in wet impregnation process show versatility of the proposed method. The pyrolysis process of the polymer may be simply used to formation of conductive carbon layers or may by coupled with carboreduction process of the host material, depending on demands. Carbon coating of cathode materials ($C/LiMn_2O_{4-y}S_y$) by CCLs improved their chemical stability towards electrolyte, and should result in higher safety of cathode composites. On the other hand, encapsulation of tin nano-grains in carbon matrix may result in formation of novel high capacity composite anode materials for Li-ion batteries, thus further electrochemical researches seems to be necessary.

Acknowledgments

The authors acknowledge a financial support from the Polish Ministry of Science and Higher Education under research grant No. N N209 088638 and from the European Institute of Innovation and Technology, under the KIC InnoEnergy NewMat project. The part of the measurements was carried out with the equipment purchased thanks to the financial support of the European Regional Development Fund in the framework of the Polish Innovation Economy Operational Program (contract no. POIG.02.01.00-12-023/08).

References

1. J.M. Tarascon, M. Armand, *Nature*, 414, 359 (2001).
2. E. Ligneel, B. Lestriez, O. Richard, D. Guyomard, *J. Phys. Chem. Solids*, 67, 1275 (2006).
3. M. Armand, J.-M. Tarascon, *Nature*, 451, 652 (2008).
4. A. Yamada, S.C. Chung, K. Hinokuma, *Journal of the Electrochemical Society* 148(3)(2001)A224
5. M. Molenda, R. Dziembaj, Z. Piwowarska, M. Drozdek, *Solid State Ionics*, 179, 88 (2008).
6. B.L. Cushing, J.B. Goodenough, *Solid State Sci.*, 4, 1487 (2002).
7. J.K. Kim, G. Cheruvally, J.H. Ahn, H.J. Ahn, *J. Phys. Chem. Solids*, 69, 1257 (2008).

8. B. Lin, Z. Wen, J. Han, X. Wu, *Solid State Ionics*, 179, 1750 (2008).
9. J.K. Kim, G. Cheruvally, J.H. Ahn, *J. Solid State Electrochem.*, 12, 799 (2008).
10. G.T.K. Fey, T.L. Lu, F.Y. Wu, *J. Solid State Electrochem.*, 12, 825 (2008).
11. Y.J. Choi, Y.D. Chung, C.Y. Baek, K.W. Kim, H.J. Ahn, J.H. Ahn, *J. Power Sources*, 184, 548 (2008).
12. H.C. Shin, W.I. Chob, H. Jang, *Electrochimica Acta* 52(2006)1472
13. S.H. Ng, J. Wang, K. Konstantinov, D. Wexler, S.Y. Chew, Z.P. Guo, H.K. Liu, *J. Power Sources*, 174, 823 (2007).
14. X. He, W. Pu, L. Wang, J. Ren, C. Jiang, C. Wan, *Solid State Ionics*, 178, 833 (2007).
15. A. Trifonova, T. Stankulov, M. Winter, *Ionics*, 14, 421 (2008).
16. Y. Li, J. Li, *J. Phys. Chem C*, 112, 14216 (2008).
17. J. Hassoun, G. Derrien, S. Panero, B. Scrosati, *J. Power Sources*, 183, 339 (2008).
18. M. Molenda, R. Dziembaj, M. Drozdek, E. Podstawka, L.M. Proniewicz, *Solid State Ionics*, 179, 197 (2008).
19. M. Molenda, R. Dziembaj, Z. Piwowarska, M. Drozdek, *J. Therm. Anal. Cal.*, 88, 503 (2007).
20. M. Molenda, R. Dziembaj, A. Kochanowski, E. Bortel, M. Drozdek, Z. Piwowarska, *Patent application,* WO 2010/021557 and US 2011/0151112.
21. M. Molenda, *Functional Materials Letters*, 4(2), 129, (2011).
22. W. Ojczyk, J. Marzec, K. Świerczek, W. Zając, M. Molenda, R. Dziembaj, J. Molenda, *Journal of Power Sources* 173, 700, (2007).
23. A.S. Ferrari, J. Robertson, *Phys. Rev. B* 61, 14095, (2000).
24. C. Fauteux, R. Longtin, J. Pegna, M. Boman, *Thin Solid Films,* 453-454, 606, (2004).
25. S. Osswald, E. Flahaut, H. Ye, Y. Gogotsi, *Chem. Phys. Lett.*, 402, 422, (2005).
26. D. Pantea, H. Darmstadt, S. Kaliaguine, L. Summchen, C. Roy, *Carbon,* 39, 1147, (2001).

New lithium electrolytes for Li-ion batteries*

M. Armand, P.G. Bruce, B. Scrosati, W.Wieczorek[1], L. Niedzicki[1], M. Marcinek[1]

ALISTORE European Research Institute

[1]Faculty of Chemistry, Warsaw University of Technology

Noakowskiego 3, 00-664 Warsaw, Poland

**This paper is an extender abstract version of the internal report of the ALISTORE ERI entitled „ Polymers vs liquids gels and ionic liquid electrolytes. Any winners?*

Introduction

The present work is not intended to be a general overview of the electrolytes studied for lithium and lithium-ion battery technologies. For these purposes there are recent excellent reviews available dealing with liquid [1], polymer [2] and ionic liquids [3] systems. Readers are welcome to use them for further extension of their knowledge regarding each group of electrolytes used. In the present paper an authorative report based on opinion of the group of experts working in the field of electrolytes for battery application is presented. This will be followed by the presentation of ideas which in our opinion open new fields of research possibly leading to an improvement of the battery performance in the future.

State of art

In the pursuit for high performance batteries, alkali metals have been recognized as good candidates for electrode materials owing to their low standard potentials and densities. Among them, lithium was the most attractive. It has the lowest standard potential among all metals, being the lightest metal in the periodic table and its cation is very small giving it a chance to diffuse quickly in solids. Alkali metals are reactive with water, giving the metal hydroxide and hydrogen gas. Therefore as early as in the 1950s electrochemistry of lithium in nonaqueous solvents was established. Its stability in certain liquids was attributed to the formation of protective passive films that is also responsible for stability of stainless steel or aluminum in oxidizing conditions. The first primary lithium cells appeared on the market where they keep their well-established position until the present days. But still there was a lot of effort made to develop lithium technology as to introduce secondary lithium cells. The problem was the plating of lithium during the recharge. Highly inhomogeneous nature of the lithium-electrolyte interface provoked growth of lithium dendrites. Their erratic shape caused their dissolution and disattachment from the electrode on discharge, leading to capacity losses (that could be overcome by putting excess lithium in a new cell). Even worse was the presence of finely divided metallic lithium inside the electrolyte, that combined with this dendritic growth could lead to short-circuits and thermal runaway. For years different electrolyte compositions were examined in the hope of finding one that could lead to uniform lithium deposition. An ether-based electrolyte was introduced into the market in 1980s, which operated satisfactorily for over 300 deep cycles, however these batteries were still not perfect and several cells failures in 1989 finished the commercial viability of lithium metal/liquid non aqueous electrolyte secondary cells.

Safety issues related to the lithium metal electrode stimulated researchers to look for new negative electrodes for lithium technology. Looking at the lithium cell one can see, that the positive electrode chemistry is of the guest-host type, i.e. lithium cations are introduced into/removed from the stable structure of the host. At the same time electrons are injected into/removed from the highest energy bands of the material. All that happens at a certain potential. This class of materials (TiS_2, $LiMn_2O_4$, and $LiCoO_2$) was introduced by Whittingam and Goodenough back in the 1970's. These materials were cycled vs. metallic lithium electrode where it is plated/stripped. Extending the approach to the positive electrode into the negative one would lead to something called a "rocking-chair", shuttle-cock" or "swing" battery in which lithium exists only in ionic state. The battery operation results from transfer of lithium between two materials of different Fermi levels combined with corresponding transfer of electrons. First materials tested were lithiated oxides: $Li_6Fe_2O_3$, $LiWO_2$ that

were cycled vs. WO_3, TiS_2 and V_2O_5. Such cells, despite being very safe and offering long cycle life were not able to enter the market because of low energy and power density as compared with other technologies. It was only at the beginning of the 1990's when Li-ion cells were marketed thanks to the application of petroleum coke as the negative electrode material. Cokes and graphitic materials offer relatively high gravimetric capacities, operating potential very close to the one of lithium metal and most of all, low price.

The general trends observed recently is the search for new electrode materials are ruled by the demand for safe, cheap and well-performing cells for automotive industry. Use of rare and expensive elements is expected to be minimized in order to lower the price and allow large-scale production; operating potentials of the electrodes should lay within the stability domain of the electrolyte in order to minimize the safety hazards that in case of large cells/battery packs are an important issue; also the cycle life should be long enough to guarantee up to 10 years operation. Of course these cells should offer as good capacities and power capabilities as possible, however these cannot be traded for the safety or unreasonably high price. The most explored materials are $LiNiO_2$ (and its intermediates with $LiCoO_2$ and $LiMnO_2$), $LiMn_2O_4$ and $LiFePO_4$.

Apart from optimization of electrodes materials, that are not to be discussed here, a lot of effort was devoted to the development of electrolytes, tailored to the specific electrochemical system.

The role of electrolyte is two, or sometimes threefold:

- It should provide ionic contact between electrodes allowing to close the circuit when the cell is operational
- It should assure electronic and spatial separation of the positive and negative electrode in order to avoid short-circuit and as a result – self discharge of the cell, which in some cases can be very spectacular (as those of failed high power Li-ion cells).

In case of electrochemical systems where electrode components are not the only reactants appearing in the overall cell reaction, the electrolyte is the source (storage) of the remaining ones.

In lithium–ion technology generally three groups of electrolytes are considered for ambient and moderate temperature application. These are: liquid systems (solutions of lithium salt in aprotic solvents), polymeric electrolytes (solid or gel systems) and solutions of lithium salts in ionic liquids.

Generally an ideal electrolyte solvent should meet the following criteria:

- be able to dissolve lithium salts to sufficient concentration
- its viscosity should be low so fast ion transport can occur within electrolyte
- be inert to all cell components especially anode and cathode materials
- it should remain liquid in a wide temperature range (low melting and high boiling temperature are desirable).

The choice of solvent for electrolyte dedicated for practical lithium cell (consisting of very low potential negative and very high potential positive electrode) is rather limited. Electrolyte should be characterized by high dielectric constant and ability to complex at least one of the ions coming from the dissociation of the electrolyte salt. In aprotic solvents (because protic ones are unstable at low potentials) we lose the ability to complex anions first of all. Then – in order to get a high dielectric constant only a limited number of polar groups to choose from remain (many of them can be easily oxidized/reduced at the electrodes) i.e. carbonyl, nitrile, sulfonyl, ester and ether groups. Some heterocyclic compounds can be considered as well as long as they lack acidic protons and are stable against oxidation and reduction. Compounds that offer high dielectric constant and form low energy complexes with lithium cations were found to be cyclic organic carbonates. Many lithium salts can be dissolved in ethylene and/or propylene carbonates. The problem is that these solvents are characterized by high viscosity and often high melting point therefore they are solid at room temperature. In order to decrease the viscosity (and in this way increase the conductivity) and melting point – simple (linear) alkyl carbonates are usually mixed with the cyclic ones. These acyclic carbonates offer low viscosities, however their dielectric constant is also low. Furthermore their boiling and flash points are also low thus limiting the safety margin of the prac-

tical cell. Mixtures of organic carbonates are the solvents of choice for the commercial cells anyway.

Coming into solutes, properties of the salt used for battery applications are as follows:

- it should be able to completely dissolve in the applied solvent at desired concentration and ions should be able to transfer through the solution
- anion should be stable towards oxidative decomposition at the cathode
- anion should be inert to electrolyte solvent
- both anion and cation should be inert towards other cell components
- anion should be nontoxic and remains thermally stable at the battery working conditions.

As can see the choice of an appropriate electrolyte salt is not easy. First of all the cation is fixed i.e. we need lithium cation as the electro active species in the electrolyte. The choice of anion is restrained by several factors. First of all the dissociation free enthalpy of its lithium salt should be as low as possible so that the dissociation constant is high and so is the maximum concentration of lithium cations. The anion should be stable at low and high potentials therefore not all the polar groups can be used to make up the anion. It should also be non-reactive towards carbonate solvents. Small and simple anions such as O^{-2} or F^{-} cannot be used because their small ionic radius induces low dissociation constants. Use of softer anions like S^{-2} or I^{-} is prohibited because of their low oxidation potentials. In order to get an anion with well-distributed charge, simple fluorine or chlorine anions were combined with strong Lewis acids such as PF_5, AsF_5, BF_3 or $AlCl_3$ in order to get PF^{6-}, AsF^{6-}, BF^{4-} and $AlCl^{4-}$, respectively, which are stable at low and high potentials and are highly soluble even in low dielectric media. Since these acids are so strong, their complexation with weak bases like fluoride or chloride does not neutralize their activity and they can react with cell components like electrolyte solvent, current collectors and electrode active materials. Depending on the anion the structure and properties of electrode-electrolyte interfaces differ (it's not only the electrolyte solvent that determines the interfacial properties).

Another class of anions is the one based on the Pearson's theory of soft and hard acids/bases. According to it, soft acids are likely to form stable salts with soft bases, as well as hard acids with hard bases. LiF is a combination of hard acid (Li^{+}) with a hard base (F^{-}). Therefore its solubility is low in low dielectric solvents. If we combine hard acid with a soft base (formal charge localized at soft centre) in which charge is well-delocalized (strong electron withdrawing groups attached to the centre by covalent bonds) a well-soluble salt of high dissociation constant should be obtained. After a new acid based on imide with 2 electron withdrawing groups (trifluoromethanesulfonyl) had been reported in 1984, in 1989 Armand et al. proposed using it in its lithiated form as an electrolyte. Despite excellent intrinsic properties of electrolytes based on LiTFSI and its analogues they have never been applied in commercial cells because of corrosion problems. The aluminum current collectors are stable at high potentials because of passive layer protecting the metal against corrosion. Many fluorinated anions like TFSI or Tf provoke aluminum corrosion and inhibit their application.

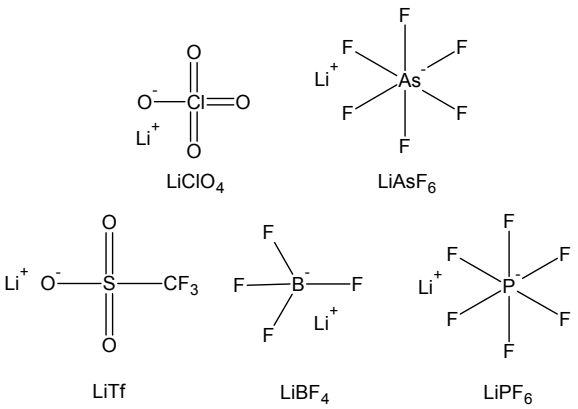

Fig. 1: Lithium salts known before the introduction of lithium-ion batteries onto market.
$LiClO_4$ - lithium perchlorate; $LiAsF_6$ - lithium hexafluoroarsenate; LiTf - $LiSO_3CF_3$ - lithium triflate - lithium trifluoromethanesulfonate; $LiBF_4$ - lithium tetrafluoroborate; $LiPF_6$ - lithium hexafluorophosphate.

Apart from salts known before 1990 ($LiClO_4$, $LiAsF_6$, $LiPF_6$, $LiBF_4$ or $LiCF_3SO_3$) – see Figure 1, so far there were very few promising introductions of new anions for lithium salts. Examples include LiTFSI ($LiN(SO_2CF_3)_2$) , then methide ones, $LiC(SO_2CF_3)_3$, $LiC(SO_2CF_3)_2(RCO)$ and $LiN(SO_2C_2F_5)_2$ (LiBETI). Unfor-

tunately, all of them, including LiTFSI, LiBETI (Fig. 2) and methide anion salts had the crippling drawback of being unable to form a passivation layer on Al current collectors when applied to a cell. $LiN(SO_2CF_3)_2$ and $LiC(SO_2CF_3)_3$ were also claimed to be too expensive for commercial application. Meanwhile, a whole class of sulfone-imide and methide-imide salts was designed and synthesized with no bigger success claimed since their introduction.

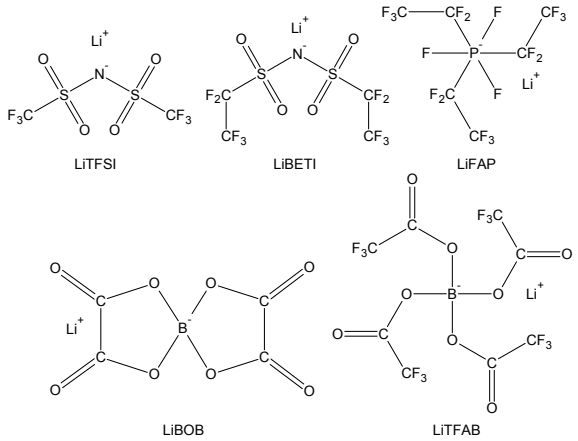

Fig. 2: New lithium conductive salts created for application in lithium-ion batteries.
LiTFSI - $Li[N(SO_2CF_3)_2]$ - lithium bis(trifluoromethane sulfone) imide; LiBETI - $Li[N(SO_2CF_2CF_3)_2]$ - lithium bis(pentafluoroethanesulfone)imide;
LiFAP - $Li[PF_3(CF_2CF_3)_3]$ - lithium fluoroalkylphosphate;
LiBOB - $Li[B(C_2O_4)_2]$ - lithium bis(oxalato)borate;
LiTFAB - $Li[B(OCOCF_3)_4]$ – lithium tetrakis (trifluoroacetoxy) borate.

The ALISTORE solution new family of immidazolium salts

The novel, promising concept of the application of new anions is based on the application of so called "Hückel anions". The name came from the transposition of the Hückel rule predicting the stability of the aromatic systems. One of the most common examples of this type of anions is 4,5-dicyano-triazole (DCTA) (Fig. 3) [4]. This particular structure is completely covalently bonded and shows very stable 6π (or 10π electron if CN bonds are involved in calculations) configuration. It can be produced from commercially available precursor and even more importantly does not comprise fluorine atoms. Salts of this type of anion were found to exhibit high (~300°C) thermal stability. LiDCTA was successfully tested in PEO matrices systems as a promising, improved electrolyte for lithium ion batteries. Unfortunately DCTA failed as a component of the EC/DMC (1:1) battery electrolyte.

To sum it all up, after almost 20 years of applications of lithium ion cells there is still a lack of potential substitutes for $LiPF_6$, which is definitely not flawless. Among the most important drawbacks of the $LiPF_6$ use in electrolyte system is the formation of HF in the cell, which destroys the cell from inside after certain time, but also $LiPF_6$ and HF toxicity.

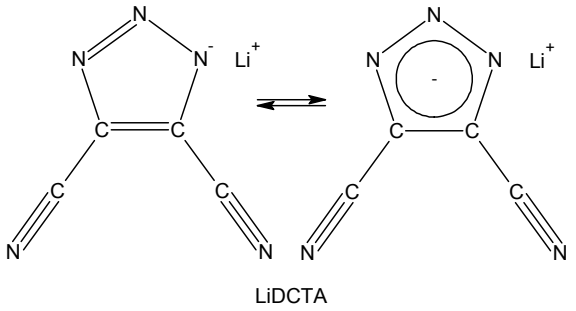

Fig. 3: LiDCTA - Hückel type salt: LiDCTA - lithium 4,5-dicyano-1,2,3-triazole.

The constant seek for more cheap, environment-friendly and easy to handle materials made a gap to fill. List of parameters for lithium salts to fulfill in order to become new predominant salt on market of lithium ion cells is not very long, but no existing salt fulfills it. Transference number above 0.5 (or at least better than $LiPF_6$ that in optimized carbonate solvent mixtures has transference number of 0.3-0.4), conductivity higher than 1 $mS \cdot cm^{-1}$ (10^{-3} $S \cdot cm^{-1}$), no decomposition in range of 0-4.5 V vs. Li and no aluminum corrosion in this range, low price (at least lower than $LiPF_6$, but the lower, the better), non-toxicity, moisture-proof (and air proof – stability in room atmosphere – easiness of handling), thermal stability up to at least 100°C and low association rate lower than $LiPF_6$ or very weakly associating $LiClO_4$ is what is necessary to obtain by researchers.

With this on mind the new "tailored" anions especially for application as lithium electrolytes in lithium ion cells have been designed and investigated.

Main idea was to design structure that would not have disadvantages of big bulky anions causing high viscosity when dissolved in organic solvents, therefore a decrease in conductivity. Also, ions of new salts should not form agglomerates after dis-

solution, due to ion pairs' and triplet's negative effect on conductivity of an electrolyte, mechanism of lithium cations insertion into the electrodes (in both charging and discharging process) and transference number of a lithium cation.

Newly designed immidazole derivatives seem to perfectly fit into this scheme. These new salts were synthesized, using the procedure shown in Figure 4.

Molecular modeling studies showed that immidazolide anions show a typical behavior of heterocyclic anion alternatives to PF_6^-: if tailored correctly they offer more dissociative lithium ion pairs compared to $LiPF_6^-$, but are not as electrochemically stable. The latter is, however, not crucial as long as the anions exceed the stability window for the intended application, for Li-ion batteries ~4.2 V.

Two anions brought to focus very recently are the 4,5-dicyano-2-trifluoromethyl immidazole (TDI) and its 2-pentafluoroethyl analogue (PDI). The lithium salts of these anions have by some of us been characterized in model polymer electrolytes [5] and stressed as "tailor made" salts for lithium battery applications [6]. Of these salts, the synthesis of LiTDI has been shown to be the most facile. The first report of this salt appeared five years ago [7], when it was prepared in good yield in connection with the finding of a new, improved synthesis route for the protonated (uncharged) form of TDI, known since the mid 70´s [8]. In Table 1 properties of the electrolytes ranging from solid polymer to ionic liquids systems in which both above mentioned salts are incorporated are summarized. The following features of the new electrolytes should be highlighted:

- thermal stability of salt
- high lithium transference number compared to previously used systems (this is particularly well seen in case of ionic liquid based electrolytes)
- ease of electrolyte preparation
- low cost of the newly design systems.

The Chalmers group [9] used LiTDI and LiPDI as templates and screen for further synthesis candidates by means of computational *ab initio* methods. New anions are proposed by first extending the heterocyclic imidazole ring to a benzimidazole ring, with two or four cyano groups symmetrically positioned on the ring, and secondly by also looking at alternatives where the fluoroalkyl substituent is replaced by a smaller, less flexible group. Ion pair configurations and dissociation energies, together with anion stabilities towards oxidation are evaluated. Information is obtained about the sensitivity of these properties with respect to ring size (imidazole or benzimidazole), the number and positioning of –CN groups, and the choice of substituent (–CF_3, –C_2F_5, or –CN) at position 2 of the heterocyclic ring. Particularly cyano substituted benzimidazoles were found to be a very promising candidates from the viewpoint of possible application in the battery technology. However they are more difficult to synthesize than their imidazole cousins. Successful finishing of the synthetic procedure will give us more information about the reaction yield and possibilities of scaling it up.

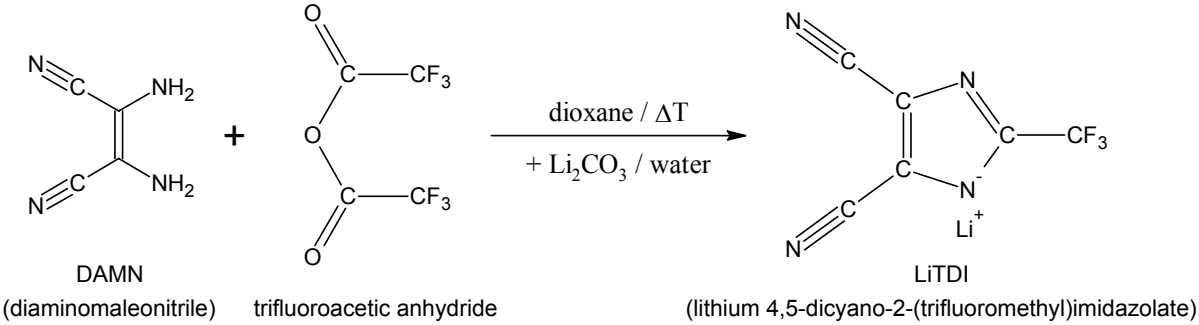

Fig. 4: Synthesis scheme for LiTDI.

Table 1. Exemplary parameters of novel salt systems used as various types electrolytes in lithium-ion batteries.

Electrolyte form\Salt	Parameter	LiTDI	LiPDI
Pristine salt (not as an electrolyte)	Thermal stability (commercial salts have stability limit around 100˚C):	257˚C	260˚C
Liquid (modern batteries for cell phones, watches)	Ionic conductivity (at least 1mS in 25˚C): Li^+ transference number up to (commercial salts have up to 0.3): Electrochemical stability up to (highest existing electrodic materials need 4.0 V):	7 mS/cm 0.5 4.7 V	6 mS/cm 0.5 4.7 V
Gel (for more expensive batteries or for safety-requiring applications like notebooks or EVs)	Ionic conductivity (at least 1mS in 25˚C): Li^+ transference number up to (commercial salts have up to 0.2): Electrochemical stability up to (highest existing electrodic materials need 4.0 V):	1.3 mS/cm 0.35 4.3 V	1.0 mS/cm 0.55 4.3 V
Solid Polymer (prototypic and small battery series, future application in EVs and notebooks)	Ionic conductivity at 25˚C (at least 0.1mS below 60˚C for EV applications): Electrochemical stability up to (highest existing electrodic materials need 4 V):	0.05mS/cm 0.1 in 40˚C (suitable pacemaker 4.0 V	0.05mS/cm 0.1 in 40˚C for batteries) 4.0 V
Ionic Liquids (nearest-future batteries)	Ionic conductivity (at least 1mS/cm in 25˚C, commercial ILs have up to 1mS/cm): Li^+ transference number up to (commercial ILs have up to 0.04): Electrochemical stability up to (highest existing electrodic materials need 4.0 V):	3 mS/cm 0.14 4.8 V	N/A N/A N/A

Ionic conductivity limits are given according to battery manufacturers requirements for battery components.

Summary

In the preceding section example of performance of LiTDI and LiPDI in all solid as well as in liquid electrolyte based batteries were shown. Although, the preliminary results are promising further studies in various electrode configurations need to be performed. It should be emphasized that the use of organic salts will extend the range of possible solvent combinations which can lead to the improvement of safety as well as reduction of environmental impact. It is also worth to mention that organic salts can be used as components in the synthesis of ionic liquids. In such a case no additional lithium salt will be required as a component of electrolyte. So far addition of the salt reduces the conductivity range of ionic liquids based electrolytes. As was shown before [5,6] addition of TDI to PEO based polymer electrolytes enhances the ambient temperature conductivity of these systems. However, as it can be concluded on the basis of the review of properties of modified polymeric electrolytes it is hardly to achieve the level of conductivity exceeding 10^{-4} S/cm at ambient temperatures.

References

1. K. Xu, Chem.Rev., 104 (2004) 4303-4418.
2. F.M. Gray, Polymer Electrolytes, RSC Materials Monographs, (1997).
3. M. Armand, F. Endres, D.R. MacFarlane, H. Ohno, B. Scrosati, Nat Mater, 8 (2009) 621-629.
4. M. Egashira, B. Scrosati, M. Armand, S. Beranger, C. Michot, Electrochem.Solid-State Lett.; Electrochemical and Solid-State Letters 6 (2003) A71-73
5. L. Niedzicki, M. Kasprzyk, K. Kuziak, G.Z. Żukowska, M. Armand, M. Bukowska, M. Marcinek, P. Szczeciński, W. Wieczorek, J.Power Sources, 192 (2009) 612-617.
6. L. Niedzicki, G.Z. Żukowska, M. Bukowska, P. Szczeciński, S. Grugeon, S. Laruelle, M. Armand, S. Panero, B. Scrosati, M. Marcinek, W. Wieczorek, Electrochim.Acta, In Press, Corrected Proof.
7. M. Bukowska, P. Prejzner, P. Szczecinski, Polish J. Chem., 78 (2004) 417.
8. R.W. Begland, D.R. Hartter, F.N. Jones, D.J. Sam, W.A. Sheppard, O.W. Webster, F.J. Weigert, J.Org.Chem., 39 (1974) 2341-2350.
9. J. Scheers, P. Johansson, P. Szczecinski, W. Wieczorek, M. Armand, P. Jacobson, Journal of Power Sources, 195 (2010) 6081

New electrode materials for hydrogen storage in batteries

Zbigniew Rogulski[1,2], Mariusz Łukaszewski[1], Piotr Piela[2], Andrzej Czerwiński[1,2]

[1]Warsaw University, Department of Chemistry, Pasteura 1, 02-093 Warsaw, Poland

[2]Industrial Chemistry Research Institute, Rydygiera 8, 01-793 Warsaw

Introduction

Hydrogen is one of the most promising energy carriers, which is considered for various applications, e.g. in power electric vehicles or hybrid electric vehicles. The main advantage of hydrogen is no direct emission of CO_2 and NO_x during its using as a fuel. The main problems that limit wide application of hydrogen are its transport and storage. H_2 gas is highly inflammable and therefore is dangerous in confined spaces. One of the promising method of safe hydrogen storage is its chemical or physically combined storage in other materials e.g. metal hydrides. The metal hydride can hold between 1% and 7% of hydrogen by weight, depending on the alloy composition [1]. As a hydrogen storage material, the metal hydride is very efficient and delivers much better volumetric efficiency than hydrogen stored in a liquid state. The performance of the metal hydride electrode depends on the composition and the microstructure of the active material. In consequence, the majority of the studies on improving the MH electrode performance are focused on these aspects. In our Laboratory we investigate new useful materials for hydrogen electrochemical storage. Our works are divided into two fields: modification of electrode materials for nickel-metal hydride batteries and preparation of new multi metal alloys for low temperature fuel cells and supercapacitors.

Modification of hydrogen storage alloy

Lithium ion/polymer batteries together with the nickel-metal hydride (Ni-MH) represent the most important energy carriers. Although the Ni-MH batteries are excellent for powering of many portable devices and hybrid (HEV) and/or electro (EV) vehicles, in low temperature the current densities are not sufficient for power of many electric devices [1-3]. This limitation prohibits effective replacement Ni–Cd batteries which are more effective in low temperatures in comparison with Ni-MH system. A huge variety of metal hydride materials has been examined for application in NiMH batteries. Some of them cannot be applied in industrial scale due to high hydrogen equilibrium pressure at room temperature or instability when in contact with the electrolyte. The most promising are Magnesium-Metal hydrides, the materials today known only from the thin film technologies [2,4].

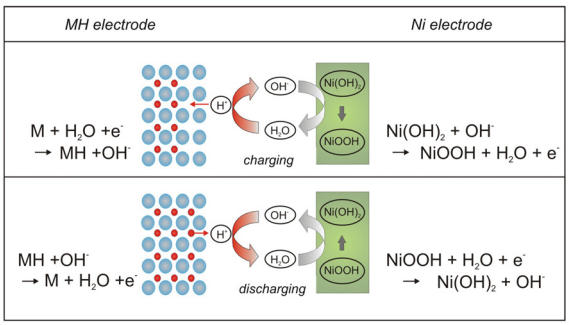

Fig. 1. A scheme of charging-discharging processes in metal hydride (Ni-MH) cell .

The hydrogen sorption process for a single-hydride-phase material is depicted in Fig. 2 [5]. The background used for symbols in the figure is an SEM image of a particle of a standard AB_5-type MH alloy. For the whole electrode to work well, the following sub-processes must proceed unhindered:

a) mass/charge transport outside the alloy particle characterized by
   - the effective diffusion coefficient of OH^- ions, D_i, and the related ionic conductivity of the alkaline electrolyte, σ_i,
   - the effective diffusion coefficient of water, D_w, and
   - the electronic conductivity, σ_e, (governed by the quality of inter-particle contact);
b) charge transfer at the surface of the particle characterized by the potential-dependent rate constants, k_1 and k_{-1};

c) phase transfer of hydrogen between the surface and the bulk of the particle characterized by the potential-independent rate constants, k_2 and k_{-2};
d) hydrogen transport inside the particle characterized by the effective diffusion coefficient of hydrogen in the alloy, D_H.

In addition, the hydrogen storage capacity of the particles, C_H, must be high. The parameters characteristic of the alloy particles themselves, namely k_1, k_{-1}, k_2, k_{-2}, D_H, and C_H, are the core performance parameters of an MH material. In the case of MH materials with a distinct α ↔ β phase transition, the kinetics of the phase transition inside the particle must be additionally considered.

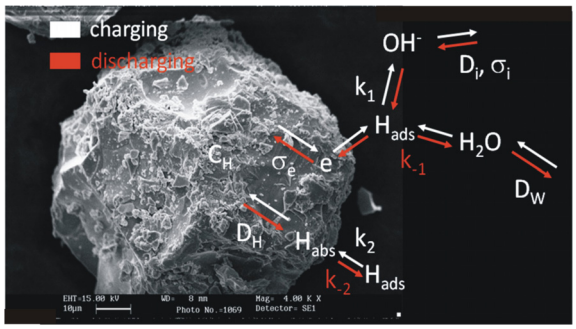

Fig. 2. The metal-hydride anode electrode process depicted on an SEM image of a LaMm–$Ni_{4.1}Al_{0.3}Mn_{0.4}Co_{0.45}$ alloy particle.

The most common way of characterizing MH alloys electrochemically is studying the behavior of electrodes prepared by pressing a certain amount of active material mixed with an binder material. The general question is: has the binding material influence for electrochemical performance of MH alloy? One of the method of determination of the intrinsic electrochemical properties of hydrogen absorbing alloy is using techniques developed in our laboratory called Limited Volume Electrodes (LVE) technique. The Limited Volume Electrode is an electrode containing a thin layer of a hydrogen storage material attached, e.g by electrochemical deposition or pressing, to a matrix which is neutral in respect to hydrogen absorption processes and acts as a current collector [6]. Fig. 3 presents a SEM image of a freshly prepared LVE electrode containing AB_5-type hydrogen storage alloy (LaMm-$Ni_{4.1}Al_{0.3}Mn_{0.4}Co_{0.45}$). The image is combined with an EDS linear scan for Au shown on the bottom of the Figure. We observe that the active alloy mass fills hollows of Au net with some uncovered parts of the net exposed to the ambient. The presence of uncovered Au was confirmed by EDS analysis showing an increase in Au net counts over the bare parts of Au wire net.

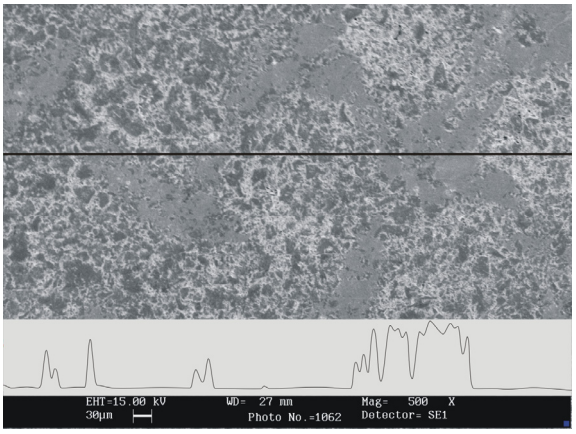

Fig. 3. SEM image and EDS linear analysis of a LV type electrode containing standard AB5 alloy. EDS analysis for gold was performed along the line indicated on the image. Vertical scale of EDS spectrum is a net count number in arbitrary units. Magnification 500×.

However, due to electrochemical neutrality of gold, this not affects results obtained for hydrogen absorption in MH alloy electrodes. An analysis of the electrode cross-section indicates the thickness of pressed alloy layer of ca. 50 µm. This value corresponds to the diameter of AB_5 alloy particles and indicates formation of an alloy layer with the thickness of a single particle. This way, ca. 25 000 single particles of hydrogen storage alloy are arranged in a single layer and each separate hole of gold matrix is filled by ca. 200-250 particles of the standard alloy. The borders between separate particles are well visible indicating that the particles do not form a bulk, continuous material and the process of hydrogen absorption/desorption in each of the particles proceeds independently. This way, hydrogen sorption/desorption in the electrodes studied may be treated as the one taking place in a particle with a spherical shape and under the conditions of a finite volume diffusion. In consequence, discussed type of limited volume electrodes exhibits the electrochemical behaviour similar to that observed for single particle metal alloy electrodes [5,6].

The LVE technique has been used as a main method for determination of electrochemical parameters (hydrogen diffusion coefficient, hydrogen capacity) of new metal hydride alloy developed in the

HydroNanoPol project (FP6). The practical specific hydrogen capacity obtained for standard and modified AB_5 alloys for 25˚C, and calculated for constant current discharging on the basis of transition time and applied desorption current, reach the values of 265 $mAhg^{-1}$ ± 5% and 258 $mAhg^{-1}$ ± 6%, respectively. These values are within the error range and correspond to ca. 85% of theoretical capacity reported by the manufacturer for the metal hydride alloy studied. Fig. 4 presents diffusion coefficient values calculated on the basis of chronopotentiometric and chronoamperometric experiments as a function of the state of charge of the electrode, SOC.

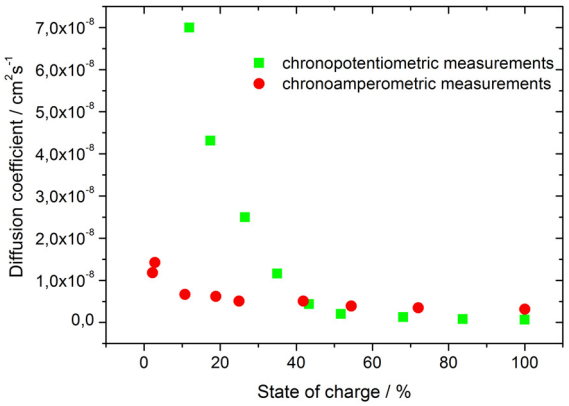

Fig. 4. Hydrogen diffusion coefficients of a LVE type electrode containing standard AB_5 alloy and calculated for constant current desorption ($45mAg^{-1}$) and constant potential desorption (-600 mV) as a function of the state of charge (SOC), T=25˚C.

In general, D values obtained by both techniques are very close and differ by less than 15 %. We observe that for both techniques D decreases with an increase in SOC reaching a constant value for SOC > 50%. For SOC equal to 100% D values are $4.9 \cdot 10^{-9}$ and $8.1 \cdot 10^{-9}$ cm^2s^{-1}, for CA and CP measurements, respectively. The influence of SOC on the value of hydrogen diffusion coefficient in various hydrogen absorbing materials is very often reported and discussed in the literature [7-9]. One of the explanations assumes that during diffusion hydrogen jumps between empty nearest-neighbour absorption sites (vacancies), in the direction determined by the concentration gradient. The occupation of these absorption sites by hydrogen increases when SOC increases. Hence, the higher the SOC the smaller the number of vacancies available for hydrogen transport and diffusion process is impeded. Influence of SOC on D can be also attributed to hydrogen concentration dependent interactions between absorbed hydrogen or to a phase transition between various phases of alloy/metal-hydrogen systems and taking place when concentration of absorbed hydrogen increases [10].

One of the most important results of HydroNanoPol project was preparation of new metal hydride alloy that has improved hydrogen storage capability in low temperatures. Fig. 5 presents the influence of temperature on the hydrogen capacity of the standard and modified alloy.

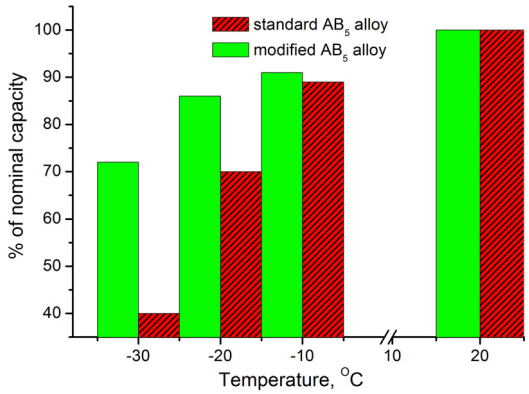

Fig. 5. A comparison of a constant current ($45mAg^{-1}$) discharge capacity calculated for LV electrodes containing standard and modified AB_5 alloy recorded at various temperatures.

For temperatures below -10˚C the capacity of the modified alloy is much higher than that of the standard one. Due to the peculiarities of binder free LV electrode construction we can conclude that the very high capacity recorded for modified alloy at -30˚C is connected only with the intrinsic properties of the alloy and is not related to the properties of binding agents or conductive materials which are simply absent in LVE. The results presented above, confirmed by independent measurements performed in Varta Microbatteries (Germany) laboratory (coordinator of the project) allow to prepare pilot set of button MH batteries with improved thermal resistance.

Application of metal hydrides in electrochemical supercapacitors

Pd and its alloys represent a large class of hydrogen-absorbing materials, which are important for chemical/electrochemical power sources [1]. Similar systems with less expensive metals systems can be applied in batteries, fuel cells or for hydro-

gen storage [2, 11]. Moreover, since hydrogen can be electrochemically inserted into and extracted from Pd-based electrodes, such materials can be treated as phase charging-discharging systems for electrochemical capacitors.

This type of devices usually utilize the capacitance of electrical double layer of various carbon materials or pseudocapacitance connected with reversible redox processes like insertion of atomic species into the crystal structure of bulk solid electrodes, e.g. conducting polymers or transition metal oxides (e.g. RuO_2, IrO_2, MnO_2) [12-15]. Due to high currents generated during hydrogen uptake and removal as well as their good practical reversibility, thin Pd-based layers electrolytically loaded with hydrogen seem particularly promising for that purpose.

Fig. 6 shows typical voltammetric and chronoamperometric responses recorded during hydrogen desorption after earlier saturation of a Pd electrode with hydrogen. These curves are typical of hydrogen extraction form thin Pd-based layers and were described in detail in earlier reports [16-22]. By the integration of hydrogen oxidation currents the amount of absorbed hydrogen was obtained.

The amount of hydrogen absorbed in Pd-based materials can be recalculated into units commonly used for description of energy storage systems, i.e. pseudocapacitance per mass unit. Under voltammetric conditions specific pseudocapacitance is obtained according to the equation:

$$C = Q^{ox}_{Habs} / (\Delta E \cdot m_M) \qquad (1)$$

where Q^{ox}_{Habs} is charge due to the oxidation of absorbed hydrogen, ΔE is the potential range in which absorbed hydrogen is completely oxidized, and m_M is mass of the hydrogen-absorbing material (i.e. the mass of Pd or Pd alloy deposit). The parameters used in the calculation are illustrated in Fig. 6a.

Other parameters used for the characterization of supercapacitors are specific power and specific energy. Specific energy can be obtained as:

$$E = (Q^{ox}_{Habs} \cdot \Delta E) / m_M \qquad (2)$$

An average value of specific power can be obtained under conditions of chronoamperometric hydrogen oxidation according to the relation:

$$P_{av} = [(Q^{ox}_{Habs} / t) \cdot (E_{abs} - E_{des})] / m_M \qquad (3)$$

where Q^{ox}_{Habs} is charge due to the oxidation of absorbed hydrogen, t is a period required for a complete hydrogen desorption and $E_{abs} - E_{des}$ is the difference between absorption and desorption potentials in chronoamperometric experiments (here 0.50 V).

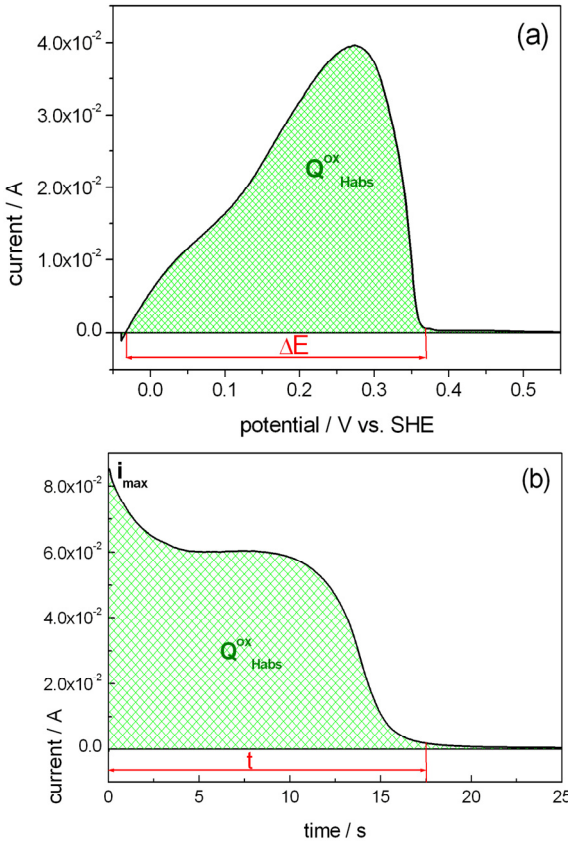

Fig. 6. (a) Voltammogram (scan rate 0.01 V s^{-1}) and (b) chronoamperogram (polarization at 0.45 V) recorded during hydrogen desorption from a Pd/RVC electrode after saturation with hydrogen at –0.05 V in 0.5 M H_2SO_4 at 25˚C. Parameters used in Eqns. 1-4 are indicated.

Additionally, maximum specific power accessible during hydrogen extraction can be calculated from the maximum value of hydrogen oxidation current (i^{ox}_{max}), i.e. at the very beginning of hydrogen extraction in a chronoamperometric experiment (see Fig. 6b):

$$P_{max} = [i^{ox}_{max} \cdot (E_{abs} - E_{des})] / m_M \qquad (4)$$

The calculations of specific pseudocapacitance, power and energy have been performed for hydrogen-saturated limite volume electrodes (thickness ca. 1 micrometer) of Pd and its alloys (Pd-Pt, Pd-Au and Pd-Rh) at various temperatures (10-55˚C). These results for room temperature (25°C) are shown in Fig. 7. It is visible that for Pd-rich Pd-Rh alloys the specific pseudocapacitance is higher than that for pure Pd, reaching a maximum for 88-95% Pd. For these alloy compositions the pseudocapacitance is by ca. 40-50% greater than for pure Pd. The increase in pseudocapacitance for Pd-rich Pd-Pt alloys is smaller than for Pd-Rh alloys and after a weaker maximum (pseudocapacitance by up to 25% greater than for Pd) for ca. 90-95% Pd, the capacitance markedly drops for lower Pd contents. In the case of Pd-Au alloys a monotonic capacity loss with increasing Au bulk content is observed.

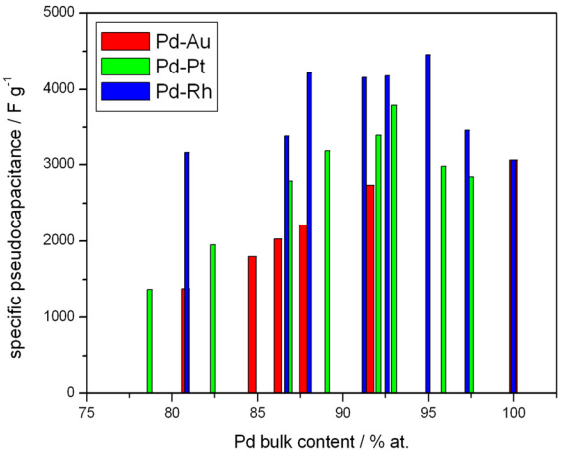

Fig. 7. Influence of alloy composition on specific pseudocapacitance (per mass of electroactive material) of hydrogen-saturated Pd alloys with Au, Pt and Rh in 0.5 M H_2SO_4 at 25˚C.

The influence of alloy bulk composition on the values of specific power and energy (per mass of the deposit) for Pd alloys with Au, Pt or Rh is presented in Figs. 8 and 9. It is demonstrated that for Pd-rich Pd-Pt alloys both average and maximum values of specific power exceed those for pure Pd, with a maximum corresponding to Pd bulk content around 90%. For these alloy compositions the specific power is markedly higher (ca. by 70%) than for pure Pd. For other alloys average specific power is not higher than for Pd. However, for Pd-Rh alloys the values of maximum specific power are intermediate between those for Pd and Pd-Pt alloys, with a maximum between 90 and 95% Pd. The values of specific energy decrease with increasing content of all the alloying metals.

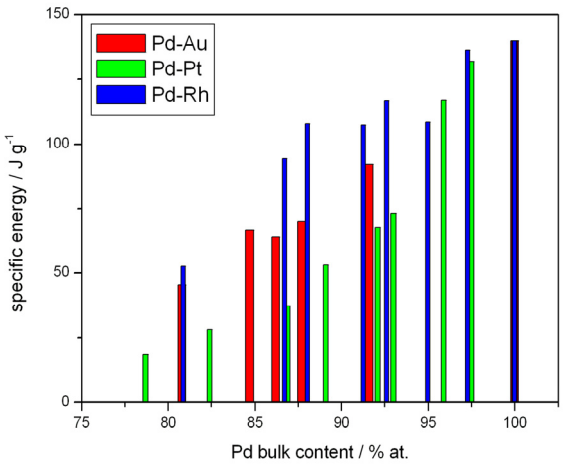

Fig. 8. Influence of alloy composition on specific energy (per mass of electroactive material) of hydrogen-saturated Pd alloys with Au, Pt and Rh in 0.5 M H_2SO_4 at 25˚C.

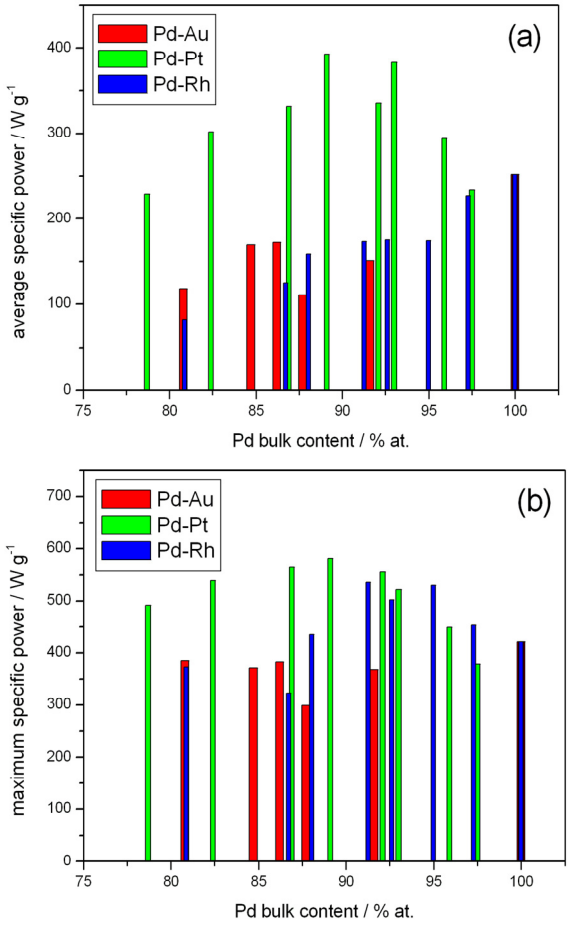

Fig. 9. Influence of alloy composition on: (a) average specific power, (b) maximum specific power (per mass of electroactive material) of hydrogen-saturated Pd alloys with Au, Pt and Rh in 0.5 M H_2SO_4 at 25˚C.

For the characteristic of a real charging/discharging system working as a supercapacitor the mass of a carrier has to be taken into account. In earlier papers [17,18] we reported on the electrochemical behavior of Pd and Pd-Rh (92-97% Pd in the bulk) layers deposited on reticulated vitreous carbon (RVC). This material has been widely described in the literature as a promising electrode material with possible applications in electrochemical power sources [23-27]. In our experiments the metal/alloy layers of a thickness of 0.6-1.0 μm were deposited on RVC with 20 ppi (pores per inch) porosity grade. Fig. 10 shows SEM image of the RVC substrate covered with a Pd-Rh alloy deposit.

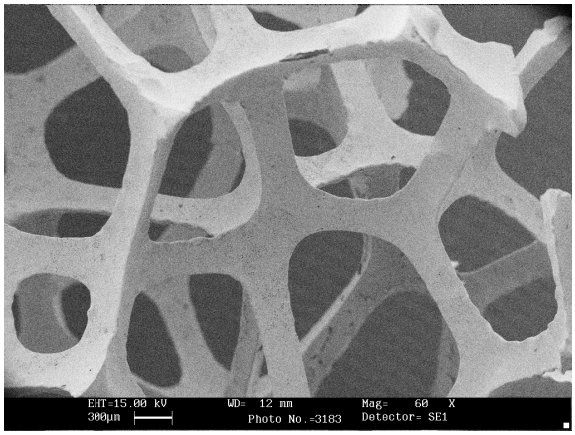

Fig. 10. RVC covered with a Pd-Rh alloy (97% Pd) layer.

The experimental values found in our studies [8-10] were in the range 240-430 F g^{-1} for Pd and up to 540 F g^{-1} for Pd-Rh alloys (97% Pd in the bulk) deposited on RVC. This tendency is consistent with the data presented in Fig. 6. It is noteworthy that the values of specific pseudocapacitance for hydrogen-saturated Pd-based systems are comparable with the data reported for supercapacitors based on reversible insertion of atomic species into bulk solid electrodes, e.g. polymers or metal oxides, and higher than the values typical of double layer electrochemical capacitors [12-15]. The average values of specific power were ca. 3 W g^{-1} for Pd/RVC and ca. 2 W g^{-1} for Pd-Rh/RVC [18], while maximum specific power reached 6 W g^{-1} In the case of Pd and Pd-Rh deposits on RVC the values of specific energy reached ca. 80 J g^{-1}.

Data presented in Figs. 7-9 lead to the conclusion that hydrogen-saturated Pd-rich (in the range of 85-95% Pd in the bulk) Pd-Pt and Pd-Rh alloys are promising electrode materials to be utilized in superccapacitors. Both these systems are characterized by higher pseudocapacitance and maximum specific power with respect to the Pd-H system. Additionally, Pd-Pt alloys exhibit also higher average specific power as compared to Pd. When these alloys are deposited on RVC substrate, their characteristics are comparable with those typical of supercapacitors utilizing various redox reactions.

Acknowledgements

This work was supported by the European Commission through HydroNanoPol (UE 032517) – a project of the 6th Framework Programme of the European Union awarded for the years 2006-2009.

References

1. F. A. Lewis, The palladium/hydrogen system, Academic Press, New York 1967.
2. J. Kleperis, G. Wójcik, A. Czerwiński, J. Skowroński, M. Kopczyk, M. Bełtowska-Brzezińska, J. Solid State Electrochem. 5 (2001) 229-249.
3. D. Linden, T.B. Reddy, Handbook of Batteries, third ed., McGraw-Hill, New York, 2002.
4. B. Sakintuna, F. Lamari-Dankrim, M. Hirscher, Int. J. Hydrogen Energy 32 (2007) 1121-1140.
5. P. Piela, Z. Rogulski, M. Krebs, E. Pytlik, M. Schmalz, J. Dłubak, M. Karwowska, A. Gumkowska, A. Czerwiński, Journal of The Electrochemical Society, 157 (3) (2010) A254-A258.
6. Z. Rogulski, J. Dłubak, M. Karwowska, M. Krebs, E. Pytlik, M. Schmalz, A. Gumkowska, A. Czerwiński, Journal of Power Sources 195 (2010) 7517–7523.
7. Yuan, N. Xu, J. Appl. Electrochem. 31 (2001) 1033.
8. X. Tuan, N. Xu, J. Alloys Compd. 316 (2001) 113–117.
9. J. Chen, S.X. Dou, D.H. Bradhurst, H.K. Liu, Int. J. Hydrogen Energy 23 (1998) 177–182.
10. S. Majorowski, B. Baranowski, J. Phys. Chem. Solids 43 (1982) 1119.
11. L. Schlapbach, A. Züttel, Nature 414 (2001) 353-358.
12. Y. Zhang, H. Feng, X. Wu, L. Wang, A. Zhang, T.Xia, H. Dong, X. Li, L. Zhang, Int J Hydrogen Energy 34 (2009) 4889-4899.
13. V. V. N. Obreja, Physica E 40 (2008) 2596-2605.
14. R. A. Huggins, Solid State Ionics 134 (2000) 179-195.

15. C. D. Lokhande, D.P. Dubal , O.-S. Joo, Current Appl. Phys. 11 (2011) 255-270.
16. A. Czerwiński, M. Łukaszewski, A. Żurowski, Patent RP 204948.
17. A. Czerwiński, M. Łukaszewski, A. Żurowski, H. Siwek, S. Obrębowski, J. New Mat. Elect. Syst. 9 (2006) 419-429.
18. M. Łukaszewski, A. Żurowski, A. Czerwiński, J. Power Sources 185 (2008) 1598-1604.
19. M. Łukaszewski, A. Żurowski, M. Grdeń, A. Czerwiński, Electrochem. Commun. 9 (2007) 671-676.
20. A. Żurowski, M. Łukaszewski, A. Czerwiński, Electrochim. Acta 51 (2006) 3112-3117.
21. K. Hubkowska, M. Łukaszewski, A. Czerwiński, Electrochim. Acta 56 (2011) 2344-2350.
22. K. Hubkowska, M. Łukaszewski, A. Czerwiński, Electrochim. Acta 56 (2010) 235-242.
23. A. Czerwiński, M. Dmochowska, M. Grdeń, M. Kopczyk, G. Wójcik, G. Młynarek, J. Kołata, J. M. Skowroński, J. Power Sources 77 (1999) 28-33.
24. J. Wang, Electrochim. Acta 26 (1981) 1721-1726.
25. J. M. Friedrich, C. Ponce-de-León, G. W. Reade, F. C. Walsh, J. Electroanal. Chem. 561 (2004) 203-217.
26. Z. Rogulski, W. Lewdorowicz, W. Tokarz, A. Czerwiński, Pol. J. Chem. 78 (2004) 1357.
27. A. Czerwiński, Z. Rogulski, S. Obrębowski, H. Siwek, I. Paleska, M. Chotkowski, M. Łukaszewski, J Appl. Electrochem. 39 (2009) 559-567.

Electrochemical capacitors for quick harvesting energy

Elżbieta Frąckowiak, Krzysztof Fic, Mikołaj Meller, Grzegorz Lota
Poznan University of Technology, Institute of Chemistry and Technical Electrochemistry, Piotrowo 3, 60-965 Poznan, Poland

Electrochemical capacitors store the energy mainly by fast charge accumulation in electrical double layer. Typical electrostatic nature of this process allows their charging and discharging in a very short time and over thousands of cycles [1]. Because they are characterised by high power rates they are successfully applied in such devices as Hybrid Electric Vehicles (HEV) where they serve as power delivery devices during acceleration or rise covering, in planes as emergency systems and in city buses or trams as alternative and efficient power sources [2]. Additionally, electrochemical capacitors can be easily discharged at high current regimes (even at 50 A g^{-1}), therefore, they can serve as great protectors for other power sources like batteries, e.g. in mobile devices such as laptops, cameras or mobile phones. Their main disadvantage is relatively low energy density, especially in comparison to batteries. On the other hand, batteries are characterised by relatively poor power rates, have a short cycle life and discharging by high current regimes is for batteries very harmful and makes their cycle life significantly shorter.

Energy released by electrochemical capacitors can be expressed by the following formula

$$E = 0.5CU^2 \qquad (1)$$

where C is capacitance and U is the operational voltage range. Therefore, supercapacitor energy density improvement can be realized by two approaches, i.e. the capacitance enhancement or operational voltage range increase.

The activated carbons with a well developed specific surface area (S_{BET} 1000-2500 m^2 g^{-1}), being most frequent electrode material for supercapacitors because of their satisfying electrochemical properties [3-4], reveal the capacitance about 150-200 F g^{-1}. This value is related with the total charge amount accumulated at the electrode/electrolyte interface [5]. Because there is no great discrepancy in capacitance values of carbon electrodes with different surface area, it might suggest that capacitance is independent of the electrode area estimated directly from nitrogen sorption. On the other hand, it rightly suggests that a significant part of this surface area is quite inert in the charge storage process. Probably, hydrophobic character of carbon surface and poor wettability by electrolyte is responsible for such situation. Hence, the improvement of the electrode wettability by surfactant addition to electrolyte [6] is a reasonable pathway for more efficient usage of the total carbon surface. Slight enhancement of wettability is observed when oxygen functional groups are introduced onto carbon surface, however, one might conclude that increase in capacitance is mainly caused by some redox reactions between functional groups and electrolyte [7]. Apart from oxygen functional groups onto carbon surface, improvement of carbon electrodes wettability may be realized by surfactant addition to electrolyte solution. It is well known that water solutions have relatively high surface tension, mainly due to strong interactions between water molecules. Surfactants, with their amphiphilic properties arising from the molecule structure, i.e., hydrophilic 'head' and hydrophobic 'tail', can effectively reduce high surface tension. Hence, they enable better electrolyte penetration into electrode structure, therefore, electrode/electrolyte interface can be significantly developed. Considering potential industrial application, well-known, cheap and widely applied compounds like sodium or lithium dodecyl sulphates, tetrapropylammonium bromide and iodide as well as Triton® X-100 were selected for further experiments. The molecule shape and dimensions are given in Figs. 1,2. The capacitance properties and other supercapacitor characteristics of the electrodes operating in alkaline (6 mol L^{-1}) electrolytes modified by surfactant addition were studied by galvanostatic cycling at current densities from 0.2 to 50 A g^{-1}, cyclic voltammetry at voltage scan rates from 5 to 100 mV s^{-1} and electrochemical impedance spectroscopy in frequency range from 1 mHz to 100 kHz using VMP3/Z Biologic, France.

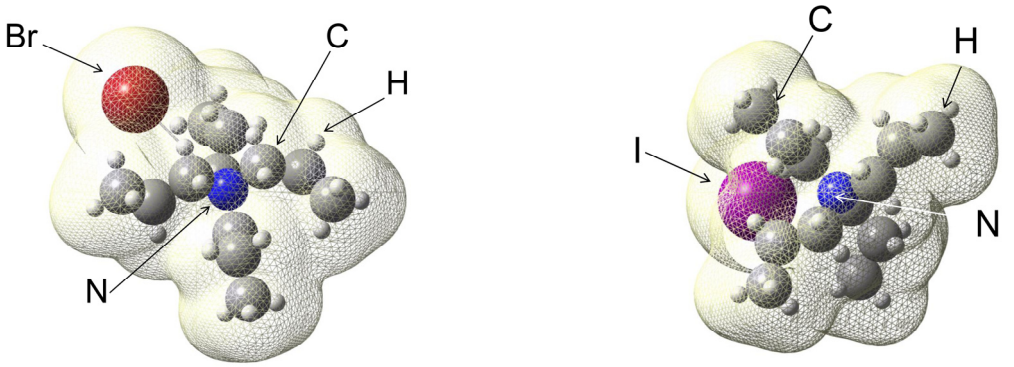

(A) (B)

Fig. 1. Molecular structure of (A) tetrapropylammonium bromide (TPAB) with a quasi-spherical shape 1.232 nm and (B) tetrapropylammonium iodide (TPAI) with diameter 1.521 nm.

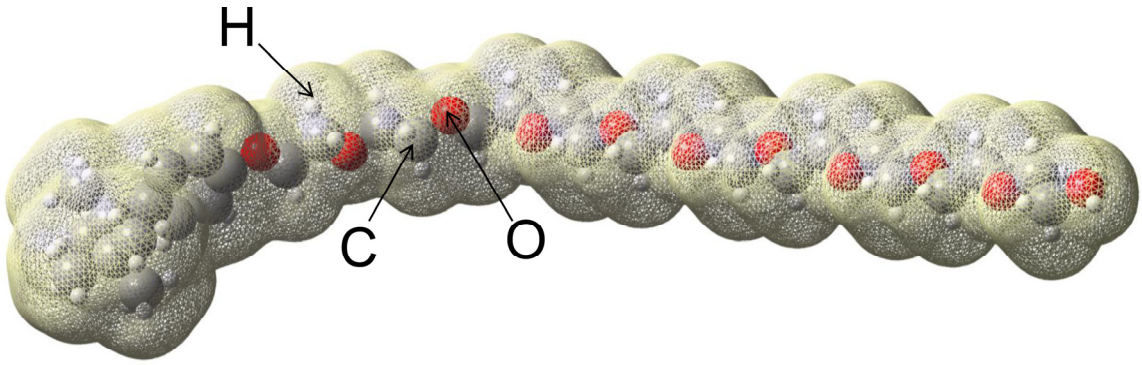

Fig. 2. Molecular structure of Triton X-100 with diameter of 0.525 nm and length of 3.621 nm.

Two-electrode capacitors were assembled in a Swagelok® system with pellets of comparable mass. Each electrode was composed of 85 wt. % of carbon, fully characterized in Ref. [8]. The investigations were performed in alkaline (6 mol L^{-1} KOH) solutions using gold current collectors, just to avoid corrosion and to preserve comparable experimental conditions. The capacitance vs. current load dependence, obtained by galvanostatic charging/discharging of the capacitor in current density range 0.2 - 50 A g^{-1} is shown in Fig. 3. In a range of small discharging current densities, i.e. 0.2 - 2 A g^{-1} no significant difference between pure electrolyte and those modified by surfactant addition is observed. The capacitance revealed by carbon electrode operating in 6 mol L^{-1} is placed in range 160-180 F g^{-1} for the smallest discharging current densities (0.2 Ag^{-1}) and is almost independent on applied type of surfactant. Some difference is observed at 5 A g^{-1} discharging current density, capacitance of carbon is almost the same for pure KOH solution and those modified by SDS while slightly lower values are observed for KOH solution with TPAB or LDS. Significantly higher (ca. 20%) capacitance values are observed both for KOH electrolyte with Triton® X-100 and TPAI additive. Furthermore, for those electrolytes in higher current densities, i.e. above 10 A g^{-1} capacitance remains almost stable, being still above 100 F g^{-1} even for extremely high current density like 50 A g^{-1}, whereas for pure KOH and those modified by other surfactants is determined to be ca. 60 F g^{-1}. For capacitor operating in alkaline solution modified by Triton® X-100 it is possible to operate in voltage range higher than 1.23 V. Cyclic voltammograms shown in Fig. 4 clearly prove that this electrolyte is stable and not decomposed even at 1.6 V. The explanation of this intriguing phenomenon consists in the fact that electrolyte with lower surface tension probably creates a thin film on pore walls and onto carbon surface in electrode bulk, therefore, the pressure prevailing in not fulfilled spaces in pores exert to electrolyte film and is too high to allow hydrogen or oxygen evolution. Stability of electrolyte was investigated during typical cycling and significant decrease of capacitance was not observed for ca-

pacitor operating at 1.6 V after 5,000 cycles of galvanostatic charging/discharging process. Unfortunately, for other surfactants positive influence on operational voltage range was not achieved.

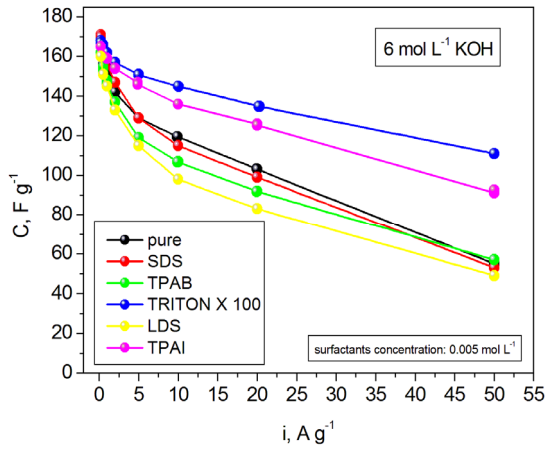

Fig. 3. Capacitance of carbon operating in 6 mol L^{-1} KOH without and with surfactants at different current loads.

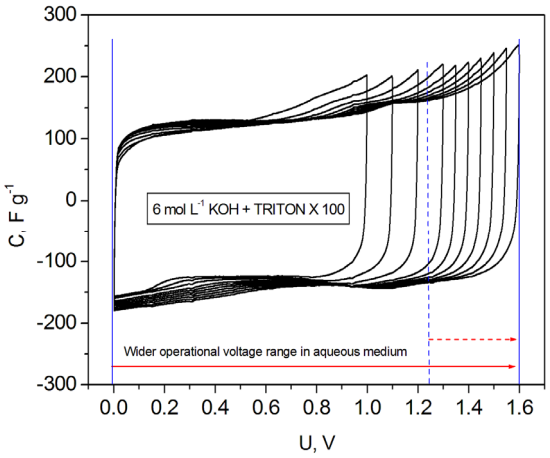

Fig. 4. Cyclic voltammetry for capacitor operating in 6 mol L^{-1} KOH with non-ionic surfactant in wider voltage range. Scan rate 10 mV s^{-1}, step wise 100 mV.

Enhancement of the capacitance value could be also realized by providing additional charge originating from faradaic reactions which can increase the capacitance of the electrodes (called pseudocapacitance) even by one order of magnitude. Electrode materials providing pseudocapacitance are mainly composed of transition metal oxides such as MnO_2, Fe_3O_4, InO_2, SnO_2, V_2O_5 or RuO_2 and may be assembled both as pure materials in asymmetric configuration e.g. with carbon electrode [9-13] as well as in transition metal oxide/carbon material composites [14] in typical symmetric configuration which is much more promising for commercial application, mainly due to the relatively high price of pure compounds, especially in case of InO_2 or RuO_2 [15]. Other promising materials providing pseudocapacitance are carbon materials enriched by heteroatoms like oxygen or nitrogen [16]. In these materials pseudocapacitance originates from redox reactions of functional groups as well as from local changes in electron density of carbon matrix being enriched by heteroatom. The nitrogen presence has a profitable effect on the capacitance values [11, 17], as well as for good capacitor performance at drastic current loads. However, an excess of nitrogen (presumably over 15%) will definitively aggravate the conducting properties, and in turn, the capacitance characteristics and supercapacitor cyclability. The form in which N participates in the carbon network is especially important. It seems that the effect of $-NH_2$ groups outside of the matrix, with N chemically bound to the carbon network ("chemical nitrogen"), will be of less importance and most probably such groups could block the entrance to the pores. Nitrogen substituted to carbon ("lattice nitrogen") in the periphery as pyridinic groups could play some useful role according to the reversible redox reaction shown in the scheme. The donor properties are responsible for filling the conduction band by electrons, in turn, more ions can be sorbed in the electrical double layer, especially for composites where carbon is optimally substituted by nitrogen. Some trials were undertaken to correlate N content in nitrogenated carbons with the electron density states from molecular quantum calculation. The energy gap, i.e., a difference between Highest Occupied Molecular Orbital (HOMO) and Lowest Unoccupied Molecular Orbital (LUMO) is tightly connected with a conductivity of material. The calculation of the gap between conduction and valence band was based on the Hartree-Fock method and the Koopmans theory. A few different compositions was assumed with varying N% content. The results showed that for the compositions with nitrogen exceeding 14% N, the gap starts to increase. Model of carbon matrix with pyridinic nitrogen of 11.88% N is shown in Fig. 5. From molecular calculation the energy gap is equal to ca. 4 eV. HOMO and LUMO are presented in Fig. 5 as transparent, colored surfaces. The orbitals being charged positively are colorized in red, the orbitals being charged negatively, are colorized in green.

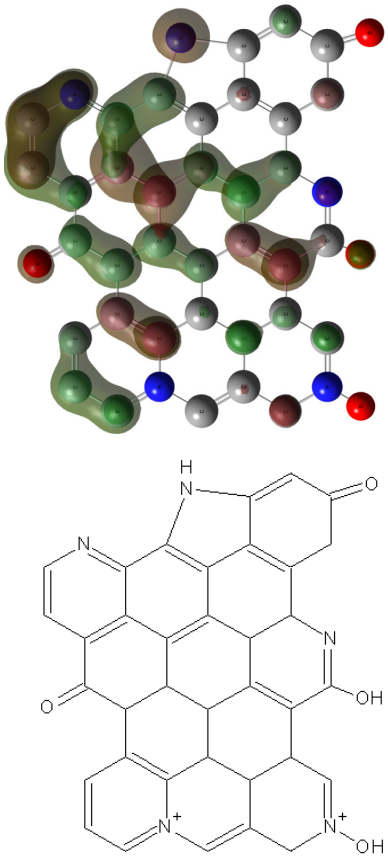

Fig. 5. Model of carbon matrix with pyridinic nitrogen of 11.88% N.

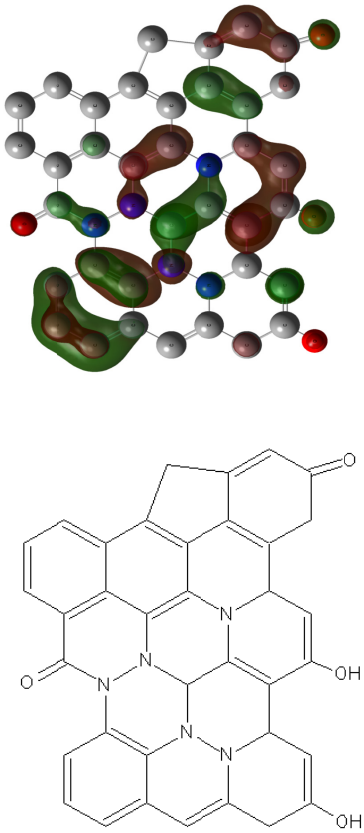

Fig. 6. Model of carbon matrix with quaternary nitrogen.

The difference of the energies between HOMO and LUMO, termed the band gap, may be interpreted as material ability to electrical conductivity. However, not only the energy of band gap can inform about this property – the shape and conformation of these orbitals are also very important. Nitrogen as whole but also type of nitrogen functionality strongly influenced and changed the primary conformation of HOMO/LUMO structure in investigated material. Generally, more developed the HOMO/LUMO structure in nitrogenated carbons, in a big simplicity, makes the electron/current flow much easier. The effect of different N functionality is shown in Fig. 6 where the nitrogen content is very close (11.92%) but more quaternary nitrogen is present in the carbon matrix. Here, the HOMO-LUMO gap is smaller than for pyridinic groups and better conductivity is expected. On the other hand, for maximal amount of nitrogen, i.e., 25.8 % N, the band gap drastically increases. Theoretical prediction matches with experimental data, the loss of conductivity has been proved by electrochemical methods. For further information and experimental details please see Ref. [11].

Inventive approach to pseudocapacitance was reported by our team and fully presented in Ref. [18-19]. In this case additional charge is provided both by electrode bulk and by electrolyte solution. These capacitors are based on iodide/iodine redox systems. Apart from electrostatic accumulation, additional charge is provided from following reactions:

$$3\ I^{-1} \leftrightarrow I_3^{-1} + 2e^- \quad (2)$$

$$2\ I^{-1} \leftrightarrow I_2 + 2e^- \quad (3)$$

$$2I_3^{-1} \leftrightarrow 3I_2 + 2e^- \quad (4)$$

$$I_2 + 6\ H_2O \leftrightarrow 2\ IO_3^{-1} + 12\ H^+ + 10\ e^- \quad (5)$$

Exceptional electrochemical behavior of carbon/iodide interface has been demonstrated and successfully used in supercapacitor application. This efficient charge storage is based on specific sorption of iodide ions as well as stable reversible redox reactions connected with various possible oxidation states of iodine from -1 to +5. An intriguing effect of iodide ions has been observed for positive electrode operating in a narrow range of potential and giving extremely high capacitance

values exceeding 1840 F g^{-1}. As opposed to typical pseudocapacitance effects, which are often characterized by some diffusion limitations and observed only at moderate regimes, our two-electrode system can be loaded until 50 A g^{-1} supplying still 125 F g^{-1}. Amazing capacitance of carbon/iodide interface has also been confirmed during long-term cycling (over 10 000 cycles). For the first time, such an innovative electrochemical system was successfully used for supercapacitor performance. The iodide ions play a useful dual role, i.e. electrolytic solution with a good ionic conductivity as well as a source of pseudo-capacitive effects. The application of this novel carbon/iodide electrochemical system is very original and it is a significant breakthrough in supercapacitor development. This bi-functional iodide electrolyte, which ensures ionic conductivity and supplies pseudocapacitive effects, has great advantages because it is inert, neutral and environmentally friendly. A good reversibility of different iodine redox couples allows reaching perfect cycling. It is necessary to stress that our system is not yet fully optimized, even though striking values 10 times exceeding typical capacitance values are observed for the positive electrode, the negative electrode imposes the final capacitor performance. It seems that asymmetric configuration with a different negative electrode should be considered. Undoubtedly, practical application of these stable reversible reactions based on iodide is relevant for supercapacitor progress.

Another possibility of supercapacitor energy increase is to apply organic electrolyte based on acetonitrile or ionic liquids. These electrolytes remain stable even in operational voltage range 0.0 – 4.0 V [20-22]. However, ionic liquids and other organic electrolytes are usually characterised by poor conductivity and high viscosity [23] which significantly hinders their penetration in the electrode structure and aggravates the charge propagation. Hence, the capacitance of the capacitors operating in such electrolytes usually does not exceed 100 F g^{-1} per electrode and they are characterised by poor power rates. On the other hand, applying protic ionic liquids, which allow occurring the quinine / hydroquinone surface redox reactions [24], slightly higher capacitance values and better power rates may be achieved [25]. Anyway, organic electrolytes are usually environment-unfriendly and the price of the capacitors operating in organic medium is still relatively high, due to demanding and complicated assembling process.

From this point of view, aqueous medium seems to be much more promising because it is cheap and ecological electrolyte. However, operational voltage range of capacitors operating in such electrolytes is thermodynamically limited to 1.0 V due to water decomposition at 1.23 V. Depending on electrode material, mainly applied aqueous electrolytes are 1 mol L^{-1} H_2SO_4 and 6 mol L^{-1} KOH solutions [26-27]. Contrarily to organic electrolytes, they are characterised by high conductivity and low viscosity, accompanied by good charge propagation and power rates of capacitor. Unlike pseudocapacitive systems, where fast transfer of ions into electrode/electrolyte interface is needed for quick redox processes, simple charging and discharging of electrical double layer in EDLCs does not need very high ion mobility. When porous structure of the electrode is well-saturated by electrolyte, ions already located on electrode/electrolyte interface are attracted and pushed off from electrode on a small distance. Hence, high mobility might aggravate fast and efficient charge propagation. Results obtained for three alkali metal (Li, Na, K) sulphate solutions proved clearly this assumption. Molecule dimensions, both for cations and anion are presented in Fig. 7. For relatively slow scan rate (1 mV s^{-1}) the difference in charge propagation is not significant for all three solutions, however, the capacitance value is the highest in case of Li_2SO_4 (170 F g^{-1}) when compared to 105 F g^{-1} for Na_2SO_4 and 78 F g^{-1} in case of K_2SO_4; at moderate scan rate (10 mV s^{-1}) Li_2SO_4 still seems to be the most promising electrolyte, taking into account charge propagation and capacitance value (147 F g^{-1}). At fast scan rate (100 mV s^{-1}), quite resistive character of voltammograms suggests some difficulties in charge propagation, anyway, the highest value of capacitance - 76 F g^{-1} is still preserved for Li_2SO_4, being significantly higher than for Na_2SO_4 (28 F g^{-1}) and K_2SO_4 (23 F g^{-1}). Such promising results obtained for 1 mol L^{-1} Li_2SO_4 solution as electrolyte for carbon|carbon electrochemical capacitor induced to further investigation. Among five values: 0.1, 0.5, 1.0 1.5 and 2.5 mol L^{-1}, the concentration 1 mol L^{-1} seems to be the most effective one. It might be a little bit contradictory taking into account conductivity vs. molar concentration dependence, where maximum of conductivity value is found to be for 2.5 mol L^{-1},

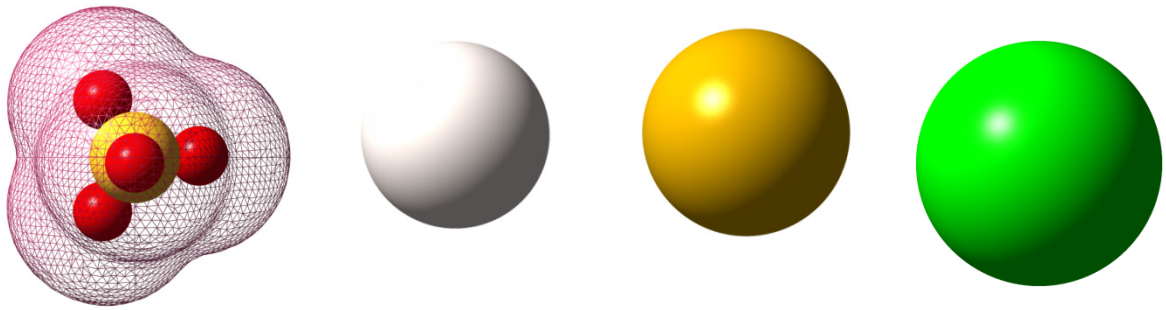

Sulphate anion, SO_4^{2-}	Lithium cation, Li^+	Sodium cation, Na^+	Potassium cation, K^+
Hydrated: 7.33 Å	Hydrated: 3.81 Å	Hydrated: 3.59 Å	Hydrated: 3.34 Å

Fig. 7. Ion shape and dimensions in aqueous solutions. The scale between pictures is not preserved; the mesh around sulphate anion represents the molecular orbitals.

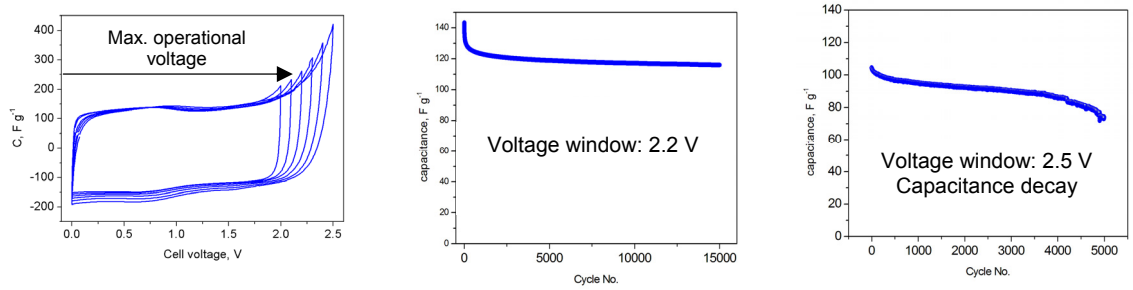

Fig. 8. Cyclic voltammetry at scan rate of 10 mV s^{-1} with a gradual 100 mV shift (A) and cyclability (±1 A g^{-1}) at voltage range of 2.2 V (B) and 2.5 V (C). Electrolyte solution: 1 mol L^{-1} Li_2SO_4.

however, it was proven that increasing conductivity not always improves electrochemical behaviour of capacitors. In this case one should take into account a lot of specific interactions between ions, ions and solvent and solvent-solvent molecules, some sterical hindrances, e.g., solvated structures of lithium cations, related with high solution concentrations that can aggravate capacitor performance. The highest capacitance values (e.g. 170 F g^{-1}) and charge propagation, observed for 1 mol L^{-1} confirms such assumptions. Additionally, for more diluted solution (0.1 and 0.5 mol L^{-1}, some resistive character of cyclic voltammograms can be observed, but it is related mainly with poor conductivity of the solution. Capacitors operating with these solutions revealed also lower capacitance (50 F g^{-1} and 62 F g^{-1} for 0.1 and 0.5 mol L^{-1}, respectively). On the other hand, resistive character of cyclic voltammograms for higher concentrations (1.5 and 2.5 mol L^{-1}) might be explained by discussed sterical hindrance caused by hydrated molecules. Additionally, it is worth to note, that capacitance values and voltammogram courses are almost the same for these two higher concentrations. It proves that electrode/electrolyte interface is saturated with ions and increasing concentration does not cause any positive effect. For diluted solutions (0.1 and 0.5 mol L^{-1}) capacitance values are significantly lower than for more concentrated solutions. At smal discharging current density, i.e., 200 mA g^{-1}, capacitor operating in 0.1 mol L^{-1} revealed the capacitance of 106 F g^{-1}; slightly higher capacitance values, i.e., 114 F g^{-1} were observed for 0.5 mol L^{-1}. For higher electrolyte concentrations capacitance values in low current density range (200 mA g^{-1} - 10 A g^{-1}) were very similar what suggests that above 1 mol L^{-1} electrode/electrolyte interface is saturated with ions. Anyway, 1 mol L^{-1} Li_2SO_4 solution as electrolyte for electrochemical capacitor seems to be the most promising one, with satisfying capacitance values, i.e., 180 F g^{-1} for 200 mA g^{-1}, about 100 F g^{-1} at 10 A g and 80 F g^{-1} at 50 A g^{-1} accompanied with a good charge propagation.

Taking into account that operational voltage range is one of the crucial and most important factor influencing energy released by capacitor, performance at wide voltage seems to be very promising. To confirm our assumption, cyclic voltammetry and galvanostatic cycling at extended voltage were applied for capacitor operating in 1 mol L^{-1} Li_2SO_4 solution. Cyclic voltammetry performed at scan rate of 10 mV s^{-1} and voltage shift of 100 mV in the range from 0.8 V to 1.6 V did not reveal any significant distortion of voltammogram even at 1.6 V (Fig. 8). It means that electrolyte is not being decomposed. Further investigations have been performed to determine a maximal voltage range for capacitor operating in neutral aqueous medium, i.e., 1 mol L^{-1} Li_2SO_4 solution. This value reaches 2.2 V.

In conclusion, new trends for enhancement of capacitor performance have been shown:

- ✓ Positive effect of some surfactants in electrolytic solution, e.g. Triton
- ✓ Significant increase of capacitance through pseudocapacitance effects from heteroatoms (N, O) incorporated into carbon matrix
- ✓ Electrolytic solution based on halides (e.g. iodides) as a source of enormous capacitance
- ✓ Extension of operating voltage in neutral medium, e.g. 1 mol L^{-1} Li_2SO_4 solution.

References

1. J.R. Miller, A. Burke, *Electrochemical Society Interface*, 2008, 17, 53.
2. A. Burke, *International Journal of Energy Research*, 2010, 34, 133.
3. E. Frackowiak, *Physical Chemistry Chemical Physics,* 2007, 9, 1774.
4. M. Heon, S. Lofland, J. Applegate, R. Nolte, E. Cortes, J.D. Hettinger, P.-L. Taberna, P. Simon, P. Huang, M. Brunet, Y. Gogotsi, *Energy and Environmental Science*, 2011, 4, 135.
5. A.B. Fuertes, F. Pico, J.M. Rojo, *Journal of Power Sources*, 2004, 133, 329.
6. K. Fic, G. Lota, E. Frackowiak, *Electrochimica Acta*, 2010, 55, 7484.
7. D. Pech, D. Guay, T. Brousse, D. Bélanger, *Electrochemistry Solid-State Letters*, 2008, 11 A202.
8. G. Lota, T.A. Centeno, E. Frackowiak, F. Stoeckli, *Electrochimica Acta*, 2008, 53, 2210
9. T. Brousse, M. Toupin, D. Bélanger, *Journal of Electrochemical Society*, 2004, 151, A614.
10. X. Liu, P.G. Pickup, *Energy and Environmental Science*, 2008, 1, 494.
11. G. Lota, K. Fic, E. Frackowiak, *Energy and Environmental Science, 2011,* 4, 1592.
12. A. Malak, K. Fic, G. Lota, C. Vix-Guterl, E. Frackowiak, *Journal of Solid State Electrochemistry*, 2010, 14, 811.
13. Ch. Peng, S. Zhang, X. Zhou, G. Z. Chen, *Energy and Environmental Science, 2010,* 3, 1499.
14. A. Malak-Polaczyk, C. Vix-Guterl, E. Frackowiak, *Energy and Fuels,* 2010, 24, 3346.
15. F. Pico, J. Ibañez, T.A. Centeno, C. Pecharroman, R.M. Rojas, J.M. Amarilla, J.M. Rojo, *Electrochimica Acta*, 2006, 51, 4693.
16. E.J. Ra, E. Raymundo-Piñero, Y.H. Lee, F. Béguin, *Carbon,* 2009, 47, 2984.
17. G. Lota, E. Frackowiak, *Fuel Cells*, 2010, 10, 848.
18. G. Lota, E. Frackowiak, *Electrochemistry Communications,* 2009, 11, 87.
19. G. Lota, K. Fic, E. Frackowiak, *Electrochemistry Communications*, 2011, 13, 38.
20. C. Arbizzani, M. Biso, D. Cericola, M. Lazzari, F. Soavi, M. Mastragostino, *Journal of Power Sources* 2008, 185, 1575.
21. A. Balducci, R. Dugas, P.L. Taberna, P. Simon, D. Plée, M. Mastragostino, S. Passerini, *Journal of Power Sources,* 2007, 165, 922.
22. P.W. Ruch, D. Cericola, A. Foelske, R. Kötz, A. Wokaun, *Electrochimica Acta*, 2010, 55, 2352.
23. M. Galinski, A. Lewandowski, I. Stepniak, *Electrochimica Acta*, 2006, 51, 5567.
24. M.A. Montes-Moran, D. Suarez, J.A. Menendez, E. Fuente, *Carbon,* 2004, 42, 1219.
25. R. Mysyk, E. Raymundo-Piñero, M. Anouti, D. Lemordant, F. Béguin, *Electrochemistry Communications,* 2010, 12, 414.
26. G. Lota, J. Tyczkowski, R. Kapica, K. Lota, E. Frackowiak, *Journal of Power Sources*, 2010, 195, 7535.
27. K. Jurewicz, R. Pietrzak, P. Nowicki, H. Wachowska, *Electrochimica Acta*, 2008, 53, 5469.

New materials for thermoelectric generators based on PbTe-MnTe and PbTe-CdTe semiconductor alloys and nanocomposites

T. Story, K. Dybko, P. Dziawa, A. Mycielski, A. Szczerbakow, M. Szot
Institute of Physics, Polish Academy of Sciences, al. Lotników 32/46, 02-668 Warsaw, Poland

Abstract

New trends in the field of thermoelectrics are discussed for PbTe-based semiconductor thermoelectric materials exhibiting density of states engineering effects strongly enhancing thermoelectric power (PbMnTe) and spontaneous formation of nano-scale two-phase crystal structures (PbTe-CdTe) – technologically scalable realization of electron crystal - phonon glass concept of new thermoelectric materials.

1. Introduction – current trends in thermoelectricity

The search for new materials for thermoelectric generators is primary driven by the idea to generate electricity using heat lost during the operation of combustion engines and industrial processing. Fuel economy envisioned is about ten percent on a global scale [1-3]. The expansion of thermoelectric devices from the well known niche applications in space missions, autonomous power supplies or Peltier coolers to a broad scale market requires development of new thermoelectric materials with largely improved figure of merit parameter ZT=2-3 [1-3]. Here the parameter $Z=\alpha^2\sigma/\kappa=P_S/\kappa$, where α is the thermoelectric power, σ – the electrical conductivity, κ – the thermal conductivity, and T - the operating temperature of a device. The thermoelectric power factor $P_S=\alpha^2\sigma$ depends on electronic parameters only and determines maximum power generation conditions [4]. In currently used semiconductor thermoelectric devices based on Bi_2Te_3, Si-Ge, $CoSb_3$ or PbTe alloys, the dimensionless thermoelectric figure of merit parameter ZT≈1 in (specific to each material) optimal temperature regime [4]. Due to the usually encountered thermoelectric mismatch between n- and p-type legs of a couple the effective figure of merit parameter of a typical device is even lower ZT_{eff}≈0.5 [4]. This imposes severe limitations to possible applications of semiconductor thermoelectric devices [1-4]. All materials should also comply with increasingly important economic and environmental criteria, e.g. concerning the limited global resources of tellurium [5].

New materials science and physical ideas for better thermoelectrics concern, in particular, already well known thermoelectric materials prepared in novel forms. These are, e.g., bulk nanocomposite materials engineered to suppress heat conduction while preserving good electrical conductivity, the so called electron crystal – phonon glass systems [4, 6-8]. It was also recently demonstrated that using special resonant doping centers one can substantially enhance electronic density of states at the Fermi level [9]. It results in an increase of thermoelectric power factor and energy selectivity of charge carrier scattering processes. The alternative direction is to search for new classes of unconventional thermoelectric materials, like oxides, intermetallic compounds, correlated electron systems or magnetic materials with spin entropy contribution to thermoelectricity.

In nanostructures composed of canonical thermoelectric materials the large increase of the figure of merit parameter Z is expected because of the qualitative changes of electronic density of states in quantum wells, wires, and dots [10,11]. The nanoscale variations of crystal lattice potential in such heterostructures result also in a reduction of their thermal conductivity. Increased Z values were already observed in various low dimensional nanostructures, like quantum wells or coupled semiconductor quantum dot systems of PbTe or Bi_2Te_3 , e.g., [6-11]. The broad scale applications of such structures would, however, critically require the development of proper nanomaterials and industrially scalable manufacturing procedures. A versatile solution to this problem is to exploit self-organization phenomena observed in semiconduc-

tor alloys, e.g., spinodal decomposition of ternary alloys into coherent clusters with varying chemical composition or spontaneous formation of nanoinclusions of second crystalline phase in semiconductor matrix (the case of immiscible materials). Thermodynamic phase diagrams of several thermoelectrically relevant pseudo-binary alloys, with the canonical examples of PbTe-PbS and PbTe-GeTe, reveal the spinodal decomposition regions. In his report we examine PbTe-CdTe pseudo-binary system. It is motivated by the recent discovery [12,13] that PbTe-CdTe heterostructures and nanometer-sized clusters (quantum dots) can be grown in the form of monocrystalline epitaxial multilayers with atomically sharp interfaces.

New materials may also be designed by smart tailoring their electronic and thermal properties, e.g. by increasing the density of electron states in the vicinity of the Fermi level via resonant doping. It results in an increase of thermoelectric power and electrical conductivity. The reduction of thermal conductivity, even below the values expected for an alloy, may be achieved by incorporating in thermoelectric materials special defects or nanoinclusions, which scatter phonons resonantly. In this work, we discuss $Pb_{1-x}Mn_xTe$ semiconductor mixed crystals, a solid solution of the well known thermoelectric IV-VI semiconductor PbTe and a magnetic semiconductor MnTe. Upon increasing Mn concentration, the band structure of PbMnTe changes favorably for its thermoelectric properties [14,15]. An increase of the bandgap and a decrease of the energy separation between the light hole and the heavy hole valence bands results in a large increase of thermoelectric power. It offers the possibility to control the thermoelectric figure of merit parameter ZT and the optimal operating temperature of PbMnTe-based thermoelectric generators. One could even envision the replacement of currently used multi-materials designs for both p- and n-type thermoelectric legs [4] by $Pb_{1-x}Mn_xTe$ alloy with varying composition (Fig. 1 and Fig. 2).

2. PbTe-based new thermoelectric materials

We experimentally verified the applicational potential of $Pb_{1-x}Mn_xTe$ ($x<0.08$) alloys by studying thermoelectric properties of bulk crystals grown from the melt by two techniques: the standard vertical Bridgman method (typical crystal shown in Fig. 3 – upper panel) and the two stage method involving the rapid quenching followed by the long term re-crystallization. The X-ray diffraction (XRD) analysis of the rock salt crystal structure as well as and the energy dispersive X-ray fluorescence (EDXRF) analysis of the chemical composition showed that in the PbMnTe crystals grown by both methods the distribution of Mn content along the ingot reveals only a moderate segregation effect. In the range of studied Mn content $x\leq0.1$ no second crystalline phase inclusions were detected.

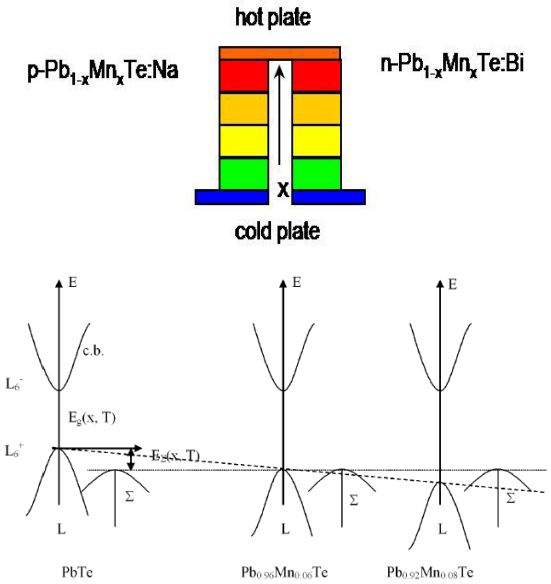

Fig. 1. Upper panel illustrates the concept of a p-n thermoelectric couple employing only n- and p-type doped $Pb_{1-x}Mn_xTe$ alloys with Mn content x varying in order to optimize thermoelectric performance over a broad temperature range. Lower panel present a model of Mn concentration dependence of band structure of $Pb_{1-x}Mn_xTe$ crystals.

In PbMnTe crystals Mn 2+ ions substitute Pb 2+ ions at cation sites and remain electrically inactive. The usually observed p-type conductivity of these crystals is due to native defects (Pb vacancies). By doping with Bi or I (for n-type) and with Na or Ag (for p-type) as well as by controlling the crystal stoichiometry with post-growth annealing both p- and n-type $Pb_{1-x}Mn_xTe$ ($x\leq0.08$) crystals were successfully prepared with carrier concentration in the range 10^{18} – $2*10^{19}$ cm^{-3}. In p-type PbMnTe crystals we observed very high thermoelectric power at room temperature α=300-600 μV/K. This was not observed for n-type crystals, which show thermoelectric power as expected from the, so called, Pisa-

renko plot for reference n-PbTe crystals. This clearly points to the important differences between the PbMnTe conduction and valence band. In the latter a remarkable, Mn-content dependent, influence of heavy hole band is expected (Fig. 1 and Fig. 2). These effects, originally proposed by us for $Pb_{1-x}Mn_xTe$ were recently experimentally found to dramatically improve high temperature thermoelectric parameters of $PbTe_{1-x}Se_x$ semiconductor alloys [16]. Applying the Harman method (based on differences between electrical resistivity measured in dc and ac regimes) we experimentally found the maximal value of the parameter ZT=0.7 for both n- and p-type PbMnTe crystals with Mn content x=0.05-0.06 at temperatures about T=400-500 K (Fig. 4).

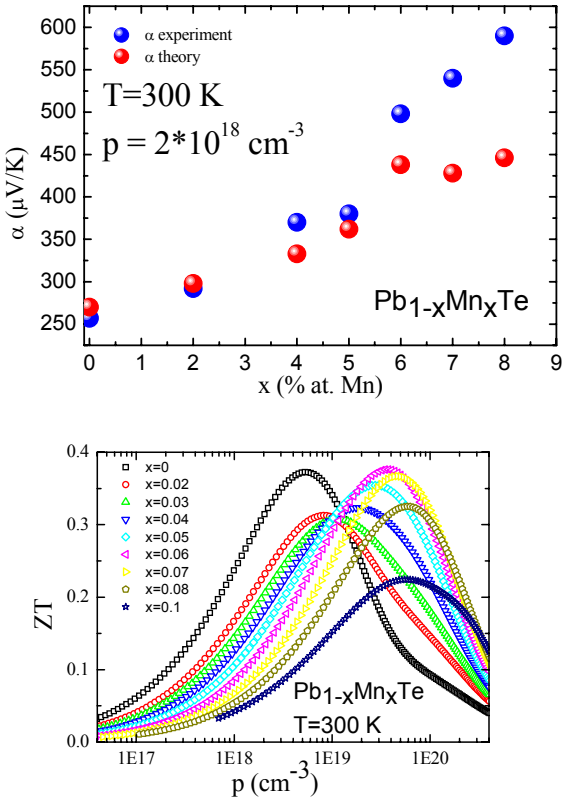

Fig. 2. Experimentally observed strong increase of thermoelectric power in p-PbMnTe alloys and its theoretical explanation based on the band structure model presented in figure 1 (upper panel). Calculations of conducting carriers and Mn content dependence of the thermoelectric figure of merit parameter ZT at room temperature (lower panel).

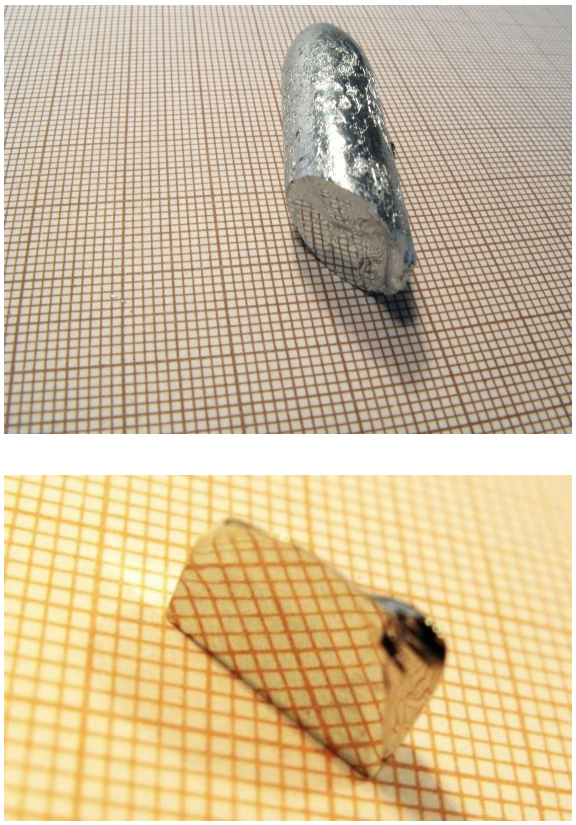

Fig. 3. Examples of thermoelectric bulk crystals grown in Institute of Physics PAS by various methods. Upper figure: $Pb_{1-x}Mn_xTe$:Na crystal (x=0.01) grown by the Bridgman method (shown is about ½ of the total length of a typical ingot). Lower figure: $Pb_{1-x}Cd_xTe$ (x=0.01) monocrystal grown by self-selecting physical vapor transport method with mirror-like natural (100) crystal facets.

The practically total immiscibility [12,13,17] and excellent matching of cubic lattice parameters of PbTe and CdTe offers a unique possibility to manufacture monocrystalline two-phase thermoelectric bulk nanocomposites (Fig. 5) of the rock-salt PbTe matrix with coherently embedded zinc-blende CdTe nanoinclusions. For the growth of PbTe-CdTe nanocomposites we applied several growth techniques. In the Cd composition range x≤0.05 homogeneous (polycrystalline) $Pb_{1-x}Cd_xTe$ solid solutions were grown by the re-crystallization and the Bridgman methods. Single phase $Pb_{1-x}Cd_xTe$ (x=0-0.12) bulk monocrystals (Fig. 3 – lower panel) of about 1 ccm volume were obtained by (self-selecting) vapor transport growth technique [18,19].

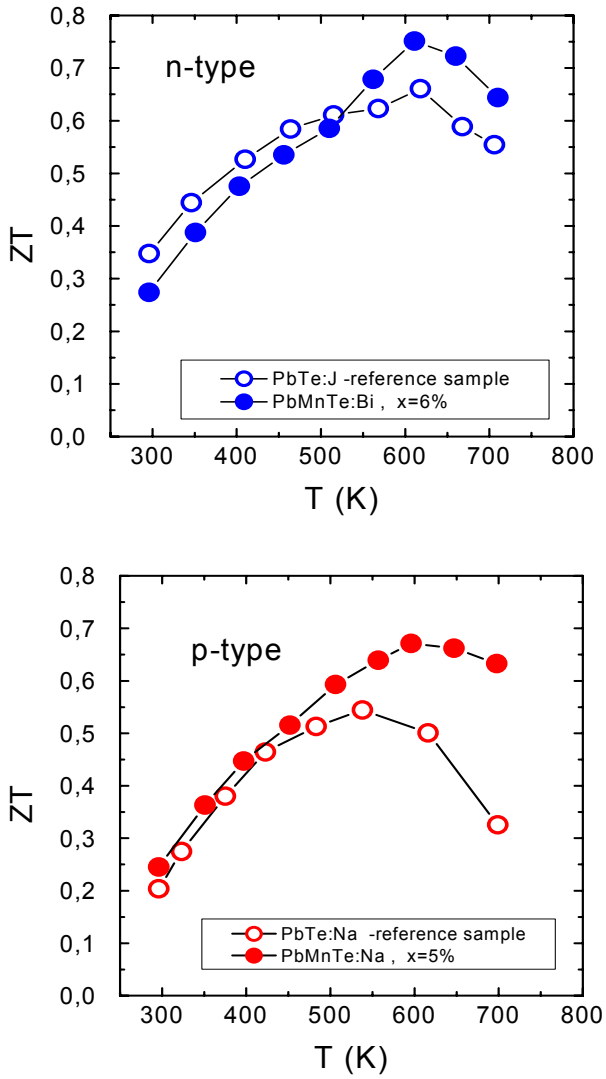

Fig. 4. Temperature dependence of the thermoelectric figure of merit parameter ZT in n-type (blue symbols, upper panel) and p-type (red symbols, lower panel) crystals of PbTe (open symbols) and PbMnTe with 5-6 at. % of Mn (full symbols). The parameter ZT was determined experimentally by the Harman method with thermal radiation correction determined at room temperature.

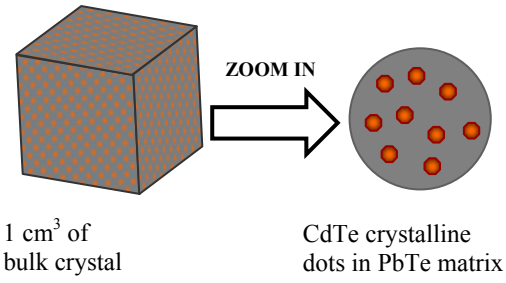

Fig. 5. An illustration of an idea of PbTe-CdTe thermoelectric bulk nano-composite.

In homogeneous $Pb_{1-x}Cd_xTe$ crystals ($x \leq 0.05$) grown by the Bridgman and the re-crystallization methods both p- and n-type conductivity was observed in as-grown materials with typical carrier concentration of 10^{18} cm^{-3}. We attribute the appearance of the n-type conductivity to Cd interstitials and the p-type conductivity to native defects (cation vacancies). This conclusion is supported by the experimentally observed smaller slope of the Vegard lattice parameter composition dependence $a_0(x)$ found in these crystals as compared to the reference monocrystals [19]. The two-crystal phase composite systems were obtained for crystals with intended Cd content x=0.1. The XRD structural analysis revealed in these materials zinc-blende CdTe inclusions occupying about 10 % of volume in the $Pb_{0.99}Cd_{0.01}Te$ rock-salt matrix. This observation was confirmed by the chemical composition analysis of the ingots showing the large differences between the total Cd content measured by the X-ray fluorescence (EDXRF) method and the XRD lattice parameter measurements (primarily sensitive to the concentration of substitutional Cd ions). Our data point to important conclusion that PbTe-CdTe nanocomposites grown from the melt consist of rock-salt $Pb_{1-x}Cd_xTe$ crystalline matrix (thermoelectrically active material) and lattice matched zinc-blende CdTe inclusions. We also carried out the experiments with controlled formation of PbTe-CdTe bulk crystalline nanocomposites by applying a proper thermal annealing regime to PbCdTe monocrystalline alloys. The formation of zinc-blende nanodots of about 10 nm in diameter that are coherently embedded in the rock-salt PbCdTe matrix was observed in high resolution transmission electron microscopy (TEM) studies. Recently, in bulk PbCdTe composites grown from the melt, the $ZT \approx 1$ figure of merit parameter was reported at temperature T=900 K [20].

Technological and experimental research activities on PbTe-CdTe nanostructures reported in literature concern almost exclusively the system of narrow bandgap PbTe quantum dots in wider bandgap CdTe matrix. This materials system, well known for its excellent mid-infrared optoelectronic properties, is of no thermoelectric relevance due to the insulating properties of undoped CdTe matrix. We developed technological procedures to prepare new layered thermoelectric material composed of the zinc-blende CdTe dots embedded in the rock-

salt PbTe semiconductor thermoelectric matrix [21]. The procedure requires special annealing regime applied to multilayer PbTe/CdTe heterostructures grown by MBE on GaAs (001) substrate. Depending on the ratio of the initial thicknesses of CdTe and PbTe layers in the heterostructure, both the growth of CdTe dots in conducting PbTe matrix and the growth of PbTe dots in insulating CdTe matrix was achieved. TEM microscopy investigations revealed highly symmetric shape of CdTe anti-dots with their diameter varying in the range from 5 to 30 nm by controlling initial CdTe layers thickness (Fig. 6).

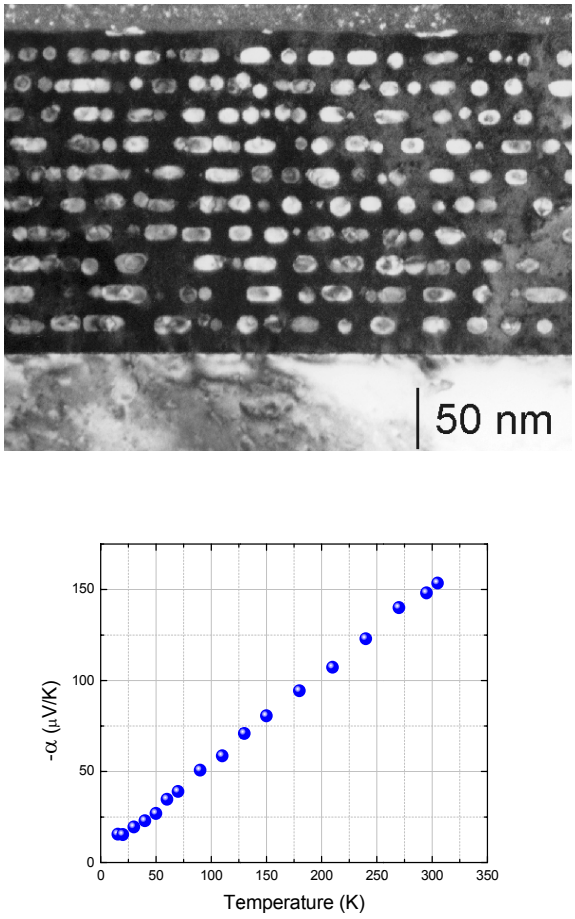

Fig. 6. Upper panel presents transmission electron microscopy (TEM) cross section image of zinc blende CdTe dots embedded in thermoelectric PbTe rock-salt crystal matrix. Lower panel shows temperature dependence of thermoelectric power of n-type PbTe-CdTe layered nanocomposite grown in Institute of Physics PAS by MBE method on GaAs (001) substrate.

Both types of electrical conductivity were achieved in such nanocomposite PbTe-CdTe multilayer materials only by crystal stoichiometry control with carrier concentration in the range $10^{17} \div 10^{18}$ cm^{-3} (Fig. 6). In PbTe-CdTe multilayer nanocomposites with CdTe dots of 5 nm-diameter the increase of the room temperature thermoelectric power of about 25 % was found as compared to the reference thermoelectric n-PbTe crystals [21]. Theoretical analysis of this effect was recently proposed based on the results of ab initio calculations of the electronic band structure of various model low dimensional PbTe-CdTe heterostructues [22].

3. Conclusions

$Pb_{1-x}Mn_xTe$ ($x \leq 0.08$) thermoelectric bulk crystals were grown from the melt by the Bridgman and the two-stage re-crystallization methods. Both types of electrical conductivity were obtained by heavily doping with Bi or I for n-type and with Na or Ag for p-type. The anticipated large increase of thermoelectric power as well as the control of the optimal operating temperature with increasing Mn content was experimentally confirmed. In $Pb_{0.95}Mn_{0.05}Te$ the $ZT \approx 0.7$ value was experimentally observed at temperatures T=400-500 K in both n- and p-type crystals revealing the potential of PbMnTe as a new graded-composition thermoelectric material. Technological procedures were developed to prepare PbTe-CdTe thermoelectric nano-composites in the form of both bulk crystals and epitaxial mulitlayers. This new thermoelectric material is composed of the zinc-blende CdTe dots embedded in the rock-salt PbTe semiconductor thermoelectric matrix. In n-PbTe-CdTe multilayer nano-composites with nanometer-sized CdTe dots the substantial increase of the room temperature thermoelectric power was observed as compared to the reference bulk crystals.

Acknowledgements

Work partially supported by the U. S. Army Research Office under contract W911NF-08-1-0231 and by the European Regional Development Fund grant POIG.01.01.02-00-108/09.

References

1. J.P. Heremans, Mat. Res. Soc. Symp. Proc. 793, 3 (2004).
2. L.E. Bell, Science 321, 1457 (2008).
3. B. Vining, Nature Materials 8, 83 (2009).
4. G.J. Snyder, E.S. Toberer, Nature Materials 7, 105 (2008).
5. A. Patyk, J. Electronic Materials 39, 2023 (2010).

6. F. Hsu, S. Loo, F. Guo, W. Chen, J.S. Dyck, C. Uher, T. Hogan, E.K. Polychroniadis, M.G. Kanatzidis, Science 303, 818 (2004).
7. B. Poudel, Q. Hao, Y. Ma, Y. Lan, A. Minnich, B. Yu, X. Yan, D. Wang, A. Muto, D. Vashaee, X. Chen, J. Liu, M.S. Dresselhaus, G. Chen, Z. Ren, Science 320, 634 (2008)
8. Y. Lan, A.J. Minnich, G. Chen, Z. Ren, Adv. Funct. Mater. 20, 357 (2010).
9. J.P. Heremans, V. Jovovic, E.S. Toberer, A. Saramat, K. Kurosaki, A. Charoenphakdee, S. Yamanaka, G.J. Snyder, Science 321, 554 (2008).
10. L.D. Hicks, M.S. Dresselhaus, Phys. Rev. B 47, 12727 (1993).
11. C.J. Vening, T.C. Harman, S.D. Calawa, M.P. Welsh, R.E. Reeder, R. Singh, A. Shakouri, Phys. reb. B 77, 235202 (2008).
12. W. Heiss, H. Groiss, E. Kaufmann, G. Hesser, M. Böberl, G. Springholz, F. Schaffler, K. Koike, H. Harada, M. Yano, Appl. Phys. Lett., 88, 192109 (2006).
13. K. Koike, H. Harada, T. Itakura, M. Yano, W. Heiss, H. Groiss, E. Kaufmann, G. Hesser, F. Schaffler, J. Crystal Growth 301-302, 722 (2007).
14. V. Osinniy, A. Jędrzejczak, W. Domuchowski, K. Dybko, B. Witkowska, T. Story, Acta Phys. Pol. A 108, 809 (2005).
15. A. Łusakowski, P. Bogusławski, T. Radzyński, Phys. Rev. B 83, 115206 (2011).
16. Y. Pei, X. Shi, A. LaLonde, H. Wang, L. Chen, G.J. Snyder, Nature 473 (7345, 66 (2011).
17. V. Leute and R. Schmidt, Z. Phys. Chem. 172, 81 (1991).
18. A. Szczerbakow, K. Durose, Prog. Cryst. Growth Character. Mater. 51, 81 (2005).
19. M. Szot, A. Szczerbakow, K. Dybko, L. Kowalczyk, E. Smajek, V. Domukhovski, E. Łusakowska, P. Dziawa, A. Mycielski, T. Story, M. Bukała, M. Galicka, P. Sankowski, R. Buczko, P. Kacman, Acta Phys. Polon. A 116, 959 (2009).
20. K. Ahn, M.-K. Han, J. He, J. Androulakis, S. Bellikaya, C. Uher, V.P. Dravid, M.G. Kanatzidis, J. Am. Chem. Soc. 132, 8669 (2010).
21. M. Szot, K. Dybko, P. Dziawa, L. Kowalczyk, E. Smajek, V. Domukhovski, B. Taliashvili, P. Dłużewski, A. Reszka, B.J. Kowalski, M. Wiater, T. Wojtowicz, T. Story, Crystal Growth and Design 11, 4794 (2011).
22. M. Bukała, M. Galicka, P. Sankowski, R. Buczko, P. Kacman, Nanoscale Research Letters 6, 126 (2011).

Development of nanostructured hybrid materials for application as catalysts in low-temperature polymer-membrane fuel cells: electrooxidation of ethanol at platinum supported on gold admixed with titanium oxide

Iwona A. Rutkowska, Sylwia Zoladek, Anna Wadas, Pawel J. Kulesza
Department of Chemistry, University of Warsaw, Pasteura 1, PL-02-093 Warsaw, Poland

Abstract

A concept of utilization of titanium dioxide matrix in electrocatalysis (ethanol oxidation in acid medium for potential application in a low temperature fuel cell cell) by admixing it with polyoxometallate (phosphomolybdate) stabilized gold nanoparticles is described here. By dispersing platinum black over the Au-containing TiO_2, the electrocatalytic activity of Pt nanoparticles towards oxidation of ethanol has been significantly enhanced. Remarkable increases of electrocatalytic currents measured under diagnostic voltammetric and chronoamperometric conditions are reported here. The most likely explanation takes into account improvement of overall conductivity (due to the presence of nanostructured gold) at the electrocatalytic interface (utilizing TiO_2 support), as well as and possibility of specific Pt-TiO_2 or Pt-Au electronic interactions and existence of active hydroxyl groups (on titanium dioxide or polyoxometallate surfaces) in the vicinity of catalytic Pt sites.

Introduction

There has been growing recent interest in development of the low-temperature direct alcohol fuel cells as an alternative technology for the systems utilizing hydrogen. Alcohols as fuels have several attractive features in comparison to the hydrogen: relatively low cost of production, easy to handle, storage and transport, high solubility in aqueous solutions. Among potential alcohols, methanol is so far the most promising organic fuel because it has several advantages in comparison to hydrogen: high solubility in aqueous electrolyte, low cost, possibility of easy handling, transportation, storage, and high theoretical density of energy (6 kWh/kg). Other alcohols that include ethanol, ethylene glycol, propanol etc. have also been considered for use in low-temperature fuel cells but, until now, only very few examples of direct alcohol fuel cells have been demonstrated [1]. It should be remembered that methanol is unfortunately fairly toxic, inflammable with a low boiling point (65^0C), and it is neither a primary fuel nor a renewable fuel. Therefore many alcohols, particularly those coming from biomass resources, have recently been considered as alternative fuels [2]. Ethanol is an example of an attractive fuel that is less toxic than methanol. Moreover, ethyl alcohol has the additional advantage that it can be obtained from biomass. Under such conditions, the use of bio-ethanol as the fuel should not change the natural balance of carbon dioxide in the atmosphere in contrast to the utilization of fossil fuels [3]. These reasons as well as high theoretical efficiency, have led to the increased interest in research on the development and optimization of electrocatalytic systems for oxidation of ethanol in acid media for potential use in low temperature fuel cells utilizing protonically conducting (e.g. Nafion) membranes. An ultimate goal of this research is not only to replace methanol as a fuel but also to develop a technology based on a commonly available renewable bio-fuel.

Ideally, ethyl alcohol can be oxidized to carbon dioxide thus delivering 12 electrons and producing theoretically the cell open circuit potential (with oxygen cathode) of 1.14 V. In other words, the overall reaction occurring in a fuel cell should ideally proceed as follows:

$$CH_3\text{-}CH_2OH + 3O_2 \rightarrow 2CO_2 + 3H_2O$$

Realistically, electrooxidation of ethanol is a complex process, and its reaction mechanism requires cleavage of the C-C bond in the ethanol molecule. Thus the reaction rate is rather low at ambient conditions [7-9]. Consequently, large amounts of undesirable toxic intermediate products, acetaldehyde

and acetic acid are formed during electrooxidations at commonly considered Pt-containing catalytic systems [4-6]. These parallel reactions cause considerable problems in practical applications of direct ethanol fuel cells not only by lowering the fuel capacity but also by producing undesirable toxic by-products.

Nanostructured platinum is so far the best-known and the most active catalyst for the activation of small organic molecules via their specific adsorption and interfacial dissociation. However, the ability of platinum to break effectively the C–C bonds is largely limited by side poisoning effects originating from the strong adsorption of CO_{ads} on Pt surfaces at low (below 60 or even 80 °C) temperatures. Several two-carbon containing molecules have been reported as undesirable intermediates during ethanol oxidation at polycrystalline Pt [9-13], most of them requiring relatively high potentials for complete oxidation [7]. It has also been suggested that the partial blocking of platinum surface by those intermediates results in slow decay with time of the ethanol oxidation currents.

For ethanol, the mechanism of its electrooxidation is different and more complex than in a case of methanol [1-13]. It is commonly accepted that the highest efficiency for electrooxidation of ethanol was achieved at nanostructured carbon-supported bimetallic PtSn or PtRu catalysts and, more recently, very promising result were obtained with PtRh type systems. Despite the relatively good performance of such bimetallic Pt-based anodes, the overall efficiency is still poor when compared to oxidation of hydrogen (at Pt) or even methanol (at PtRu). The main products remain acetaldehyde (2-electron oxidation) and acetic acid (4-electron oxidation) thus further modification of existing catalysts is necessary to obtain higher efficiency. There is a need to remove not only the poisoning CO adsorbates but also to activate the ethanol molecule and to break C-C bonds effectively. As already mentioned, modification of the platinum-based surface is often achieved by adding the second additive namely by introducing the second alloying metal. This additive or modifying agent as well as a carrier (support) must be also characterized by good stability in addition to desired activity.

Gold nanoparticles have attracted attention as an alternative or complimentary (to platinum) metal in catalytic applications [14]. While gold is rather inactive as a bulk metal, gold nanostructures, e.g. Au nanoparticles, were demonstrated to exhibit the size and support dependence during the gas-phase oxidation of carbon monoxide [14,15]. The systems composed of gold and platinum were found to produce highly reactive bimetallic catalysts. It was postulated for Pt-Au catalysts that the degree of CO-poisoning of Pt sites was largely diminished through the interracial oxidation of CO to CO_2 by the surface oxo species existing on Au sites. In particular, Au-Pt bimetallic nanoparticles were found to exhibit high activity during CO oxidation thus making the systems more CO-tolerant, in comparison to bare (pure) Pt or Au nanoparticles [16-18]. Furthermore, the use of Pt-decorated Au nanoparticles favored markedly direct oxidation of formic acid to CO_2 by inhibiting formation of undesirable CO-type poisoning species through so called "ensemble effect" [19]. To fabricate stable (ultra-thin film protected) gold nanoparticles, most of research concerns organic ligands including alkanothiols and their derivatives that can be successfully employed to obtain monolayer coverages on gold. We have recently modified noble metal nanoparticles with inorganic monolayers of a Keggin-type polyoxometallates. Heteropolyacids of molybdenum and tungsten are able to adsorb irreversibly on metals and to undergo reversible stepwise multi-electron transfer reactions of importance to electrocatalysis. Attractive features of the polyoxometallate stabilized and activated noble metal nanoparticles in electrocatalysis have been recently demonstrated [20-23]. We have also developed and described a unique chemical method of fabrication of $PMo_{12}O_{40}^{3-}$ stabilized gold nanoparticles (Au-PMo_{12}) [24,25]. We utilize such functionalized or activated gold clusters as supports for dispersed platinum (Fig. 1) and show their usefulness during electrocatalytic oxidation of ethanol.

Recently, some attention has been paid to the possibility of immobilization and activation of the platinum-based nanoparticle catalysts in such an active matrix as nanostructured metal oxide, e.g. titanium dioxide [26,27], and tungsten oxide [28]. Titanium dioxide (TiO_2) has been studied because of its unique optical, electronic and chemical properties as well as its low cost [29,30]. TiO_2 is known to be stable in acidic and alkaline solutions [31] and, due to its high porosity, large surface area [32] and non-toxic properties, titanium dioxide has been

widely considered as the catalyst support. The increase of the activity of platinum during oxidation of ethanol by dispersing it in TiO_2 support has been ascribed in terms of the Pt–TiO_2 interactions capable of changing electronic properties of the Pt catalyst (the electronic effect) [33,34]. In addition, the so called bi-functional mechanism [35] is operative in the presence of titanium dioxide, and poisoning of platinum surface by CO passivating adsorbates (that are formed during oxidation of alcohols), tends to significantly decrease. TiO_2 is believed to activate interfacial water molecules to form oxygen-containing species (OH_{ads}) on Pt at lower potentials than on bare platinum. These hydroxyl species react with CO-like intermediates, form CO_2, and release the catalytic active sites for the further alcohol oxidation (Fig.2). In addition TiO_2 matrix enhances the stability of the immobilized platinum nanoparticles by preventing their agglomeration.

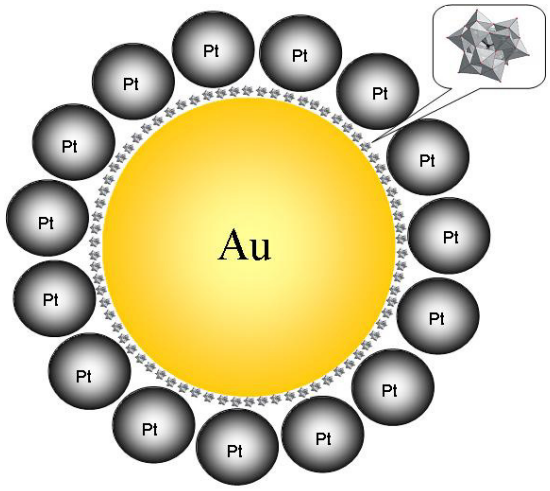

Fig. 1. Cartoon of gold nanoparticle stabilized with PMo_{12} monolayer modified with platinium nanoparticles.

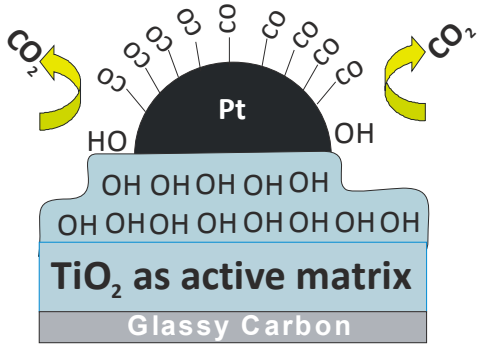

Fig. 2. Cartoon of titanium dioxide to use as active matrix.

In the present work, we impregnate titanium dioxide matrix with gold nanoparticles and combine them with catalytic nanostructured platinum. Bimetallic Au-Pt nanoparticles are of significant interest to the field of electrocatalysis. For example, a synergistic effect was reported for the Pt-Au nanoparticles during electrooxidation of methanol [36-39]. The size of bimetallic Au-Pt nanoparticles played an important role in the overall electrocatalytic activity [38]. It was also found that addition of gold tended to shift the onset potential for methanol electrooxidation towards lower values [40]. Further, gold was believed to provide sites for oxidizing poisonous CO-like species to CO_2 [41,42].

Our research aims at investigation of the influence of the hybrid TiO_2-support admixed with gold nanoparticles (ca. 30-40 nm) on the activity of the nanostructured Pt catalyst towards electrooxidation of ethanol. Highly effective electrocatalytic systems have utilized phosphododecamolybdate-modified (stabilized) gold nanoparticles introduced to TiO_2 matrix. In the present work, impregnation of TiO_2 with nanostructured gold has been followed by deposition of conventional platinum black nanoparticles (ca. 7-9 nm). Electrochemical diagnostic experiments have involved cyclic voltammetric and chronoamperometric measurements in the ethanol acid solutions. Ethanol is which which oxidation is a complex process requiring development of highly efficient electrocatalytic systems.

Fabrication and Characterization of Electrocatalytic Material

Fig. 3 show a transmission electron microscopic image (TEM) of gold nanoparticles modified with PMo_{12} (A) and titanium dioxide modified with Au-PMo_{12} nanoparticles (B). It is apparent from the TEM data (Fig. 3A) that the Au-PMo_{12} nanoparticles were highly monodisperse and characterized by diameters on the level 30-40 nm. In Fig. 3B we expect that particles of dark appearance stand for gold clusters whereas those of light appearance should be correlated with less dense structures, namely with dispersed titanium dioxide.

We can see that good dispersion of Au and TiO_2 nanoparticles may be attributed to the presence of anionic PMo_{12} monolayers assembled on gold favoring not only their attachment to the positively charged surfaces of titanium dioxide but also being

responsible for electrostatic repulsion between themselves thus preventing their agglomeration.

a)

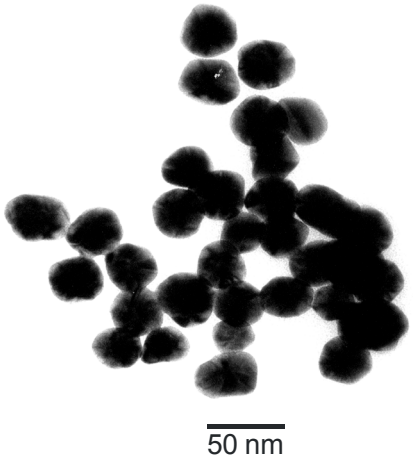

b)

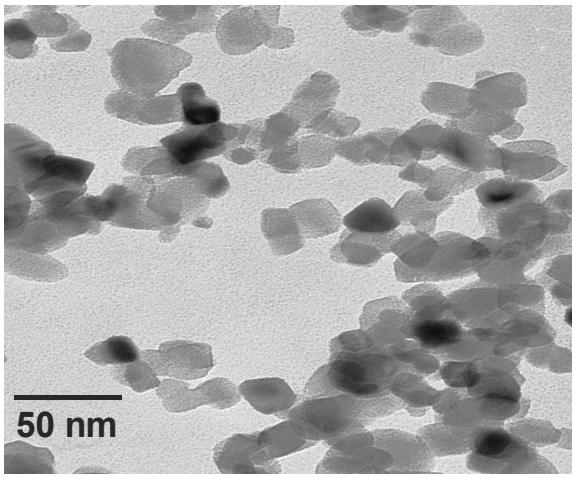

Fig. 3. TEM examination of PMo_{12}-protected gold nanoparticles (A) and titanium dioxide modified with Au- PMo_{12} nanoparticles (B).

We prepare catalytic layers composed of nanostructured TiO_2 containing gold nanoparticles (Au-PMo_{12}) and platinum nanoparticles. First, 0.04 g of TiO_2 powder was weighed and subsequently dispersed in 2 cm^3 of deionized water using an ultrasonic bath. The suspension of TiO_2 (1 μdm^3) was next deposited on surface of the glassy carbon disk electrode (GC) and let dry in air at room temperature (22°C) for 30 min. Later, 1 μdm^3 of the suspension of (Au-PMo_{12}) was placed onto the previously described TiO_2 layer and dried in air as mentioned above. In the following step, 1 μdm^3 of the colloidal suspension of bare platinum nanoparticles (prepared by dispersing 0.071 g of commercial platinum black through sonication for 30 min in 2 cm^3 of distilled water to obtain a homogenous mixture) was introduced onto the nanostructured film of TiO_2 and Au-PMo_{12} nanostructures. For comparison, we also considered the catalytic system containing bare platinum black dispersed over TiO_2 nanoparticles prepared as above, i.e. as for the electrocatalytic film composed of titanium dioxide, Au-PMo_{12} and platinum black. In all cases, the platinum loading was equal to 500 $\mu g \cdot cm^{-2}$ after depositing each catalytic system on glassy carbon electrode. As a rule at the end, we were covered the films by ultrathin layers of Nafion polyelectrolyte by depositing 1 μdm^3 of the Nafion solution (prepared by introducing 5 mass% of the commercial Nafion solution into ethanol at 1 to 10 volume ratio).

Electrochemical Diagnostic Experiments – Oxidation of Ethanol

Our initial diagnostic experiments (permitting evaluation of utility of the catalysts designed by us for potential application in alcohol fuel cells) have involved cyclic voltammetric monitoring of redox reactions of interest. Fig. 4 illustrates cyclic voltammetric responses of bare platinum black nanoparticles (black line), Pt black nanostructures immobilized within titanium dioxide support catalyst (red line), and platinum black nanoparticles deposited onto TiO_2-supported Au-PMo_{12} (green line) recorded in 0.5 mol dm^{-3} C_2H_5OH + 0.5 mol dm^{-3} H_2SO_4 solution. An important issue is that the ethanol oxidation process was characterized by the highest currents following dispersion of platinum black within the TiO_2 support containing Au-PMo_{12} (Fig. 4, green line). We can see that the onset potential of ethanol oxidation was shifted to the less positive values in comparison to its behavior at bare platinum black (black line) and at Pt nanoparticles dispersed within Au-free TiO_2 (red line).

Further diagnostic experiments have been based on monitoring and examining current-time (chronoamperometric) characteristics at certain applied potentials (as low as possible having in mind potential operation in a low-temeperature fuel cell as anode). Fig. 5 illustrates the long-term chronoamperometric responses of platinum black (black line), Pt nanoparticles supported onto TiO_2 (red line), and Pt nanoparticles supported onto TiO_2 admixed with Au-PMo_{12}Pt (green line) upon application of 0.2 V (Fig. 5A) and 0.1 V (Fig. 5B). These data show that, under such conditions, the meas-

ured currents for the oxidation of ethanol are relatively the highest for Au-PMo_{12}-containing samples. If we compare black and red lines in Fig. 5 we can indicate that TiO_2 matrix seems to be an attractive support for platinum during the ethanol oxidation process. The main role of nanostructured gold carriers is, in addition to the already mentioned possible interactions with platinum, to improve the overall charge distribution at the electrocatalytic interface. On the whole, the increased catalytic efficiency shall be related to improved removal of poisoning species such as CO_{ads} from the platinum active sites. So far there is no evidence for enhanced C-C bond splitting necessary for the oxidation of ethanol. The activation effect may also involve direct specific interactions (chemical or electronic) between titania and Pt or even Au sites. It cannot be excluded that interactions between platinum or gold and titanium oxide may result in changes in the surface electronic structures and thus in changes in the adsorption energies of carbon monoxide or even ethanol on these surfaces. Further research is along this line.

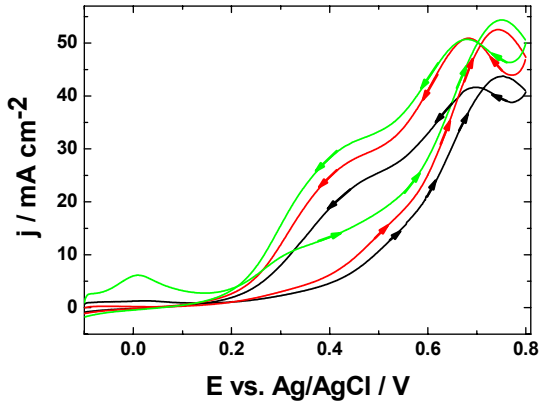

Fig. 4. Cyclic voltammetric curves for ethanol electrooxidation at simple Pt black (black line), Pt nanoparticles supported onto TiO_2 (red line), and Pt nanoparticles supported onto TiO_2 admixed with Au-PMo_{12}Pt (green line) deposited on glassy carbon. Electrolyte: 0.5 mol dm^{-3} C_2H_5OH + 0.5 mol dm^{-3} H_2SO_4. Scan rate: 10 mV s^{-1}.

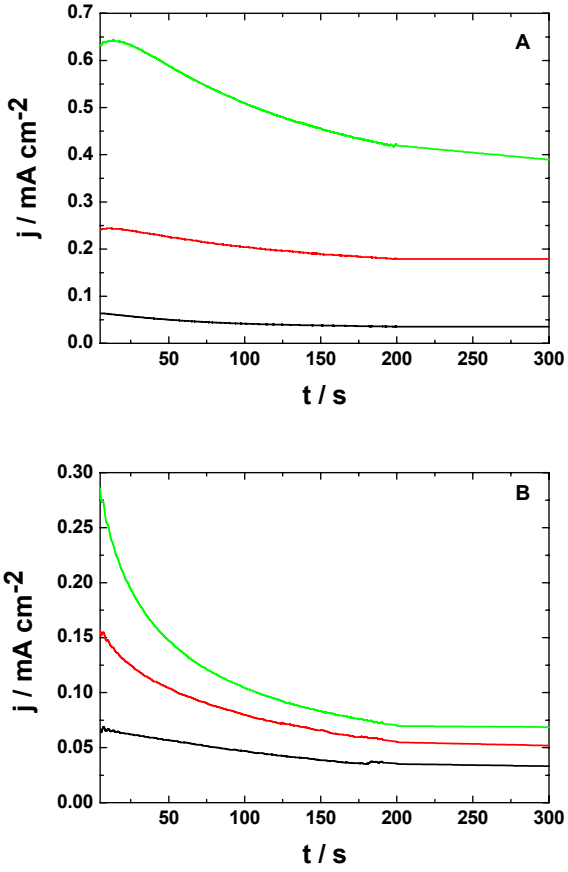

Fig. 5. Chronoamperometric responses recorded at 0.1 V (A) and 0.2 V (B) vs. Ag/AgCl for the oxidation of ethanol at simple Pt black (black line), Pt nanoparticles supported onto TiO_2 (red line), and Pt nanoparticles supported onto TiO_2 admixed with Au-PMo_{12}Pt (green line) deposited on glassy carbon. Electrolyte: 0.5 mol dm^{-3} C_2H_5OH + 0.5 mol dm^{-3} H_2SO_4.

Conclusions

Application of the titanium dioxide-supported Au-PMo_{12} matrix for dispersed Pt nanoparticles has led to the highest activity in terms of shifting potential for ethanol oxidation towards more negative values and increasing electrocatalytic currents under both voltammetric and chronoamperometric conditions. It is reasonable to expect that incorporation of nanometric gold structures into semiconducting TiO_2 increases the oxide conductivity due to the possibility of hopping electron transfers between gold sites. Dispersion of gold within TiO_2 is facilitated by the fact that anionic phosphomolybdate modified Au nanoparticles are likely to be electrostatically attracted by positively charge oxo-

cationic species existing on titanium dioxide in acid media.

Finally, it should be noted that dispersion of gold within TiO_2 is facilitated by the fact that anionic phosphomolybdate modified Au nanoparticles are likely to be electrostatically attracted by positively charge oxo-cationic species existing on titanium dioxide in acid media. Further, the capping layers of Keggin-type phosphomolybdates, which are known to undergo fast stepwise multi-electron redox processes as well as to activate Pt-based electrocatalysts during ethanol oxidation [21], may also contribute to the overall enhancement effect.

Acknowledgements

The support from Ministry of Science and Higher Education (Poland) under the grant N N204 031235 and Foundation of Polish Science (FNP) under the Chair (*Mistrz*) Project are appreciated.

References

1. C. Lamy, J.-M. Léger, S. Srinivasan, Direct methanol fuel cells – from a 20th century electrochemists' dream to a 21st century emerging technology, in : J.O.M. Bockris, B.E. Comway (Eds.), Modern Aspects of Electrochemistry, Vol. 34, Plenum Press, New York, 2000 (Chapter 3), pp.53-117
2. C. Lamy, A. Lima, V. LeRhun, F. Delime, C. Coutanceau, J. Léger, Journal of Power Sources 105 (2002) 283
3. J.W. Gosselink, Int. J. Hydrogen Energy 27 (2002) 1125
4. H. Hitmi, E.M. Belgsir, J.-M. Léger, C. Lamy, O. Lezna, Electrochim. Acta 39 (1994) 407.
5. T. Iwasita, E. Pastor, Electrochim. Acta 39 (1994) 531.
6. J.-M. Léger, S. Rousseau, C. Coutanceau, F. Hahn, C. Lamy, Electrochim. Acta 50 (2005) 5118.
7. E. Pastor, T. Iwasita, Electrochim. Acta 39 (1994) 547.
8. N.R. Detacconi, R.O. Lezna, B. Beden, F. Hahn, C. Lamy, J. Electroanal. Chem. 379 (1994) 329.
9. [9] J.P.I. de Souza, S.L. Queiroz, K. Bergamaski, E.R. Gonzalez, F.C. Nart, J. Phys. Chem. B 106 (2002) 9825.
10. J. Willsau, J. Heitbaum, J. Electroanal. Chem. 194 (1985) 27.
11. T. Iwasita, B. Rasch, E. Cattaneo, W. Vielstich, Electrochim. Acta 34 (1989) 1073.
12. S.C. Chang, L.W.H. Leung, M.J. Weaver, J. Phys. Chem. 94 (1990) 6013.
13. J.W. Shin, W.J. Tornquist, C. Korzeniewski, C.S. Hoaglund, Surf. Sci. 364 (1996) 122.
14. M. Haruta, Catal. Today 36 (1997) 153.
15. Y. Iizuka, T. Tode, T. Takao, K.-I. Yatsu, T. Takeuchi, S. Tsubota, M. Haruta, J. Catal. 187 (1999) 50.
16. H.G. Lang, S. Maldonado, K.J. Stevenson, B.D. Chandler, J. Am. Chem. Soc. 126 (2004) 12949.
17. S.G. Zhou, K. McIlwrath, G. Jackson, B. Eichhorn, J. Am. Chem. Soc. 128 (2006) 1780.
18. W. Li, H. Ma, J. Zhang, X. Liu, X. Feng, J. Phys. Chem. C 113 (2009) 1738.
19. N. Kristian, Y. S. Yan, X. Wang, Chem. Commun. (2008) 353
20. M. Chojak, A. Kolary-Zurowska, R. Wlodarczyk, K. Miecznikowski, K. Karnicka, B. Palys, R. Marassi, P.J. Kulesza, Electrochim. Acta 52 (2007) 5574.
21. P.J. Barczuk, A. Lewera, K. Miecznikowski, A. Zurowski, P.J. Kulesza, J. Power Sources 195 (2010) 2507.
22. P.J. Kulesza, K. Karnicka, K. Miecznikowski, M. Chojak, A. Kolary, P.J. Barczuk, G. Tsirlina, W. Czerwinski, Electrochim. Acta 50 (2005) 5155.
23. K. Karnicka, M. Chojak, K. Miecznikowski, M. Skunik, B. Baranowska, A. Kolary, A. Piranska, B. Palys, L. Adamczyk, P.J. Kulesza, Bioelectrochemistry 66 (2005) 79.
24. M. Lublow, K. Skorupska, S. Zoladek, P. J. Kulesza, T. Vo-Dinh H.J. Lewerenz, Electrochem. Commun. 12 (2010) 1298.
25. S. Zoladek, I.A. Rutkowska, K. Skorupka, B. Parys, P.J. Kulesza, Electrochim. Acta (2011) in press accessible on line
doi: 10.1016/j.electacta.2011.04.020
26. P. K. Shen and A. C. C. Tseung, J. Electrochem. Soc. 141 (1994) 3082.
27. B. E. Hayden, D. V. Malevich, D. Pletcher, Electrochem. Commun. 3 (2001) 395.
28. F. Micoud, F. Maillard, A. Bonnefont, N. Job, M. Chatenet, Physical Chemistry Chemical Physics 12 (2010) 1182.
29. R.S. Mane, W.J. Lee, H.M. Pathan, S.-H. Han, J. Phys. Chem. B 109 (2005) 24254.
30. N.A. Galiote, A.J.F. Carvalho, F. Huguenin, J. Phys. Chem. B 110 (2006) 24612.
31. D.B. Chu, X.F. Zhou, C.J. Lin, Chem. J. Chinese U. 21 (2000) 133.

32. B.E. Hayden, D.V. Malevich, D. Pletcher, Electrochem. Commun. 3 (2001) 390.
33. K. D. Schierbaum, S. Fischer, P. Wincott, P. Hardman, V. Dhanak, G. Jones, G. Thornton Surf. Sci. 391 (1997) 196.
34. J. M. Herrmann, J. Disdier, P. Pichat, Stud. Surf. Sci. Catal. 11 (1982) 27.
35. J. H. Liu, C. B. Yu, Chem. J. Chin. Univ. 24 (2003) 2263.
36. P. N. Njoki, A. Jacob, B. Khan, J. Luo, C. J. Zhong, J. Phys. Chem. B 110 (2006) 22503.
37. P. N. Njoki, J. Luo, L.Y. Wang, M. M. Maye, H. Quaizar, C. J. Zhong, Langmuir 21 (2005) 1623.
38. D. Mott, J. Luo, P. N. Njoki, Y. Lin, L. Y. Wang, C. J. Zhong, Catal. Today 122 (2007) 378.
39. D. Mott, J. Luo, A. Smith, P. N. Njoki, L. Y. Wang, C. J. Zhong, Nanoscale Res. Lett. 2 (2007) 12.
40. W. Tang, S. Jayaraman, T. F. Jaramillo, G. D. Stucky, F. W. McFafland, J. Phys. Chem.C 113 (2009) 5014.
41. Y. Lou, M. M. Maye, L. Han, J. Luo and C. Zhong, Chem. Commun. 5 (2001) 473.
42. W. Li, H. Ma, J. Zhang, X. Liu, X. Feng, J. Phys. Chem. C 113 (2009) 1738.

Cathode materials for SOFC

Konrad Świerczek
AGH University of Science and Technology
Faculty of Energy and Fuels, Department of Hydrogen Energy
al. A. Mickiewicza 30, 30-059 Krakow, Poland

Introduction

Lowering of the operation temperature of Solid Oxide Fuel Cells from present 1000°C down to an intermediate range of 600–800°C (so called IT–SOFC) is considered as a strategic goal for development and commercialization of SOFC technology. Operation at lower temperatures requires an application of suitable cathode material, which possesses high catalytic activity towards an oxygen reduction process in that temperature range. In classical SOFC with zirconia–based electrolyte, working at 1000°C, $La_{1-x}Sr_xMnO_3$ oxide plays role of the cathode. This compound exhibits perovskite structure and is usually referred to as LSM. LSM is characterized by a high, practically purely electronic conductivity at high temperatures (> 900°C). However, at 600–800°C the efficiency of LSM cathode is significantly decreased [1, 2].

Among numerous compounds considered for application in IT–SOFC (as cathode materials, but also as electrolyte or anode materials), majority crystallize in cubic or pseudo–cubic perovskite structure [3]. Such structure is typical for ABO_3–type oxides and is often a building block for more complex structures (e.g. double perovskites $AA'B_2O_6$ and $A_2BB'O_6$, Ruddlesden–Popper $A_{n+1}B_nO_{3n+1}$–type oxides and others) [4]. Majority of perovskite and perovskite–related materials show presence of some type of structural distortion, which is related to BO_6 octahedra tilting and / or distortion of AO_{12} and BO_6 polyhedra. Perovskite structure is also responsible for the effective transport of electrons, owing to the overlapping 3*d* orbitals of transition metal B present in octahedral position with 2*p* orbitals of oxygen atoms. The ionic transport is also possible and it occurs via oxygen vacancies. The possibility of high, mixed ionic–electronic is highly desirable, because it may improve effectiveness of the cathode performance in SOFC in the intermediate and low temperature range [5].

There are many strict requirements for a successful candidate cathode material, among them the following seem to be particularly important [1, 2, 5, 6]:

- high temperature thermal and chemical stability in the oxidizing atmosphere,
- high chemical stability in relation to used electrolyte and interconnector,
- Cr tolerance in case of usage of Cr containing interconnectors,
- CO_2 tolerance,
- high total electrical conductivity (> 100 $S \cdot cm^{-1}$),
- in case if the material is used in IT–SOFC, high mixed ionic–electronic conductivity (MIEC) with as high as possible ionic transport,
- high catalytic activity for the oxygen reduction reaction,
- adequate thermomechanical properties, thermal expansion coefficient (TEC) matched with that of electrolyte and interconnector,
- possibility of preparation of cathode layers with appropriate porosity, adhesion and mechanical strength,
- as low as possible cost of substrates for synthesis and effective preparation method,
- environmental friendliness.

Oxides having perovskite structure have been recently a subject of extensive studies [7–13] and the main research activities concentrate on their functional properties, i.e. application as cathodes in IT–SOFC. It has been found [2] that kinetics of the cathode reaction (oxygen reduction) may limit the electrochemical effectiveness of SOFC. Despite that the microscopic mechanism of the catalytic process of the oxygen reduction has not been yet entirely explored, it has been established that the rate of oxygen adsorption on the cathode material depends on the concentration of oxygen vacancies and electrons in the cathode. A deviation from stoichiometry towards the oxygen deficiency intro-

duces donor centers, ionization of which leads to a change in the concentration of charge carriers. Therefore, the oxygen nonstoichiometry and the presence of dopants shift position of the Fermi level, which, according to electronic theory of catalysis is a vital factor for catalytic activity of the cathode material [5].

Overview of the considered cathode materials

Literature data concerning possible cathode materials allows to present the following overview for the main groups of studied compounds (italic font – positive aspects, underlined font – negative aspects) [1–3, 7, 8]:

manganites – $Ln_{1-x}A_xMnO_{3\pm\delta}$ (Ln = La – Yb, Y; A = Ca, Sr, Ba, Pb)

- *are suitable for a high temperature SOFC with YSZ electrolyte,*
- *possess high electronic conductivity at temperatures above 900°C,*
- *have excellent thermomechanical properties and stability, TEC = 10–12·10^{-6} K^{-1},*
- *are suitable for composite cathodes (e.g. LSM–YSZ),*
- *have good long term and microstructural stability,*
- *partial substitution of Mn with other stable-oxidation-state cations improves stability and sometimes improves oxygen transport,*
- *moderate addition of variable-valence cations decreases polarization resistance of the material,*
- *nano-sized particles of catalytically active MIEC significantly improve LSM cathode performance at lower temperatures,*
- the overpotential of $Ln_{0.6}Sr_{0.4}MnO_3$ manganites decreases in the following way Y > Yb > La > Gd > Nd > Sm > Pr,
- <u>the effectiveness of the manganite-based cathode below 900°C is strongly limited,</u>
- <u>materials exhibit negligible ionic conductivity up to 900°C,</u>
- <u>their electrical conductivity varies strongly, depending on the preparation technique,</u>
- <u>the solid solution range of doping with A^{2+} cations is limited (x = 0.4–0.7),</u>

ferrites and cobaltites – $Ln_{1-x}A_xCo_{1-y}Fe_yO_{3-\delta}$

- *are suitable for the intermediate temperature SOFC (600–800°C) with ceria-based (e.g. $Ce_{1-x}Gd_xO_{2-x/2}$ – CGO) or $La_{1-x}Sr_xGa_{1-y}Mg_yO_{3-(x+y)/2}$ (LSGM) electrolyte,*
- *possess high mixed ionic-electronic conductivity at 600-800°C range (depending on the composition σ_e = 100-1000 S·cm^{-1}; σ_i up to 0,75 S·cm^{-1} at 800°C),*
- *have high catalytic activity at lower temperatures,*
- *are suitable for composite cathodes (e.g. LSCF-CGO),*
- their long-term structural, microstructural and chemical stability is only partially studied,
- despite high values of oxygen diffusion coefficient *D* (10^{-6}–10^{-5} cm^{2}s^{-1}) and surface exchange coefficient *k* (10^{-5}–10^{-3} cm·s^{-1}) for $La_{1-x}Sr_xCo_{1-y}Fe_yO_{3-\delta}$ (LSCF) at ~800°C, literature data shows no general, composition related tendencies,
- there are contradictory data on the activation energy for the oxygen diffusion and the oxygen exchange reactions,
- mechanism of the cathodic reaction is still poorly understood,
- kinetics of the cathodic reaction is also poorly understood,
- due to the low values of ionic transference number (10^{-7}–10^{-3}) the actual measurements of this value are problematic,
- <u>the materials have high thermal expansion, which is increasing with A and Co amount (TEC = 15–25·10^{-6} K^{-1}),</u>
- <u>high chemical expansion related to the oxygen vacancy formation is observed,</u>

other perovskites, brownmillerites, Ruddlesden–Popper–type and other oxides

- *possess promising, high mixed ionic–electrical conductivity,* <u>but usually lower than in case of LSCF oxides,</u>
- *have significantly lower thermal expansion (especially $LaFe_{1-x}Ni_xO_3$ and Ruddlesden–Popper–type oxides),*
- further studies are needed to clarify their chemical, structural and long–term stability,
- there is a lack of comprehensive data for a wide range of chemical compositions.

Among the mentioned materials perovskites from $La_{1-x}Sr_xCo_{1-y}Fe_yO_{3-\delta}$ (LSCF) group seem to be particularly interesting in terms of their possible application. In the following section a discussion of selected issues regarding structural properties, oxygen nonstoichiometry and transport properties of LSCF oxides is provided.

Structural properties of LSCF perovskites

In $La_{1-x}Sr_xCo_{1-y}Fe_yO_{3-\delta}$ ($0 \le x \le 1$; $0 \le y \le 1$; $0 \le \delta \le 0{,}5$) system an existence of single phase solid solutions is observed in whole chemical composition range (x, y) and in a relatively wide δ range [14]. At room temperature $LaCoO_3$ possesses rhombohedral symmetry with *R-3c* space group. Strontium substituted compounds have identical structure for compositions with $x \le 0.5$ in $La_{1-x}Sr_xCoO_3$. For higher Sr content these perovskites adopt regular symmetry. An especially broad range of oxygen nonstoichiometry, $2.29 < 3-\delta < 3.00$, is observed for $SrCoO_{3-\delta}$. However, synthesis of fully stoichiometric $SrCoO_3$ is difficult and so far the best results were obtained by electrochemical oxidation. In oxygen deficient samples there is a strong tendency for oxygen vacancy ordering. On the other side of the chemical composition diagram, $LaFeO_3$ possesses *Pnma* orthorhombic symmetry in wide temperature range. With the increasing x in $La_{1-x}Sr_xFeO_3$ initial orthorhombic symmetry ($0 \le x \le 0.2$) is replaced by rhombohedral ($0.4 \le x \le 0.7$) and for even higher strontium content cubic structure is observed. Oxygen vacancy ordered samples were observed in case of $LaCoO_{3-\delta}$, $La_{0,5}Sr_{0,5}CoO_{2,5}$, $SrCo_{1-y}Fe_yO_{3-\delta}$ and $La_{1-x}Sr_xFeO_{3-\delta}$. In contrast to this, there is no literature evidence of ordered oxygen sublattice in case of $La_{1-x}Sr_xCo_{1-y}Fe_yO_{3-\delta}$ ($0 < x < 1$; $0 < y < 1$; $0 < \delta < 0.5$). This might be explained by the existence of disorder in both cationic sublattices as cobalt / iron and lanthanum / strontium are statistically placed.

Exemplary structural data for $La_{1-x}Sr_xCo_{0.2}Fe_{0.8}O_{3-\delta}$ series ($0 \le x \le 0.8$) are presented below. Fig. 1 shows dependence of normalized (to pseudo–cubic perovskite) unit cell parameters as a function of Sr amount. In case of $LaCo_{0.2}Fe_{0.8}O_{3-\delta}$ material orthorhombic structure was observed. For materials with $0.2 \le x \le 0.6$ rhombohedral structure was identified, however in case of $La_{0.4}Sr_{0.6}Co_{0.2}Fe_{0.8}O_{3-\delta}$ compound the degree of the distortion was so small that for its proper identification neutron diffraction (ND) studies were required (Fig. 2).

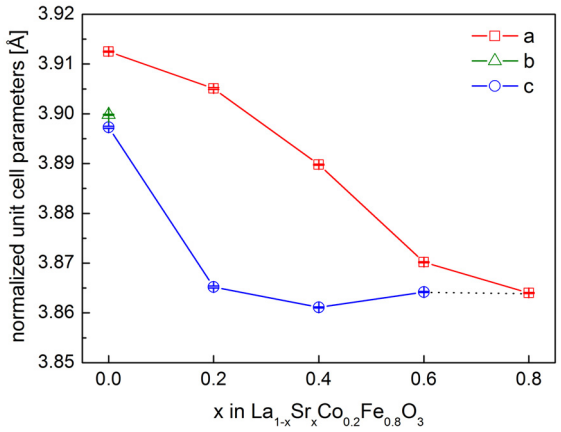

Fig. 1. Dependence of normalized unit cell parameters for $La_{1-x}Sr_xCo_{0.2}Fe_{0.8}O_{3-\delta}$ ($0 \le x \le 0.8$) as a function of chemical composition.

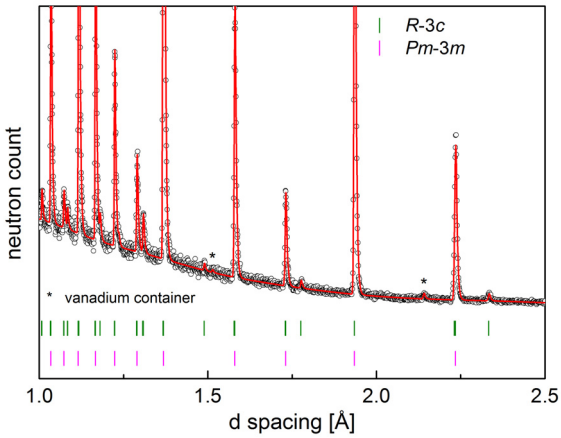

Fig. 2. ND diffractogram for $La_{0.4}Sr_{0.6}Co_{0.2}Fe_{0.8}O_{3-\delta}$ with clearly visible R-3c–related reflections.

Frequently, perovskite materials show structural phase transitions from lower symmetry to higher symmetry during heating. One of the typical examples is *Pnma* → *R-3c* transition, which, due to the structural aspects, is of the first order. On the other hand, another typical one, *R-3c* → *Pm-3m*, is continuous. In order to avoid occurrence or minimize effects of the possible phase transition (which affects thermomechanical properties of the cathode) high temperature structural studies of the considered material are required. Nevertheless, usage of materials having high symmetry at room temperature is advised, so in the case of $La_{1-x}Sr_xCo_{0.2}Fe_{0.8}O_{3-\delta}$, compounds with $x \ge 0.6$ are preferential. However, high amount of strontium causes unwanted effects related to the chemical expansion, as discussed below.

Oxygen nonstoichiometry and chemical expansion of LSCF

Fig. 3. shows thermogravimetric (TG) measurements of "as prepared" $La_{1-x}Sr_xCo_{0.2}Fe_{0.8}O_{3-\delta}$ materials. Due to the preparation technique (soft chemistry, EDTA–based method) an initial small decrease of mass may be attributed to the oxidation of residual carbon and / or desorption of CO_2. For $La_{0.4}Sr_{0.6}Co_{0.2}Fe_{0.8}O_{3-\delta}$ and $La_{0.2}Sr_{0.8}Co_{0.2}Fe_{0.8}O_{3-\delta}$ perovskites, above ~200°C an increase of mass occurs. Depending on the composition, at higher temperatures a decrease of the mass was recorded. The magnitude of this effect increases with the increasing Sr content; for sample with x = 0.2 is almost nonexistent. These both effects may be explained as a result of changes of the oxygen stoichiometry: the "as prepared" samples were relatively fast cooled down after synthesis at high temperature, therefore the high-temperature oxygen nonstoichiometry was partially preserved in the samples having high Sr amount. During slower heating these materials equilibrated and oxygen uptake was visible. At higher temperatures the oxygen was again released, creating oxygen vacancies.

On the basis of thermogravimetric measurements (performed in air as well as TG reduction studies) the equilibrium concentration of the oxygen vacancies in air as a function of temperature was estimated. In Fig. 4 Arrhenius–type plot of such dependence is presented. One can see that for samples with higher Sr content the formation energy of oxygen vacancies significantly decreases. High concentration of mobile vacancies should greatly intensify ionic conductivity, but on the other hand has strong negative impact on the thermomechanical properties of the materials. Oxygen leaving the material causes reduction of 3*d* metals (Co and Fe), and in consequence, causes the increase of their ionic radii:

$$O_O = V_O^{\bullet\bullet} + 2e^- + 0.5O_2 \uparrow$$
$$2M(Co,Fe)^{4+} + 2e^- = 2M(Co,Fe)^{3+}$$

This in turn is observed as a significant increase of the thermal expansion of the sample (so called chemical expansion). In case of $La_{0.2}Sr_{0.8}Co_{0.2}Fe_{0.8}O_{3-\delta}$ material average TEC increases from $15.9 \cdot 10^{-6}$ K^{-1} in 100–500°C range to $32.8 \cdot 10^{-6}$ K^{-1} in 600–800°C range [15]. Such high values of TEC cause major problems with adhesion at cathode | electrolyte interphase and may induce decohesion during repetitive heating – cooling of the cell.

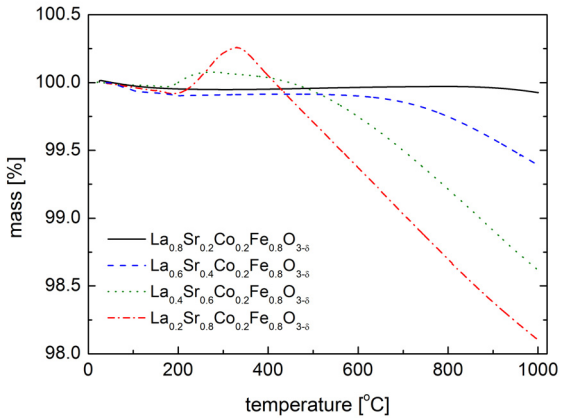

Fig. 3. Thermogravimetric measurements (relative changes of mass as a function of temperature) performed in air for "as prepared" $La_{1-x}Sr_xCo_{0.2}Fe_{0.8}O_{3-\delta}$ materials. Heating rate was 2.5 deg·min^{-1}.

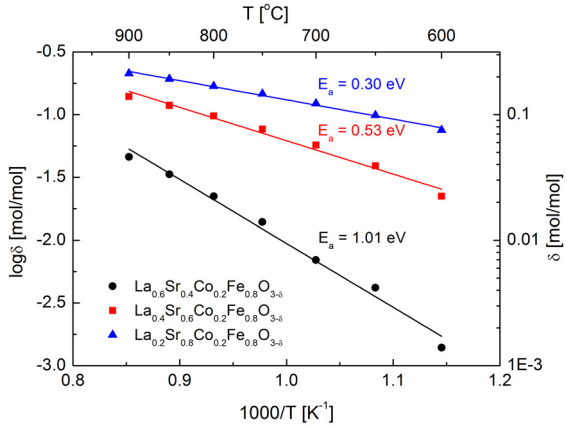

Fig. 4. Equilibrium concentration of oxygen vacancies for $La_{1-x}Sr_xCo_{0.2}Fe_{0.8}O_{3-\delta}$ as a function of temperature in air. E_a – enthalpy of formation.

Electrical properties of LSCF oxides

Literature data concerning ionic conductivity of LSCF perovskites indicate that even for the optimized materials it is about three or more orders or magnitude lower than the electronic one. The electronic conductivity of these materials may be very high, well above 100 S·cm^{-1}. Fig. 5 presents results of electrical conductivity measurements versus temperature for considered oxides in a wide temperature range up to 950°C. At lower temperatures (< 500°C) the activated type of conductivity was observed. At higher temperatures, depending on the chemical composition of the sample, a maximum on the σ(T) dependence appears, which corresponds quite well with the temperature at which

oxygen vacancies are created (Fig. 3). The decrease of the electrical conductivity above this temperature is related to breaking of M–O–M double exchange mechanism due to the formation of the oxygen vacancies and also due to the changes of the average oxidation state of Co and Fe. The temperature at which characteristic maximum of electrical conductivity is observed has important technological meaning: it indicates formation of oxygen vacancies, which are catalytic centers for oxygen reduction. With higher strontium content in LSCF this temperature decreases and higher catalytic activity of the cathode material may be expected.

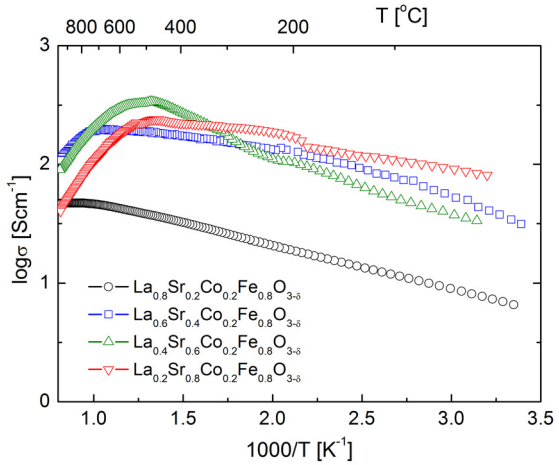

Fig. 5. High temperature electrical conductivity of $La_{1-x}Sr_xCo_{0.2}Fe_{0.8}O_{3-\delta}$ perovskites. Data from [5] and [16].

Conclusions

Among many considered candidates, LSCF cathode materials show attractive properties in terms of their application in IT–SOFC cells. Their physicochemical characteristics are strongly dependent on the amount of Sr^{2+} cations, which allows for optimization of the materials in order to obtain desired properties.

Due to the size of this paper, many important issues, which are crucial for the successful cathode material, were not discussed (e.g. chemical stability towards electrolytes and interconnects, issues regarding porosity, mechanical properties, manufacturing of cathode layers, usage of composite cathodes). Interested reader may find discussion regarding these topics in literature [1–3].

Acknowledgement

The author acknowledge a financial support from the European Institute of Innovation and Technology, under the KIC InnoEnergy NewMat project.

References

1. J.W. Fergus, R. Hui, X. Li, D.P. Wilkinson, J. Zhang, (Eds.), Solid Oxide Fuel Cells Materials Properties and Performance, CRC Press, 2009
2. S.C. Singhal, K. Kendall, (Eds.), High Temperature Solid Oxide Fuel Cells: Fundamentals, Design and Applications, Elsevier, 2003
3. T. Ishihara, (Ed.), Perovskite Oxide for Solid Oxide Fuel Cells, Springer 2009
4. R.H. Mitchell, Perovskites Modern and Ancient, Almaz Press Inc., Canada, 2002
5. J. Molenda, K. Świerczek, W. Zając, J. Power Sources 173 (2007) 657
6. E. Ivers-Tiffée, A. Weber, D. Herbstritt, J. Eur. Ceram. Soc. 21 (2001) 1805
7. E.V. Tsipis, V.V. Kharton, J. Solid State Electrochem. 12 (2008) 1039
8. E.V. Tsipis, V.V. Kharton, J. Solid State Electrochem. 12 (2008) 1367
9. J. Richter, P. Holtappels, T. Graule, T. Nakamura, L.J. Gauckler, Monatsh Chem. 140 (2009) 985
10. S.J. Skinner, Fuel Cells Bull. 339 (2001) 6
11. C. Sun, R. Hui, J. Roller, J. Solid State Electrochem. 14 (2010) 1125
12. W. Zhou, R. Ran, Z. Shao, J. Power Sources 192 (2009) 231
13. S. P. Jiang, J. Mater. Sci. 43 (2008) 6799
14. K. Świerczek, B. Dabrowski, L. Suescun, S. Kolesnik, J. Solid State Chem. 182 (2009) 280
15. K. Świerczek, Solid State Ionics 179 (2008) 126
16. K. Świerczek, M. Gozu, J. Power Sources 173 (2007) 695

The IV. generation vessels for hydrogen storage applied in vehicles. Modelling, technology and experiment

Wojciech Błażejewski, Paweł Gąsior, Jerzy Kaleta and Marek Rybaczuk
Wrocław University of Technology, Poland

I. Introduction

Role of gaseous fuels, particularly hydrogen in automotive applications

The role of gaseous fuels (mainly: methane, hydrogen) in transport, especially automotive, is steadily growing. There are known many reasons for this situation, including economic, environmental, operational, political, etc. The increasing importance of hydrogen begins, both to power internal combustion engines and fuel cells. In recent years, the EU carried out, or still continue many projects (eg: StorHy, HyWay, HyComp, HyCube), aimed at dissemination of hydrogen in the automotive industry. The dominant technology, especially in cars, is the storage of hydrogen in high-pressure tanks, which are labeled as CH2 (Compressed Hydrogen). Hydrogen is stored in the vessels of the latest (4-th generation) at the nominal working pressure equal to 700 bar.

High pressure vessels. Application, advantages, requirements

The introduction at large-scale lightweight, highly stressed composite vessels for hydrogen requires an effective solution of many problems. It is necessary that the distance which car can be overcome by a single refueling, was not less than 600 km. This results in necessitate of increasing the vessels operating pressure up to 70 MPa. Modern high pressure vessels for compressed hydrogen storage are made of composite materials (usually carbon-epoxy). Their great popularity is connected with a significant reduction in weight of the composite vessels, compared to steel ones, while ensuring a sufficiently high mechanical strength. Other advantages of composite vessels are:

- no sparks with abrasions and impacts,
- lack of splinters in the event of the destruction of the tank (eg overshoot, burst),
- high chemical resistance,
- lack of a plastic-brittle transition at low temperatures.

Presently in the world, research and development works are focused on two main directions, namely:

- optimization of manufacturing technology in order to reduce weight, and thus production costs, enabling in turn the mass use of vessels,
- ensure the safe use of vessels during the 10 to 15 years of operation.

The following some examples of authors scientific activity are presented, including results from participation in national and European projects (eg StorHy, InGas, HyComp, HyCube) and research for industrial partners.

II. Composite high pressure vessels. Manufacturing technologies

Composite high pressure vessels for gaseous fuels storage are produced by following techniques: winding technology; braiding technology.

Winding technology

The main production method of vessels is winding. This technology is well described in the literature and will not be discussed in detail here. In winding technology the type of the curve called isotensoide has been applied to form bottoms in composite tanks. They form determining fibre wound over bottom, i.e., the form of bottom, has been chosen in a way making stresses in composite strength wall equal at every point. Results of authors presented in [1, 2, 3, 4] indicate that the structure of wound composite elements (the way in which bands are arranged) has influence onto initiation and development of defects and onto final strength of material. The notion of structure has wider meaning comparing with anisotropy since the structure depends not solely on angle of architecture but also on their arrangement. Fig. 1. presents axonometric view of chosen fragments indicated by frame.

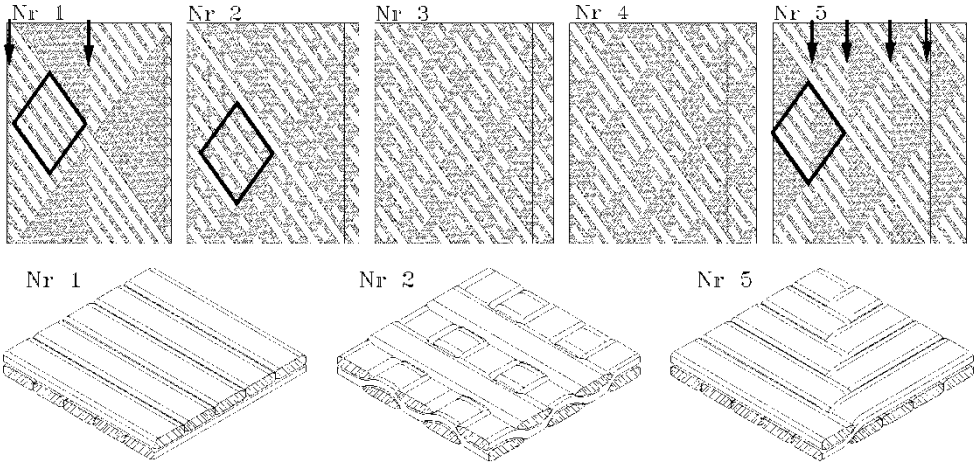

Fig. 1. The axonometric views of the fragments of winds Nr. 1, 2 and 5 marked by frames.

The following steps are proposed during manufacturing of the prototype of each composite tank using winding technology:

- acceptance of approximate linear sizes of tank,
- choice of wind making use, for example, of the above mentioned table method,
- acceptance of the width of rowing beam ex,
- acceptance of the number and sequence of layers wound of wind,
- estimation of strength,
- determination of winding parameters (including ratio of rowing beams, number of winds, length of winding),
- model tries of winding,
- designing and manufacturing of liner,
- manufacturing of tank prototype,
- verifying tests,
- analysis of results of research and return to initial stage if necessary.

Braiding technology

The method of braiding is a simple, but at the same time extremely effective process for the manufacture of semi-closed profiles, or finished products from the long fibers. The main advantage of the braiding process comparing to unidirectionally reinforced or laminated composites is the ability to adapt to the unusual shapes of cores and fiber continuity when changing core diameter. This allows the preparation of oval, rectangular and other made-cutting shapes. In the case of triaxial braiding it is possible to perform cross-sections of heterogeneous elements, where the process takes place simultaneously in three planes. An important advantages of braiding technology is speed and full automation of the process, reduction of labour costs associated with fiber laying, and finally the preforms are produced much more accurately and faster than by winding technique. Since labour comprises from 60 to 80% of the total cost of most manufactured composite elements, the reduction due to braiding method can significantly reduce the price of the final product.

Another advantage of this method is the use of dry fibers, so that it is unnecessary to use "prepregs", which may double the price of production. Low costs of materials used as well as labour, predestine this method to perform the composite reinforced elements with continuous fibers, especially in the case of pipes, fittings and pressure vessels.

In the process of vessels braiding, authors have used 5-axis KUKA robot and braiding frame HERZOG 288-1 (both devices at the disposal of the TU Dresden). Below the process of braiding of carbon fiber vessel is presented. The whole process was done completely automatically. The vessel was maintained in the robot gripper, which is also responsible for the displacement of the object relatively to the so-called convergence point of the fibers. Application of a robot arm which is characterized by high rigidity allows for the attachment of the vessel's liner and manipulate it at all directions. Generating the composite structure of the vessel was done automatically by the movement of spools (bobbins) of fiber in a circle bearing. Both the robot's movements and the bobbins are programmed so as to eliminate the influence of the operator on the process.

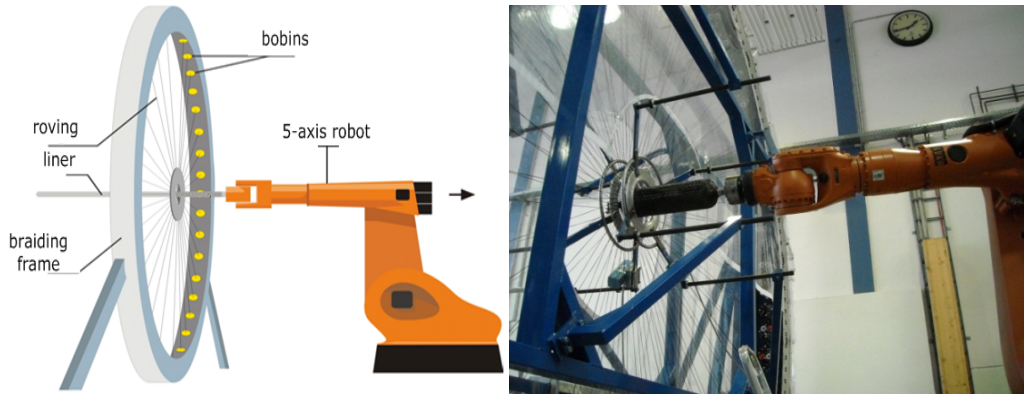

Fig. 2. Scheme and view of braiding frame with manipulator (Institut für Leichtbau und Kunstofftechnik (ILK), Technische Universität Dresden).

Following braided layers were obtained without interruption of work, only by changing the direction of the object (the robot gripper). On the braiding frame 288 bobbins were installed. They moved at a controlled rate. In this way the collected fibers intertwined with each other, creating a preset composite structure. The braiding geometry (pattern) can be modified by changing the number of spools and their location on the frame as well as by movement of the robot arm. Such produced tanks were infiltrated by epoxy resin and put into test campaign.

III. Modelling of strain state and damage accumulation of composite vessels

Examination of running damage process and current damage level may be effectively performed as an effect of some hybrid procedure, i.e. it should consist of well verified numerical model (of the multi-scale type) of vessel together with local measurements making use of well located limited number of sensors.

Good numerical model (for every type of vessel) should allow:

- description of winding geometry (so called parquet problem, described above),
- the constitutive equation of composite (making use of some homogenization procedure for example),
- description of the stress and strain states in vessel (applying the model of continuum and FEM),
- formulation of the problem of initiation of material damage,
- acceptance of quantity responsible for damage accumulation (measure of damage) and formulation of fatigue hypothesis.

The model should indicate location of sensors and their number what constitute basis for experiment.

Modeling of materials with complicated internal structure (corresponding to sufficiently short scales or equivalently to sufficient magnifications of observations) remains still an open problem. Modern constructional materials like fiber reinforced composites constitute a challenge. The basic problem is to find the correspondence between visible microscopic structure and material properties, mainly mechanical ones, responsible for macro scales usually put forward in engineering applications.

The identification of material parameters based on experimental measurements has the key meaning. The experiment should allow:

- local measurements of strain at places indicated by the model (here, application of optical fibers sensors is preferred),
- measurement of quantity correlated with accumulation of damage of vessel (registration of AE for example),
- modelling and experiments for vessels (expensive ones) may be preceded by modelling and experiments for tube specimens.

Especially useful in modelling of composite structures applied in tanks construction approaches are listed below [5, 6, 7, 8]:

- modelling making use of nonstandard models of continual media (using homogenisation),
- modelling in terms of cellular automata,
- modelling applying theory of dynamical systems.

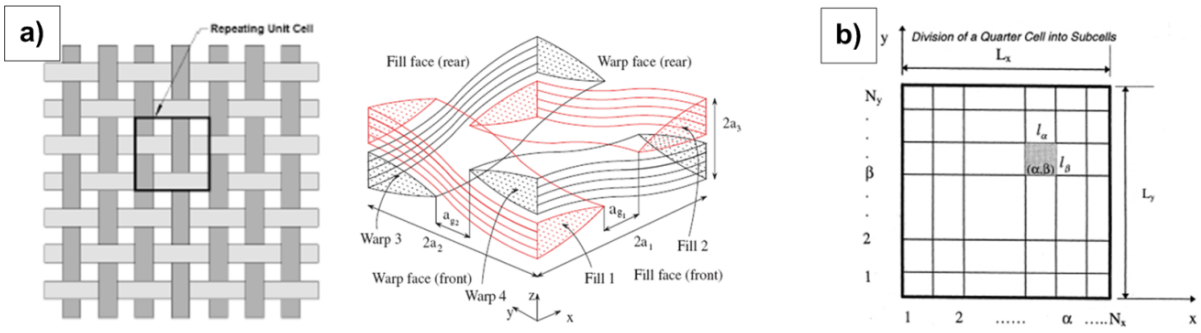

Fig. 3. The structure and quarter of Representative Volume Element (a) and division of a quarter of unit cell into subcells in plane material properties homogenisation (b) [17].

The main purpose of modelling of composite materials is establishing of constitutive equations describing entire large specimens due to known structure and material properties of separate phases forming composite as well as architecture of fibres (transition from micro- through meso- to large scales). The homogenisation method allows determination of material properties (for example Young modulus) and it consists in suitable averaging over chosen volume and over separate phases properties. At macro level, the structure of composite becomes invisible but one knows the stress-strain dependence which in fact corresponds to phase and fibres properties. It is possible to assume that fibre reinforced polymeric composites have periodic structure what enables establishing of the Representative Volume Element (RVE) – Fig. 3.

We predict the behaviour of composite making use the found RVE and the homogenisation procedure. According to distribution of fibres the RVE may be decomposed into sub cells (Fig. 3b) and the homogenisation procedure may run in few steps.

In turn application of fractal geometry methods allows modelling of acoustic emission (AE). Numerically simulated acoustic events may be compared with acoustic events registered during experimental examinations of specimens and pressure vessels.

IV. Safety of high pressure vessels. Integrated structural monitoring systems

The ever increasing popularity of composite structures is first of all due to the considerable reduction in weight in comparison with metal structures, at an appropriately high mechanical durability. Nevertheless, the safety requirements require that the stress-strain state of composite structure be monitored. Standard NDE methods such as radiography, interferometric holography, ultrasonic scanning or visual inspection are usually not effective in on-line monitoring. Even if they were used for periodic checks, they would not be able to detect promptly defects critical to the condition of the monitored structure. Moreover, conventional measurement devices, such as electrical resistance strain gauges, often get damaged in adverse environmental conditions.

State-of-the-art measuring methods based on optical fibre technology are increasingly often used to monitor the structural health of industrial objects. Optical fibre sensors have many advantages over the conventional devices [9]. These sensors can be easily inbuilt in the structure of composite or can be installed on the outer surface without changing its mechanical properties. Moreover, sensors are spark less and resistant against electromagnetic disturbance. They have large range of measurements and can work in adverse conditions (high dust concentration, high temperature, high pressure, significant deformations).

Thanks to their high potential for multiplexing it is possible to create a nervous system of the object being monitored, enabling health and damage assessment. In addition, optical fibre based sensors ensure spark-proof safety which is an important consideration for inflammable applications [10].

Optimal solution requires hybrid approach what means the both numerical model of composite tank and measurement system are required. The numerical model allows an optimal arrangement of sensors reducing their number and current comparison of measured strains with values derived from model. The original FEM model required application of so-called homogenisation procedures and it enabled determination of strains within variety of length scales as well as damage accumula-

tion. An example of real-data measurements from high-pressure vessel cyclic test is presented in Fig. 4.

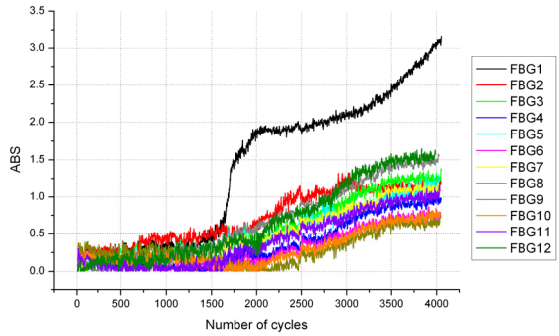

Fig. 4: Analysis of damage accumulation coefficient (ABS) versus number of pressure cycles for all FBG sensors installed on tested vessel with programmed defects [9].

V. Regulation Codes and Standards. Testing of high pressure vessels for hydrogen storage

The most countries in the world (USA, Japan, Europe) have established laws and regulations connected with hydrogen storage systems that require commercial products to meet all applicable codes and standards to demonstrate that they are safe, perform as designed and are compatible in the systems in which they are used, ie. [11, 12, 13, 14, 15]. Hydrogen has an established history of industrial use as a chemical feedstock, but its use as an energy carrier on a large-scale commercial basis remains largely undeveloped and untested [16]. The biggest challenge is that so called harmonized documents are still missing. It means that there are many various regulations describing requirements for high pressure storage components, however there are still carried out intensive efforts to new and balanced standards.

The above-mentioned standards, in addition to the requirements connected with materials used for the production of pressure vessels, pressure ranges (ie: the nominal operating pressure, pressure test), design criteria, describe also the whole range of tests that must be successfully passed to the final design has been approved for production (so called: cylinder design qualification tests).

The most popular tests for high pressure composite vessels (IV generation):

- Hydrostatic pressure burst test (see: Fig. 6),
- Ambient temperature pressure cycling test (see: Fig. 5),
- Extreme temperature pressure cycling,
- Acid environment test,
- Bonfire test (see: Fig. 8),
- Penetration test (see: Fig. 7),
- Composite flaw tolerance tests,
- High temperature creep test,
- Accelerated stress rupture test,
- Impact damage test,
- Permeation test,
- Pressure relief device requirements,
- Hydrogen gas cycling test,
- Leak-before-break (LBB).

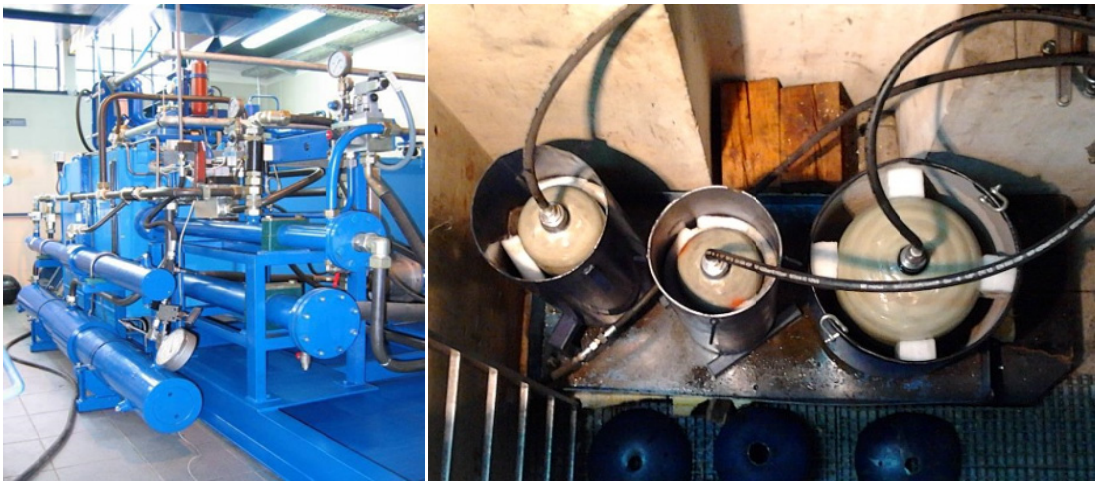

Fig. 5. Hydraulic equipment for cyclic tests and high pressure vessels inside safety chamber

Fig. 6. Burst test of high pressure vessel in the test range conditions.

Fig. 7. High pressure vessel during the penetration test.

Fig. 8. The bonfire test of high pressure vessel and view of the vessel after this test if PRD failed.

In Institute of Materials Science and Applied Mechanics (IMSAM) Wroclaw University of Technology (WRUT) different kinds of test in a range of pressure vessels for scientific and industrial partners are implemented (including: EIT/KIC programme, 6th FP and 7th FP of EU projects). In IMSAM among other things following test are realized: cycling test in a pressure range 2÷140 MPa (at ambient temperature and extreme conditions, -40 °C and 85 °C with 90% humidity), burst test (with maximum pressure 240 MPa), impact damage test, penetration test, accelerated stress rupture test as well as high temperature creep test. Short descriptions of the most critical tests are presented below.

Ambient temperature pressure cycling

Before the pressure cycling test the test tank is filled with a non-corrosive fluid such as oil, inhibited water or glycol, and then pressure cycled between not more than 2 MPa and not less than 1,25 times the working pressure (that is 87.5 MPa for 70 MPa hydrogen vessels) at a rate not exceeding 10 cycles per minute. The fuel tank is pressure cycled until failure or to a minimum 45000 cycles. View of the hydraulic test setup at IMSAM is presented in Fig. 5.

Hydrostatic pressure burst test

The tested fuel tank before the burst test is filled with a fluid such as water and then pressure is gradually increased until its failure. It is necessary to ensure that the pressure measuring device is monitoring the true value of tank pressure, particularly when the pressurization rate exceeds 0.35 MPa/s. For this purpose, it is possible to make a five second hold at the minimum design burst pressure. For a70 MPa type vessel, a burst pressure shall exceed 164.5 MPa. An example of the burst test realized at the test range conditions is presented in Fig. 6.

Extreme temperature pressure cycling

First part of this test is realized at extreme high conditions, what means the temperature not less than 85 °C, and 95 % or greater relative humidity. After 48 hour of conditioning vessel is pressure cycled between not more than 2 MPa nor less than 1,25 times the working pressure (87.5 MPa) at the same conditions for 22500 cycles. Then tank with working fluid is conditioned for next 48 hours at -40 °C or lower as measured in the fluid and on the fuel tank surface. Finally it is pressurized from not more than 2 MPa to not less than the working pressure (70 MPa) for next 22500 filling cycles at extreme low temperature conditions.

VI. Summary

The paper presents the results of own research in the field of modelling, technology, manufacturing and testing of high pressure composite vessels for hydrogen storage as an automotive fuel.

Acknowledgments

The work has been supported partly by research projects: "InGas" (7th FP), "HyComp" (7th FP), HyCube (EIT KIC) and by Wrocław Research Centre EIT+ within the project "The Application of Nanotechnology in Advanced Materials" – NanoMat (POIG.01.01.02-02-002/08) financed by the European Regional Development Fund (Innovative Economy Operational Programme, 1.1.2).

References

1. W. Błażejewski, „Metodyka doboru struktury kompozytowego oplotu nośnego zbiorników wytwarzanych metodą nawijania," Czasopismo Techniczne. Mechanika. , tom 106, nr 1, pp. 9-14, 2009.
2. W. Błażejewski, „Zastosowanie metody tablicowej w projektowaniu oplotu kompozytowego butli wysokociśnieniowych," Kompozyty, tom 10, nr 2, pp. 154-158, 2010.
3. W. Błażejewski, P. Gąsior i J. Kaleta, „Aspekty bezpieczeństwa w zakresie ciśnieniowego magazynowania wodoru w zbiornikach samochodowych," Biuletyn Polskiego Stowarzyszenia Wodoru i Ogniw Paliwowych, nr 5, pp. 22-28, 2010.
4. W. Błażejewski, P. Gąsior, R. Rybczyński i J. Kaleta , „Lekkie, wysokociśnieniowe, kompozytowe, monitorowane zbiorniki do paliw gazowych w pojazdach," Przegląd Mechaniczny, tom 70, nr 1, pp. 13-20, 2011.
5. D. Aniszewska i M. Rybaczuk, „Fractal characteristics of defects evolution in parallel fibre reinforced composite in quasi-static process of fracture," Theoretical and Applied Fracture Mechanics, tom 52, pp. 91-95, 2009.
6. D. Aniszewska i M. Rybaczuk, „Modelling defects growth in composites using fractals characteristics," w Composites2009 2nd ECCOMAS, London, 2009.
7. J. Czopor i M. Rybaczuk, „Fibers breaking process in composites models and numerical simulations applying cellular automata," Theoretical and Applied Fracture Mechanics, tom 52, pp. 154-157, 2009.
8. T. Czapliński, Ł. Maciejewski, A. Przygoda i G. Ziętek, „A model of textile reinforced composite; homogenisation and identification," w 18th Conference on CMM, Zielona Góra, 2009.

9. W. Błażejewski, P. Gąsior i J. Kaleta, „Application of Optical Fibre Sensors to Measuring the Mechanical Properties of Composite Materials and Structures," w Advances in Composite Materials - Ecodesign and Analysis, B. Attaf, Red., InTech, 2011.
10. P. Gąsior, W. Błażejewski i J. Kaleta, „Smart fibre optic methods for structural health monitoring of high pressure vessels for hydrogen storage," in: WHEC - World Hydrogen Energy Conference, Essen, 2010.
11. ISO 15869 - Gaseous hydrogen and hydrogen blends -- Land vehicle fuel tanks.
12. „Draft ECE Compressed Gaseous Hydrogen Regulation, Revision 12b".
13. ISO 23273-2:2006. Fuel cell road vehicles - Safety specifications - Part 2: Protection against hydrogen hazards for vehicles fuelled with compressed hydrogen.
14. JARI S 001 - Technical Standards for Containers for Compressed Hydrogen Vehicle Fuel Device.
15. SAE J2579 - Technical Information Report for Fuel Systems in Fuel Cell and Other Hydrogen Vehicles.
16. „http://www1.eere.energy.gov/hydrogenandfuelcells/storage/hydrogen_storage_testing.html," [Online].
17. J. Kaleta, W. Błażejewski, P. Gąsior i M. Rybaczuk, „Optimisation of the IV generation tanks for hydrogen storage applied in vehicles. Modelling and experiment," in: WHEC - World Hydrogen Energy Conference, Essen, 2010.

INFLUENCE OF ALUMINIUM ELECTRODE PREPARATION ON POWER CONVERSION EFFICIENCY OF POLYMERIC SOLAR CELLS

A. Iwan, M. Palewicz, M. Ozimek and A. Chuchmala

Electrotechnical Institute, Division of Electrotechnology and Materials Science,
M. Sklodowskiej-Curie 55/61 Street, 50-369 Wroclaw, Poland

Keywords: polymers, P3HT, PCBM, solar cells

INTRODUCTION

Photovoltaic devices based on semiconducting polymers are a promising route to low-cost solution-processed solar cells. Being into consideration the polymer structure used as an active layer in the construction of photovoltaic devices mainly polythiophenes and poly(p-phenylene vinylene)s blended with [6,6]-phenyl-C_{61}-butyric acid methyl ester (PCBM) are investigated [1-3].

In this paper the photovoltaic properties of devices based on poly(3-hexylthiophene-2,5-diyl, regioregular) (P3HT) were investigated. The photovoltaic properties of P3HT were tested by fabrication the organic photovoltaic devices with the three kinds of configurations: ITO/P3HT/Al, ITO/P3HT:PCBM (1:1, w/w)/Al and ITO/PEDOT:PSS/P3HT:PCBM (1:1, w/w)/Al. For the constructed devices impedance spectroscopy were analyzed. The main goal of the paper was investigation of influence of aluminium electrode preparation via thermal evaporation and the magnetron sputtering on power conversion efficiency (PCE) of polymeric solar cells.

EXPERIMENTAL

Solar cells were fabricated on an indium tin oxide (ITO)-coated glass substrate in air atmosphere. PEDOT:PSS was spin cast from aqueous solution to form a film on the ITO substrate. A solution containing a mixture of P3HT:PCBM in chloroform solution with weight ratio 1:1 was then spin cast (10000 (or 2000) turns per minute, 25 sec.) on top of the PEDOT:PSS or ITO layer. Then, an aluminum electrode (~100 nm) was deposited by thermal evaporation (5×10^{-4} Torr) or magnetron sputtering (~50 nm). For the preparation of Al electrode by magnetron sputtering high purity aluminium target with a diameter of 107 mm and thickness of 3 mm was used. Before deposition, the working chamber was evacuated to a base pressure of 5×10^{-4} Pa using turbo molecular pump and then backfilled with pure argon. The total pressure during the process was 3×10^{-1} Pa. The substrates temperature was below 50°C during deposition. Before starting the experiment, the target was pre-sputtered with a shutter located in between the target and the substrates.

Current density–voltage (J–U) characteristics of the devices were measured using a Keithley 6517B electrometer and DC microvoltmeter V623. Solar cell performance measurements utilized a xenon lamp with an illumination of 100mW/cm^2 with an AM1.5G. The area of one photovoltaic pixel was about 4.5 mm^2. The devices were measured with impedance spectroscopy (IS) by Solartron precision LCR meter Model SI1260 in the frequency range of 1 Hz to 1 MHz with 20 mV test signal.

The photovoltaic properties of P3HT were investigated by fabricating the polymeric photovoltaic devices with ITO as anode, the blend polymer with PCBM in weight ratio 1:1 as active layer, and Al as cathode. Polymer was applied as donor in polymeric photovoltaic devices, while fullerene was used as an acceptor. PEDOT:PSS was used in two-layer devices as a hole transporting layer. The devices comprising PEDOT:PSS with P3HT:PCBM (1:1, layer spin cast with 10000 turns per minute) showed the best photovoltaic parameters such as a V_{OC} of 0.60 V, J_{SC} of 4.61 mA/cm^2, FF of 0.21, and PCE of 5.7×10^{-1} %. The device comprising P3HT:PCBM layer spin cast with 2000 turns per minute showed lower photovoltaic performance. For devices lack of PEDOT:PSS layer or lack of PCBM, photovoltaic parameters were very low and similar to the parameters obtained for device with Al electrode prepared by magnetron sputtering. For example, device ITO/PEDOT:PSS/P3HT:PCBM (1:1)/Al (with Al electrode prepared by magnetron sputtering) showed a V_{OC} of 0.34 V, J_{SC} of 2.16 mA/cm^2, and a FF of 0.19, giving a PCE of 1.4×10^{-4} %.

CONCLUSIONS

Our study showed that exist influence of Al electrode preparation and kind of devices along with thickness of the active layer on photovoltaic parameters and impedance spectroscopy. The best photovoltaic parameters were obtained for device ITO/PEDOT:PSS/P3HT:PCBM/Al with the Al electrode prepared by thermal evaporation. For all devices depressed semicircles, or partial semicircles, were identified by IS. Resistances of device prepared by magnetron sputtering are in general lower than for device prepared by thermal evaporation, which gives significantly shorter relaxation times. This is ascribed to the micro contacts, which could be the result of electrode fabrication by magnetron sputtering. Energetic ions bombarding polymer layer could enter deep into it and even reach the bottom electrode. Moreover, the structure of polymers could be altered during this process, what changes their electrical properties.

REFERENCES

1. B.C. Thompson, M.J. Frechet, *Angew. Chem. Int. Ed.*, 47(2008)58
2. M. Palewicz, A. Iwan, *Current Physical Chemistry*, 1(2011)27
3. G. Dennler, M.C. Scharber, C.J. Brabec, *Adv. Mater.* 21(2009)1323

INFLUENCE OF CO AND CU SUBSTITUTION ON STRUCTURAL, ELECTRICAL, TRANSPORT AND ELECTROCHEMICAL PROPERTIES OF THE $Li_xNi_{0.9-y}Co_yMn_{0.1}O_2$ CATHODE MATERIALS

A. Milewska, J. Molenda

AGH University of Science and Technology, Faculty of Energy and Fuels, Department of Hydrogen Energy
al. A. Mickiewicza 30, 30-059 Krakow, Poland

Keywords: lithium ion battery, layered oxide, $LiNi_{1-y-z}Co_yMn_{0.1}O_2$, intercalation, transport properties

INTRODUCTION

Increasing requirement on the portable devices for energy storing is stimulating research on lithium ion batteries. The industry's main requirements with regards to Li ion batteries are their safety, stability and effectiveness of the charge/discharge process, which mainly depends on the used cathode material. Among cathode materials for the lithium ion batteries, the layered oxides stand out because of the high electrical conductivity, that is maintained during lithium intercalation / deintercalation process, that provides into higher current gained from the cell and shorten the charging time.

RESULTS

$LiNi_{0.65}Co_{0.25}Mn_{0.1}O_2$, $LiNi_{0.63}Cu_{0.02}Co_{0.25}Mn_{0.1}O_2$ and $LiNi_{0.55}Co_{0.35}Mn_{0.1}O_2$ cathode materials were synthesized by a soft chemistry EDTA - based method. All synthesized compounds have a well developed layered structure with trigonal *R*-3*m* symmetry. Increase in cobalt content causes that *a* lattice parameter is decreasing. Higher content of cobalt in $LiNi_{0.9-y}Co_yMn_{0.1}O_2$ suppress the cation mixing. Similar effect is observed for Cu-substituted $LiNi_{0.63}Cu_{0.02}Co_{0.25}Mn_{0.1}O_2$ and $LiNi_{0.63}Cu_{0.02}Co_{0.25}Mn_{0.1}O_2$ oxides.

Low temperature electrical conductivity and thermoelectric power results are presented. Higher electrical conductivity and higher number of effective charge carriers in pristine $LiNi_{0.9-y}Co_yMn_{0.1}O_2$ oxides are correlated with the increase of concentration of the Ni^{3+} ions.

Increase of manganese amount to 0.2 mol in $LiNi_{0.2}Co_{0.6}Mn_{0.2}O_2$ decreases the electrical conductivity few orders of magnitude and arises the activation energy to 0.3 eV (from 0.18 eV for $LiNi_{0.65}Co_{0.25}Mn_{0.1}O_2$).

The observed decrease of *a* parameter with lithium deintercalation is mainly related to the compensation of the charge and oxidation of nickel ions: $Ni^{2+} \rightarrow Ni^{3+} \rightarrow Ni^{4+}$. *c* parameter is increasing due to increasing electrostatic repulsion between $((Ni,Co,Mn)O_2)_n$ sheets, when Li amount is decreasing. Below the critical concentration of the lithium in the deintercalated oxides the *c* parameter starts to decrease and the *a* parameter starts to increase what is involved with structural instability of the deintercalated oxides.

Decrease of electrical conductivity during lithium deintercalation is related to the decrease of carrier concentration in the e_gNiCo band.

In the transition metals oxides containing cobalt the charge compensation during deeper lithium deintercalation occurs via formation of holes in the oxygen 2p band [1-3]. The obtained results show that the the structural instability of deintercalated materials occurs until whole amount of nickel is oxidized to Ni^{4+} ions. Ones can expect that during deeper deintercalation of lithium the oxygen ions participate in the charge compensation and as a result some part of nickel ions remain in the $3d^7$ configuration (Ni^{3+}). The obtained results of electrical conductivity and the results showing the changes of structural parameters in deintercalated materials indicate that more stable cathode material based on $LiNi_{0.9-y}Co_yMn_{0.1}O_2$, is that with lower concentration of cobalt, i.e. $LiNi_{0.65}Co_{0.25}Mn_{0.1}O_2$. $Li_xNi_{0.65}Co_{0.25}Mn_{0.1}O_2$ retains structural stability up to x_{Li}=0.35 mol.

Doping of $LiNi_{0.63}Cu_{0.02}Co_{0.25}Mn_{0.1}O_2$ oxide with Cu improves electrical conductivity. Electrical conductivity of $LiNi_{0.63}Cu_{0.02}Co_{0.25}Mn_{0.1}O_2$ is better than that of the most often investigated $LiNi_{1/3}Co_{1/3}Mn_{1/3}O_2$ [4]. In additional, similar to $LiNi_{0.65}Co_{0.25}Mn_{0.1}O_2$ oxide, $LiNi_{0.63}Cu_{0.02}Co_{0.25}Mn_{0.1}O_2$ retains structural stability up to x_{Li}=0.35 mol.

The electrochemical tests show that the discharge capacity of the $Li_xNi_{1-y}Co_yMn_{0.1}O_2$ (y = 0.25, 0.35) cathodes is improved with decreasing cation mixing effect, i.e. with lower nickel content. Poor capacity retention in the first cycle for the cell $Li/Li_xNi_{0.63}Cu_{0.02}Co_{0.25}Mn_{0.1}O_2$ is observed, however the capacity retention during the next cycles is equal 100 %.

ACKNOWLEDGEMENTS

This work is supported by the Ministry of Science and Higher Education Republic of Poland under Singapore-Poland Joint Research Project nr SINGAPUR/99/2007.

REFERENCES

1. G. Ceder *et al, Nature,* 392 (1998) 694.
2. L. A. Montoro *et al, J. Electrochem. Soc*., **147** (2000) 1651.
3. W.-S. Yoon *et al, J. AM. Chem. Soc*., **127** (2005) 17479.
4. M. Gozu *et al*, *Journal of Power Sources,* **194** (2009) 38.

SYNTHESIS AND PROPERTIES OF $LiFePO_4$ – CATHODE MATERIAL FOR Li-ION BATTERIES

W. Zając, D. Baster and J. Molenda

AGH University of Science and Technology, Faculty of Energy and Fuels, Department of Hydrogen Energy
al. A. Mickiewicza 30, 30-059 Krakow, Poland

Keywords: Li-ion batteries, LiFePO4, cathode materials

INTRODUCTION

Alternative energy sources such as sun, wind and nuclear require effective energy storage technologies. One of possibilities is chemical energy storage in rechargeable Li-ion batteries, which offer the highest gravimetric and volumetric energy density among currently used electrochemical power sources [1]. Another application of lithium batteries, which is in common use nowadays, is power supply for portable electronics, such as notebooks, digital cameras, mobile phones etc. If certain issues concerning capacity, safety and cost are overcome, lithium batteries could be used in power grids, hybrid and electric vehicles, and possibly many other functions will be found. The most promising cathode material for lithium cells is lithium iron phosphate $LiFePO_4$ with olivine-type structure. The main advantages of $LiFePO_4$ are its high theoretical capacity, high discharge potential (~3.5 V vs. Li), high thermal stability, which guarantees safety of use and stable capacity after numerous work cycles, moreover it is environmentally benign and of low cost. However, phospho-olivine possesses low ionic and electronic conductivity which results in low lithium chemical diffusion coefficient, and in turn low charge/discharge rates. Consequently, thorough modification of the material is needed in order to obtain effectively working Li-ion cell cathode. Macroscopic transport properties can be improved on two main ways: by decreasing the lithium-ion diffusion path length within $LiFePO_4$ particle, which can be achieved by reduction of particle size, or by covering of $LiFePO_4$ grains with highly lithium and electron-conducting layer such as carbon [2-4]. Preferably, both methods should be implemented at the same time.

EXPERIMENTAL

Nano-sized $LiFePO_4$ powder was obtained by a low temperature method developed by Delacourt et al. [5]. The method is based on precipitation from water-ethylene glycol solution containing LiOH, $FeSO_4$ and H_3PO_4. Obtained powder was dried in vacuum at 50°C and annealed at 300-800°C for 12 h under H_2/Ar mixture flow. Crystal structure of the obtained material was characterized using X-ray diffraction (XRD) method with Panalytical X'Pert Pro diffractometer. Powder microstructure was examined by SEM microscopy. Electrochemical properties of the cathode materials were studied in a $Li/Li^+/LiFePO_4$-type cell [6,7].

RESULTS AND DISCUSSION

XRD measurements confirmed single phase phospho-olivine *Pnma* structure of the obtained samples. The highest discharge capacity was received for $LiFePO_4$ annealed at 300°C. Comparison of discharge capacity values for $LiFePO_4$ annealed in inert and reducing atmosphere showed superior effect of the latter. The observed behavior can be rationalized by presence of Fe^{3+}-containing contamination, which was detected in the as-prepared samples by Moessbauer spectroscopy. H_2/Ar mixture turned out to be highly capable of reducing Fe^{3+} to Fe^{2+}, and in turn increasing material's electrochemical capacity.

CONCLUSIONS

Grains size and electrochemical properties, especially discharge capacity dependent on the final heating temperature of the material.

ACKNOWLEDGMENT

This work was supported by EU under the grant No. UDA-POIG 01.01.02-00-108/09-01.

REFERENCES

1. R.V. Kumar, T. Sarakonsri, Introduction to Electrochemical Cells, in High Energy Density Lithium Batteries. Materials, Engineering, Applications, eds. K.E. Aifantis, S.A. Hackney, R.V.Kumar, WILEY-VCH, 2010.
2. J.B. Goodenough, J. Power Sources 174 (2007) 996.
3. J. Molenda, J. Marzec, Funct. Mater. Lett. 1 (2008) 97.
4. O. Topkraci, H.A.K. Topkraci, L. Ji, X. Zhang, KONA Powder Part. J. 28 (2010) 50.
5. C. Delacourt, P. Poizot, S. Levasseur, C. Masquelier, Electrochem. Solid-State Lett. 9 (2006) A352.
6. W. Zając, D. Rusinek, J. Molenda, Ceramic Mater. 63 (2011) 261.
7. W. Zając, J. Marzec, W. Maziarz, A. Rakowska, J. Molenda, Funct. Mater. Lett. 4 (2011) 117.

RESEARCH ON THE CHOICE OF SUPERCAPACITOR MATERIALS WITH AN ELECTROLYTE ON THE BASIS OF IONIC LIQUIDS

A. Szmaja, B. Szubzda and R. Kuliński
Electrotechnical Institute Division of Electrotechnology and Materials Science
M. Sklodowskiej-Curie 55/61, 50-369 Wrocław, Poland

Keywords: supercapacitors, ionic liquids, temperature influence

INTRODUCTION

The purpose of the presented research is to elaborate a capacitor model which is characterized by the possibly smallest sizes and mass and which can accumulate a big amount of energy. This requirement results from the target application of the device in supply systems of mechanical vehicles both for hybrid electric vehicle (HEV) and electric vehicle (EV). This application, where the combustion engine produces waste heat, brings about the necessity to comply with other requirements for supercapacitors: efficiency and reliability in higher working temperatures. It is particularly important that this application can be safely used in means of transport – it is non-toxic and non-explosive.

All of these requirements make it necessary to employ electrolytes on the basis of room temperature ionic liquids (RTILs). They are non-volatile, non-flammable and non-toxic, thus improving their features as an electrolyte in higher temperatures [1,2]. Moreover, they are characterized by a high value of the so called potential window due to which they are able to accumulate more energy per mass or sizes than supercapacitors which use other typical electrolytes.

EXPERIMENTAL

The research plan comprised:

- choice of electrolyte – physical and electrochemical examinations of chosen ionic liquids in higher temperatures,
- choice of electrode material - physical and electrochemical examinations of chosen carbon materials,
- choice of separator material – examinations of wettability and model electrochemical examinations, including resistance.

In the subsequent research stages, the following are to be carried out:

- checking the influence of co-solvents on physical and electrochemical properties of ionic liquids as electrolytes with a particular emphasis on simultaneous influence of adding a co-solvent and higher temperature,
- research on the choice of the current collector material,
- elaborating a technology of depositing electrodes and performing a series of test models.

For the purpose of carrying out the presented cycle of research, six low temperature aproton ionic liquids were chosen which contained cations of imidazolium and pyrrolidinium: [BMIM][BF_4], [BMIM][PF_6], [BMIM][Tf_2N], [EMIM][BF_4], [EMIM][Tf2N], [PYR_{14}][Tf_2N].

As materials for electrodes, two activated carbon were researched: carbon A – obtained by thermal carbonization of plant originated materials. Carbon B – obtained by chemical decomposition of oil materials.

The research on the choice of separators comprised the materials on the basis of cellulose and woven polymers: polyamide and polypropylene.

The research cycle included:

- porosity examinations and distribution of pores of carbon materials,
- determination of influence of temperature (in the range of 25°C - 135°C) on: viscosity, electrical conductivity, electrochemical potential window of chosen ionic liquids,
- research on electrochemical properties in the same range of temperatures of supercapacitor models with the employment of all combinations of the researched materials: electrolytes, electrode materials and separators. In this way were carried out: cyclic voltammetry, galvanostatic charge-discharge, and impedance spectroscopy in the 2-elelctrode system.

CONCLUSIONS

The research results confirmed advantages of ionic liquids as electrolytes for applications in systems working in higher temperatures.

They allowed for determination of dependencies existing between viscosity, conductivity and capacitance, electrical resistance and potential window of supercapacitor models.

For each of the researched six ionic liquids, an optimal system was determined i.e. electrode material–separator-working temperature, where the most advantageous values of potential window, cell resistance and electric capacitance are achieved. These are the key data for obtaining the required values of power and energy density of an appliance.

REFERENCES

1. M. Mastragostino, F. Soavi, *Journal of Power Sources* 174 (2007) 89–93
2. M. Galiński, A. Lewandowski, I. Stępniak, *Electrochimica Acta* 51 (2006) 5567–5580

ELECTROCHEMICAL ACTIVITY OF C/Li_2MnSiO_4 COMPOSITE CATHODE MATERIAL SYNTHESIZED BY SOL-GEL METHOD

M. Świętosławski[1], M. Molenda[1], M.M. Zaitz[1], W. Maziarz[2] and R. Dziembaj[1]

[1]Faculty of Chemistry, Jagiellonian University, Ingardena 3 30-060 Krakow, Poland

[2]Institute of Metallurgy and Material Science, Polish Academy of Sciences, Reymonta 25, 30-059 Krakow, Poland

Keywords: Li-ion batteries, Li_2MnSiO_4, carbon coating, nanocomposite, CCL

INTRODUCTION

Development of portable electronic devices is much faster than development of energy storage systems which power them. Recently, lithium-ion batteries became the most popular portable energy source. The main challenge in improving Li-ion batteries characteristic is to find a proper cathode material with high energy density and appropriate chemical stability at the same time. Beside that cathode material should be cheap and environmentally friendly [1].

Lithium manganese orthosilicate Li_2MnSiO_4, a member of polyanionic cathode material family, with its high chemical stability due to a presence of strong covalent bonds Si-O, seems to be worth a closer look. Theoretical ability of deinsertion of two lithium ions per unit formula leads to very high theoretical capacity of 333 mAh/g [2]. Moreover, potentially low production cost and low environmental impact of Li_2MnSiO_4 makes it promising cathode material for lithium-ion batteries. Unfortunately lithium manganese orthosilicate reveals very low electrical conductivity. Reducing grain size and coating the material with carbon can significantly improve electrical properties of the composite [3].

The aim of this work is examination of electrochemical behaviour of C/Li_2MnSiO_4 and CCL/Li_2MnSiO_4 obtained by sol-gel method.

EXPERIMENTAL

The C/Li_2MnSiO_4 composite was produced in one-step synthesis using sol-gel method (Pechini type) [4]. Controlled calcination of the obtained gel resulted in formation of Li_2MnSiO_4 nanosized grains encapsulated in conductive carbon matrix formed from organic compounds with carbon load ca. 35 wt.%. Preparation of composites with different amounts of carbon required burning out primary carbon and coating Li_2MnSiO_4 with conductive carbon layers. CCL/Li_2MnSiO_4 composites were produced by wet polymer precursor deposition on active material grains and controlled pyrolysis. As a carbon polymer precursor poly(N-vinylformamide) with pyromellitic acid (PMA) additive was used [5, 6]. For comparison standard composite was prepared by mixing Li_2MnSiO_4 with commercial carbon black (CB) additive (CB/Li_2MnSiO_4 composite).

Composites were studied using thermal analysis (TG/SDTA-EGA), X-ray diffraction (XRD), N_2 adsorption measurements (N_2-BET), electrical conductivity studies (EC) and transmission electron microscopy (TEM) to find the relations between structure, morphology and electrochemical properties.

All the obtained samples were tested in Li-ion battery cell. Galvanostatic charge-discharge cycling tests were performed in CR 2032 coin cells Li/Li^+/(C/Li_2MnSiO_4) using 1M $LiPF_6$ solution in EC/DEC (1:1) as electrolyte. Tests were conducted within 2.7-4.7 V potential range at C/200 and C/100 rates at room temperature.

CONCLUSIONS

C/Li_2MnSiO_4 composite was successfully synthesized in a one step process. It was found that electrochemical properties of obtained composites strongly depended on thickness and morphology of carbon layer covering the active material grains. The best performance revealed CCL/Li_2MnSiO_4 composites, at initial charge high capacity up to 227 mAh/g was observed while first discharge cycle resulted in 101 mAh/g.

ACKNOWLEDGMENT

The authors acknowledge a financial support from the Polish Ministry of Science and Higher Education under research grant No. N N209 088638 and from the European Institute of Innovation and Technology, under the KIC InnoEnergy NewMat project. One of the authors (M.Ś.) acknowledge a financial support from the International PhD-studies programme at the Faculty of Chemistry Jagiellonian University within the Foundation for Polish Science MPD Programme. The part of the measurements was carried out with the equipment purchased thanks to the financial support of the European Regional Development Fund in the framework of the Polish Innovation Economy Operational Program (contract no. POIG.02.01.00-12-023/08).

REFERENCES

1. J. M. Tarascon, M. Armand, *Nature* 414(2001)359
2. R. Dominko, *Journal of Power Sources* 184(2008)462
3. A. Nyten, A. Abouimrane, M. Armand, T. Gustafsson, J. O. Thomas, *Electrochemistry Communications* 7(2005)156
4. M. Molenda, M. Świętosławski, A. Rafalska-Łasocha, R. Dziembaj, *Functional Material Letters* 2(2011)135
5. M. Molenda, R. Dziembaj, E. Podstawka, L.M. Proniewicz, Z. Piwowarska, *Journal of Power Sources* 174(2007)613
6. M. Molenda, R. Dziembaj, A. Kochanowski, E. Bortel, M. Drozdek, Z. Piwowarska, *Patent appl.:* WO 2010/021557 and US 2011/0151112

NON-METAL DOPED TITANIA AS ELECTRODE MATERIAL FOR ENERGY STORAGE AND CONVERSION DEVICES

A. Lisowska-Oleksiak[1], K. Siuzdak[1,2], L. Vignau[2]

[1]Chemical Faculty, Gdansk University of Technology
Narutowicza 11/12 , 80-233 Gdańsk, Poland
[2]Organic Electronics Group University of Bordeaux, Bordeaux Institute of Technology,
Laboratoire IMS – ENSCBP – IPB, UMR CNRS 5218, 16, Avenue Pey Berland
33607 Pessac Cedex, France

Keywords: titania electrodes, non-metal doping, electrochemical capacitors, solar cells

INTRODUCTION

Progress in technology related to synthesis of electrode materials stimulates commercial application of advanced devices in both a) energy conversion from solar to electric and in b) electric energy storage. Nowadays the most popular approach in the field of solar cells is focused on Grätzel type systems so called dye sensitized solar cell DSSC and inverted organic solar cells [1, 2]. All these type of devices require semiconductor film active under electromagnetic wave illumination with an appropriate position of valence and conduction bands. The material of the first choice is TiO_2. The energy band gap of anatase is 3.25 eV which means that maximum on absorption spectra is positioned in the UV region. There are several ways to shift the maximum towards the red light. One is based on non-metal doping of titania structure. The dopants known to cause the expected red shift are: nitrogen, boron, iodine, sulphur, phosphorus. The doping triggers changes in valence state of titanium. New surface redox activities may appear giving rise to electrode psedocapacitance. Thus, application of non-metal doped TiO_2 in electrochemical capacitors may occur beneficial. Expected enhanced pseudofaradaic current of non-metal doped TiO_2 electrodes opens new possibilities for fast charging / discharging processes [3]. The aim of our work is to develop technological procedures for synthesis of non-metal doped TiO_2 for further tests and potential application in electrochemical devices like a) supercapacitors and b) solar cells. Focusing on new materials for two different applications is favourable in respect for possible commercial stage of novel doped TiO_2 synthesis technology.

EXPERIMENTAL

Non-metal doped TiO_2 synthesis procedure is based on hydrothermal treatment of appropriate Ti(IV) complex containing chemical bond between Ti centre atom and dopant atom(s). Proposed synthesis proceeds without solid-state diffusion-control doping stage [4]. Ti(IV) halides (Hal) ($TiCl_4$, TiI_4) dissolve in aprotic solvents AP (AP: DMF, DMSO, ACN) due to formation of soluble complexes. The general formula of the complexes molecule can be given as $Ti(Hal)_4$ $(AP)_2$. Three types of "smart" powders have been produced [3-5]. There are N-TiO_2, I-TiO_2 and S-TiO_2. All of them exhibit red shift in absorbance spectrum in comparison to pure TiO_2. The co-precipitation of alkali metal halides during thermal stage guaranties fine powder formation of a mean crystalline size below 20 nm [4,5]. Cyclic voltammetry measurements for electrodes S-TiO_2 and electrodes I-TiO_2 exhibit redox activity in a vicinity responding to Ti(III)/Ti(II) one electron transfer. Appearance of this kind of redox process is a consequence of dopand introduction. Observed increase in pseudofaradaic surface current allows to use S-TiO_2 and I-TiO_2 as a components in electrode materials for electrochemical capacitors.

The second application of doped TiO_2 aims on solar cells. Preliminary tests of non-metal doped TiO_2 in solar cells (type of FTO/X/N3dye/Z-50 electrolyte/Pt/FTO) proves their advantages character in comparison to pure TiO_2, as photon to electron efficiency highly increases for cells with doped materials, see Table below:

X 1 µm	efficiency p-e /%	V_{oc} / V	J_{sc} / mA cm^{-2}	*FF*
TiO_2	0.54	0.64	1.49	0.57
S-TiO_2	2.45	0.75	5.95	0.55
I-TiO_2	3.18	0.76	7.26	0.58

FF – fill factor, V_{oc} –open circuit voltage, J_{sc} – short circuit current density

CONCLUSIONS

The synthesis method for non-metal doped TiO_2 is found to be efficient and straightforward. All doped TiO_2 nanopowders, active under visible light illumination, can be effectively employed in solar cells of different configuration. Moreover, S-doped TiO_2 and I-doped TiO_2 with Ti(III)/Ti(II) surface redox activity are good for application in supercapacitors.

ACKNOWLEDGMENT

This work is supported by Polish Ministry of Science and Higher Education under grant NN209245238. K.S. is thankful for a scholarship InterPhD for her stay at University of Bordeaux.

REFERENCES

1. A. Hagfeld, G. Boschloo, L. Sun, L. Kloo, H. Petterson, Chem. Rev 110 (2010) 6596.
2. J. Weichert, R.B. Dunbar, H.C. Hesse, W. Wiedemann, L. Schmidt-Mende, Adv. Mat. 23 (2011) 1810.
3. K. Siuzdak, M. Wilamowska, A. Lisowska-O Proc., ISEE-Cap 11 Poznan, 12-16 June 2011 p.112.
4. K. A. Lisowska-Oleksiak, K. Szybowska, Polish Patent Application P 387327 (24.02.2009).
5. A. Lisowska-Oleksiak, K. Siuzdak, V. Jasulajtienè Electrochim. Acta 55 (2010) 5851.

HIGH SURFACE AREA AND NANOPOROUS CARBON FROM CHITOSAN FOR SUPERCAPACITORS

A. Kucińska and J. P. Łukaszewicz
Faculty of Chemistry
Nicholas Copernicus University, ul. Gagarina 11
87-100 Torun, Poland

Keywords: chitosan, charcoal, carbonization, nanopores

INTRODUCTION

Nitrogen-rich carbon adsorbents are potentially applicable to the construction of super capacitors (SC). Chitosan is a biopolymer obtained by deacetylation of another commonly accessible biopolymer, chitin. Chitosan structure is characteristic because of amino groups linked to the chain of six-member saccharide rings i.e. poly-(D)glucosamine. The polymer is rich of nitrogen and possesses specific acid-base properties and chelation abilities directly resulting from the presence of NH_2- groups. The similarity to cellulose suggests that chitosan can be transformed in an active carbon by a simple heat-treatment in oxygen-free conditions. However, carbonisation of pure cellulose is a more complex case since the achievement of more advanced surface parameters (total pore volume, specific surface area) needs additional treatments (preliminary oxidation) and/or specific carbonisation conditions (hydrothermal carbonisation) of pure cellulose. There is lack of work describing successful transformation of chitosan to an active carbon of satisfactory surface parameters. Such a carbon could potentially find several important applications since carbonisation of nitrogen-rich raw materials frequently results in a high content of nitrogen in the carbonizate, mostly in the form of nitrogen-containing base-type functional groups. If the concept of a direct chitosan carbonisation could really yield high surface-active carbons it would have been realised a long time ago, but in practice no satisfactory results have been achieved so far. We have assumed that proper surface parameters are achievable provided the carbonisation of the considered raw material (chitosan) is supported by an additional activating procedure, as in the case of pure cellulose carbonisation. Our attention was focused on less aggressive procedure involving the application of a bulge agent, which should help the development of a porous sponge-like structure of a chitosan driven char. Past experience in the fabrication of carbon films [1] for chemical sensing applications proves that inorganic carbonates like Na_2CO_3 and/or K_2CO_3 act as bulge agents when added to the carbon matrix precursor.

EXPERIMENTAL

A series of carbon samples were prepared in a similar manner. Dry chitosan powder was provided by Sigma Aldrich (75-85% deacetylation, medium molecular weight, CAS Number: 9012-76-4). In this form chitosan has limited ability to absorb water and water solutions, therefore HCl was used to partly depolymerise chitosan chains and protonate NH_2- groups. Both phenomena help to solubilise the polymer. 10 g of chitosan was mixed with 45-100 cm^3 of water and neutral pH of the slurry was noticed. Then, 3 cm^3 of 1 M HCl water solution was added, but surprisingly the pH of the slurry did not change. Only the consistency of the slurry altered since after HCl addition it became more uniform and sticky and resembled a thick paste. The pH did not change because, as expected, protons in the acid solution chemically bonded to the NH_2- groups in the polymer. Neutral pH let to admit carbonate solution (4 - 17 % Na_2CO_3) and no spectacular reaction results were visible i.e. CO_2 was not released due to direct reaction of sodium carbonate with the strong acid. The concentration of sodium carbonate in the modifying solution and in the paste was low enough to avoid its instant precipitation. The chitosan-based paste was placed in a tubular stove and subsequently subjected to a heat-treatment: heating from 20 to 600 ^{0}C (10 ^{0}C / min), 600 ^{0}C (1 hour), cooling from 600 ^{0}C to room temperature (free cooling). The obtained black char was subjected to several chemical analyses (SEM/SEM-EDX, XRD, XPS, low temperature adsorption of nitrogen). The samples of chitosan which originated from virgin char were treated with 0.1 M HCl. A spectacular evolution of a gas in form of fine bubbles after immersing the char in acid solution was observed.

CONCLUSIONS

Etched char takes up high quantities of nitrogen, proving the presence of a well-developed surface area and pore structure. BET surface area increases after etching from ca. 1 m^2/g to 440 +/- 17 m^2/g. PSD suggests that the carbon is strictly nanoporous. Elemental composition of the surface (XPS measurement) proves that the removal of sodium is almost complete while the surface nitrogen level exceeds 6 % atomic. The nitrogen in the surface layer is chemically accessible and may reveal its presence in some surface processes. High-resolution N1s spectrum allows to state that most of the nitrogen atoms are constituents of NH_2- groups. The bulge agent forms Na_2CO_3 nano-crystallites. Their etching leaves empty cavities in the matrix, which contribute significantly to the total pore volume and surface area. The procedure allows a high level of nitrogen content to be retained in the surface region.

REFERENCES

1. J. P. Lukaszewicz, M. Skompska, *Sens. Actuators B 113(2006)970.*

$GdBaCo_{2-x}Me_xO_{5.5-\delta}$ LAYERED PEROVSKITES AS CATHODE MATERIALS FOR INTERMEDIATE TEMPERATURE FUEL CELLS

Andrzej Kulka[1], Yang Hu[2], Guilhelm Dezanneau[2], Janina Molenda[1]

[1]Faculty of Energy and Fuels, AGH University of Science and Technology
Al. Mickiewicza 30, 30-059 Kraków, Poland
[2]Laboratoire SPMS, Ecole Centrale Paris (UMR CNRS 8580),
Grande voie des vignes, 92295 Chatenay-Malabry Cedex, France

Keywords: Layered perovskites, cathode material, IT-SOFC

INTRODUCTION

Due to better materials compatibility, better long-term stability and reduced cost the operational temperature of Solid Oxide Fuel Cells (SOFC) must be reduce down to the 600-800°C. In order to minimize cathode polarization in this temperature range and hence obtain better cell performance new cathode materials with sufficient electrochemical properties must be found.

Particularly, $GdBaCo_2O_{5.5-\delta}$ has been reported to possess very good transport properties i.e. high surface exchange coefficient and oxygen diffusivity what with its very high electrical conductivity makes it a good candidate for cathode material for SOFC cells.

In this work we investigate $GdBaCo_2O_{5.5-\delta}$, $GdBaCo_{1.7}Fe_{0.3}O_{5.5-\delta}$, $GdBaCo_{1.4}Fe_{0.6}O_{5.5-\delta}$, $GdBaCo_{1.7}Ni_{0.3}O_{5.5-\delta}$ and $GdBaCo_{1.4}Ni_{0.6}O_{5.5-\delta}$ in terms of crystal structure, oxygen nonstoichiometry, electrical conductivity and single button-type SOFC cell in order to investigate effect of substitution of Co by Fe and Ni.

EXPERIMENTAL

All powders were fabricated via soft chemistry method using $Gd(NO_3)_3{\cdot}6H_2O$ $Ba(NO_3)_2$, $Co(NO_3)_2{\cdot}6H_2O$, $Fe(NO_3)_3{\cdot}9H_2O$, $Ni(NO_3)_3{\cdot}9H_2O$ and citric acid as a substrates. The water solutions of substrates in appropriate ratios were first rapidly evaporated, subsequently obtained precursors were ground thoroughly in agate mortar and heated at 850°C for 4 h. Obtained powders were once again ground in agate mortar and heated at 1050°C for 8h.

All samples exhibit layered perovskite structure with doubled *c* parameter and either orthorhombic Pmmm space group symmetry ($a_p \times 2a_p \times 2a_p$ where a_p is the basic cubic perovskite cell parameter) or tetragonal P4/mmm space group symmetry ($a_p \times 2a_p \times 2a_p$), depending on Fe and Ni content.

From the thermogravimetric measurements it was found that Fe and Ni doping affects oxygen content. At elevated temperatures for all samples mass loss was observed what was ascribed to formation of oxygen vacancies. It was noticed that depending on the Fe and Ni content the oxygen release and uptake rate changes. The obtained enthalpies of formation of the oxygen vacancies are very low and indicate that examined compounds are promising cathode materials for SOFC technology.

Electrical conductivity for all samples is very high and changes with Fe and Ni content (i.e. max~1000 $S{\cdot}cm^{-1}$ for $GdBaCo_2O_{5.5-\delta}$ and max~170 Scm^{-1} for $GdBaCo_{1.4}Fe_{0.6}O_{5.5-\delta}$). The behavior of electrical conductivity changes with temperature, and at lower temperature semiconductor-type behavior was observed whereas at certain temperature (dependent on Ni and Fe content) .

It was noticed from results of button-type SOFC cell measurements that substitution of Co by Fe lead to increase of obtained power density at lower temperature (~600°C) and its decrease at elevated temperature (~750°C). Ni doping improved SOFC performances in whole temperature range.

In order to conduct compatibility experiments, all cathode materials were mixed with $Ce_{0.8}Gd_{0.2}O_{1.9}$ electrolyte in 1:1 volume ratio, put into the tube furnace, heated up to 1000°C and kept in this temperature for 100h. In a case of Fe doping no other extra phase was observed. Substitution of Co buy Ni leads to formation of $BaCeO_3$ after annealing with $Ce_{0.8}Gd_{0.2}O_{1.9}$ electrolyte.

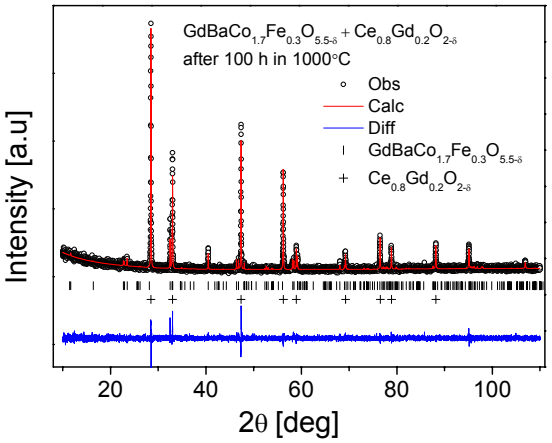

Fig1. XRD pattern for mixture of $GdBaCo_{1.7}Fe_{0.3}O_{5.5-\delta}$ + $Ce_{0.8}Gd_{0.2}O_{1.9}$.

CONCLUSIONS

$GdBaCo_{2-x}M_xO_{5.5-\delta}$, with M = Fe, Ni were synthesised. All materials exhibit layered perovskite structure with space group symmetry dependent on M doping. Electrical conductivity as a function of temperature was measured. Compatibility tests and button-type SOFC cell measurements were also performed.

ACKNOWLEDGMENT

This work was supported by NCBiR under the grant No. OZE/2/2010-AGH.

CHARACTERIZATION OF $GdBa_{0.5}Sr_{0.5}Co_{2-x}Fe_xO_{5.5\pm\delta}$ DOUBLE PEROVSKITES FOR APPLICATION IN IT-SOFC CELLS

Chihiro Kuroda[1], Konrad Świerczek[2]

[1]Faculty of Engineering, Shibaura Institute of Technology
3-7-5 Toyosu, Koto-ku, 135-8548 Tokyo, Japan
[2]AGH University of Science and Technology, Faculty of Energy and Fuels, Department of Hydrogen Energy
al. A. Mickiewicza 30, 30-059 Krakow, Poland

Keywords: structural properties, transport properties, cathode materials, A-site double perovskites, IT-SOFC

INTRODUCTION

Unique structural properties of so called A-site double (or sometimes layered) perovskites of general formula $AA'M_2O_{6-\delta}$ (A - lanthanide, A' - almost solely Ba, M - one of 3*d* metals or their mixture), together with their very high, mixed ionic-electronic conductivity make these compounds particularly interesting for application as cathode materials in Solid Oxide Fuel Cells working at intermediate temperatures (600-800°C). A-site ordering is inducted by a large difference in ionic radii between A and A' cations, and for example is observed in $GdBaCo_2O_{5.5\pm\delta}$ perovskite [1].

In this report we show characterization of structural (XRD) and transport properties (electrical conductivity and Seebeck coefficient), evaluation of the oxygen non-stoichiometry δ and chemical stability in relation to $Ce_{0.8}Gd_{0.2}O_{1.9}$ electrolyte, as well as preliminary electrochemical properties (IT-SOFC performance and impedance spectroscopy) of $GdBa_{0.5}Sr_{0.5}Co_{2-x}Fe_xO_{5.5\pm\delta}$ series of materials.

EXPERIMENTAL

$GdBa_{0.5}Sr_{0.5}Co_{2-x}Fe_xO_{5.5\pm\delta}$ (x = 0, 0.5, 1, 1.5 and 2) compounds were synthesized by ceramic method with Gd_2O_3, $BaCO_3$, $SrCO_3$, Co_3O_4 and Fe_2O_3 used as substrates. After milling in high efficiency Spex SamplePrep 8000M mill, materials were pressed into pellets and sintered in air at 1200°C for 100h. Structural studies were performed using Panalytical X'Pert Pro diffractometer with Rietveld analysis. Dependence of δ on temperature was evaluated on the basis of TG method performed on TA Q5000IR apparatus. The electrical conductivity (σ) was measured using four-probe DC method with simultaneous measurements of Seebeck coefficient (α). Chemical stability in relation to $Ce_{0.8}Gd_{0.2}O_{1.9}$ electrolyte was evaluated by analyzing of XRD data of cathode material - electrolyte mixtures heated at 800°C and 1000°C in air for 100h. Electrochemical performance (voltage - current density curves and impedance spectroscopy) was tested in button-type, electrolyte-supported IT-SOFC cells.

RESULTS AND DISCUSSION

Substitution of bigger Ba^{2+} cations (1.61Å) by smaller Sr^{2+} cations (1.44Å) decreases the tendency for separation of the cations into two distinctive layers (see Fig. below). Nevertheless, in case of Co-rich compounds from the studied $GdBa_{0.5}Sr_{0.5}Co_{2-x}Fe_xO_{5.5\pm\delta}$ system, we observed formation of A-site double perovskite structure, but with the increasing content of iron, the increasing amount of secondary phase, having simple perovskite structure appeared.

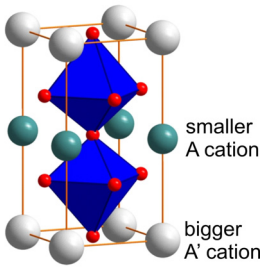

Fig. below shows the variation of unit cell parameters as a function of x for the studied materials.

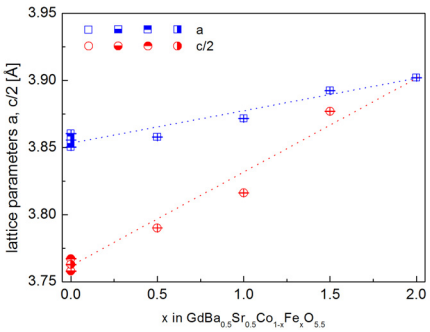

The measured electrical conductivity of the samples is very high, for instance for $GdBa_{0.5}Sr_{0.5}Co_{1.5}Fe_{0.5}O_{5.5\pm\delta}$ exceeds 700Scm^{-1} at 600°C and 500Scm^{-1} at 800°C. This, together with large oxygen nonstoichiometry and good chemical stability towards $Ce_{0.8}Gd_{0.2}O_{1.9}$ electrolyte, as well as promising, initial electrochemical measurements of IT-SOFC cells based on $GdBa_{0.5}Sr_{0.5}Co_{2-x}Fe_xO_{5.5\pm\delta}$ cathode make these materials attractive for application.

CONCLUSIONS

Characterization of physicochemical properties of $GdBa_{0.5}Sr_{0.5}Co_{2-x}Fe_xO_{5.5\pm\delta}$ perovskites indicates their attractiveness for application as cathode materials in IT-SOFC cells.

ACKNOWLEDGMENT

This work is supported by NCN under grant No. UMO-2011/01/B/ST8/04046.

REFERENCES

1. A. Chang, S.J. Skinner, J.A. Kilner, *Solid State Ionics* 177 (2006) 2009

EVALUATION OF $Ln_2CuO_{4\pm\delta}$ (Ln: La, Pr, Nd) OXIDES AS CATHODE MATERIALS FOR IT-SOFC

Kun Zheng[1], Agnieszka Gorzkowska-Sobaś[2], Konrad Świerczek[1]

[1]AGH University of Science and Technology, Faculty of Energy and Fuels, Department of Hydrogen Energy
al. A. Mickiewicza 30, 30-059 Krakow, Poland

[2]Department of Chemistry, University of Oslo, Centre for Materials Science and Nanotechnology FERMiO
Gaustadalleen 21, NO-0349 Oslo, Norway

Keywords: structural properties, transport properties, cathode materials, IT-SOFC, thin layers, PLD

INTRODUCTION

Recently, oxides from Ruddlesden-Popper series, particularly of $Ln_2MO_{4\pm\delta}$ type ($Ln_{n+1}M_nO_{3n+1}$, n = 1, Ln: lanthanides, M: 3*d* metals) have drawn a lot of attention in terms of their possible application as cathode materials in Solid Oxide Fuel Cells, especially in 600-800°C range. Their main advantage is related to moderate thermal expansion, while at the same time these materials possess sufficiently high mixed ionic-electronic conductivity [1]. In this report we show characterization of structural and transport properties, evaluation of the oxygen non-stoichiometry and chemical stability in relation to ceria-based electrolyte, as well as initial data showing electrochemical properties of $Ln_2CuO_{4\pm\delta}$ (Ln: La, Pr, Nd) oxides. The obtained results are compared to our previous report regarding properties of $Ln_2NiO_{4\pm\delta}$ (Ln: La, Pr, Nd) materials [2].

EXPERIMENTAL

The mentioned $Ln_2CuO_{4\pm\delta}$ compounds were synthesized using EDTA-based soft chemistry method [3]. XRD studies were performed using Panalytical X'Pert Pro diffractometer in 10-110° range with CuK_α radiation. The x-ray patterns were analyzed using Rietveld method. The initial oxygen excess δ, present in the materials, and it's temperature dependence in air was evaluated on the basis of TG reduction process, performed on TA Q5000IR apparatus. The electrical conductivity was measured using four-probe DC method with Seebeck coefficient measurements carried out simultaneously using dynamical method. Chemical stability towards $Ce_{0.8}Gd_{0.2}O_{1.9}$ was evaluated by analyzing of XRD data gathered for cathode material - electrolyte mixtures heated at 800°C and 1000°C in air for 100h. Electrochemical performance of $Pr_2CuO_{4-\delta}$ cathode was tested in button-type, electrolyte-supported IT-SOFC cells, analyzing voltage as a function of current density curves and impedance spectroscopy data.

Thin layers of $Pr_2CuO_{4\pm\delta}$ cathode material were deposited using SURFACE™ PLD setup equipped with KrF excimer laser. The c-plane sapphire, Si (001) and fused silica wafers were used as substrates. The layers were characterized by XRD, SEM and electrical conductivity measurements.

RESULTS AND DISCUSSION

Structural analysis revealed that obtained $Nd_2CuO_{4\pm\delta}$ and $Pr_2CuO_{4\pm\delta}$ materials possess *I4/mmm* tetragonal structure, while $La_2CuO_{4\pm\delta}$ shows *Bmab* orthorhombic symmetry. Additionally, electrical conductivity (σ) of $La_2CuO_{4\pm\delta}$, which is almost temperature-independent (~10Scm^{-1}) and positive values of Seebeck coefficient (α) are different, comparing to activated-type of σ and negative values of α for $Nd_2CuO_{4\pm\delta}$ and $Pr_2CuO_{4\pm\delta}$. The highest electrical conductivity was observed for $Pr_2CuO_{4\pm\delta}$, which exceeds 100 Scm^{-1} in 500-900°C range. This compound was selected as the cathode material for the constructed IT-SOFC cells. The exemplary data of the cell's performance are shown below. The maximum power output was measured to be ~0.12Wcm^{-2} at 800°C and ~0.27W·cm^{-2} at 900°C, these values are lower, comparing to cells based on $Pr_2NiO_{4\pm\delta}$ cathode material [2]. This may be related to the fact that in the working range the values of δ are negative for Cu-based material (oxygen vacancies) and positive for Ni-based material (interstitial oxygen).

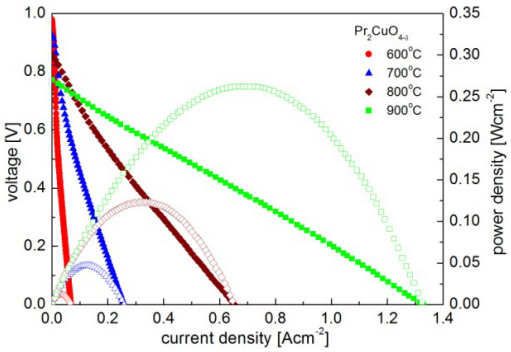

$Pr_2CuO_{4\pm\delta}$ thin films exhibit similar activation energy as the bulk materials, with the electrical conductivity values varying depending on the deposition conditions and post situ thermal treatment. This is followed by the microstructure evolution, which is reflected by the surface images and XRD patterns.

CONCLUSIONS

Characterization of physicochemical properties of $Ln_2CuO_{4\pm\delta}$ (Ln: La, Pr, Nd) oxides was performed, showing that $Pr_2CuO_{4\pm\delta}$ is attractive in terms of possible application as cathode material in IT-SOFC cells.

ACKNOWLEDGMENT

This work is supported by NCBiR under grant No. OZE/2/2010-AGH.

REFERENCES

1. E.V. Tsipis, V.V. Kharton, *J. Solid State Electrochem.* 12 (2008) 1367
2. J. Han, K. Zheng, K. Świerczek, *Funct. Mater. Lett.* 4 (2011) 151

PREPARATION OF CERIA BASED MEMBRANE FOR IT-SOFC

K. Furczoń, M. Molenda, A. Kochanowski, S. Zapotoczny and R. Dziembaj
Faculty of Chemistry, Jagiellonian University, Ingardena 3, 30-060 Krakow, Poland

Keywords: fuel cells, IT-SOFC, solid electrolyte, ceria, gelcasting

INTRODUCTION

Increasing requirement on the portable devices for energy storing is stimulating research on lithium ion batteries. The industry's main requirements with regards to Li ion batteries are their safety, stability and effectiveness of the charge/discharge process, which mainly depends on the used cathode material. Among cathode materials for the lithium ion batteries, the layered oxides stand out because of the high electrical conductivity, that is maintained during lithium intercalation / deintercalation process, that provides into higher current gained from the cell and shorten the charging time.

RESULTS

Solid Oxide Fuel Cells (SOFC) are considered as the most efficient energy conversion devices, what can bring many source of possible applications. However, one of main disadvantages of the fuel cells is a high operating temperature (~1000 °C), related to use of YSZ (yttrium stabilized zirconia) as electrolyte. To reduce the operating temperature a new electrolyte material must be applied. One of the most promising material for this application seems to be lanthanide doped cerium oxide. Ceria doped with trivalent cations shows an adequate high ionic conductivity. For further SOFC applications, this material must reveal both the highest ionic conductivity and the lowest electronic conductivity. The high chemical stability under oxidizing as well as reducing atmospheres is also required. Moreover, this material should be compatible with the applied electrodes materials. Not only the chemical properties of the new materials are in great importance, the physical properties must fulfill certain demands. For instance one of them is an ability to form them into a thin, strong and gas-proof membrane [1-8]. Great influence on sintering properties and membrane formation has the powder grain size. High surface energy of nanomaterials leads to decreasing of the sintering temperature [10]. Thus application of nanopowders in gelcasting process (GC) may be used to formation of strong and non-porous ceramic shapes in decreased temperature [11].

EXPERIMENTAL

In the present work the cerium(IV) oxide with different amount of dopants was synthetized by means of modified reserve microemulsion method [9]. The microemulsion is a thermodynamically stable system of nanosized water droplets, stabilized by surfactant and cosurfactant, dispersed in a continuous oil phase. In the reverse micelles (nanoreactors) a precursor of samarium or gadolinium doped ceria were prepared. The obtained precursors were calcined in 500 °C in order to form oxide materials. From this method the nanometric powders of doped ceria were produced. The morphology and the crystal structure of the samples were characterized by powder X-ray diffraction (XRD) and N2-BET surface area analysis as well as dynamic light scattering measurements (DLS). The optimal sintering temperature of such nanopowder was determined by dilatometers measurements and is much lower than that for conventional ceria powder [11].

Gelcasting process was applied in order to obtained thin, gas-proof and durable membranes. It was shown in our previous work that it is possible to obtain high-quality membrane from the ceria nanopowder [11].

In this work the Sm or Gd doped ceria membranes were prepared in GC process. The obtained membranes were later investigated by scanning electron microscopy (SEM) and atomic force microscopy (AFM). Finally high-temperature electrical conductivity measurements (EC) and impedance spectroscopy (IS) were applied for characterization of electrical properties of the prepared membranes.

ACKNOWLEDGMENT

The authors acknowledge a financial support from the Polish Ministry of Science and Higher Education under research grant No. N N209 099337 and from the European Institute of Innovation and Technology, under the KIC InnoEnergy NewMat project. The part of the measurements was carried out with the equipment purchased thanks to the financial support of the European Regional Development Fund in the framework of the Polish Innovation Economy Operational Program (contract no. POIG.02.01.00-12-023/08).

REFERENCES

1. B.C.H. Steel, Solid State Ionics 129 (2000) 95.
2. N. Kim, J.F. Stebbins, Chemistry of Materials 19 (2007) 5742.
3. B. Zhu, International Journal of Energy Research 30 (2006) 895.
4. Y. Zheng, Y. Shi, H. Gu, L. Gao, H. Chen, L. Guo, Materials Research Bulletin 44 (2009) 1717.
5. X. Zhou, F. Deng, M. Zhu, G. Meng, X. Liu, Journal of Power Sources 164 (2007) 293.
6. S. Fabris, S. de Gironcoli, S. Baroni, G. Vicario, G. Balducci, Physical Review B 71(2005) 041.
7. X. Sha, Z. Liu, X. Huanga, J. Miaoa, Z. Ding, X. Xin, W. Sua, Journal of Alloys and Compounds 428 (2007) 59.
8. F. Ye, T. Mori, D.R. Ou, A.N. Cormack, Solid State Ionics 180 (2009) 1127.
9. R. Dziembaj, M. Molenda, L. Chmielarz, M. Drozdek, M.M. Zaitz, B. Dudek, A. Rafalska-Łasocha, Z. Piwowarska, Catalysis Letters 135 (2010) 68.
10. A.V.Belyakov, Refractories and Industrial Ceramics, 2, (2009).
11. M. Molenda, K. Furczoń, A. Kochanowski, S. Zapotoczny, M. Szuwarzyński, B. Dudek, R. Dziembaj, Solid State Ionics 188, (2011), 135-139

SYNTHESIS AND CHARACTERIZATION OF PARA- AND META- POLYBENZIMIDAZOLES FOR HIGH TEMPERATURE PROTON EXCHANGE MEMBRANE FUEL CELLS

M. Malinowski, A. Iwan, G. Paściak
Electrotechnical Institute Division of Electrotechnology and Materials Science
M. Sklodowskiej-Curie 55/61, 50-369 Wrocław, Poland

Keywords: fuel cells, polybenzimidazoles, PEM membranes

INTRODUCTION

There are two commonly used electrochemical devices which allow of direct transformation from chemical energy into the electricity: batteries and fuel cells. Batteries as a widely used energy container exhibit well-known disadvantages that lead to the limitation of performance and area of applications. The other are fuel cells. It seems to they have still become better thus are considered as a sophisticated substitution of batteries. From large group of fuel cells, mainly due to extended range of applications Proton Exchange Membrane Fuel Cell (PEM-FC) has to be distinguished. Particularly, high temperature PEM-FC accomplished significant features such as more efficient ORR reaction, higher exchange current density, desirable resistance on contaminations, improved gas transport and water management, better gas diffusion coefficient, simplified stack structure and increased thermal dissipation. The commonly used polymers in PEM-FC as a membrane are Nafion and fluorinated polybenzimidazoles (F-PBI) [1, 2]. Polybenzimidazoles (*p*-PBI and *m*-PBI) are also investigated as high temperature PEM-FC. However, *p*-PBI has very rigid molecular structure and for this reason not good solubility in common solvents such as DMA or NMP [1-3]. Polybenzimidazoles (PBI) are commonly used for PEM fuel cells due to properties such as good ion conductivity and high temperature operation. These polymers provide well value of such parameters as chemical resistance, thermal stability, ion conductivity and mechanical strength but they have still problem with processability and solubility.

The main goal of this work was obtained *p*-PBI and *m*-PBI for application in high temperature PEM-FC. In this study, we prepared acid doped *p*-PBI thin film using a sulfuric acid as a solvent in high temperature. Obtained polymers were investigated by TGA, FTIR and to best of our knowledge first time by impedance spectroscopy (IS) in the context of chemical characterization.

EXPERIMENTAL

All materials were purchased from Aldrich and used as received. *p*-PBI and *m*-PBI were synthesized by polycondensation of 3,3'-diaminobenzidine (DAB) with terephthalic acid, TA (*p*-PBI) and isophthalic acid, IA (*m*-PBI), with a molar ratio of 1.25:1.25 mmol in poly(phosphoric acid) (PPA). The general procedure for the synthesis of PBI was as follows: DAB was dissolved in 12.6 g of PPA at about 150 °C. To the solution TA (or IA) was added, and the mixture was reacted at 200 °C for 24 h. Polymer was precipitated in distillated water and next filtrated, and washed with distillated water. The polymer was dried at 70 °C for 72 h. *p*-PBI was obtained as brown powder, while *m*-PBI as dark green powder.

Solubility of both polymers was tested in DMA, PPA and H_2SO_4. *p*-PBI and *m*-PBI were soluble only in H_2SO_4 (95%) after heating to about 150 °C. Film was cast from the acid solution onto glass plate and heating from 50 to 150 °C for 20 h. The obtained film was dark-brown or light brown depended on the polymer used. Both polymers were insoluble in DMA and PPA even after heating to 160 °C. In contrary to results presented in the paper [3], *m*-PBI synthesized by us was insoluble in DMA solution.

Solubility of PBI in strong protic acid such as H_2SO_4 can be explained by protonation of nitrogen atom (-N=, proton acceptor) in PBI by hydrogen atom of hydroxyl group in H_2SO_4. However, lack of solubility of *p*-PBI and *m*-PBI in H_2SO_4 in room temperature is probably caused by very rigid structure of these polymers and probably very high molecular weight. Differences between para- and meta- PBI was observed in the time of solubility. Meta substitution in PBI caused immediate solubility in hot H_2SO_4, while *p*-PBI was soluble in hot H_2SO_4.after 30 minutes of heating.

CONCLUSIONS

Synthesized with good yield two polymers were soluble only in H_2SO_4 after heating to 150 °C, what is caused by protonation of nitrogen atom and self-organization of the polymer structure. *p*-PBI and *m*-PBI membranes can be prepared via solution casting of polymer (in hot H_2SO_4). Polymers were analyzed by FTIR, TGA and IS.

ACKNOWLEDGMENT

The research is supported by Wroclaw Research Centre EIT+ under the project "The Application of Nanotechnology in Advanced Materials" – NanoMat (POIG.01.01.02-002/08) financed from the European Regional Development Fund (Operational Programme Innovative Economy, 1.1.2)

REFERENCES

1. Q. Li, J. O. Jansen, R. Savinell, N. J. Bjerrum, Prog. Polym. Sci. 34 (2009) 449-477
2. J. A. A. Asensio, E. M. Sanchez, P. Gomez-Romero, Chem. Soc. Rev. 39, (2010), 3210-3239
3. T-H. Kim, T-W. Lim, J-C. Lee, J. Power Surces, 172 (2007) 172-179

OVIERVIEW OF THE EU FP7 SUAV PROJECT

P. Pianko-Oprych, Z. Jaworski and B. Zakrzewska

Faculty of Chemical Technology and Engineering
Institute of Chemical Engineering and Environmental Protection Processes, West Pomeranian University of Technology, al. Piastow 42, 71-065 Szczecin, Poland

Keywords: fuel cells, polybenzimidazoles, PEM membranes

INTRODUCTION

The main objective of the 7th Framework Programme SUAV project is to design, optimise and build a 100-200 W microtubular Solid Oxide Fuel Cell (mSOFC) stack. The mSOFC stack will be integrated with a battery into a hybrid power system used to generate energy in a mini unmanned aerial vehicle (mini-UAV) or in the future to feed other light-weight man-portable applications. Additional components will also be included in the hybrid power system such as fuel processor to generate reformate gas from propane and other electrical, mechanical and control balance of plant. An important goal of the SUAV project is to achieve a significant improvement in miniaturisation of the mini-UAV platform and also further optimisation of the mission duration.

EXPERIMENTAL AND MODELLING

The lifetime of the mSOFC stack is influenced by its components, design and the way how it is manufactured and operated. In order to improve the long term stability of SOFC performance the investigation and understanding of processes and mechanisms depending on the operating conditions is of major importance. Therefore the SUAV project involves testing and modelling of the individual fuel cells, stacks, seals, interconnectors and other system components in fuel cell operating conditions. The operating parameters will include temperature, fuel composition, fuel utilization, air utilization, current density and transient characteristics. During the experimental analysis and development work the optimum cell geometry will be defined and stack will be designed, built and tested. Hydrogen will be the fuel in the first instance but catalysed propane will also be considered since this is the fuel to be used in the UAV. The stack design will take also into consideration the unique electrical and thermo-mechanical characteristics of the individual components. In the second step, full mSOFC power generation system will be created by integrating mSOFC stack with the necessary balance of plant components and controller. The system will be operated in the laboratory facilities and the required system data as flow, temperature, pressure for the system analysis will be collected.

One of the key issues for successful transition of SOFC fuel cell technology to the commercial phase is elimination of the residual stress inherent to the multilayer nature of the cell, thermal stress induced by uneven temperature distribution in stack operation and mechanical interactions with the other stack components [1]. Detailed understanding of those mechanisms and processes in fuel cells and their impact on the overall system performance will be achieved by developing tailored numerical methodology. The numerical methodology will be developed based on multi-scale fuel cell modelling including a simulation tool such as a commercial package CFD ANSYS-Fluent together with the AspenONE infrastructure. Modelling will help to optimise the stack geometry for high fuel utilisation and acceptable thermal characteristics. The modelling results will support the development work and will identify, in terms of flow characteristics, pressure and temperature levels, the best components of the fuel cell generator (reformer catalyst, pre-reformer) and/or other auxiliaries (control valves, pumps). Numerical results will lead to cost limitations of the novel fuel cell generation system.

CONCLUSIONS

The SUAV project will give the following advances in mSOFC technology: improvements in understanding and modelling of micro-tubular SOFC stack transient behaviour and operation as well as improvements in understanding of integration issues for balance of plant and optimisation of SOFC/battery capabilities.

ACKNOWLEDGMENT

This work is supported by JTI-CP-FCH Joint Technology Initiatives - Collaborative Project (FCH) under grant 278629.

Acknowledgment to the partners of SUAV: Ellart de Wit[1], Michael Walter[1], Michaela Kendall[2], Kevin Kendall[2], Tihamer Hargitai[3], Fredrik Silversand[3], Anna-Karin Jannasch[3], Marcus Lenberg[3], Charlotte Karlsson[3], Vincenzo Antonucci[4], Antonino S. Arico[4], Marco Ferraro[4], Rene Langermann[5], Caroline Turner[6], Matthew Maynard[6], Erich Erdle[7], Pierre Tantot[8], Eric Georges[8], Jacques Chapius[8], Waldemar Bujalski[9], Aman Dhir[9], Kate Howe[9], Tom Pike[9]

[1]HyGear Fuel Cell Systems B.V., Netherlands, [2]ADELAN LTD, UK, [3]CATATOR AB, Sweden [4]Consiglio Nationale Delle Ricerche, Italy, [5]EADS Deutschland GMBH, Germany, [6]EADS UK, UK, [7]Erdle Erich Korad - efceco, Germany, [8]Survey Copter, France, [9]University of Birmingham, UK

REFERENCES

1. A. Nakajo, F. Mueller, J. Brouwer, J. Van herle, D. Favrat, T. Hocker, *2nd International Workshop on Degradation Issues of Fuel Cells, Book of abstract and posters* JRC (2011) 33

Trends in LT/HT-PEMFC Core Technology Components R&D

Stanko Hočevar
National Institute of Chemistry, Ljubljana, Slovenia

Keywords: PEMFC

The search for better catalysts of oxygen reduction reaction in PEMFC that will use as small as possible load of noble metal catalyst will be reviewed form theoretical as well as experimental point of view. Recent results on activity and durability of Pt skin-type PtCu3 alloyed carbon supported catalysts will be presented and discussed.

Among the new approaches to HT proton conducting membranes development a special attention will be devoted to those that use various proton-conducting ionic liquids in combination with functional polymers and those using various heteropolyacids in combination with functional polymers. A comparison will be made with the characteristics of phosphoric acid doped polybenzimidazole-based membranes.

Application of materials for building interconnectors in fuel cells

R. Wlodarczyk, A. Kacprzak, Z. Bis
Czestochowa University of Technology
Department of Energy Engineering, ul. Brzeznicka 60A
42-200 Czestochowa, Poland

Keywords: stainless steel, graphite, sinters, interconnectors, fuel cells

The main focus and aim of the present article is to propose materials for building one of the elements of fuel cells i.e. bipolar plates. *Bipolar plates* are also termed *interconnectors* and are the elements which separate electrodes with electrolyte into individual cells. Their mass accounts for ca. 80% of cell's mass and they involve 45% of costs of production. Because of a number of functions performed by interconnectors for fuel cells, choice of materials for bipolar plates is extremely difficult.

The proposed method of material preparation and product properties provide a proposal for solution for the problem of high costs of production of the cell and the problem of choice of material for interconnectors in fuel cells. The present project focuses on materials obtained by means of *powder metallurgy*. The method of powder metallurgy is attractive since it opens up opportunities for obtaining parts with complicated shapes, which eliminates the stage of final mechanical processing of materials and suitably selected parameters of the process of compaction and sintering will allow for obtaining the products with desired structural and strength properties which are resistant to corrosion.

An important aspect of the project will be an in-depth analysis of properties of sinters obtained in different sintering atmosphere (dissociated ammonia, hydrogen, vacuum) and compacted at different compaction pressures [1-3]. When searching for materials which meet the requirements formulated by the Ministry of Energy (USA) [4], the authors proposed *sintered alloy steels* and *graphite-based composites* (the material widely used in technology of fuel cells, which, however, is brittle and difficult to be machined) with *addition of steel*.

The present study presents analysis of the properties of sintered alloy steels in terms of their practical use for production of interconnectors in fuel cells. The investigations encompassed measurements of mechanical properties, microstructural examinations and analysis of surface profile in sintered samples. The main criterion for selection of a particular material for components of fuel cells is their corrosion resistance in operating conditions of hydrogen fuel cells. In order to determine resistance to corrosion in the environment of operation of fuel cells, potentiokinetic curves (as a function of temperature) were registered in synthetic solution 0.1M H_2SO_4 + 2 ppmF^- at 80°C. The technology also ensures that the obtained materials show the required and expected porosity.

ACKNOWLEDGMENT

This work is supported by the Ministry of Education and Science in the years 2009-2012 under grant N N513 396 736.

REFERENCES

1. R. Wlodarczyk R., A. Dudek, Solid State Phenomena 165 (2010) 231-236
2. R. Wlodarczyk, A. Dudek, Steel Research 81 (2010) 1288-1291
3. R. Włodarczyk, A. Dudek, R. Kobyłecki, Z. Bis, Monografie Komitetu Inżynierii Środowiska PAN 59, III Kongres Inżynierii Środowiska: Polska Inżynieria Środowiska pięć lat po wstąpieniu do Unii Europejskiej, Lublin 2009, 273-280.
4. U.S. Department of Energy (*DOE*) www.energy.gov (September, 2011).

DEVELOPING SURFACE OF Ni AND Ni/Cu POWDER ELECTRODES BY CYCLIC OXIDATION/REDUCTION PROCESSES

A. Jaron
Faculty of Chemical Engineering and Technology
Cracow University of Technology, ul. Warszawska 24
31-155 Krakow, Poland

Keywords: powder electrodes, cyclic oxidation/reduction, Ni, Ni/Cu alloy

INTRODUCTION

Porous sinters made from different metals have been widely applied in the processes of gas and liquid filtration in chemical and petrochemical industries, as well as for the production of electrical energy and semiconductors. Additionally, sinters characterized by an expanded specific surface used as electrodes in electrochemical processes and as a catalyst or catalyst carriers [1-3].

The presented paper discusses a possibility of developing surface of Ni and Ni/Cu powder electrodes by cyclic oxidation/reduction processes for their further use as electrode precursors, in electrochemical processes of hydrogen production.

EXPERIMENTAL

The subject of the studies was the powders of the Ni (Alfa Products) and Ni70/Cu30 alloy (Goodfellow), both of 99.99% purity. Taking into consideration the application of the obtained sinters in electrochemical process of industrial release of hydrogen, the selection of the powders depended mainly on the low overvoltage of the hydrogen release on these metals.

In order to obtain a powder deposit of repeatable geometric parameters, forming boat-cartridge clips of nickel foil were made by the method described in paper [4].

The cyclic oxidization/reduction of the powder samples was conducted in a tubular furnace in temperature of 600°C, according to the procedure described below. The samples were placed in a cold furnace within the range of constant temperature each time. The system was washed in argon for 90 min (volumetric flow of 10dm^3/h), in order to eliminate the air form the apparatus, and next the heating up process to the temperature of 600°C was started at the rate of 10°C/min. After the required temperature was reached, the sample was thermostated for 5min. Next, an oxidizing factor (air) was incorporated into the system and the heating up was continued for 60min. After the oxidization process had been finished, the system was washed in argon for 90 min and next the reduction factor (H_2) was introduced in to furnace. The process of reduction was conducted at 600°C for 60min. Inertial cooling of the system was performed in argon atmosphere to room temperature after each cycle. The cyclic oxidization/reduction was repeated for 8 times.

The application of a furnace of a large diameter enabled the reduction of whole series of samples (25 items) in identical conditions, with the assuring of the proper excess of the gases.

The studies of a samples surface were conducted with the use of an FEI scanning microscope. The aim of morphology studies of the samples surface was to establish a qualitative assessment of its porosity and topography. The porosity characteristic of the sinters surface was carried out on the basis of SEM images with the use of ImageTool v. 3.0– stereographic analysis software.

CONCLUSIONS

As established in the performed research, the cyclic oxidation reduction process of nickel and Ni/Cu alloy powder as the SEM study shown, leads to a considerable development of their surface. This creates a possibility of their implementation as electrode in electrochemical processes of hydrogen production.

ACKNOWLEDGMENT

This work is supported by the Polish Ministry of Science and Higher Education under grant 3086/B/T02/2011/40.

REFERENCES

1. P. Los, A. Rami, A. Lasia, J. of app. electrochem. 23 (1993) 135-140
2. J. Jianga, , M. Gasik, J. Laine., M. Lampinen, J. of Alloys and Comp. 322 (2001) 281–285
3. A. Jaron, Z. Zurek, Arch. of Met. and Mat., 53 (3), (2008) 847-853
4. A. Jaron, Z. Zurek, Solid State Ionic, 181 (2010) 976-981

HYDROGEN ABSORPTION ABILITY AND CORROSION BEHAVIOUR OF METAL HYDRIDE MATERIALS

H. Bala, I. Kukuła, K. Giza, B. Marciniak[1], E. Różycka-Sokołowska[1] and H.Drulis[2]

Department of Chemistry, WIPMiFS, Czestochowa Univ.Technol.,
ul. Dąbrowskiego 69, 42-200 Częstochowa, Poland
[1]Institute of Chemistry and Environment Protection, AJD, Al. Armii Krajowej 15,
42-200 Częstochowa, Poland
[2] Institute of Low Temperatures and Structural Research, Polish Acad. Sciences,
Ul. Okólna 2, 50-422 Wrocław, Poland

Keywords: La(Ni,M)$_5$-composite materials, charge/discharge, corrosion

INTRODUCTION

In many papers the galvanostatic charge /discharge curves are applied to characterize the usefulness of the metal-hydride electrode materials [1-4]. At constant temperature and pressure the plot of charge/discharge curves strongly depends of many factors, like applied cathodic/anodic current densities [2], state of material saturation with hydrogen [4], state of activation (cycle number) [2], the method of electrode preparation (particle size, presence of conducting additions, kind and amount of binders etc) [5] and others. In our previous paper [6], we have shown possibilities to determine some important parameters from charge/discharge (-*i*/+*i*) curves of massive electrodes, such as effectiveness of hydrogen absorption, equilibrium potential of H_2O/H_2 system and its exchange current density. We have also indicated for possibilities of determining further kinetic parameters for these electrodes, not only for H_2/H_2O system but also for O_2/OH^- one, which is very important from the danger of electrode overcharge point of view.

EXPERIMENTAL METHOD

Three alloys with formal formulae: $LaNi_5$, $LaNi_4Zn$ and $LaNi_4Bi$ have been produced by arc-melting, the ingots have been ball-milled into powder and sieved. The pellets (ϕ 5 mm, $h \approx 3$ mm) containing 0.030±0.001 g of the tested materials have been pre-pared with 20-50 μm powder fraction, bonded with 2% of epoxy resin and pressed (0.1 kNcm^{-2}). The galvanostatic measurements have been carried out using CHI Instruments station. The cathodic charging with the current density of −186 mAg^{-1}(−0.5C) lasted 9000s in all experiments. The discharging process (+0.5C) has been breaking off every time when the electrode potential achieved value of 0.00 V vs HgO/Hg.

RESULTS AND CONCLUDING REMARKS

In most of papers authors attach rather low significance to the plots of the cathodic charge curves. However, in early charge steps (up to ca 300s) the $E^{(-i)}$ potential changes are very evident and systematic for the following cycles. In order to present these changes more clearly it is convenient to apply logarithmic scale for charge time axis [7]. Only for the first cycle (i.e. in the absence of oxides, the $E^{(-i)}$ consistently increases. This cathodic potential increase may be ascribed to the material mechanical degradation and its effective surface development resulting from hydrogen absorption [7]. It is possible to prove on the basis of Evans diagrams that $E^{(-i)}$ increase of 0.12V is caused by surface development by an order of magnitude. Thermo-dynamic analysis allows to ascribe the particular steps of the charge curves to the partial processes of not only water reduction but reduction of oxide phases produced during electrode discharging as well.

Knowledge of time periods found for particular reduction processes allows to determine the material corrosion rate. As it results from Faraday's law, the amount of Ni_3O_4 produced in anodic cycle is negligible but the amounts of NiO are $3.0 \cdot 10^{-4}$ g which is equal to 0.8% of the initial electrode mass and corresponds to the $LaNi_5$ corrosion rate of 0.14 mgcm^{-2}h. Similar analysis performed for Bi substituted alloy indicates its greater corrosion rate (3.3 mgcm^{-2}h) which is caused by presence of LaBi phase in this alloy and production of $Bi_2O_3/Bi(OH)_3$ deposit during discharge step. What is more, the Bi substituted alloy absorbs much less hydrogen than the reference, $LaNi_5$ compound. On the other hand, Zn is the addition which distinctly decreases the hydrogen equilibrium pressure whereas the hydride capacity for this alloy exceeds that for $LaNi_5$ compound. The corrosion rate of Zn substituted alloy is comparable with that for the $LaNi_5$ reference.

ACKNOWLEDGEMENTS

The research was co- supported by Wrocław Research Centre EIT+ under the project-NanoMat (*POIG.01.01.02-02-002/08)* financed by the European Regional Development Fund (*Innovative Economy Operational Programme,* 1.1 .2*)* and by MNiSW (grant Nr N-N507 514638).

REFERENCES

1. J.J.G.Willems, *Philips J.Research*, 39 (1984) 65
2. D.Mu, Y.Hatano, T.Abe, K.Watanabe, *J.Alloys Comp.,* 334 (2002) 232
3. J.Wu, R.Li, H.Su, X.Wang, *J.Alloys Comp.,* 289 (1999) 251
4. M.Tliha, H.Mathlouthi, J.Lamloumi, A.Percheron-Guegan, *Int.J.Hydrogen En.,*32 (2007) 611
5. I.Kukula, H.Bala, *Ochr.przed Korozją* 53 (2010) 225
6. H.Bala, K.Giza, I.Kukula, *J.Appl.Electrochem.* 40 (2010) 791
7. I.Kukuła, H.Bala, *Ochr.przed Korozją* 54 (2011) 494

KINETICS OF INTERACTION OF HYDROGEN WITH THIN C-Pd FILMS

Anna Kamińska, Mirosław Kozłowski, Sławomir Krawczyk
Tele and Radio Research Institute
Ratuszowa 11, 03-450 Warsaw, Poland

Keywords: hydrogen sensor, C-Pd film

INTRODUCTION

Nanocomposite C-Pd films with porous structure and palladium nanograins placed in/on carbon matrix are promising materials for hydrogen sensor applications. It is connected with highly developed surface area of these films and such properties of palladium as highly selective hydrogen adsorption/desorption. The sensing mechanism of C-Pd films is based on the resistivity changes of Pd in the presence of hydrogen. Interaction between hydrogen and palladium nanograins begins with adsorption of H_2 on palladium surface following homolytic dissociation of hydrogen molecules to H atoms. These hydrogen atoms diffuse into Pd nanograins and occupy the interstitial sites of the lattice, forming solid solution [1,2]. At higher hydrogen pressure, further incorporation of hydrogen atoms induces a phase transition from α- to β-phase and creating of palladium hydride characterized by higher resistance than metallic palladium [3].

EXPERIMENTAL

The nanostructural C-Pd films were obtained by Physical Vapour Deposition method. In PVD process two separated sources containing fullerene C_{60} and palladium acetate $Pd(OAc)_2$ were used to prepare the films on alundum substrate with earlier deposited titanium electrodes. The structure and morphology of these films were characterized by Scanning Electron Microscopy. These studies exhibit that films are flat and composed of small uniform, angular grains (sizes of 200-400nm).

Sensing measurements were performed in various hydrogen concentrations in nitrogen. The flow of hydrogen through experimental chamber caused the increase of the films resistance due to formation of palladium hydride.

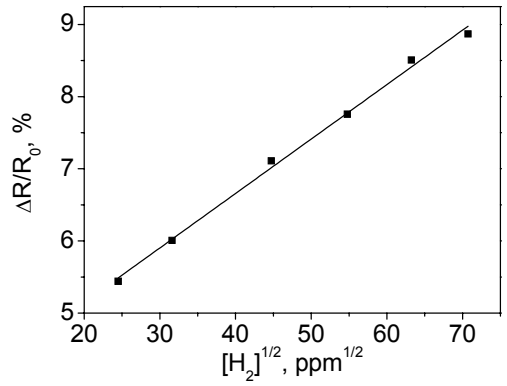

Fig. 1. C-Pd film sensitivity versus $[H_2]^{1/2}$.

The sensitivity (defined as relative change between resistance measured after exposure to hydrogen and the film initial resistance, $\Delta R/R_0$) reached 9% at 5000 ppm H_2. The response time ($t_{90\%}$) decrease in the function of increasing hydrogen concentration and achieve 90 s at highest examined H_2 concentration. Both C-Pd film sensitivity and response rate change in the function of H_2 concentration. We found the linear correlations between C-Pd film sensitivity (Fig.1) as well as response rate and $[H_2]^{1/2}$ (Fig. 2). Linear character of this relations is consistent with Sieverts law [3].

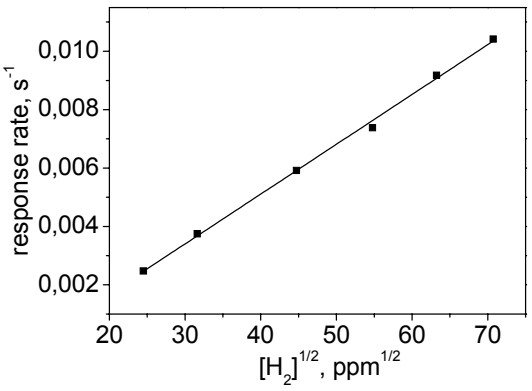

Fig. 2. C-Pd film response rate versus $[H_2]^{1/2}$.

CONCLUSIONS

The sensitivity and response rate of C-Pd films increase with hydrogen concentration. The changes of these values are in good accordance with Sieverts law.

ACKNOWLEDGMENT

This project is co-financed by the European Regional Development Fund within the Innovative Economy Operational Programme 2007-2013 (title of the project "Development of technology for a new generation of the hydrogen and hydrogen compounds sensor for applications in above normative conditions") No UDA-POIG.01.03.01-14-071/08-06.

REFERENCES

1. J.-S. Noh, J.M. Lee, W. Lee, *Sensors* 11(2011)825
2. X.Q. Zeng, M.L. Latimer, Z.L. Xiao, S. Panuganti, U. Welp, W.K. Kwok, T. Xu, *Nano Lett.* 11(2011)262
3. E. Lee, J.M. Lee, J.H. Koo, W. Lee, T. Lee, *Int. J. Hydrogen Energ.* 35(2010)6984

STRUCTURAL CHANGES IN C-Pd THIN FILMS DUE TO TEMPERATURE MODIFICATION IN CVD PROCESS

E. Kowalska, M. Kozłowski, J. Radomska, H. Wronka, E. Czerwosz

Tele and Radio Research Institute, ul. Ratuszowa 11

03-450 Warsaw, Poland

Keywords: hydrogen, sensor, palladium nanograins

INTRODUCTION

Nanostructures based on palladium nanocrystals and nanoporous carbon matrix are promising materials for hydrogen gas sensing applications. One of the factors which decides about using such materials in hydrogen detection is presence of palladium nanograins which absorb hydrogen. Well-developed specific surface area of carbonaceous matrix also could play a positive role in hydrogen adsorption. In literature one can find many examples of the use of Pd as hydrogen sensing elements (nanowires, nanoparticles, thin films) [1-3] because of its ability to adsorb/absorb large amounts of H_2.

Here we present results of studies of changes in a structure of C-Pd films obtained by PVD/CVD. These changes were caused by different temperature modification in CVD process. The morphology, topography and microstructure of films were changed when the temperature was varied.

For obtaining C-Pd films sensitive to hydrogen we apply two processes: 1) Physical Vapour Deposition (PVD) as the first stage to form the initial nanocomposite C-Pd films and 2) Chemical Vapour Deposition as the second stage to modify PVD films into porous structure and to extract palladium nanograins on the films' surface. Such change in the structure causes better sensitivity of films for hydrogen present in the ambient atmosphere.

EXPERIMENTAL

Fullerene C_{60} and palladium acetate PdC_2O_4 are precursors of the initial nanocomposite films in PVD process. Both compounds are evaporated from two separated sources using different current conditions. Thin (200-300nm) films obtained in this way on ceramic substrates (Fig.1a) are composed of amorphous carbon grains (80-100nm) and Pd nanocrystals (<10nm). Next, these films are modified by chemical CVD method at different temperature. We use xylene C_8H_{10} as an additional source of carbon in transformation process. This process is performed in a quartz reactor at different temperatures 500, 550, 600, 650, 700 and 750°C. The structure and morphology of these films are studied by SEM. These microscopic studies show that too low temperature (~500°C) is insufficient to transform carbon matrix into porous structure. Palladium grains obtained at this temperature are of sizes 100 - 400nm (Fig.1b). At the temperature of 750°C carbon matrix also is not porous but Pd nanograins (with size of 10 - 20nm) are displaced on the all surface of film (Fig.1d). Only films obtained at the temperature of 600 - 700°C are in form of carbonaceous porous matrix with palladium nanograins place inside the film as well as on its surface. It should be noticed too that Pd nanograins are grouped at big carbonaceous grain's edges at low temperature and with increasing temperature they migrate into these grains.

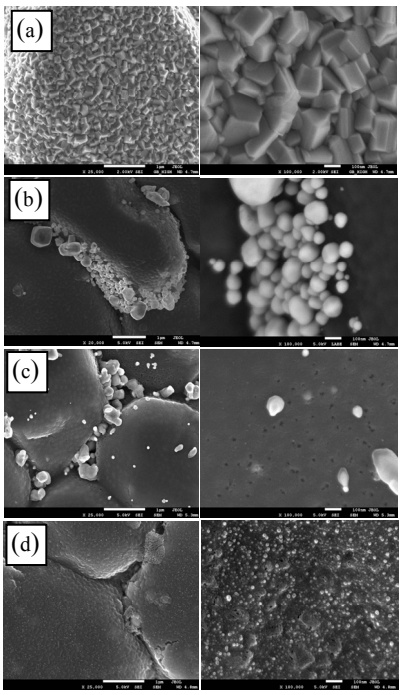

Fig.1 SEM images with different magnifications of (a) PVD film; (b) CVD film after 500°C; (c) CVD film after 650°C and (d) CVD film after 750°C.

CONCLUSIONS

From SEM observation we conclude that temperature ~ 650°C is optimal to transform carbon matrix of PVD film into porous structure and to obtain Pd nanograins on the film surface. With the temperature increase we observe the decrease of Pd particles sizes.

ACKNOWLEDGMENT

This project is co-financed by the European Regional Development Fund within the Innovative Economy Operational Programme 2007-2013 (title of the project "Development of technology for a new generation of the hydrogen and hydrogen compounds sensor for applications in above normative conditions" No UDA-POIG.01.03.01-14-071/08-06)

REFERENCES

1. S. Mubeen, T. Zhang, B.Yoo, *J. Phys. Chem. C* 111(2007)6321
2. W-Ch. Li, T.J. Balk, *Materials* 2(2009)2496
3. I. Pavlovsky, P. Soundarrajan, Z. Yaniv, Sensor & Transducers Journal 73(2006)793

FABRICATION OF NANOPOROUS MOLECULAR SIEVES FOR METHANE AND HYDROGEN STORAGE

A. Cyganiuk, O. Górska, A. Kucińska and J. P. Łukaszewicz

Faculty of Chemistry

Nicholas Copernicus University, ul. Gagarina 11

87-100 Torun, Poland

Keywords: gas separation, Salix viminalis, carbon molecular sieves

INTRODUCTION

High surface area and nanopore volume are key properties of carbon adsorbents enabling their applicability for methane and hydrogen storage. The discovery of a novel raw material for carbon molecular sieve fabrication is described. The invention deals with the application of widely accessible wood from *Salix viminalis* as a precursor for carbonization [1]. High temperature carbonization intermediately yields carbon molecular sieves of very narrow pore size distribution (PSD) in the range below 1 nm. Two methods for PSD evaluation were employed i.e. Horvath-Kawazoe [2] and Nguyen-Do [3] approach. Each of them is based on other assumptions on the mechanism of gas adsorption, but in both cases slit-like shape of pores is assumed what was widely accepted for active carbons. The Horvath-Kawazoe model considers a phase transition (at a specified relative pressure) in the layer of adsorbed gas leading finally to the filling of pores having a specific size. The Nguyen-Do model takes into account the formation of adsorbate layer on the pore walls. Despite the different theoretical background, both approaches yielded practically identical results pointing out a very narrow pore size distribution (PSD) what was the main target of the proposed approach of CMS fabrication (inexpensive fabrication of perfect molecular sieves). The effective diameter of pores is below 1 nm, what makes CarboSal® [4] molecular sieves a unique and very promising material for separation applications, especially for gas separation. Beside that gas accumulation may be regarded as another possible field of application. As mentioned, the study reports an unique way of nanoporous carbon molecular sieves fabrication using unconventional raw material i. e. *Salix viminalis* wood. The plant is inexpensive, easy to grow and harvest. Specific properties of *Salix viminalis* wood lead directly to the formation of carbon molecular sieves during pyrolysis of the raw material. Additional activation procedures are useful for the development of pore structure of carbon molecular sieves. Some typical parameters of the pore structure of such carbons make them similar to CNTs. It opens the way to wide application of novel nanoporous CMS in practice.

EXPERIMENTAL

CMS were fabricated from the dried wood of *Salix viminalis*. Pieces (ca. 4 x ca. 1 mm) of the wood were at first preliminary carbonised at 600^{0}C for 1 hour. A constant flow of nitrogen (99.99 %) was maintained during the whole procedure: heating to the desired temperature, 1 hour of heating at a constant temperature and cooling. Then, some samples underwent a subsequent carbonization for 3 hours at 600^{0}C.

Pore structure and specific surface area were determined by a widely accepted method exploiting the phenomenon of low temperature adsorption of chemically neutral gases. Nitrogen was applied as an inert adsorptive. For some samples, argon was applied instead of nitrogen to verify the conclusions derived from the N_2 adsorption data. Nitrogen (and argon) adsorption isotherms were recorded at the temperature of liquid nitrogen (-196^{0}C) by means of Micromeritics ASAP 2010 equipment. The standard software provided by the manufacturer of ASAP 2010 was employed for the regression of primary obtained adsorption data (nitrogen adsorption vs. relative partial pressure of the adsorptive).

Chromatographic gas separation tests were performed using a Schimadzu GC-14B gas chromatograph supplied with a TCD detector kept at a constant temperature of 110^{0}C. The tests were performed at several temperatures (70, 60, 50, 40 and 30^{0}C). The morphology of the carbon samples was investigated by means of an electron microscope (LEO 1430 VP, Electron Microscopy Ltd.) supplied with an EDS/EDX microspectrometer (Quantax 200-XFlash 4010, Bruker Ltd.). The diameter of most pores (ca. 0.8 nm) is comparable to the size of simple molecules, thus enabling separation. The sieving effect was proven in an industrially important process of CH_4/N_2 separation at 30-70^{0}C and providing effective accumulation of methane.

CONCLUSIONS

Separation of a methane/nitrogen gas mixture was investigated by means Carbon Molecular Sieves obtained from a newly discovered "green" resource: *Salix viminalis*. This plant grows quickly, yields hard wood and is frequently cultivated for energy purposes (renewable green fuel). Carbonisation of the wood yields carbons with a very narrow pore size distribution.

REFERENCES

1. J. P. Lukaszewicz, A. Arcimowicz, B. Klemp-Dyczek, *Patent application, Patent Office of Poland (2006)*.
2. G. Hórvath, K. Kawazoe, J. Chem. Eng. Jap. 16(1983)470.
3. C. Nguyen, D. D. Do, Langmuir, 15(1999)3608.
4. J. P. Lukaszewicz, R. P. Wesołowski, Trade mark registration pending, Patent Office of Poland (2007).

TOPOGRAPHY AND STRUCTURE OF HYDROGEN SENSITIVE C-Pd FILMS

Izabela Stępińska, MirosławKozłowski, Joanna Rymarczyk, Anna Kamińska ,
Piotr Dłużewski, Elżbieta Czerwosz
Tele- & RadioResearch Institute
Ratuszowa 11 Street
03-450 Warszawa, Poland

Keywords: hydrogen, sensor

INTRODUCTION

Palladium is an ideal material for hydrogen sensing because of its selective absorption of hydrogen gas and ability of formation a chemical species known as a palladium hydride. Hydrogen sensor designs rely on the fact that palladium metal hydride's electrical resistance is greater than this metal's resistance. Absorption of hydrogen in such film is accompanied by a measurable increase in electrical resistance [1]. In case of Pd nanoparticles, the increase of their volume after hydrogen absorption can lead to nanograins connection and creation of conductivity paths [2]. Our Pd-C film sensor is based on another properties that depend on the Pd nanograins sizes and their distribution in carbonaceous matrix. In this film, nanosized palladium particles swell when the hydride is formed, and in the process of expanding, some of them form new electrical connections with their neighbors The increased number of conducting pathways results in an overall net decrease in resistance. Depending on the structure of carbonaceous matrix (porous or amorphous carbon) and size and distribution of Pd nanograins in these film we can observe first or second type of changes undergoing due to hydrogen absorption. Here we report the topography and structure studies of films that show high sensitivity on hydrogen.

EXPERIMENTAL

The nanostructural C-Pd films were obtained by Physical Vapor Deposition (PVD) method. In this process two separated sources containing fullerene C60 and palladium acetate Pd(OAc)2 were used to prepare films. All films were deposited on oxidized Si substrates. The parameters of PVD process such as sources temperature (or current through these sources of C60 – IC and palladium acetate IPd), sources-substrate distance – d and duration time of the process - T influence on the structure, thickness and resistance of deposited film (Tab.1).

Tab.1 PVD process parameters and resistance of obtained films.

Sample no	I_C [A]	I_{Pd} [I]	d [cm]	T [min]	Resistance [kΩ]
1	2.1	1.1	69	8	1000
2	2.1	1.2	54	8	30000
3	2.1	1.2	54	10	0.0003

These films were characterised by scanning electron microscopy (SEM), Fourier Transformed Infrared absorption spectra (FTIR), atomic force microscopy (AFM) and measurement of resistance changes observed during hydrogen absorption.

Palladium nanograins sizes and their distribution within the film were studied with transmission electron microscopy (TEM).

FTIR spectra allow us for conclusion how the fullerene and palladium acetate were decomposited during PVD process.

In these processes the carbonaceous matrix is formed and in this matrix Pd nanoparticles are placed. The matrix composes of carbonaceous grains with various sizes and shapes. Topography of studied films reflects a mechanism of film growth. We observe islands growing layer after layer on the substrate (Fig.1a). Fulfilled with such islands surface of film is presented in Fig.1b.

a) b)

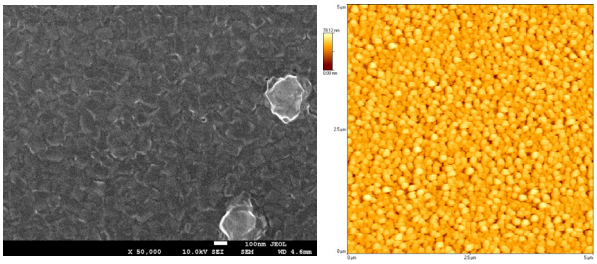

Fig. 1 a) SEM image of sample 2; b) AFM image of film's 2 surface fulfilled with islands

CONCLUSIONS

We found that electric properties, structure and topography of C-Pd films obtained by PVD method are strongly depended on PVD process parameters. Pd grains have different shapes, sizes and distributions within film depending on these parameters.

ACKNOWLEDGMENT

This project is co-financed by the European Regional Development Fund within the Innovative Economy Operational Programme 2007-2013 No UDA-POIG.01.03.01-14-071/08-06.

REFERENCES

1. F. J. Ibanez, F. P. Zamborini, Langmuir 22 (2006), 9789-9796
2. F. Favier, E.C. Walter, M.P. Zach, T. Benter, R.M. Penner, Science 293 (2001), 2227–2231

THERMAL STABILITY OF THIN Ni_3Al NANO AND ULTRACRYSTALLINE FOILS AS A POTENTIAL MATERIAL FOR HYDROGEN PRODUCTION

P. Jóźwik, A. Małecka, T. Czujko, Z. Bojar
Faculty of Advanced Materials and Technology
Military University of Technology, ul. Kaliskiego 2
00-908 Warsaw, Poland

Keywords: production, thermal stability, Ni_3Al intermetallic alloy, thin foils

INTRODUCTION

Ordered Ni_3Al–based intermetallic alloys are a group of advanced high-temperature structural materials which are characterized by relatively low density, excellent oxidation and corrosion resistance. These properties make them a considerable candidate for many high-tech applications [1-5]. In recent years, good catalytic properties of these materials during the decomposition of chemical compounds such as methane and methanol were confirmed [3-5].

In this respect, application of thin Ni_3Al foils as microchanneled reactors for hydrogen production is considerable promising.

Potential opportunity to use nano and ultracrystalline materials with attractive catalytic activity requires intensive study related to their structural stability in working conditions. Therefore, in this paper the problem of thermal stability of crystallites/grains at elevated temperature has been shown.

EXPERIMENTAL

Foils made of Ni_3Al-based alloy (Ni-22.1Al–0.26Zr–0.1B at.%) characterized by single-phase Ni_3Al (γ′) or diphase (γ′+/γ+γ′/) structure was selected. The foils were obtained by recrystallization in argon atmosphere followed by cold work to 98% rolling reduction at liquid-nitrogen temperature. As a result of these processes the nanocrystalline structure (d_0-23nm) for single and diphase material and ultracrystalline single-phase structure (d_0-120nm) were obtained. More details about fabrication process were shown previously [6, 7]. Investigation of thermal stability was carried out in long-lasting annealing for 50 and 100 hours at the temperature 300, 400, 500 and 600°C in air. After annealing Ni_3Al foils in micro- and nanocrystalline form were mechanically polished to remove oxides formed on the surface.

Analysis of structural stability was carried out by crystalline size measurements. The crystallite size was calculated from Cauchy/Gaussian approximation by linear regression plot using XRD diffractometer Seifert 3003. Additionally, grain size measurements obtained by electron backscatter diffraction technique (EDAX, Quanta 3D FEG), were carried out.

CONCLUSIONS

Temperature and annealing time have an impact on the structural stability of nano and ultracrystalline structure of investigated materials. The change course of crystallite/grain size measured by XRD and EBSD method were similar for all studied foils.

Nanocrystalline Ni_3Al sheet in all ranges of temperature didn't show clear stabilisation of crystallites/grains growth. Obtained results indicate that nanocrystalline diphase material showed significantly better thermal stability in 300 and 400°C than single-phase one. Existence of second phase in diphase γ+γ′ structure significantly inhibits grain growth of nanocrystalline structure up to 500°C when the participation of second phase decrease (below 0.5%) and material behaves similar to his single-phase Ni_3Al (γ′) counterpart.

The relatively stable growth of crystallites/grains in ultracrystalline material was observed at 300 and 400°C after 50 hours of annealing. Further annealing didn't significantly affect structural stability of investigated samples.

Obtained results showed that ultracrystalline Ni_3Al-based foil may be successfully introduced to catalytic system with working temperature up to 400 °C. In this range good catalytic activity of this material was proved during past experiments [5]. However, nanocrystalline materials possess better catalyticall properties on activation stage when the crystallites/grains growth may promote quicker forming of active centers on the surface.

ACKNOWLEDGMENT

The authors gratefully acknowledge the financial support by the Polish Ministry of Science and Higher Education (R0702502 and OR00004905)

REFERENCES

1. V. K. Sikka, S. C. Deevi, S. Viswanathan, R. W. Swindeman, M. L. Santella, Intermetallics, 8 (2000) 1329.
2. S. Deevi, V. Sikka, Intermetallics, 4 (1996) 357.
3. D. H. Chun, Y. Xu, M. Demura, K. Kishida, M. H. Oh, T. Hirano, D. M. Wee, Catalysis Letters, 106(2006) 71.
4. Yan Ma, Ya Xu, Masahiko Demura, Toshiyuki Hirano, Applied Catalysis B: Environmental 80 (2008) 15.
5. P. Jozwik, R. Grabowski, Z. Bojar, Materials Science Forum 636(2010) 895.
6. Z. Bojar, P. Jóźwik, J. Bystrzycki, Scripta Materialia, 55(2006) 399.
7. P. Jóźwik, Z. Bojar, Archives of Metallurgy and Materials, 52(2007) 321.

HIGH TEMPERATURE ACTIVATED AB_2 NANOPOWDERS FOR HYDROGEN COMPRESSION APPLICATIONS

E.D. Koultoukis[1,2], S.S. Makridis[1,*], D. Fruchart[2] and A.K. Stubos[1]

[1]Institute of Nuclear Technology and Radiation Protection, NCSR "Demokritos", Ag. Paraskevi, 15-310, Athens, Greece

[2]Laboratoire de Cristallographie du CNRS, 25 Avenue des Martyrs, BP 166, 38042 Grenoble Cedex 9, France

Keywords: Zr-based hydrides, intermetallic compounds, hydrogen compressors, AB2, efficient hydrogen storage

INTRODUCTION

Many scientists all over the world are trying to come up to a solution for longer term hydrogen storage. Moreover, a lightweight high-pressure hydrogen storage vessel starts to become a reality for onboard hydrogen storage technology, while its rapid development has led the working pressure to be much higher than it used to be. As a result, the need for efficient hydrogen compressors has begun to emerge.

The two main types of hydrogen compressors are the mechanical and the non-mechanical. The second family is mainly represented by the solid-state hydrogen compressor and the electrochemical hydrogen compressor [1].

Non-mechanical hydrogen compressors have several advantages over mechanical compressors, including smaller size, lower capital, operating and maintenance costs. Moreover the absence of moving parts eliminates the problems related to wear, noise and intensity of energy usage. Finally this type of compressors has the capability of high-purity hydrogen supply [1].

It is also well known that the hydrogen absorption-desorption plateau pressure of a metal hydride varies with the temperature according to Van't Hoff's equation. Thus, the metal hydride compressors are thermally powered systems that use the properties of reversible metal hydride alloys to compress hydrogen without contamination [1]. They also provide the ability of connecting them to an outlet of an electrolyser [2] as long as the traces of dilute electrolyte, vapor and oxygen have been removed from the hydrogen produced [3].

Moreover, using the heat rejected by the electrolyser to feed the compressor will enhance the overall efficiency of the system [3], while the temperature of the produced hydrogen that exits the device is at about 90 °C. As a result, all the PCIs have been performed at ambient temperature of 20 °C, 90 °C, and 60 °C for extra information.

EXPERIMENTAL

The alloys have been prepared from pure elements by melting into an induction levitation furnace, under argon inert atmosphere. All samples have been re-melted at least for two times to ensure homogeneity.

Powder X-Ray diffraction (XRD) measurements have been done using CuK_a radiation in a Phillips Cubix_XRD diffractometer.

SEM/EDX measurements have been conducted by a FESEM Zeiss Ultra Plus.

All PCI measurements have been accomplished at 20 °C, 60 °C and 90 °C, using a high-pressure Sievert's type apparatus. This device is equipped with two parallel hydrogen circuits (one for the sample cell and one for the reference cell). A differential pressure gauge checks the pressure variations (interpreted either as H/M or H_2 wt. %) on the sample, by comparing it to the reference empty cell.

All alloys have a similar AB_2 type of composition, containing the same elements. The activation procedure that took place was exactly the same for all samples in order to ensure that all measurements will be conducted under the same conditions. Moreover, this is of crucial importance, because has been considered that the alloys must be activated in the same way, since they will work in a single device and remain in the tanks for compression processes to ensure pure nanopowders.

The purpose of this study is to find alloys with suitable properties in order to build a n-stage metal hydride-based hydrogen compressor, working between 20 and 90 °C, in the way the following in Fig.1.

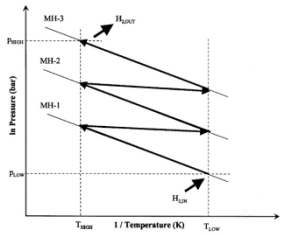

Fig.1 Operation of a 3-stage metal hydride compressor [2]

CONCLUSIONS

Structural and hydrogenation properties have been investigated for a series of Zr-based hydrides in order to be used in MHC. The plateau pressures seem to be appropriate, i.e. the desorption pressure is above the absorption pressure for the next stage. The exchanging amount of hydrogen is low, but this is an advantage for the alloys for not experience ageing.

ACKNOWLEDGMENT

This work is supported of the ATLAS-H2 European Project PIAP-GA-2009-251562.

REFERENCES

1. Aline Léon (ed.), Hydrogen Technology, Springer-Verlag, Heidelberg, Berlin, 2008.
2. JP Vanhanen, MT Hagström, PD Lund PD, Int J Hydrogen Energy 24(1999)441
3. F Laurencelle, Z Dehouche, J Goyette, TK Bose, Int J Hydrogen Energy 31(2006)762

MAGNESIUM HYDRIDE-CALCIUM ALANATE COMPOSITES AS A MATERIAL FOR HYDROGEN STORAGE

E. Kościuczyk, Z. Zarański and T. Czujko
Faculty of Advanced Materials and Technology
Military University of Technology, ul. Kaliskiego 2
00-908 Warsaw, Poland

Keywords: hydrogen storage, hydrides, composites

INTRODUCTION

The investigation of inexpensive, low temperature and reversible materials that could match the requirements for hydrogen storage system to be used in automobile applications has been mostly focused on complex hydrides in the past decade.

Especially, since the work of Chen *et al.*[1], Luo [2] and Vajo *et al.*[3] on mixtures of $LiNH_2$/LiH, $LiNH_2$/MgH_2 and $LiBH_4$/MgH_2, there have been many publications devoted to complex hydrides thermodynamically destabilized by ball - milling with other hydrides [4-7].

The advantage of such reactions is that the enthalpies of complex hydrides can be reduced by providing an alternate reaction pathway that liberates hydrogen. It has also been found that new phases could be formed during the high-energy ball-milling of different ratios of known hydrides [2, 3].

Recently, it has been shown [4, 5] that the hydrogen desorption temperature of the composite constituent with the higher desorption temperature in the systems, substantially decreases linearly with increasing volume fraction of the constituent having lower desorption temperature.

In the present work the composite approach is applied to the MgH_2+$Ca(AlH_4)_2$+LiCl system. The composites with various volume fractions of both constituents – LiCl is the residual by-product of calcium alanate synthesis – were processed by mechanical milling under protective argon atmosphere. Hydrogen desorption was tested using a Differential Scanning Calorimeter (DSC) analysis. The aim of this work is to analyze the influence of $Ca(AlH_4)_2$ additives on magnesium hydrogen decomposition process.

EXPERIMENTAL

As-received commercial MgH_2 (Alfa Aesar; ~98wt.% purity) and synthesized $Ca(AlH_4)_2$ powders were mixed to MgH_2+X wt.% $Ca(AlH_4)_2$ compositions, where X = 5, 15 and 25.

The $Ca(AlH_4)_2$ complex hydride was obtained by mechano-chemical synthesis according to the reaction: $CaCl_2 + 2LiAlH_4 \rightarrow Ca(AlH_4)_2 + 2LiCl$. For the MgH_2+ $Ca(AlH_4)_2$ composites continuous mechanical milling was carried out for 30 minutes in argon using planetary mill Fritsch 7 Pulverisette Premium Line. The balls-to-powder weight ratio was ~40 and the rotational speed of milling vial was ~600 rpm.

Morphological examination of powders was conducted with SEM Philips microscope LaB_6 XL-30. The crystalline structure of as milled powders was characterized by Seifert powder diffractometer. Monochromated $CoK\alpha_1$ radiation was used in this study.

The thermal behaviour of powders was studied by differential scanning calorimetry (DSC) (SETARAM Labsys™) with heating rate of 5 °C/min and argon flow rate of 100 ml/min.

CONCLUSIONS

The DSC hydrogen desorption onset temperature of the MgH_2 constituent in the MgH_2+$Ca(AlH_4)_2$ decreases linearly with increasing weight fraction of complex hydride component. This behaviour can be related to catalytic influence of active Al, which is formed during calcium alanate decomposition or interaction between Al and Mg affecting enthalpy of H_2 realising from MgH_2 hydride.

ACKNOWLEDGMENT

This work is supported by the State Committee for Scientific Research of Poland under grant N N507 352735.

REFERENCES

1. P. Chen, Z. Xiong, J. Luo, J. Lin, K.L. Tan, Journal of Physical Chemistry B 107(2003)10967.
2. W. Luo, Journal of Alloys and Compounds, 381(2004)284.
3. J.J. Vajo, S.L. Skeith, F. Mertens, Journal of Physical Chemistry B 109(2005)3719.
4. J.J. Vajo, G.L. Olson, Scripta Materialia 56(2007)829.
5. T. Czujko, R.A.Varin, Z. Wronski, Z. Zaranski, T. Durejko, Journal of Alloys and Compounds 427(2007)291.
6. R.A.Varin, T. Czujko, Z.S. Wronski, Nanomaterials for Solid State Hydrogen Storage, Springer Science + Business Media, New York, USA, 2009.
7. R.A. Varin, T. Czujko, R. Pulz, Z.S. Wronski, Journal of Alloys and Compounds 483(2009)252.

THERMODYNAMIC AND ELECTROCHEMICAL PROPERTIES OF La-Ni-In SYSTEM

H. Drulis[1], K. Giza[3], A. Hackemer[1], L. Folcik, Ł. Gondek[2], H. Figiel and H. Bala[3]

[1]Trzebiatowski Institute of Low Temperatures and Structure Research PAS, Okolna Str.2 P.O.Box 1410, 50-950 Wrocław, Poland

[2]AGH University of Science and Technology, Faculty of Physics and Applied Computer Science, al. A. Mickiewicza 30, 30-059 Krakow, Poland

[3]Czestochowa University of Technology, Faculty of Materials Processing Technology and Applied Physics, Al. Armii Krajowej 19, 42-200 Częstochowa, Poland

Keywords: metal hydrides, pressure-composition isotherms , electrochemical charge/discharge characteristics

INTRODUCTION

Many intermetallic compounds absorb reversibly large amounts of hydrogen gas and are considered as potential materials for hydrogen storage. Whereas, for any practical use, the advantage of high storage capacity is always desirable, a too high absorption /desorption hydrogen pressure is not a good parameter when hydride materials are considered as negative electrodes in MH batteries. Fortunately, the thermodynamic properties of metal hydrides based on $LaNi_5$ can be easily modified by partial substitution of nickel elements and the needs necessary for hydride negative electrodes can be fulfilled. In this paper, the hydrogen absorption properties of $LaNi_{5-x}In_x$ alloys and their electrochemical hydrogenation abilities are examined. Hydrogen sorption properties of $LaNi_{5-x}In_x$ alloys have been reported in [1] but as far as we know, an electrochemical investigations were not performed up to now. The performance of Ni-MH battery, measured by parameters such as current capacity, durability, discharge ability closely depends on the properties of the hydride forming alloy, used as the active material of the anode.

EXPERIMENTAL

The three samples of intermetallic compounds LaNi4.9In0.1, LaNi4.8In0.2 and LaNi4.5In0.5 were studied. The alloys were subsequently exposed to a high purity (99.999N) of hydrogen under pressure of the order of 20 bars at room temperature. The amount of hydrogen absorbed by the samples was calculated volumetrically. The absorption pressure-composition isotherm (*p-c-t*) measurements were carried out at several temperatures and hydrogen pressures up to 40 bars using a fully computerized PRO2000 apparatus.

Galvanostatic charge/discharge experiments were carried out at room temperature in a three-electrode glass cell using a CHI 1140 A workstation. The 6M KOH, Pt wire and saturated calomel electrode (SCE) were used as an electrolyte solution, counter and reference electrodes, respectively. The galvanostatic cycle were performed charging electrodes with charge rate of 185 mA/g for 2h and then discharging at the same rate 185 mA/g. Hydride electrodes were manufactured from $LaNi_{5-x}In_x$ powder material mixed with an acetylene carbon black and PVDF as a binder. The *p-c* isotherms for $LaNi_{4.9}In_{0.1}$ shows one plateau for isotherms at temperatures lower than T < 325 K and the two plateaus at temperatures higher than T > 325 K. The presence of two plateaus system indicates that there must exist at least three single-hydride phases for a given conditions of temperature and hydrogen pressure. Apart from the α – and β- phase ($LaNi_{4.9}In_{0.1}H_{\approx 6}$), the new unknown hydride phase appears with a hydrogen content extended over the region $LaNi_{4.9}In_{0.1}H_{1.3\text{-}1.8}$. We called this a σ^*- phase. The lower plateau is heavily altered by the increase of indium content and temperature. Thermodynamic functions of the enthalpy, ΔH, and the entropy, ΔS, have been calculated using the Van't Hoff plots which were constructed from the *pct* middle plateau values of hydrogen pressure. The curves of the electrochemical discharge capacity versus the cycle number for the $LaNi_{5-x}In_x$ composite electrodes are shown in Fig.1.

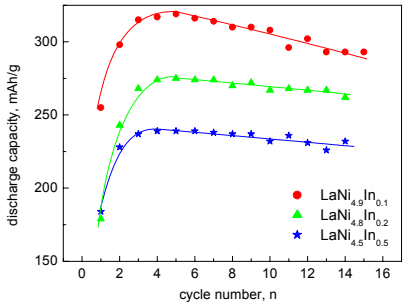

Fig. 1. Discharge capacities as a function of cycle number of $LaNi_{5-x}In_x$ (x= 0.1, 0.2, 0.5) alloy electrodes.

CONCLUSIONS

Indium substitution for Ni in $LaNi_5$ modifies the hydrogenation behavior, decreasing the equilibrium pressure of hydrogen at the cost of the reduced hydriding capacity.

ACKNOWLEDGMENT

The research was supported by Wrocław Research Centre EIT + under the project "The Application of Nanotechnology in Advanced Materials" - NanoMat (POIG.01.01.02-02-002/08*)* financed by the European Regional Development Fund (Innovative Economy Operational Program , 1.1 .2)

REFERENCES

1. A. Drašner, Z. Blažina, *J. Alloys Compds.* 420 (2006) 213

PD-C NANOFILMS FOR HYDROGEN SENSORS

Elżbieta Czerwosz, Ewa Kowalska, Joanna Radomska, Halina Wronka, Mirosław Kozłowski
Tele and Radio Research Institute, ul. Ratuszowa 11
03-450 Warsaw, Poland

Keywords: hydrogen, sensor

INTRODUCTION

Palladium is an ideal material for hydrogen sensing because it selectively absorbs hydrogen gas and forms a chemical species known as a palladium hydride. Hydrogen sensor designs rely on the fact that palladium metal hydride's electrical resistance is greater than this metal's resistance. Absorption of hydrogen in such film is accompanied by a measurable increase in electrical resistance [1]. Our Pd-C film sensor is based on an opposing property that depends on the Pd nanograins sizes and distribution in carbonaceous matrix. In this film, nanosized palladium particles swell when the hydride is formed, and in the process of expanding, some of them form new electrical connections with their neighbors [2]. The increased number of conducting pathways results in an overall net decrease in resistance. Depending on the structure of carbonaceous matrix (porous or amorphous carbon) and size and distribution of Pd nanograins in these film we can observe first or second type of changes undergoing due to hydrogen absorption.

EXPERIMENTAL

The nanostructural C-Pd films were obtained by Physical Vapor Deposition (PVD) method and next they were modified by Chemical Vapor Deposition (CVD) process. In PVD process two separated sources containing fullerene C_{60} and palladium acetate Pd(OAc)2 were used to prepare the initial films. The parameters of PVD process such as sources temperature (or current through these sources), sources-substrate distance and duration time of the process influence on the structure and thickness of deposited film. CVD process with xylene as carbon's source was carried out in argon flow and such parameters as xylene flow rate, CVD process temperature and time of duration of the process are reflected in the final form of Pd-C film. the change of other parameters (time and temperature).

All films are fully characterised by transmission and scanning electron microscopy, Fourier Transformed Infrared absorption spectra, X-ray diffraction and measurement of resistance changes observed during hydrogen absorption.

We found that with changing parameters of PVD and CVD processes we can obtain several types of films that are composed of: 1) Pd nanograins placed in porous carbon matrix (Fig.1a); 2) Pd nanograins placed in amorphous and nano-carbon matrix (Fig.1b), 3) for film deposited on alundum ceramic where the topography of alundum is reflected by the film Pd nanograins are deposited in all volume and on a surface of big areas of alundum grain (Fig.1c) or 4) Pd nanograins are place an edge of big alundum grains (Fig.1d).

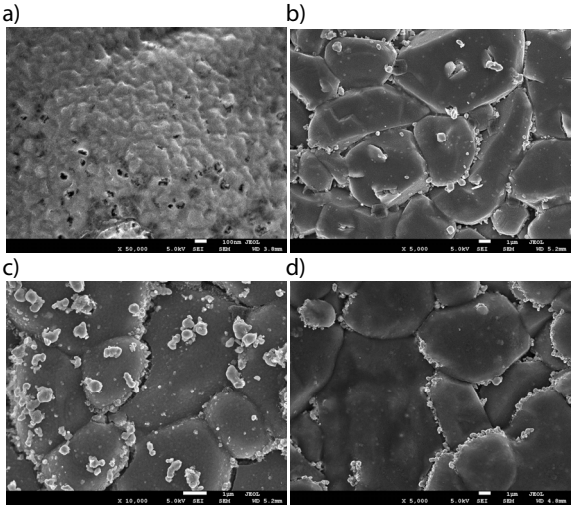

Resistance characteristics versus hydrogen absorption depend on the type of film's structure.

CONCLUSIONS

Manipulating deposition PVD and modification process CVD parameters we are able to obtain many type of films reacting in different way on the hydrogen present in ambient atmosphere. We can also change the sensitivity of these films by changing their structure.

ACKNOWLEDGMENT

This project is co-financed by the European Regional Development Fund within the Innovative Economy Operational Programme 2007-2013 (title of the project "Development of technology for a new generation of the hydrogen and hydrogen compounds sensor for applications in above normative conditions") No UDA-POIG.01.03.01-14-071/08-06.

REFERENCES

1. F.A. Lewis, The Palladium Hydrogen System, Academic Press, London, 1967, p. 50.
2. F. Favier, E.C. Walter, M.P. Zach, T. Benter, R.M. Penner, Science 293 (2001) 2227–2231.

MOLECULAR DYNAMICS AND ELECTRICAL CONDUCTIVITY OF BENZIMIDAZOLIUM AZELATE

P. Ławniczak, K. Hołderna-Natkaniec[1], M. Zdanowska-Frączek and Cz. Pawlaczyk

Institute of Molecular Physics, Polish Academy of Sciences, Smoluchowskiego 17, 60-179 Poznań

[1]Department of Physics, Adam Mickiewicz University, Umultowska 85, 61-614 Poznań

Keywords: proton dynamics, proton conductor, heterocyclic, NMR, fuel cells

INTRODUCTION

Benzimidazolium Azelate (abbreviated as BenAze) belongs to a large family of salts composed of heterocyclic molecules and different dicarboxylic acids. In search of anhydrous materials, that could be applied as solid electrolytes in fuel cells, we have investigated the electric properties of these salts in a wide temperature range [1,2]. Continuing our study, the ^{1}H NMR technique as well as impedance spectroscopy have been used to check a correlation between the local molecular dynamics and the electrical conductivity of BenAze. The mechanism of the electrical conductivity was established also.

EXPERIMENTAL

Conductivity investigations were carried out by means of impedance spectroscopy for the powder samples, using AlphaA Frequency Analyzer from Novocontrol in frequency range from 1Hz to 10MHz. Measurements were made in wide temperature range, from 120K to above 360K, near melting point.

The molecular dynamics of BenAze have been studied by means of ^{1}H solid -state NMR. The second moment of the ^{1}H NMR line (M_2) as well as the slope line widths of the first derivative of the resonance lines were determined from the ^{1}H NMR spectra recorded by the continuous wave method on a home made spectrometer operating at 25 MHz. The values of M_2 found by numerical integration of the recorded experimental curves were corrected for the finite modulated field. Measurements were performed on heating in a wide temperatures range of (100K-380K).

The results of ^{1}H NMR study have been correlated with the ones obtained by means of the electric conductivity measurements (Fig.1). It was found that below 243K both conductivity and ^{1}H NMR second moment M_2 are almost constant what corresponds to the "rigid" structure of compound studied. Rigid structure was confirmed by calculations of M_2 performed according to the formula given by van Vleck [3] and taking into account the structural parameters (solid line, top part of Fig.1).

On heating above 243K the conductivity of BenAze increases. This process is accompanied by the reduction the second moment of the ^{1}H NMR line. To interpret the second moment values different models of proton motions have been considered and the type of motion was proposed. The motions are accompanied by proton diffusion in the hydrogen bonds visible as an additional narrow contribution of line of ^{1}H NMR spectra.

The presence of a very narrow line in the NMR spectrum, whose width does not change in a wide range of temperatures, indicates that the protons can undergo a diffusive translational motion even in low temperatures (above 243 K). This result demonstrates that the nature of the electric conduction in BenAze is fairly well explained in the framework of the Grotthuss type diffusion mechanism of proton transport.

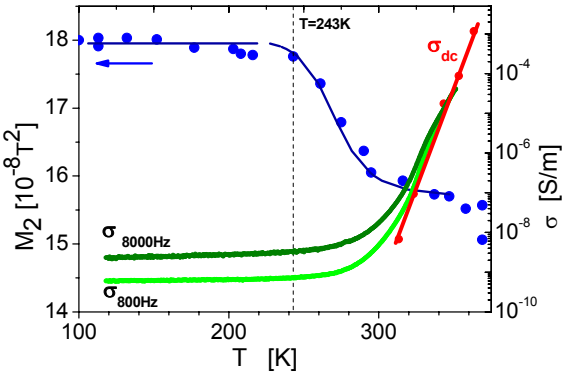

Fig. 1. The second moment of the ^{1}H NMR line (M_2), electric conductivity σ_{ac} (green lines) and σ_{dc} (in red) *versus* temperature. The σ_{dc} conductivity of BenAze shows typical Arrhenius behavior, with the conductivity process activation energy equal to E_A=2,11eV.

CONCLUSIONS

The molecular dynamics as well as the proton motion have been studied by means of ^{1}H solid-state NMR in a wide range of temperatures. The results have been correlated with the results of the conductivity studies. The following conclusions have been obtained:

1. Conduction of the BenAze crystal is a cooperative process involving both molecular motions prior to the proton exchange and migration along the hydrogen bonded chain.
2. A favoured type of conductivity in the compound studied is the protonic one.
3. Benzimidazolium Azelate cations do not diffuse in the bulk of the sample even near melting temperature.(while the 180 flip of benzimidazole only lightly influences M_2).

ACKNOWLEDGMENT

This work was supported by the funds for Science in Poland as a research project N N202 368 139

REFERENCES

1. P. Ławniczak, K. Pogorzelec-Glaser, Cz. Pawlaczyk, A. Pietraszko, L. Szcześniak *J. Phys. Condes. Matter* **21** (2009) 345403
2. K. Pogorzelec-Glaser, A. Pietraszko, J. Baran, B. Hilczer, J. Malecki, M. Polomska, P. Ławniczak *CrystEngComm* **13** (2011) 3698
3. J. H. Van Vleck, *Phys. Rev.* **74** (1948) 1168

CONDUCTIVITY SPECTRA UNIVERSALITIES OF PROTON CONDUCTORS BASED ON HETEROCYCLIC CATIONS

P. Ławniczak, Cz. Pawlaczyk and M. Zdanowska-Frączek

Institute of Molecular Physics, Polish Academy of Sciences, Smoluchowskiego 17, 60-179 Poznań

Keywords: proton conductors, universal dynamic response, dicarboxylic acids, heterocyclic molecules

INTRODUCTION

Ion conducting materials, independently on differences in their structure, disordered or even crystalline, show in different thermal conditions the same type of electric properties (e.g. conductivity spectra), which is often called "universal dynamic response" [1,2]. In this work we show that the same phenomenon is observed in crystalline proton conductors, for example in some compounds synthesized from dicarboxylic acids and heterocyclic substances (imidazole, 1,2,4-triazole, 2-methylimidazoele and benzimidazole). The structure of these crystals promotes their proton conductivity: they have a layer type structure with layers held by hydrogen bond networks between acid and heterocyclic molecules. The structure and electric conductivity of many materials of this crystal family were recently studied in our group [3-5]. In this contribution we present universality of the conductivity spectra in some selected compounds.

EXPERIMENTAL AND RESULTS

Conductivity measurements were carried out by means of impedance spectroscopy (AlphaA Frequency Analyzer from Novocontrol) on disc samples made by pressing of the powdered as grown crystals.

In figure 1, the so called first universality of the conductivity spectra of benzimidazolium azelate (BenAze) is presented. The frequency conductivity dependence was scaled using the Summerfield method [6]:

$$\frac{\sigma'(\nu)}{\sigma_{dc}} = F\left(\frac{\nu}{\sigma_{dc}T}\right)$$

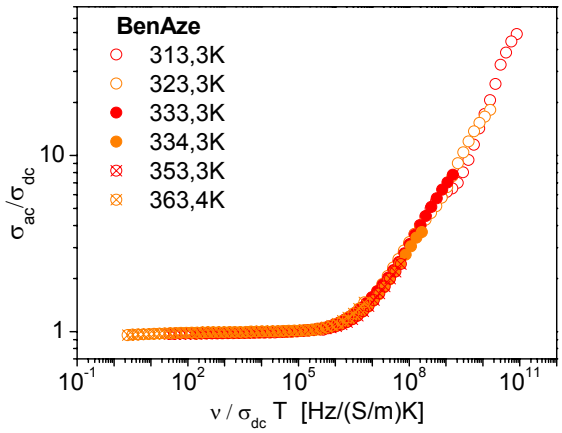

Fig. 1. First universality for BenAze: all isotherms create one curve with characteristic plateau, which corresponds to long range movements of ions.

Figure 2 shows typical low temperature behavior, so called "second universality" of 2-methylimidazolium azelate (MetImiAze).

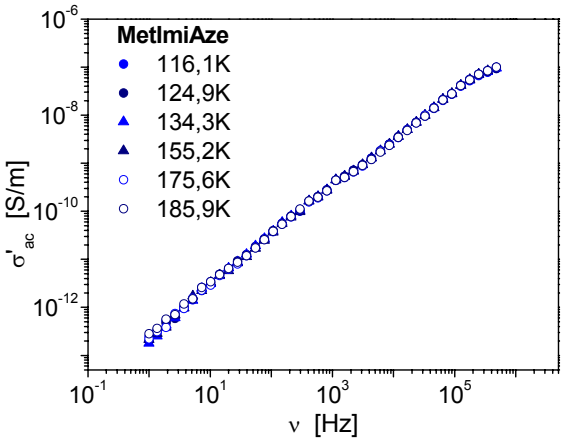

Figure 2. Second universality (Nearly Constant Loss): at low temperatures a linear frequency dependence of the *ac* conductivity is observed independently on the temperature.

CONCLUSION

Also proton crystalline conductors, similarly as other disordered and crystalline ion conductors, show the universal dynamic response.

ACKNOWLEDGMENT

This work was supported by the funds for Science in Poland as a research project N N202 481439

REFERENCES

1. J. Dyre, P. Maass, B. Roling, D.L. Sidebottom, *Rep. Prog. Phys.* 72 (2009) 046501
2. D. Laughman, R. Banhatti, K. Funke, *Phys. Chem. Chem. Phys.* 12 (2010) 14102
3. K. Pogorzelec-Glaser, A. Pietraszko, J. Baran, B. Hilczer, J. Malecki, M. Polomska, P. Ławniczak, *CrystEngComm* 13 (2011) 3698
4. Cz. Pawlaczyk, A. Pawlowski, M. Polomska, K. Pogorzelec-Glaser, B. Hilczer A. Pietraszko, E. Markiewicz, P. Ławniczak, L. Szcześniak, *Phase Transition.* 83 (2010) 854
5. P. Ławniczak, K. Pogorzelec-Glaser, Cz. Pawla-czyk, A. Pietraszko, L. Szcześniak, *J. Phys. Condes. Matter* 21 (2009) 345403
6. S. Summerfield, *Philos. Mag. B* 52 (1985) 9

BIOTECHNOLOGICAL FABRICATION OF HYBRID CATALYSTS FOR OXYGEN REDUCTION ELECTRODES

A. Cyganiuk, A. Kucińska, A. Olejniczak and J. P. Łukaszewicz
Faculty of Chemistry
Nicholas Copernicus University, ul. Gagarina 11
87-100 Torun, Poland

Keywords: Salix viminalis, hybrid catalyst, biotechnological impregnation

INTRODUCTION

The paper describes a novel sensing and electrode material consisting of a porous carbon matrix with nanoclusters of metal oxides. The presence of metal oxide clusters in electrically conductive carbon matrix enables catalytic activity of such hybrid materials. The fresh cut stems of *Salix viminalis* preserve the ability towards capillary suction of the solvent (water) and dissolved metal ions. Due to the capillary action the metal ions get distributed over the whole stem and accumulated in cells. In this way one provides uniform distribution of metal ions in the stem and later (after carbonization of the stem) in carbon matrix. The raw organic matter (plant tissues) incorporating metal ions in cells, is subjected to a heat treatment in oxygen-free conditions. The organic matter (plant tissues) transforms into porous carbon matrix while metal ions transform into the metal oxide clusters of nanometric size. This idea is described in detail in a patent application submitted to a patent office. The obtained complex carbon based materials exhibit high specific surface area ranging from 400 to 1000 m^2/g. The proposed method leads to the formation of the complex metal oxide which exhibits high catalytic activity in numerous reactions. *Salix viminalis* is an example of so-called short-rotation coppice, planted as an easily renewable source of energy. The plant is widely known due to its contribution to "green" energy production.

EXPERIMENTAL

Fresh cut stems of *Salix viminalis* (ca. 20-50 cm long) were immersed in a water solution containing equimolar quantities of $La(NO_3)_3$ (0.01–0.1 M) and $Mn(NO_3)_2$ (0.01–0.1 M). The stems retained the ability of metal ion transport i. e. a gradual rise of the solution along the stems kept in vertical position. After saturation with La^{3+} and Mn^{2+} ions, the stems were dried, diminished and carbonized (600–800 ^{0}C, two-step procedure) in an inert gas atmosphere (N_2), or in vacuum. The first step consisted of fast heating of up to 600 ^{0}C and maintaining the temperature for ca. 1 h [1]. Then, the material was cooled to room temperature. In the second stage, the row charcoal from the first stage was placed on the retort again and heat-treated at the desired temperature and time. After this, the obtained carbon material was again cooled and used in further experiments and tests. Beside the experiment with simultaneous bio-impregnation by La and Mn ions we performed bio-impregnation with single ions Ti and Ce. In the case of Ce the impregnation followed the above described procedure involving La and Mn ions i.e. a 0.1 M water solution of $Ce(NO_3)$ was applied. The problem appeared when we tried to introduce titanium firstly to the plant's cells, secondly to carbon matrix via carbonization of metal ion containing *Salix viminalis* tissues. Titanium (IV) water soluble salts are characteristic because of very low pH, sometimes achieved artificially by an addition of concentrated HCl. Otherwise Ti^{4+} ions undergo intensive hydrolysis yielding insoluble $Ti(OH)_4$. The substance in form of a white precipitate is useless for the wood impregnation. Additionally, strong acidic pH caused the denaturizing of *Salix viminalis* tissues. Therefore, firstly acidic Ti^{4+} water solution was obtained and subsequently Ti^{4+} ions were chelated by means of an appropriate ligand (patent application in progress [2]). After chelation pH was set at 7 by means of a base water solution. Preliminary chelation helped to avoid the formation of $Ti(OH)_4$. Such obtained solution of chelated Ti(IV) ions were suitable for a successful bio-impregnation. Experimental data were collected by means of several instrumental techniques like: XRD, SEM, AFM, FT-IR, XPS and catalytic activity tests [1].

CONCLUSIONS

Bio-impregnation of living *Salix viminalis* tissues has been proposed as a method for a hybrid catalysts fabrication. The method exploits a natural phenomenon of metal ion transport in living plants. Bio-impregnated parts of *Salix viminalis* underwent carboniozation transforming organic matter into carbon matrix while metal ions (La^{3+}, Mn^{2+}, Ce^{3+} and $Ti^{4+}_{(chelated)}$)participated at the formation of metal oxide nano-crystallites. Both diminishing and dispersion of the crystallites were very good. The hybrids exhibited high catalytic activity in several reactions including test processes like ketonization or dehydration of n-butanol. The La/Mn, Ti and Ce containing hybrid materials despite of the same properties of carbon support, exhibited dramatically different catalytic activity in some test reactions

REFERENCES

1. A. Cyganiuk, R. Klimkiewicz, A. Olejniczak, J. P. Lukaszewicz, *Carbon 48(2010)99*.
2. A. Cyganiuk, J. P. Lukaszewicz, *Patent application, Polish Patent Office, 2011, Warsaw*.

A FULLY AUTOMATED CONTROL SYSTEM FOR ELECTRICAL CONDUCTIVITY MEASUREMENTS OF SOLIDS UNDER EXTREME CONDITIONS

M. Zdanowska-Frączek, Z. J. Frączek

Institute of Molecular Physics, Polish Academy of Sciences, Smoluchowskiego 17, 60-179 Poznań, Poland

Keywords: high pressure, impedance spectroscopy, solid electrolytes

INTRODUCTION

In this contribution we describe a fully automated system for the electrical properties studies of solids under extreme conditions (high pressure, high as well as low temperatures). The system is especially suitable for low temperature measurements of electric permittivity, dielectric relaxation and phase transitions in ferroelectrics. Recently, the system has been utilized for the measurements of the solid electrolytes. The electric conductivity of ionic and electronic materials can be measured as a function of temperature, pressure and time by means of impedance spectroscopy. Impedance spectroscopy where measurements are made over a wide frequency range is a particularly useful technique for conductivity measurements of ionic conductors as contributions of various processes, occurring under different external conditions, can be separated in the frequency domain.The technique is also ideally suited for studying ageing phenomena in solid electrolytes at constant temperature as well as constant pressure.

THE SYSTEM DESCRIPTION

The pressure-temperature control system consists of three parts: temperature control system (based on Oxford Instruments equipment), high pressure generating and control system and electrical measurements system. Data collections were made using an program based on Agilent Vee Pro 7.0 platform.

High pressures are generated by means of the three stage IF-012 A Unipress helium gas compressor. Pressure was measured to an accuracy of 0.2 MPa by means of a manganine gauge (previously calibrated by reference to the pressure-induced phase transition of bismuth) with a Keithley 2400 Source Meter. The pressure chamber was made of heat-treated beryllium-copper alloy. The most difficult part of holding high-pressure helium gas is the electric plug. New structure of electric plug (especially suitable for low temperature measurements) based on corundum crystal was designed and used. The samples used for the dielectric or conductivity measurements were covered with golden electrodes and placed between two parallel golden plates. The samples of size of approximately 5x5x1 are sufficient for measurements. The pressure chamber was placed into Oxford flow cryostat.

The temperature of the sample was set and stabilized using the Oxford Instruments automatic temperature controller ITC4. The temperature was measured with an accuracy to 0.01 K by means of Pt100 sensor located inside the pressure chamber. Measurements can be performed on heating and cooling with different rate. For example, the heating/cooling rate in the vicinity of the phase transition is usually equal 0.02 K/min.

Electrical properties of solids were measured using an impedance analyzer Hewlett-Packard HP 4284A or HP 4285A for the frequencies from 100 Hz to 1 MHz and from 75 kHz to 30 MHz respectively.

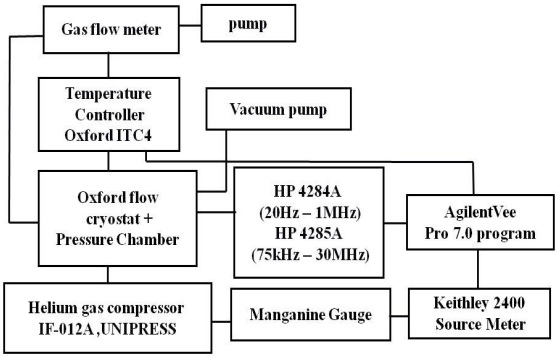

Fig.1 Schematic diagram of an apparatus for conductivity measurements of solids under external pressure.

Due to illustration of technical possibilities of presented technique the conductivity data of selected proton conductors are presented.

ACKNOWLEDGMENT

This work was supported by the funds for science in Poland as a research project N N202 368 139.

CATALYTIC PROPERTIES OF THIN Ni_3Al FOILS IN METHANOL DECOMPOSITION

P. Jóźwik[1], R. Grabowski [2], M. Domańska[1], Z. Bojar[1]

[1]Faculty of Advanced Technology and Chemistry
Military University of Technology, ul. Kaliskiego 2, 00-908 Warsaw, Poland
[2]Jerzy Haber Institute of Catalysis and Surface Chemistry, Polish Academy of Sciences, Cracow, Poland

Keywords: hydrogen production, methanol decomposition, catalytic stability, thin Ni_3Al foils

INTRODUCTION

In the near future methanol is expected to be a promising alternative energy source (as a fuel). It can be efficiently produced from a wide variety of sources, e.g. biomass, natural gas or coal which are more abundant resources than crude oil. In comparison to hydrogen and methane, methanol as liquid is easily stored, transported, and used [1,2].

The methanol decomposition to hydrogen and carbon monoxide is an endothermic process and therefore it gives possibility to recover of waste heat from industries and automobile exhaust gases. Integrated heat-exchangers/reactor can possibly realize new processing concept – connecting exothermic combustion with endothermic methanol brake down.

The Ni_3Al intermetallics present, as compared to nowadays utilized nickel-based superalloys, excellent oxidation and corrosion resistances and good catalytic properties [3-4]. In respect to this the Ni_3Al thin foils can be used in high-performance applications in the form of honeycomb structures, which have an advantage in lightweight, high-stiffness and high specific area surface. Thus far we have successfully fabricated thin Ni_3Al foils by cold rolling of commonly casted ingots without additional treatment. The proposed technology allows to obtain foils with thickness below 50μm and micro and nanostructure [5,6].

EXPERIMENTAL

The nearly single-phase Ni_3Al foils with chemical compositions Ni-22.1Al–0.26Zr–0.1B at.% were obtained by cold rolling at room temperature for 95 % cold work and next recrystallization at the temperature up to 1100^{O}C for time up to 1.5 hours in an argon atmosphere. Thin Ni_3Al foils (approx. 50μm thickness) obtained by mentioned processing technology were mechanically polished for the next step. Additionally, comparative analysis of catalytic activity of pure nickel thin foil was performed in similar conditions.

The catalytic experiments of hydrogen production from methanol were carried out in the fixed-bed quartz tube reactor. Prior to the catalytic experiments the foils were annealed in reducing atmosphere (Ar + 5%H_2) at 300^{O}C for 1 hour. The initial feed mixtures with different feed composition (methanol, water and argon) were introduced into reactor with the flow rate 30ml/min (1,8l/h). Feed mixtures were obtained by argon flow through the saturator containing pure methanol or mixture of methanol and water. The catalysts were tested in a temperature range 250^{O}C to 600^{O}C. The temperature was increased by 50^{O}C and each temperature was maintained constant by half an hour and the products were analyzed on-line by mass spectrometer Quadera 200. Additionally, the thin foils of Ni_3Al or pure Ni foil were continuously tested for 24 hours at reaction temperature 480^{O}C in (95%MeOH+5%H_2O) mixture.

The surface morphology after tests of catalysis was observed by scanning electron microscopy (BSE and SE detectors). The phase structure of the surface products after catalysis was examined by X-ray diffraction using Seifert 3003 diffractometer with CuK_α radiation.

CONCLUSIONS

Heavily cold rolled and recrystallized Ni_3Al foils with microcrystalline structure demonstrated good catalytic properties in methanol decomposition at a temperature range 250-580^{O}C - depending on feed mixture composition.

Small addition of water (5%) to the feed mixture influences positively methanol conversion on both the micro and nanocrystalline Ni_3Al catalysts and has also important influence on H_2 and CO formation rate – in these cases almost complete conversion (approx. 100%) and high rate of reaction (approx. 6μmol/g_{cat}) were observed. In opposite, much less value of conversion (approx. 60%) and rate of reaction (approx. 3.5μmol/g_{cat}) were observed for nickel foil catalyst at analyzed conditions.

Good catalytic stability of Ni_3Al thin foil surfaces at long – 24 hours lasting examinations was also shown. Existence of carbon nanofibres and nickel nanoparticles forming spontaneously on the both foils surfaces during catalytic reactions was observed.

ACKNOWLEDGMENT

The authors gratefully acknowledge the financial support by the Polish Ministry of Science and Higher Education (R0702502 and OR00004905)

REFERENCES

1. G. Olah, Alain Goeppert & G Prakash Publisher: Weinheim, Wiley-VCH, 2006.
2. J. Sehested, Catalysis Today, 2006, 111, 102-110.
3. V. K. Sikka et al. Intermetallics, 8 (2000) 1329.
4. P. Jozwik, R. Grabowski, Z. Bojar, Materials Science Forum 636(2010) 895.
5. Z. Bojar, P. Jóźwik, J. Bystrzycki, Scripta Materialia, 55(2006) 399.
6. P. Jóźwik, Z. Bojar, Archives of Metallurgy and Materials, 52(2007) 321.

HYBRID MATERIALS FOR SOLAR ENERGY CONVERSION: ENZYMATIC CO_2 REDUCTION TO METHANOL

T. Baran,[1] P. Stufano,[2] M. Aresta[2,3] and W. Macyk[1]

[1]Faculty of Chemistry, Jagiellonian University,
Ingardena 3, 30-060 Kraków, Poland
[2]Department of Chemistry, University of Bari,
Orabona 4, 70125 Bari, Italy
[3]CIRRC, Interuniversity Consortium for Chemical Reactivity and Catalysis
Celso Ulpiani 27, 70126 Bari, Italy

Keywords: photocatalysis, carbon dioxide reduction, semiconductor materials, enzymatic processes

INTRODUCTION

High emission and concentration of carbon dioxide, excessive use of fossil fuels and increasing demand for energy and raw materials are really serious problems. Various methods of capture, storage and utilization of carbon dioxide are intensively study. Moreover, utilization of CO_2 as a carbon source in synthesis of chemicals and fuels is under evaluation. These reactions, mimicking photosynthesis, would reduce utilization of fossil fuels [1]. An interesting case is enzymatic reduction of CO_2 to methanol, that could be used as a raw chemical and fuel [2]. Such reduction occurs in water and is promoted by three enzymes: formate dehydrogenase, formaldehyde dehydrogenase, and alcohol dehydrogenase, while the necessary energy is provided by NADH which is oxidized to NAD^+. The main problem is related to the consumption of three moles of NADH per one mole of methanol produced. In Nature, NAD^+ is reduced back to NADH with help of solar light; in the industrial application such reduction would have to be performed implementing the most energetically and economically convenient technologies, like photocatalysis. In our studies semiconductor photocatalysts based on zinc sulphide and titanium dioxide were used for reduction of oxidized form of coenzyme to NADH.

Studies on NADH regeneration were a first step in research project on carbon dioxide reduction to methane using photocatalytic-enzymatic hybrid systems. Because of kinetics of enzymatic reaction, NADH concentration in the system should be relatively high, therefore photocatalytic process should be characterized by a possibly high yield. The final goal was to develop an active photocatalytic-enzymatic hybrid system for carbon dioxide reduction, as shown in Figure 1.

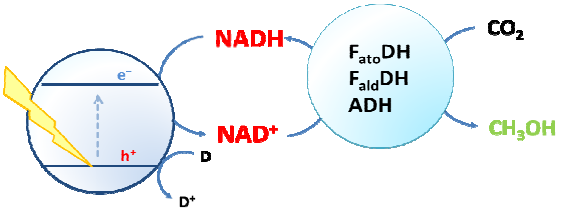

Fig. 1. The idea of hybrid technology for carbon dioxide reduction.

EXPERIMENTAL

Photocatalytic NADH regeneration was carried out according to the following procedure. The photocatalyst powder was suspended in distilled, deoxygenated water. Isopropanol or glycerol, if any, was added as a sacrificial electron donor and NAD^+. Before experiment water was degased by bubbling nitrogen to remove oxygen. Suspension in a closed reactor was illuminated with XBO lamp as a light source. Influence of several parameters, such as the photocatalyst, hole scavenger and light source was tested in this study.

Enzymatic CO_2 reduction was carried out using photocatalytically regenerated NADH. pH was kept at about 7.2 by addition of buffer solution. Reaction was carried out at 37°C. Carbon dioxide was bubbled to saturate the solution. Enzymes were used in immobilized form (co-encapsulation of the three enzymes into silica-alginate solid matrix).

CONCLUSIONS

Combination of enzymatic method of carbon dioxide reduction with photocatalytic regeneration of enzymes activator (NADH) is a modern, novel and promising approach to convert carbon dioxide into methanol through consecutive reduction catalyzed by three different dehydrogenases. Tested system is more interesting then classical enzymatic conversion because NADH is produced *in situ* in a cheap process without the use of electricity nor thermal energy. Additionally water and cheap alcohols (glycerol or isopropanol) were used as a substrate for reaction (as electron donors).

The chemical co-factor regeneration in a separated compartment is a proof of concept that the recycling of NAD^+ is possible and more sophisticated systems have to be developed for an efficient and economically viable biotechnological synthesis of CH_3OH from CO_2.

REFERENCES

1. M. Aresta, *Carbon dioxide as a chemical feedstock,* Wiley (2010).
2. A. Dibenedetto, P. Stufano, W. Macyk, T. Baran, C. Fragale, M. Costa, M. Aresta, *ChemSusChem* (2011) accepted.

KIC InnoEnergy
Innovation in Sustainable Energy

Tomasz Szmuc
Vice-Rector for Science
AGH University of Science and Technology
al. A. Mickiewicza 30, 30-059 Krakow, Poland

1. Introduction

KIC InnoEnergy SE is a European Company (Societas Europaea – SE) established by international consortium gathering leading European Universities, research centers, and important companies working in the area of sustainable energy. The KIC InnoEnergy consortium was built as an answer to the call (2nd April 2009) of the European Institute of Innovation and Technology (EIT) related to shaping new paradigms for innovation in the three areas:

1. Sustainable Energy
2. Climate Changes Mitigation and Adaptation
3. Future ICT Society.

Applications submitted by several European consortia were carefully reviewed (including reviewers from US) and after final selection three projects (one in every above mentioned area) were accepted for realization starting with 1st January 2010. Project submitted by KIC InnoEnergy was selected in the area of Sustainable Energy.

The main goal of the Project is to create a persistent structure and to define long term rules for collaboration of different institutions (research / business oriented) forming eco-system to achieve the best quality research in the area of energy, to make a breakthrough improvement in innovation and in deployment (commercialization) of research results, as well as to assure highest level teaching of students including shaping their entrepreneurial skills. This long term (7-15 years of co-financing) Project should improve development and innovation in energy area, but also should apply joint collaboration of universities and industry based on common business, as well as should change mentality of young people by significant improvement of their entrepreneurship. The goal specified by the so-called Research – Innovation – Education triangle. The triangle and tools supporting cooperation specified in the related vertices are shown in Fig. 1.

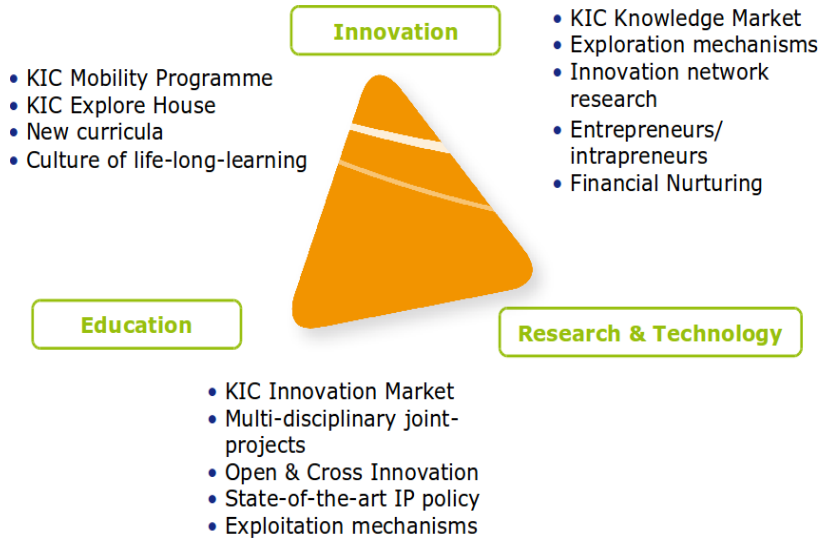

Fig. 1. Research – Innovation – Education Triangle.

Realisation of these purposes requires several years. The total budget of KIC InnoEnergy is almost 700 MEUR for 2011-2014. However, only 25% of the budget is supplied by EIT. The remaining 75% will come from KIC Partners own activities. KIC InnoEnergy is in fact a company with a 7 year industrial plan. With a strong cooperation with EIT, InnoEnergy Legal Entity is managing and coordinating activities performed by our partners.

Apart from KIC InnoEnergy Project (chosen in domain of Sustainable Energy), EIT coordinates two other ones in the domain of Climate Changes Adaptation and Mitigation (http://eit.europa.eu/kics1/climate-kic.html), and Future ICT Society (http://eit.europa.eu/kics1/eit-ict-labs.html). Each of these consortiums is composed of 5 or 6 Collocation Centers.

2. *Structure and main partners*

Consortium KIC InnoEnergy was coordinated in the preparatory phase by the Karlsruhe Institute of Technology (KIT) known as one of the most prestigious German universities. European company – KIC InnoEnergy SE was established as a target management structure in the 1st year of the Project run. The management structure consists of 2 levels (Fig. 2), where on the upper one the KIC InnoEnergy SE coordinates the whole consortium. Activities within Collocation Centers are coordinated by lower level units, i.e. limited liability company or foundation depending on country where CC is implemented.

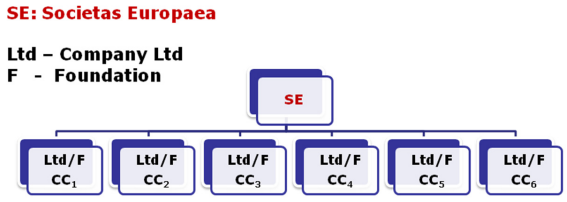

Fig. 2. Management structure.

Every Collocation Centre coordinates Consortium's activity in the field of its specialty. It is possible to develop common projects among a group of different CCs, providing that the best CC in each field supervises the whole work. It is worth emphasizing that the KIC InnoEnergy Collocation Centres coordinate complementary subjects that cover all the priority domains in the European Energy Set Plan. Below you will find a list of partners (the coordinating institution is underlined) and the theme (in bold). Additionally, we would like to mention that our global partners are the companies EdF and Total.

- **CC Sweden**: Royal Institute of Technology (Stockholm), Uppsala University, Vattenfal, ABB. **Smart European Electricity Grids and Storage**
- **CC Benelux**: TU Eindhoven, KU Leuven, VITO, TNO, EANDIS, Philips. **Intelligent Energy Efficient Building and Cities**
- **CC Germany**: Karlsruhe Institute of Technology, U Stuttgart, SAP, INTEL, ENBW. **Power from Fossils and Biogenic Sources**
- **CC Alps Valleys**: Grenoble INP & Grenoble Ecole de Management, Paris Tech, Grenoble, CEA (Commissariat a l'Energie Atomique), INSA, CNRS, AREVA, Schneider Electric, Alstom. **Sustanaible Nuclear Energy and Converging Nuclear-Renewables Technologies**
- **CC Iberia**: Univeristat Politecnica de Catalunya (UPC – Barcelona), ESADE (Higher School of Business) Barcelona, CIEMAT, IBERDROLA, Gas Natural, Union Fenosa. **Renewables**: **Solar (PV& CSP), Wind, Wave and Tidal Energy Systems**
- **CC PolandPlus**: AGH University of Science and Technology, Silesian University of Technology, University of Silesia, Wroclaw Technical University, Central Mining Institute (GIG), Institute of Chemical Processing of Coal (IChPW), Jagiellonian University, Tauron, LOTOS, PGNiG. **Clean Coal Technologies and New Paradigm for Carbon Management**

3. *Conclusion*

The KIC is a new and prospective concept for remarkable improvement of innovation in Europe. The new paradigm is based on arrangement of ecosystem, where all main actors (universities, companies) will jointly cooperate in priority areas. The main difference in comparison to existing frameworks is business orientation of the collaboration. KIC InnoEnergy is an example of implementation of the general idea, where main European institutions (both on university and industry sides) are involved. The consortium is opened for collaboration with external partners. Please refer to the Consortium web page: **http://www.kic-innoenergy.com** for further details.

Photoelectrochemical properties of anion-doped TiO_2*

Anita Trenczek-Zając
AGH University of Science and Technology, Faculty of Materials Science and Ceramics
al. A. Mickiewicza 30, 30-059 Krakow, Poland

**This paper was written based on the Ph.D. thesis supervised by Professor Marta Radecka.*

Introduction

Titanium dioxide TiO_2 is one of the best known wide-band gap semiconductors. It is promising in variety of applications such as decomposition of organic contaminations [1], super-hydrophilic layers [2], anodes in photoelectrochemical cells, PEC [3]. In the PEC with the use of water an environmentally friendly conversion of the solar energy into the chemical energy of hydrogen is possible, which was demonstrated in 1972 by Fujishima and Honda [4] for the first time. However, undoped TiO_2 suffers from a large band gap (of about 3 eV) resulting low photoelectrochemical activity.

The aim of this work was to determine the influence of selected anionic TiO_2 sublattice modification methods on its photoelectrochemical properties.

Experimental

Methods of TiO_2 modification include incorporation of nonstoichiometry in polycrystalline titanium dioxide – TiO_{2-x}, doping with nitrogen of stoichiometric and nonstoichiometric titanium dioxide – TiO_2:N, as well as doping with oxygen of titanium nitride – TiN:O. Thin films of TiO_2:N and TiN:O were deposited in the magnetron sputtering process from Ti target in the controlled flow of gaseous mixture of Ar-O_2-N_2.

The effect of anion sublattice modification of thin films and polycrystalline titanium dioxide on chemical composition and structural, microstructural, optical, electrical and photoelectrochemical properties have been evaluated.

Results and discussion

TiN:O thin films

Thin films of TiN_xO_y were sputtered with different oxygen rate flow η_{O2}. XRD measurements shows that with an increasing η_{O2} the *fcc* unit cell of TiN changes, a progressive amorphisation along with a decrease in lattice parameter is observed. This effect seems to have a direct consequence of substitution of oxygen for nitrogen in anionic sublattice. Based on RBS and XPS studies the chemical composition of thin films was determined. A slight non-stoichiometry in TiN towards nitrogen excess is observed. Films deposited in the highest oxygen rate flow are characterized by atomic composition: N/Ti=0.41, O/Ti=0.52 [5,6].

An optical reflectance spectra of TiN and TiN:O thin films deposited onto transparent substrates allowed to calculate a plasma frequency ω_p according to the Drude theory. On the Fig. 1 ω_p along with electrical conductivity as a function of oxygen rate flow is presented. Decrease in plasma frequency is observed together with η_{O2} increase which is a direct consequence of the decrease of charge carrier concentration [6].

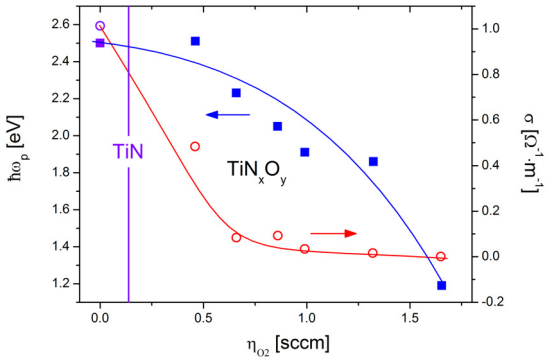

Fig. 1. Plasma frequency ω_p calculated based on the Drude model adjustment to the experimental data and conductivity σ of TiN_xO_y thin films deposited with different oxygen rate flow η_{O2}.

TiO_2:N thin films

TiO_2:N thin film deposition conditions were chosen in such a way to incorporate nitrogen into stoichiometric or nonstoichiometric TiO_{2-x} with an oxygen deficiency. Based on XRD results it was suggested that TiN-TiO solid solution (titanium oxynitrides) is created at the high nitrogen rate flow.

In Fig. 2 influence of nitrogen rate flow η_{N_2} on N/Ti and O/Ti atomic ratio (based on XPS calculation) in case of stoichiometric and nonstoichiometric films is presented. It can be concluded that point defects in the form of oxygen vacancies in TiO_{2-x} structure favours nitrogen ions incorporation into the oxygen sublattice. No such dependence is observed in the case of stoichiometric films.

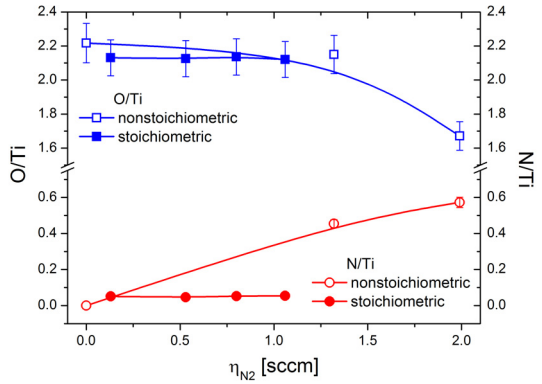

Fig. 2. Dependence of thin films composition expressed as a N/Ti and O/Ti atomic ratio vs. nitrogen flow rate.

Photoelectrochemical measurements in the PEC cell were carried out in white light illumination and in the dark. I_{ph}-V characteristics for stoichiometric films are presented in Fig. 3. Nitrogen doping leads to the decrease in the photocurrent. The inset shows influence of nonstoichiometry on I_{ph}-V characteristic. Stoichiometric samples are characterized by much higher values of the photocurrent than nonstoichiometric. It is connected with point defects which acts as a recombination centres. The positive impact of nitrogen doping on the enhanced contribution coming from light excitation at longer wavelengths was also studied. In contrast to the stoichiometric samples, a rise in the photocurrent $I_{vis}(\lambda)/I_{uv}(300\ nm)$ with the increase in the nitrogen flow rate is observed for the nonstoichiometric TiO_{2-x}:N thin films at all considered wavelengths. It can be concluded that doping with nitrogen improves the photoelectrochemical properties over the visible range in the case of slightly nonstoichiometric samples [7].

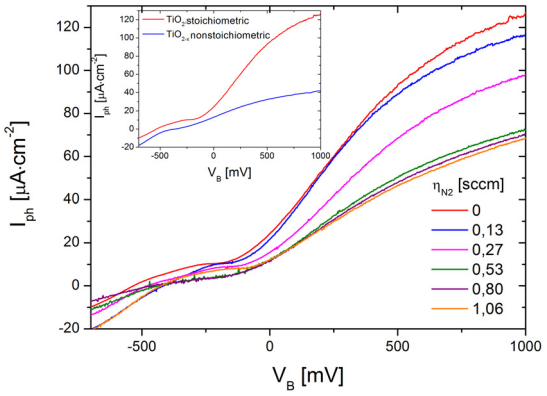

Fig. 3. Photocurrent-voltage dependence for thin films of stoichiometric TiO_2. Inset – nonstoichiometry influence on the photocurrent-voltage characteristic.

Oxidized TiN thin films and powders

TiN samples were oxidized in air in wide range of temperature. Rutile phase appears between 200°C and 300°C and TiN phase persist up to 400-500°C. Optical absorption *A* (*A*=100-(*R*+*T*)) for thin films oxidized at 400°C and 450°C compared with results for anatase and TiO_2 phase mixture is presented on the Fig. 4a. The fundamental absorption edge of a film oxidized at 450°C is shifted towards visible range as related to its position in the anatase and TiO_2 phase mixture thin films. Band gap energy E_g and dopant energy E_d calculated based on the spectral dependence of reflectance are presented in Fig. 4b. Increase in the temperature results in the decrease in the band gap energy. In the range of 400-700°C additional optical transition is observed [8,9].

Nonstoichiometric TiO_{2-x}

TiO_2 powder was sintered into pellets and reduced in Ar/H_2 atmosphere in wide range of temperatures. XRD studies show rutile phase in lower reduction temperature and different Magneli phases in higher temperatures. Based on the spectral dependence of reflectance *R* and photoelectrochemical measurements the values of band gap energy E_g was calculated. The comparison of those values and data obtained by other authors [10] is presented in Fig. 5. Increase in the nonstoichiometry is accompanied by increase in the band gap energy. Additional states in the forbidden band gap of TiO_{2-x} gives supplementary absorption of photons with energy $h\nu<E_g$.

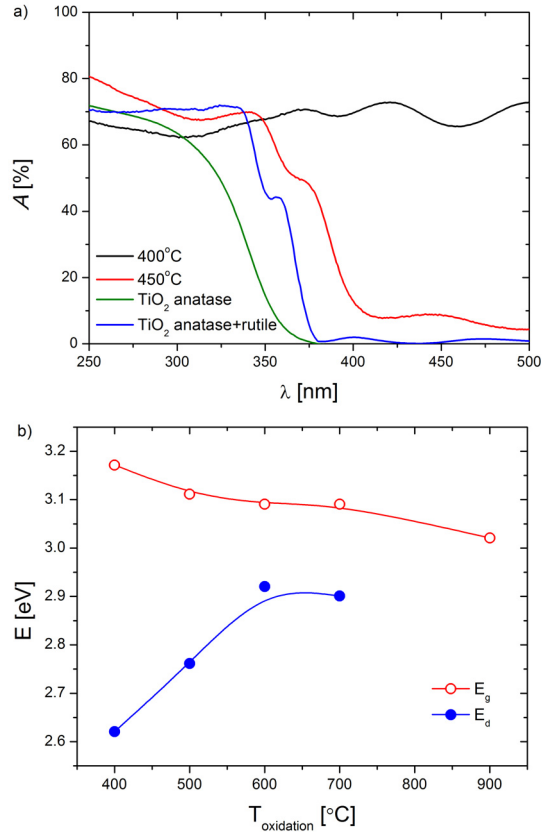

Fig. 4. Spectral dependence of the absorption for TiN thin films oxidized at 400°C and 450°C in comparison with anatase and TiO_2 phase mixture (a). Influence of the oxidation temperature on the band gap energy Eg and Ed (b).

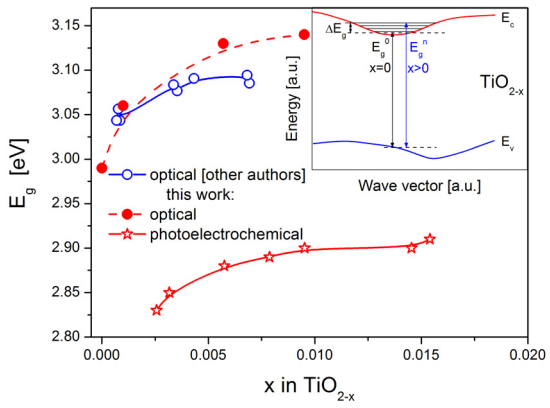

Fig. 5. Band gap energy E_g vs. nonstoichiometry x in TiO_{2-x}. Inset – schematic diagram explaining changes of E_g with nonstoichiometry.

Current density I_{ph} corresponding to darkness and to white light illumination is presented in Fig. 6 as a function of electric bias, V_B, versus saturated calomel electrode, SCE. The dark current assumes negligible values at positive potential. Exposure to light causes a considerable increase in photocurrent. The threshold potential of anodic current start at about −0.4V and corresponds to the flat band potential, V_{FB}. The highest photocurrent is observed for $TiO_{1.994}$ photoanode and for $TiO_{1.954}$ the lowest values of photocurrent. This may be correlated with the disappearance of rutile phase with the increasing deviation from stoichiometry because the presence of rutile seems to be a prerequisite condition for good photoelectrochemical performance of the photoanode [11].

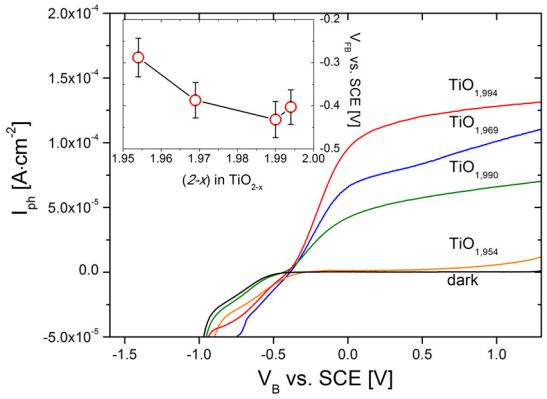

Fig. 6. Current–voltage characteristics, I_{ph}–V_B, for TiO_2 monitored in the dark and after illumination by white light. Inset – flat band potential, V_{FB}, vs. (2–x) in TiO_2.

Conclusions

Composition of the gaseous atmosphere in the magnetron thin films sputtering process influences on the structural, optical, electrical and photoelectrochemical properties. Thin films deposited at oxygen flow rate η_{O_2}<0.5 sccm crystallize in cubic structure of $TiN_{1-x}O_x$ solid solutions. For higher rates films crystallize in anatase structure. Changes in oxygen content in gaseous atmosphere allows for sputtering TiO_2 layers with different non-stoichiometry. Based on the XPS analysis it was found that the amount of nitrogen incorporated into the anionic sublattice is larger in the case of nonstoichiometric TiO_{2-x}:N thin films than that for the stoichiometric samples. This suggests that the nonstoichiometry in the oxygen sublattice creates conditions quite favourable for accommodation of a larger amount of nitrogen. In case of TiO_2 anodes much higher values of photocurrent are observed in comparison with nonstoichiometric one. Doping TiO_2 with nitrogen improves photoelectrochemical properties in the visible range of light.

Based on owns studies and other authors an update of the phase diagram proposed by Granier

et al. [12] for the ternary phase Ti–N–O obtained under equilibrium conditions was proposed (Fig. 7) [5].

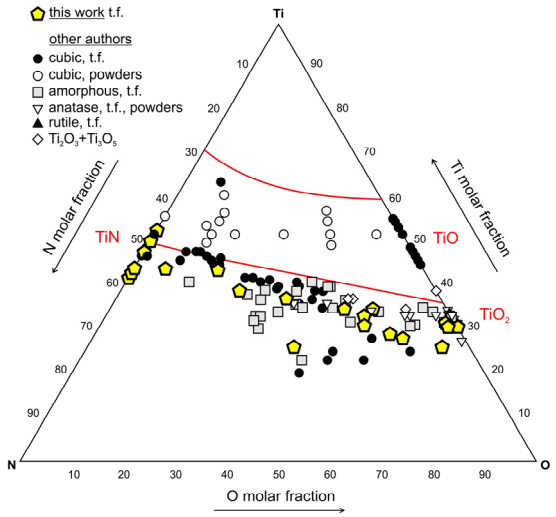

Fig. 7. Ti-O-N ternary phase diagram. t.f – thin films.

TiN oxidation in the air leads to $TiO_{2-x}N_x$ formation in rutile form and the decrease in the conductivity is a result of insulating rutile growth. TiO_{2-x} polycrystalline materials demonstrate increase in the nonstoichiometry departure and with electrical conductivity along with increase of reduction temperature. The energy band gap determined from both optical and photocurrent measurements increased with an increased deviation from stoichiometry, *x*. This phenomenon could be explained by a gradual filling up of a narrow conduction band in the rutile phase. The detrimental effect of the reduction on the main photoelectrochemical parameters such as the flat band potential and the photoelectrochemical efficiencies was observed at the highest *x* values for which the rutile phase existed.

Acknowledgments

The author would like to give her thanks to Professor Marta Radecka for undertaking the effort of supervising this thesis, for the inspiration and all the help given; to Professor Katarzyna Zakrzewska from the Department of Electronics Faculty of Electrical Engineering, Automatics, Computer Science and Electronics AGH UST and her co-workers for the opportunity to conduct a part of measurements and a helpful discussion; to Professor Sylvie Bourgeois (Université de Bourgogne, France) and her co-workers. The author would like to also kindly acknowledge the Foundation for Polish Science for financial support.

References

1. J.E. Lee, S.M. Oh, D.W. Park, Thin Solid Films 457 (1) (2004) 230-234
2. H. Irie, S. Washizuka, Y. Watanabe, T. Kako, K. Hashimotoz, J. Electrochem. Soc. 152 (11) (2005) E351-E356
3. M. Radecka, Thin Solid Films 451-452 (2004) 98-104
4. A. Fujishima, K. Honda, Nature 238 (1972) 37-38
5. M. Radecka, E. Pamuła, A. Trenczek-Zajac, K. Zakrzewska, A. Brudnik, E. Kusior, N.-T.H. Kim-Ngan, A.G. Balogh, Solid State Ionics 192 (2011) 693-698
6. A. Trenczek-Zajac, M. Radecka, K. Zakrzewska, A. Brudnik, E. Kusior, S. Bourgeois, M.C. Marco de Lucas, L. Imhoff, J. Power Sources 194/1 (2009) 93-103
7. A. Trenczek-Zajac, M. Radecka, K. Zakrzewska, A. Brudnik, E. Kusior, B. Lyson, K. Kowalski, J. Nanosci. Nanotechnol. (accepted for printing)
8. Brudnik, M. Bucko, M. Radecka, A. Trenczek-Zajac, K. Zakrzewska, Vacuum 82 (2008) 936-941
9. A. Trenczek-Zajac, K. Kowalski, K. Zakrzewska, M. Radecka, Mat. Res. Bull 44/7 (2009) 1547-1552
10. F. Vratny, F. Micale, Trans. Faraday Soc. 59 (1963) 2739-2749
11. M. Radecka, A. Trenczek-Zajac, K. Zakrzewska, M. Rękas, J. Power Sources 173/2 (2007) 816-821
12. B. Granier, C. Chatillon, M. Allibert, J. Am. Cer. Soc. 65/10 (1982) 465-469

INVESTIGATION OF $GdBaCo_{2-x}Fe_xO_{5.5-\delta}$ - CATHODE MATERIAL FOR INTERMEDIATE TEMPERATURE SOLID OXIDE FUEL CELLS*

Andrzej Kulka

AGH University of Science and Technology, Faculty of Energy and Fuels, Department of Hydrogen Energy
al. A. Mickiewicza 30, 30-059 Krakow, Poland

**This paper was written based on the Master Thesis supervised by Professor Janina Molenda.*

Introduction

Reducing the operational temperature down to the 600-800°C has become one of the main goals in SOFC technology. However, in this temperature range the cathodic overpotential constitutes a big part of overall potential losses in SOFC cell. Thus new cathode materials with satisfactory electrochemical properties must be found, in order to obtain good cells performances. Recently, layered cobaltites $ReBaCo_2O_{5.5-\delta}$ (Re - rare earth element) have been proposed as potential cathode materials for SOFC applications. It was noticed that these compounds are formed by$[CoO_2][BaO][CoO_2][ReO_\delta]$ plane sequence along the c direction. In addition if Re = Gd and in case of $\delta < 1$ the oxygen vacancies were found to locate in gadolinium planes at (0,0,1/2) positions. Furthermore, at RT the coexistence of two types of cobalt coordination environments with different spin state was observed: pyramidal CoO_5 (Co^{3+} intermediate spin state, IS, $t^5_{2g}e^1_g$) and octahedral CoO_6 (Co^{3+} low spin state, LS, $t^6_{2g}e^0_g$)[1]. Particularly, $GdBaCo_2O_{5.5-\delta}$ has been reported to exhibit very good transport properties i.e. high surface exchange coefficient and oxygen diffusivity [2,3]. Moreover this compound has been reported to undergo metal-insulator (MI) transition, which was connected with the spin state switch in the Co^{3+} ions located at the octahedra (from low spin $t^6_{2g}e^0_g$ to high spin $t^4_{2g}e^2_g$ state) and resulted in very high electric conductivity[1,2].

Experimental

In this work the comparison between $GdBaCo_2O_{5.5-\delta}$, $GdBaCo_{1.7}Fe_{0.3}O_{5.5-\delta}$ and $GdBaCo_{1.4}Fe_{0.6}O_{5.5-\delta}$ has been presented in terms of crystal structure, oxygen nonstoichiometry, electrical conductivity and single button-type SOFC cell measurements in order to investigate effect of substitution of Co by Fe. All powders were fabricated via soft chemistry method. The phase characterization was performed using a Rigaku RU-300 18 kW Bragg-Brentano diffractometer coupled to a rotating anode X-ray source (Cu K_α source). XRD measurements were also performed as a function of temperature. The obtained diffractograms were analyzed using Rietveld method. Mass changes of samples as a function of temperature were studying by thermogravimetric measurements using STA-SDT 2960 TA Instruments apparatus. The initial oxygen contents were obtained from reduction measurements in 5% H_2 in Ar atmosphere. Transport properties were characterized by high temperature electrical conductivity, measured by four-probe DC method (in air and as a function of oxygen partial pressure) and Seebeck coefficient measurements (dynamical method with temperature gradient equal 2-3°C). In order to investigate the influence of substitution of Co by Fe on the SOFC performance, electrolyte supported button-type SOFC cells with different cathode materials were fabricated. Button-type cell performances were examined using home-made SOFC test unit.

Results and discussion

X-ray diffraction indicate that both $GdBaCo_2O_{5.5-\delta}$ and $GdBaCo_{1.7}Fe_{0.3}O_{5.5-\delta}$ samples exhibit orthorhombic Pmmm space group symmetry with doubled *b* and *c* cell parameters ($a_p \times 2a_p \times 2a_p$ where a_p is the basic cubic perovskite cell parameter), while $GdBaCo_{1.4}Fe_{0.6}O_{5.5-\delta}$ was found to exhibit tetragonal P4/mmm space group symmetry, with only *c* cell parameter doubled ($a_p \times a_p \times 2a_p$). In Fig. 1 the XRD patterns at RT for all samples are presented. Cell parameters are listed in Table 1. Those values show that after substitution of Co by Fe, the

Table 1. Cell parameters for $GdBaCo_{2-x}Fe_xO_{5.5-\delta}$

Cell parameters for $GdBaCo_{2-x}Fe_xO_{5.5-\delta}$				
Fe content	*a* [Å]	*b* [Å]	*c* [Å]	V_p ($V_p = a_p^3$) [Å^3]
0.0	3.8770(3)	7.8211(5)	7.5346(7)	57.11(8)
0.3	3.8758(9)	7.8243(8)	7.5660(2)	57.36(3)
0.6	3.8944(1)	3.8944(1)	7.5944(4)	57.59(1)

volume of the cell tends to increase. The radius of the HS Fe^{3+} ions is 0.645 Å and is slightly higher compared to the radius of the IS Co^{3+} (0.56 Å) at the pyramidal site[4] what can explain observed increase of the volume of the cell.

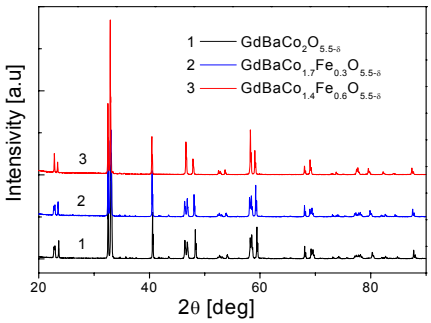

Fig. 1. XRD patterns at RT for $GdBaCo_{2-x}Fe_xO_{5.5-\delta}$

In Fig. 2 exemplary XRD patterns as a function of temperature for $GdBaCo_2O_{5.5-\delta}$ are presented. One can see that with increase of the temperature, XRD patterns change, and for higher temperatures it was found that crystal structure can be described as a P4/mmm space group symmetry ($a_p \times a_p \times 2a_p$). This indicates that oxygen vacancies are no longer ordered at (0,0,1/2) positions, additionally, it was found that the introduction of Fe has led to the lowering of the phase transition temperature.

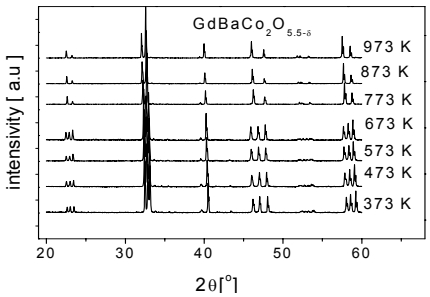

Fig.2. XRD patterns as function of temperature for $GdBaCo_2O_{5.5-\delta}$

In Fig. 3 exemplary thermogravimetric measurements result is shown.

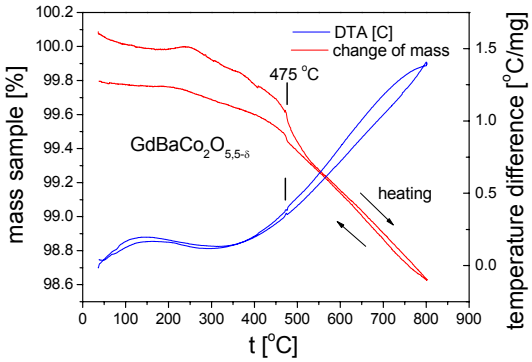

Fig.3. TG-DTA results for $GdBaCo_2O_{5.5-\delta}$

The temperature of phase transition from low temperature phase (Pmmm $a_p \times 2a_p \times 2a_p$) to high temperature phase (P4/mmm $a_p \times a_p \times 2a_p$) is marked, one can notice the change of the slope of mass dependence as a function of temperature for these two phases. For high temperature phase the change of the mass sample decrease more abruptly, than for low temperature one. It can be ascribed to the different oxygen uptake/release rates in these two regions, with greater one for high temperature phase. Additionally, it was noticed that enthalpies of oxygen vacancy formations at higher temperatures (600-800°C) are extremely small (i.e. 0.3 eV for pO_2=0.2). In Fig. 4 the electrical conductivities for all samples as a function of temperature are presented.

An increase in conductivity observed at lower temperatures, $T < T_s$ (T_s-temperature of spin state transition) is typical for semiconductor-type behavior. Furthermore at specific temperature T_s, change of electrical behavior was observed and for $GdBaCo_2O_{5.5-\delta}$ it has been attributed to the metal-insulator transition caused by change of spin state of cobalt ions in octahedral environment[1]. It has been noticed that with increasing Fe content the temperature of this transition shifts to the higher

values (100°C ,180°C and 300°C for x: 0.0, 0.3, 0.6 respectively). At temperatures T > T_t (T_t-temperature of phase transition) decrease of the electrical conductivity was observed. Taking into account results of TG measurements (Fig.3), for samples with Fe content *x*: 0.0 and 0.3 it corresponds well with increase of concentration of the oxygen vacancies within greater oxygen uptake/release rate regime. In Fig. 5 exemplary result of electrical conductivity as a function of oxygen partial pressure for different temperatures is shown. It can be noticed that with increase of the oxygen partial pressure electrical conductivity also increases, what is typical for p-type semiconductors.

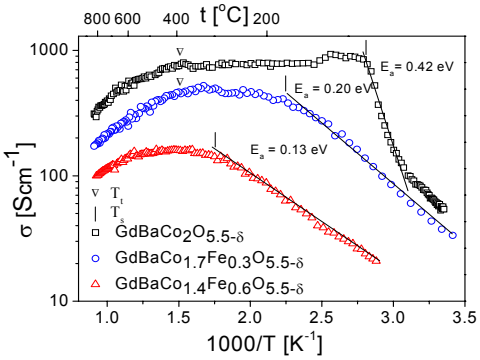

Fig.4. Electrical conductivity as function of temperature for $GdBaCo_{2-x}Fe_xO_{5.5-\delta}$

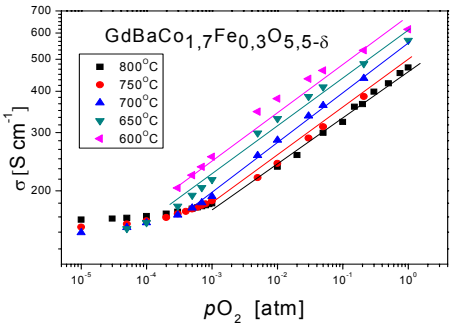

Fig.5 Electrical conductivity as a function of oxygen partial pressure for $GdBaCo_{1.7}Fe_{0.3}O_{5.5-\delta}$ for different temperatures

In Fig. 6 exemplary voltage and power density as a function of current density characteristics are shown. As can be seen, voltage drop with increasing current is almost linear, therefore indicating that major part in the whole electrical losses can be ascribed to the ohmic resistivity of the electrolyte. It is caused by the specific construction of the single SOFC cells where thick (~800μm) $Ce_{0.8}Gd_{0.2}O_{2-\delta}$ electrolyte was used. The obtained values of maximum power density of a single SOFC cell indicate that at high temperatures, the maximum power density decreases with Fe content, while at lower temperature, a slightly improved performance can be observed for composition with *x* = 0.3 (0.029 W/cm^2 at 600°C).

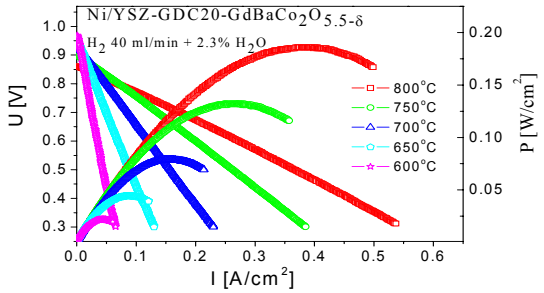

Fig. 6. Voltage and power density as a function of current density characteristics for selected cathode materials.

Conclusion

In conclusion, all materials exhibit layered perovskite structure with space group symmetry dependent on Fe content. In investigated compounds both structural and spin state transition occurs. Different oxygen uptake/release rates are present for low and high temperatures. High electrical conductivity and very low enthalpies of oxygen vacancies formation suggest that these materials are potential cathode materials in SOFC application. The highest maximum power density at 600°C was obtained for Fe content *x* = 0.3.

References

1. C. Frontera *et al.,* Phys. Rev. B 65, 180405(R) (2002).
2. A.A. Taskin *et al.,* Phys. Rev. B 71, 134414 (2005).
3. A.A. Taskin *et al.,* Appl. Phys. Lett. 86, 91910 (2005).
4. R.D. Shannon, Acta Crysallogr. Sect. A: Cryst. Phys., Diffr., Theor. Gen. Crystallogr. A32, 751 (1976).

Activity of the Polish Hydrogen and Fuel Cell Association

The Polish Hydrogen and Fuel Cell Association (PHFCA) was founded on the 19th of July 2004 at AGH University of Science and Technology. The initiatives undertaken by the Association have been focused on education in the field of hydrogen and fuel cells technology application in Poland, stimulation of interest in hydrogen and fuel cell technologies and dissemination of current achievements as well as supporting of cooperation between industry and scientific institutions in this area. The one of the significant achievements was creation of the graduate studies program entitled: "Hydrogen Energy" at the Faculty of Energy and Fuels at AGH in March 2009. This specialty is the unique one in Poland. During last 7 years Association has organized 3 international conferences "Polish Forum of Hydrogen and Fuel Cells", 3 periodic trainings for students and postgraduate students – "The Summer School of Hydrogen and Fuel Cells". Every year Association is organizing academic lectures at AGH Open Technical University in the hydrogen technology field and is organizing the contest entiled: "Best thesis in the field of hydrogen technology and fuel cells" (the abstracts of the master and Ph.D. theses awarded in the last edition of the contest are presented in the current Bulletin). Every year PHFCA is participating in the Science Festival, which takes place in May in Krakow. To date PHFCA published 6 annals of the Bulletin of Polish Hydrogen and Fuel Cells Association. Bulletin contains, among other, lectures from the last Forum or Summer School.

The Polish Forum of Hydrogen and Fuel Cells conference is devoted to a presentation of Polish achievements and stimulation of growth and development in fuel cells and hydrogen technology areas. The invited world-leading scientists presented and shared their experience in these fields. Forum particularly intends to discuss fundamental material-related issues. Forum is organized every 2 years. I Polish Forum took place on 5-7 September 2007 in Zakopane, Poland. The II Polish Forum took place in Kocierz, Poland, on 7-10 September 2009. Current Bulletin was dedicated to the III Polish Forum "Smart Materials for Hydrogen and Renewable Energy". The event was organized on the 29-30 November 2011 in Warsaw as satellite to major Strategic Energy Technology Plan Conference 2011 (www.setplan2011.pl), which is related to Polish EU Presidency.

The list of the invited guest on the II Polish Forum of Hydrogen and Fuel Cells:

K. Funke *"First and Second Universality" in disordered ion-conducting materials*
L. Gauckler *Design, materials and processes for micro solid oxide fuel cells (SOFC micro fuel cells)*
I. Kosacki *Small but perfectly working - novel materials for energy*
M. Mogensen *Nano-scale in SOFC electrodes*
I. Riess *Catalysis of electrochemical processes and the suppression of chemical ones are needed in mixed reactant fuel cells. Can this be achieved?*
J.T.S. Irvine *Fuel electrodes for solid oxide fuel cells*
L. Suescun *Perovskite materials for SOFC cathodes. Tailoring of the crystal structure*
J. Thomas *State-of-the-art MD simulation of PEMFC electrolytes*
P. Knauth *Physical chemistry of proton-conducting polymers*
A. Takasaki *Hydrogen storage systems for automotive application. The case of Japan*

The II Polish Forum in Kocierz, Poland, 7-10 September 2009

The Summer School of Hydrogen and Fuel Cells organized every two years in September (every year interchangeably with Forum) at AGH UST is dedicated to young scientists, Ph.D. students and power industry employees. It gives possibility for young researchers to get access to the actual state of knowledge related to the research achievements and application problems in the area of new sources of energy and methods of its transformation. I Summer School took place on 6-8 September 2006, II Summer School took place on 3-5 September 2008, III Summer School took place on 15-17 September 2010.

Posters of the Summer Schools of Hydrogen and Fuel Cells organized by PHFCA

II and III Summer Schools of Hydrogen and Fuel Cells, 3-5 September 2008, 15-17 September 2010

Lectures in the hydrogen technology field organized at AGH Open Technical University on December every year serve the popularization of the ideas of new, ecological energy sources in the society and are addresses mainly to the students, secondary schools students and citizens of Krakow.

Lectures in the hydrogen technology field at AGH Open Technical University

Today the PHFCA counts 157 ordinary members (including over 50 professors or senior scientists in this figure), 2 honorary members and 12 supporting members:

- AGH University of Science and Technology, Krakow
- ETCplus SA, Ostrowiec Swietokrzyski
- Central Mining Institute, Katowice
- Institute of Physical Chemistry Polish Academy of Sciences, Warsaw
- Electrotechnical Institute, Division of Electro-technology and Materials Science, Wroclaw
- Institute of Molecular Physics Polish Academy of Sciences, Poznan
- Division of the Institute of Non-Ferrous Metals in Poznan, Central Laboratory of Batteries and Cells, Poznan
- NAFCELLS Centre of Excellence, Wroclaw
- Warsaw University of Technology, Warsaw
- Warsaw University of Technology, CERED Centre of Excellence, Plock
- The West Pomeranian University of Technology, Szczecin
- The Department of Management and Quality Systems, Faculty of Mechanical Engineering, Military University of Technology, Warsaw

Approaching scientific conferences

2011

- Hydrogen and Fuel Cells Conference
  1 - 5 December 2011, Puerto Morelos, Mexico

- European Fuel Cell "Piero Lunghi Conference
  14 - 16 December 2011, Rome, Italy
  http://www.europeanfuelcell.it/

- International Conference on Renewable Energy Technologies (iCORET 2011)
  15-17 December 2011, Coimbatore, Tamil Nadu, India
  http://www.psgtech.edu/icoret11/

2012

- 2nd Annual Electric Energy Storage Conference
  10-12 January 2012, Phoenix, AZ, USA

- Advanced Automotive Battery Conference 2012 (AABC 2012)
  6-10 February, 2012, Omni Orlando Resort, Orlando, Floryda, USA
  http://www.advancedautobat.com

- EV Battery Forum 2012
  20-22 March, 2012, Barcelona, Spain

- Advanced Characterization, Theory and Mechanisms of Processes in Rechargeable Batteries Across Length Scales
  4-9 March, 2012, Ventura, CA, USA
  http://www.grc.org/programs.aspx?year=2012&program=batteries

- Advanced Lithium Ion Battery International Symposium
  18 - 20 April, 2012, Charlotte, NC, USA
  www.acius.net

- Fuel Cells 2012 Science & Technology
  11-12 April 2012, Berlin, Germany
  http://www.fuelcelladvances.com/

- EVS- Electric Vehicle Symposium
  6-9 May, Los Angeles, California, USA
  http://evs26.org/

- International Symposium on Ceramic Materials and Components for Energy and Environmental Applications
  20 - 23 May 2012, Dresden, Germany
  http://www.cmcee12.de/

- Battcon 2012 – Stationary Batteries in our Mobile World
  15-17 May, 2012, Hollywood, Floryda, USA
  http://www.battcon.com

- WHEC 2012 19th World Hydrogen Energy Conference 2012
  3 - 7 June 2012, Toronto, Canada
  http://www.whec2012.com/

- Renewable Energy World Europe
  12-14 June, 2012, Cologne, Germany
  http://www.renewableenergyworld-europe.com/

- 10th European SOFC forum 2012
  26-29 June, Lucerne, Switzerland
  http://www.efcf.com/events/

- 7 Kongres Technologii Chemicznej (7th Congress of Chemical Technology)
  8-12 July 2012, Krakow, Poland
  http://www.techem7.pl/

- International Symposium on Metal-Hydrogen Systems
  21-26 December, Kyoto, Japan
  http://www.mh2012.jp/

New books

Fuel Cells: From Fundamentals to Systems
U. Stimming, D. Jones
Wiley 2010

Fuel Cell Science: Theory, Fundamentals and Biocatalysis
A. Wieckowski, J. Norskov, S. Gottesfeld
Wiley 2010

Fuel Cell Micro
Sh. Obara
Springer 2010

Fuel Cell Electronics Packaging
K. Kuang, K. Easler
Springer 2010

Fuel Cell Technology: Reaching Towards Commercialization
N. Sammes
Springer 2010

Fuel Cells: Modeling, Control and Applications
W. Gou, K. Na, B. Dion
CRC Press 2010

Advances In Solid Oxide Fuel Cells V, Vol. 30
N. P. Bansal, P. Singh
Wiley 2010

Handbook of Fuel Cell Modelling
E. Fontes
Elsevier 2010

Proton Exchange Membrane Fuel Cells: Materials Properties and Performance
D. P. Wilkinson, J. Zhang, R. Hui, J. Fergus, X. Li
CRC Press 2010

Modeling and Diagnostics of Polymer Electrolyte Fuel Cells
U. Pasaogullari, Ch.-Y. Wang
Springer 2010

The Economic Dynamics of Fuel Cell Technologies
B. Springer
Springer 2010

Analytical Modelling of Fuel Cells
A. Kulikovsky
Elsevier 2010

Direct Methanol Fuel Cells
A. S. Arico, V. Baglio, V. Antonucci
Nova Science Publishers 2010

On Solar Hydrogen and Nanotechnology
L. Vayssieres
Wiley 2010

The Metal-Hydrogen System: Basic Bulk Properties (Springer Series in Materials Science)
Y. Fukai
Springer 2010

Hydrogen Bonding and Transfer in the Excited State
K.-L. Han, G.-J. Zhao
Wiley 2010

Hydrogen and Syngas Production and Purification Technologies
K. Liu, Ch. Song, V. Subramani
Elsevier 2010

Renewable Energy and Climate Change
V. Quaschning
Wiley-IEEE Press 2010

Renewable Energy, 4th Edition. Physics, Engineering, Environmental Impacts, Economics & Planning
B. Sorensen
Academic Press 2010

Electric and Hybrid Vehicles. Power Sources, Models, Sustainability, Infrastructure and the Market
G. Pistoia
Academic Press 2010

Automotive Electricity: Electric Drive
J. Beretta
Wiley 2010

Lithium-ion Batteries
Ch. R. Park
InTech 2010

Battery Management Systems for Large Lithium-Ion Battery Packs
D. Andrea
Artech House 2010

High Energy Density Lithium Batteries: Materials, Engineering, Applications
K. E. Aifantis, S. A. Hackney, R. V. Kumar
Wiley 2010

Advanced Methods of Solid Oxide Fuel Cell Modeling
J. Milewski, K. Swirski, M. Santarelli, P. Leone
Springer 2011

Hydrogen Fuel Cells for Road Vehicles
P. Corbo, F. Migliardini, O. Veneri, P. Corbo, F. Migliardini, O. Veneri
Springer 2011

Pem Fuel Cells with Bio-Ethanol Processor Systems: A Multidisciplinary Study of Modelling, Simulation, Fault Diagnosis and Advanced Control
M.S. Basualdo, R. Outbib, D. Feroldi
Springer 2011

Cogeneration Fuel Cell-Sorption Air Conditioning Systems
I. Pilatowsky, R. J. Romero, C. A. Isaza, S. A. Gamboa, W. Rivera, P. J. Sebastian
Springer 2011

Fuel Cells and Hydrogen Storage
S.C. Singhal, X.-D. Zhou, H. Wang, H.D. Abru, J. Benziger, A. Bocarsly, M.J. Cheah, P. Majsztrik, B. Satterfield, Q. Zhao, S. Sachdeva, J. A. Turner, J.L. Horana, A. M. Herring, M. T. Kelly
Springer 2011

Advances in Solid Oxide Fuel Cells VII: Ceramic Engineering and Science Proceedings
N.P. Bansal, P. Singh
Wiley 2011

Catalysis in Electrochemistry: From Fundamental Aspects to Strategies for Fuel Cell Development
E. Santos, W. Schmickler
Wiley 2011

Fuel Cells: Technologies for Fuel Processing
D. Shekhawat, J.J. Spivey, D. A. Berry
Elsevier 2011

Polymer Electrolyte Fuel Cell Degradation
M. M. Mench, E. C. Kumbur, T. N. Veziroglu
Academic Press 2011

PEM Fuel Cells, Theory and Practice
F. Barbir
Academic Press 2011

Hydrogen and Fuel Cells, 2nd Edition Emerging Technologies and Applications
B. Sorensen
Academic Press 2012

Hybrid Hydrogen Systems: Stationary and Transportation Applications, Series: Green Energy and Technology
S. Al-Hallaj, K. Kiszynski
Springer 2011

Renewable Energy System Design
Z. Salameh
Elsevier 2011

Advanced Lithium-Ion Batteries: Recent Trends and Perspectives
M. Lu, G.-A. Nazri, P. Balaya, A. Manthiram, A.Yamada, Y. Yang
Wiley 2011

Lithium-ion Batteries: Advanced Materials and Technologies
X. Yuan, H. Liu, J. Zhang
CRC Press 2011

Authorities of the Association

PRESIDENT
Prof. dr hab. inż. Janina Molenda
Faculty of Energy and Fuels, Head of Department of Hydrogen Energy
AGH University of Science and Technology
al. Mickiewicza 30, 30-059 Kraków
molenda@agh.edu.pl

VICE-PRESIDENT
Dr hab. Piotr Tomczyk, prof. AGH
Dean of Department of Hydrogen Energy
AGH University of Science and Technology
al. Mickiewicza 30, 30-059 Kraków
ptomczyk@uci.agh.edu.pl

VICE-PRESIDENT
Dr inż. Grzegorz Paściak
Electrotechnical Institute Division of Electrotechnology
and Materials Science
M. Skłodowskiej-Curie 55/61, 50-369 Wrocław
pasciak@iel.wroc.pl

VICE-PRESIDENT
Dr inż. Janusz Jewulski
Institute of Power Engineering
Augustówka 36, 02-981 Warszawa
janusz.jewulski@ien.com.pl

SECRETARY
Mgr inż. Zdzisław Matysiak
Ecoenergy Cieszyn Association
Bobrecka 29, 43-400 Cieszyn
zdzisław-matysiak@o2.pl

TREASURER, ADMINISTRATION, WEBSITE
Dr inż. Anna Milewska
Faculty of Energy and Fuels
AGH University of Science and Technology
al. Mickiewicza 30, 30-059 Kraków
anna.milewska@agh.edu.pl
hydrogen@agh.edu.pl

AUDITING COMMITTEE
CHAIRMAN OF AUDITING COMMITTEE
Prof. dr hab. Henryk Figiel

MEMBERS OF AUDITING COMMITTEE
Prof. dr hab. Roman Dziembaj
Doc. dr inż. Dariusz Dzirba
Dr inż. Piotr Jasiński
Doc. dr hab. Stanisław Filipek

www.hydrogen.edu.pl

ISSN 1896-7205
cena 25zł

www.hydrogen.edu.pl